# The Role of Death Receptor 3 in Health and Disease

A thesis submitted in candidature for the degree of

**DOCTOR OF PHILOSOPHY**

By

**Melanie Jane Bull**

January 2009
Medical Biochemistry and Immunology,
Cardiff University,
Wales College of Medicine
Cardiff, CF14 4XN, UK.





ProQuest LLC
789 East Eisenhower Parkway
P.O. Box 1346
Ann Arbor, MI 48106-1346

**DECLARATION**

This work has not previously been accepted in substance for any degree and is not concurrently submitted in candidature for any degree.

Signed ..... (Melanie Bull) Date 19/02/2009..

**STATEMENT 1**

This thesis is being submitted in partial fulfillment of the requirements for the degree of PhD

Signed ..... (Melanie Bull) Date 19/02/2009.....

**STATEMENT 2**

This thesis is the result of my own independent work/investigation, except where otherwise stated.

Other sources are acknowledged by explicit references.

Signed ..... (Melanie Bull) Date 19/02/2009.....

**STATEMENT 3**

I hereby give consent for my thesis, if accepted, to be available for photocopying and for inter-library loan, and for the title and summary to be made available to outside organisations.

Signed ..... (Melanie Bull) Date 19/02/2009.....

**STATEMENT 4: PREVIOUSLY APPROVED BAR ON ACCESS**

I hereby give consent for my thesis, if accepted, to be available for photocopying and for inter-library loans **after expiry of a bar on access previously approved by the Graduate Development Committee.**

Signed..... (Melanie Bull) Date .....

**Acknowledgements**

I would first like to thank my supervisors Dr Eddie Wang and Dr Anwen Williams for all of their advice, encouragement and hard work over the past few years. Your enthusiasm never failed to motivate me and without your support and patience throughout the ups and downs, I doubt this thesis would ever have been completed. I would also like to thank Dr Awen Gallimore for her involvement in the creation of the project.

Secondly I would like to thank all of the members of the DR3 team and my other colleagues within Medical Biochemistry and Medical Microbiology for their daily advice and entertainment. I have thoroughly enjoyed my time within the lab and I would like to thank you all for making it a great experience. I would also like to thank the I3-IRG and the MRC for funding the project.

Finally I would like to thank my family, Richard, Lloyd, Mum, Dad, Ellie, Mick and James, for their lifelong support and belief in me. I would especially like to thank my partner Richard and my son Lloyd for undertaking the whole experience with me. Despite the long hours and frustrations you kept me smiling through it all.

## Summary

Death receptor 3 (DR3) is a death domain-containing type I transmembrane protein. It can bring about a wide range of responses from apoptosis to proliferation through association with intracellular signaling molecules. The only accepted ligand for DR3 is TNF-like protein 1A (TL1A). An important role for DR3 in inflammatory disease states is emerging with links being made with inflammatory bowel disease (IBD), Rheumatoid Arthritis, atherosclerosis, allergic lung inflammation and in renal inflammation. The project undertaken in this thesis investigated the role of DR3 in a murine model for rheumatoid arthritis, namely antigen-induced arthritis (AIA), using mice genetically deficient in DR3. A further aim of this project was to generate reagents for use in DR3 research through the employment of DR3 gene cloning strategies.

DR3 deficient animals displayed a high degree of protection from mAIA in terms of resolution of joint swelling and the pathological degenerative alterations occurring within the joint. At day 21 post-arthritis induction, a time-point when maximal structural damage would likely be observed, $DR3^{-/-}$ animals showed a significant reduction in all histopathological parameters including a complete absence of bone erosion. This effect was shown to be DR3 specific through the administration of TL1A to control animals. Mice receiving increasing concentrations of TL1A showed a dose-dependent increase in synovial hyperplasia and bone erosion. DR3 deficient mice also displayed protection from cartilage depletion following induction of AIA. In an attempt to dissect a mechanism for this reduced disease severity, an analysis of osteoclast numbers and F4/80+ osteoclast precursor cell numbers within the joints was undertaken. DR3 sufficient mice displayed significantly more osteoclasts at sites of focal bone erosion which could not be attributed to differences in F4/80+ precursor cell numbers.

The results presented here identify a potentially novel target for the treatment of human inflammatory joint disease.

**Table of contents**

**List of Tables**

**List of Figures**

**Suppliers and Company Addresses**

**Abbott Laboratories**, Maidenhead, Berkshire, UK

**Amersham Pharmacia Biotech**, Little Chalfont, Bucks, UK.

**Alpha Diagnostics International**, US

**Autogen Bioclear,** Wiltshire, UK

**Beckman Instruments** Ltd., High Wycombe, Bucks, UK.

**BD Pharmingen** UK Ltd., Cowley, Oxford, UK.

**Bio-Rad**, USA

**Caltag** Ltd., Silverstone, Towcester, UK.

**Clontech laboratories** Inc., Basingstoke, Hampshire, UK.

**Eurogentec** Ltd., Hythe, Southampton, UK.

**Fisher Scientific** Ltd., Loughborough, Leics., UK.

**Genscript**, USA

**GraphPad** Software Inc., San Diego, CA, USA.

**Greiner**, Stonehouse, Gloucestershire, UK.

**Hamamatsu,** Hamamatsu City, Japan

**Hybaid** Ltd., Ashford, Middlesex, UK.

**Hycor Biomedical** Inc., Penicuik, Edinburgh, UK.

**IBA**, USA

**Invitrogen**, Groningen, The Netherlands.

**Improvision** Ltd., Coventry, Warwickshire, UK.

**Leica** Camera AG, Solms,Germany.

**Melford**, Suffolk

**Merck** Pharmaceuticals, West Drayton, UK.

**Miltenyi Biotec** Ltd., Bisley, Surrey, UK.

**New England Biolabs,**USA.

**Oxoid** Ltd., Hampshire, UK.

**Perbio Pierce**, Belgium

**Perkin-Elmer** Life Sciences, Boston, USA.

**Pharmacia Biotech**, Cambridge, UK

**ProImmune** Ltd., Oxford Science Park, Oxford, UK.

**Promega Ltd.,** Southhampton, UK.

**Qiagen**, West Sussex, UK

**Reichert**, USA

**Roche Diagnostics** GmBH Roche, Mannheim, Germany.

**Santa Cruz** Autogen Bioclear UK Ltd., Calne, Wiltshire, UK.

**Serotec** Ltd, Kidlington, Oxford, UK.

**Sigma-Aldrich** Co. Ltd., Poole, UK.

**Sorvall** Kendro Lab. Products Ltd., Bishops Stortford, Herts., UK.

**Thermoelectron Corp,** USA

**Vector Laboratories**, California, USA

**Weiss-Gallenkamp**, Loughborough, UK

**Abbreviations**

| | |
|---|---|
| aa | Amino acids |
| ADAMTS | A disintegrin and a metalloprotease with thrombospondin motifs |
| AIA | Antigen-induced arthritis |
| ATP | Adenosine triphosphate |
| bp | Base pairs |
| BSA | Bovine serum albumin |
| CD | Cluster of differentiation |
| CHO | Chinese hamster ovary |
| CIA | Collagen-induced arthritis |
| ct | c terminal |
| DcR | Decoy receptor |
| DR | Death receptor |
| dH2O | Distilled water |
| DMEM | Dulbeccos modified eagle's medium |
| DMSO | Dimethyl sulfoxide |
| DN | Dominant negative |

| | |
|---|---|
| DNA | Deoxyribonucleic acid |
| dNTP | Deoxynucleotide triphosphate |
| EDTA | Ethylene diamine tetraacetic acid |
| ELISA | Enzyme-linked immunosorbent assay |
| FADD | Fas-associated death domain |
| FCS | Foetal calf serum |
| GFP | Green fluorescent protein |
| GM-CSF | Granulocyte macrophage colony stimulating factor |
| H and E | Haematoxylin and eosin |
| hDR3 | Human DR3 |
| HRP | Horse radish peroxidase |
| IBD | Inflammatory bowel disease |
| Ig | Immunoglobulin |
| IFN | Interferon |
| IL | Interleukin |
| kb | Kilobases |
| kDa | Kilodaltons |

| | |
|---|---|
| L | Ligand |
| LacZ | Beta-galactosidase gene |
| LB | Lauria bertani |
| LT | Lymphotoxin |
| MAP | Multiple antigenic peptide |
| MCP | Monocyte chemotactic protein |
| M-CSF | Macrophage colony stimulating factor |
| mDR3 | Murine DR3 |
| MMP | Matrix metalloproteinase |
| mRNA | Messenger RNA |
| NFκB | Nuclear factor kappa B |
| nt | n terminal |
| OD | Optical density |
| OPG | Osteoprotegerin |
| ORF | Open reading frame |
| PBMC | Peripheral blood mononuclear cells |
| PBS | Phosphate buffered saline |

| | |
|---|---|
| PBS-T | Phosphate buffered saline (tween-20) |
| PCR | Polymerase chain reaction |
| PEG | Polyethylene glycol |
| RA | Rheumatoid arthritis |
| RANK | Receptor activator of NFκB |
| RIP | Receptor interacting protein |
| RNA | Ribonucleic acid |
| Rpm | Revolutions per minute |
| RPMI | Media developed at the Roswell Park Memorial Institute |
| RT-PCR | Reverse transcription PCR |
| SDS | Sodium dodecyl sulphate |
| SOL | Soluble |
| TBE | Tris/Borate/EDTA |
| TBS | Tris-buffered saline |
| TE | Tris-EDTA buffer |
| TEMED | N N N' N'-tetraethylenediamine |
| TL1A | TNF-like protein 1A |

| | |
|---|---|
| TNF | Tumour necrosis factor |
| TNFR | Tumour necrosis factor receptor |
| TNFRSF | Tumour necrosis factor receptor superfamily |
| TRADD | TNF receptor associated death domain |
| TRAF | TNFR-associated factor |
| TRAP | Tartrate resistant acid phosphatase |
| Tris | Tris (hydroxymethyl)methylamine |
| UV | Ultraviolet |
| v/v | Volume to volume ratio |
| w/v | Weight to volume ratio |
| X-gal | 5-bromo,4-chloro-3-indolyl-β-D-galactopyranoside |

# Introduction

# 1. Introduction

## 1.1 The Tumour Necrosis Factor (TNF) Superfamily

The discovery of the TNF superfamily was made following the identification of the proteins TNF and Lymphotoxin (LT). TNF was originally named in 1975 when it was described as a factor capable of bringing about the necrosis of tumours (Carswell et al., 1975). LT was first described in 1968 also as a tumour necrosing factor (Williams and Granger, 1968). When the sequences and structures of these proteins were later determined in 1985, it became apparent that they displayed homology and were capable of binding the same cell surface receptors (Aggarwal et al., 1985). Thus the beginnings of a receptor/ligand superfamily started to emerge. The TNF superfamily now comprises at least 29 receptors and 19 ligands (Aggarwal et al., 2003) which interact to bring about a variety of cellular effects. Table 1.1 provides a list of receptors and ligands belonging to the TNF superfamily, patterns of cellular expression and some of the general biological functions they are associated with.

### 1.1.1 General Structure of Receptors and Ligands

TNF receptors (TNFRs) are characterised by the presence of a cysteine-rich region in their extracellular domain (MacEwan, 2002). Apart from the receptors osteoprotegerin (OPG) and decoy receptor 3 (DcR3) which are produced as secreted proteins, TNF receptors are type I trans-membrane proteins (Bossen et al., 2006). A small subset of these receptors displays an additional region of homology within the cytoplasmic tail which is known as the death domain. At least 8 family members containing the death domain have been identified and these are

indicated in table 1.1. The death domain confers the ability to bring about programmed cell death or apoptosis (Orlinick and Chao, 1998).

| Receptor | Cellular Expression | Death Domain? | Ligand | Cellular Expression | General Roles |
|---|---|---|---|---|---|
| **TNFR1** | Generally ubiquitous expression | Yes | TNFα/LTα | Immune c ells | Host defence/inflammation/septic shock |
| **TNFR2** | Immune cells/endothelial cells | No | TNFα/LTα | Immune c ells | Host defence |
| **LTβR** | NK cells/T cells | No | LTα/β | Immune c ells | Host defence/organogenesis |
| **FAS** | Generally ubiquitous expression | Yes | FASL | Splenocytes/thymocytes | Host defence/immune cell homeostasis |
| **CD40** | Immune cells | No | CD40L | T cells/B cells | Immune cell homeostasis |
| **RANK** | Osteoclasts | No | RANKL | T cells/osteoblasts | Osteoclastogenesis |
| **OPG** | Osteoclasts/endothelial cells | No | RANKL | T cells/osteoblasts | Decoy receptor |
| **DR3** | T cells/B cells/endothelial cells | Yes | TL1A | Endothelial cells/T cells/macrophages | T cell homeostasis and activation/inflammation |
| **DR4** | Generally ubiquitous expression | Yes | TRAIL | NK cells/T cells/DCs | Host defence |
| **DR5** | Generally ubiquitous expression | Yes | TRAIL | NK cells/T cells/DCs | Host defence |
| **DR6** | T cells | Yes | ? | ? | ? |
| **DcR1** | Generally ubiquitous expression | No | TRAIL | NK cells/T cells/DCs | Decoy receptor |
| **DcR2** | Generally ubiquitous expression | No | TRAIL | NK cells/T cells/DCs | Decoy receptor |
| **DcR3** | T cells | No | TL1A | Endothelial cells | Decoy receptor |
| **41BB** | Activated T cells/monocytes/NK cells | No | 41BBL | B cells/DCs/macrophages | T/B cell activation |
| **BAFFR** | B cells/T cells | Yes | BAFF | T cells/DCs/monocytes/macrophages | B cell homeostasis/autoimmunity |
| **BCMA** | Immune cells | No | BAFF/APRIL | Immune c ells | B cell homeostasis/autoimmunity |
| **CD27** | T cells | No | CD27L | NK cells/T cells/B cells | T cell activation |
| **CD30** | Reed-sternberg cells | No | CD30L | T cells/monocytes | Th2 cell function |
| **EDAR** | Ectodermal derivative | Yes | EDA2 | Skin | Hair/teeth morphogenesis |
| **Fn14** | Endothelial cells/fibroblasts | No | TWEAK | Monocytes | Inflammation/cellular migration/proliferation |
| **GITR** | T cells | No | GITRL | ? | T cell homeostasis |
| **HVEM** | T cells | No | LIGHT/LTα | Immune cells | Viral entry |
| **NGFR** | Nervous system | Yes | ? | ? | CNS development |
| **OX40** | T cells | No | OX40L | T cells/B cells | T/B cell homeostasis |
| **RELT** | Lymphoid tissues | No | ? | ? | T cell homeostasis |
| **TACI** | Immune cells | No | BAFF/APRIL | Immune cells | B cell homeostasis |
| **TROY** | Embryo skin/epithelium/hair follicles | No | ? | ? | Embronic development |
| **XEDAR** | Ectodermal derivative | No | EDA2 | Skin | Hair/teeth morphogenesis |

**Table 1.1. TNFRSF members.** A list of TNFRSF receptors and their ligands. Some general biological functions and patterns of cellular expression are listed. Produced using (Aggarwal 2003), (Bossen, Ingold et al 2006) and (MacEwan 2002).

TNF family ligands are type II proteins that may also be cleaved from the membrane under certain conditions to bring about their effects (Aggarwal et al., 2003). TNF family ligands share a region of homology of approximately 150 amino acids within their extracellular domains. 15%-35% of this region is conserved between different ligands (Orlinick and Chao, 1998).

### 1.1.2 Signalling

Prior to receptor interaction, all TNF ligands are thought to form homotrimers which either bind to their respective receptors via cell-cell contact or are cleaved from the membrane enabling them to bring about their effects at a distance from their local environment (MacEwan, 2002). Receptors also signal as trimer complexes following ligand interaction or as is the case with TNFR1 and TNFR2, may also form a complex prior to ligand association via a pre-ligand-binding assembly domain (Chan et al., 2000). Signalling through TNFRs is best exemplified using the well characterised TNFR1 receptor. This is depicted in figure 1.1.

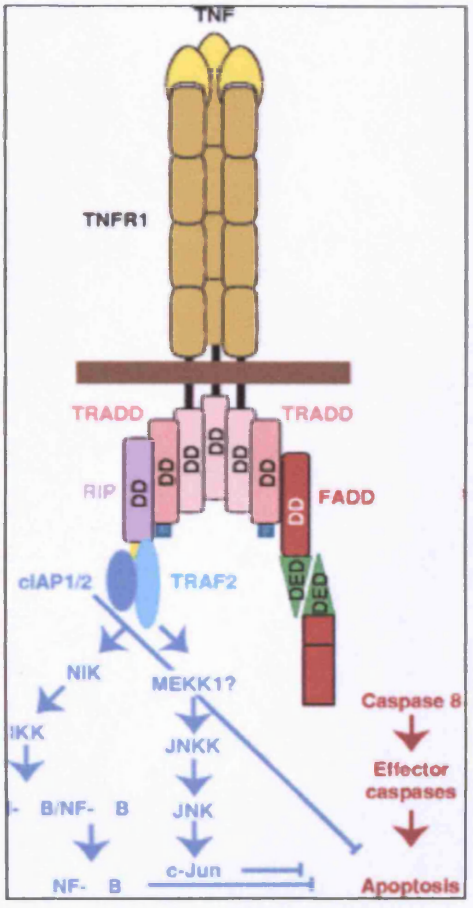


**Figure 1.1. Signalling via TNF and TNFR1.** TNFR1 signalling is mediated via the recruitment of TRADD, FADD and TRAF2. Reproduced from (Ashkenazi and Dixit, 1998)

Following TNF-TNFR1 association, intracellular adaptor molecules are recruited to the complex to initiate downstream effects. In the death domain-containing receptors such as TNFR1, the death domain itself acts as the site for interaction with signalling molecules. Such molecules include TNFR-associated death domain (TRADD), Fas-associated death domain (FADD) and receptor-interacting protein (RIP) (MacEwan, 2002). TRADD associates with the death domains of the trimerised receptors and subsequently recruits TNFR-associated factor 2 (TRAF-2) and RIP which serve to initiate the NFκB pathway and cellular proliferation and differentiation (Hsu et al., 1996). TRADD can also recruit FADD resulting in the interaction of caspase 8 and the induction of downstream effector caspases subsequently initiating apoptosis (Hsu et al., 1996). However, TNFR1 generally only signals for apoptosis when protein synthesis is blocked (Ashkenazi and Dixit, 1998). Unlike TNFR1, Fas via FasL engagement, only signals for apoptosis via the recruitment of FADD (Ashkenazi and Dixit, 1998). Thus TNFRSF members are capable of initiating a range of responses from apoptosis to cellular proliferation and differentiation.

### 1.1.3 Knockout and Transgenic Models

Gene knockout and transgenic models of the TNFRSF and their ligands have provided useful insight into the non-redundant biological effects of these molecules and in assessing their role in disease. The characteristics of those models which have most relevance to this thesis will now be described.

#### 1.1.3.1 TNFR1/TNFα

TNFR1 is a ubiquitously expressed receptor which binds both TNFα and LTα. Its principle functions are however, generally ascribed to its association with TNFα and it is this interaction that will be considered. TNFR1 deficient mice are viable and develop into adulthood. They display both normal thymopoiesis and spleen and lymph node anatomy (Peschon et al., 1998). Cell numbers within the thymus, spleen, lymph nodes and bone marrow are also normal and the removal of autoreactive T cells from the thymus is not impaired (Pfeffer et al., 1993). However, when infected with the bacteria *listeria monocytogenes* at a sublethal dose, TNFR1 deficient mice do not survive (Peschon et al., 1998). Additionally, they display a reduced accumulation of neutrophils within the lungs following inhalation of inflammatory agents (Peschon et al., 1998). TNFR1 deficient mice do however display resistance to endotoxic shock (Pfeffer et al., 1993).

In addition to TNFR1$^{-/-}$ mice, transgenic mice which constitutively expressive the human TNFα gene have also been generated. Similar to the TNFR1 deficient animals, TNFα transgenics develop normally and survive into adulthood. However, an ankle swelling and impaired movement phenotype is evident in these mice with 100% penetrance and progressive weight loss is also a common feature. Histopathological analysis of the joints from these animals shows consistence with arthritic disease with evidence of synovial hyperplasia and joint destruction. These features are all completely prevented via treatment with anti-TNF agents (Keffer et al., 1991).

#### 1.1.3.2 FAS

Both genetically engineered and naturally occurring FAS deficient mice exist. Lpr (lymphoproliferation) mutants contain a mutation within the FAS gene rendering it non-functional. Naturally occurring FASL mice also exist which have inactive FASL and these are termed gld (generalised lymphoproliferative disease) mice (Roths et al., 1984). All of these mice are characterised by lymphadenopathy and splenomegaly (Adachi et al., 1995). Genetically engineered Fas deficient animals develop lymphadenopathy and splenomegaly by 8 weeks of age and this is mainly attributed to the accumulation of T lymphocytes (Adachi et al., 1995). Hyperplasia of the liver is also present but thymus size and composition is normal (Adachi et al., 1995). Lpr mutants are also characterised by autoimmune diseases including synovitis, pulmonary vasculitis and a syndrome similar to systemic lupus erythematosus. High levels of autoantibody production are also seen. Additionally they display a proliferative glomerulonephritis which may account for the 50% mortality at 5 months of age (Cohen and Eisenberg, 1991). Gld mice similarly display autoimmunity and a reduced lifespan (Cohen and Eisenberg, 1991).

#### 1.1.3.3 RANK

Mice which are genetically deficient in RANK display a bone phenotype which is characterised by runted growth, an absence of tooth eruption and severe osteopetrosis (Dougall et al., 2008). Histological analysis revealed an absence of osteoclasts within the bone, and spleen cells from these animals cultured *in vitro* in the presence of RANKL and M-CSF fail to undergo osteoclastogenesis (Dougall et al.,

2008). Thymus development is normal, however splenomegaly is evident and there is an absence of lymph nodes (Dougall et al., 2008).

#### 1.1.3.4 OPG

OPG deficient mice develop normally from the embryonic stage, however they display an osteoporotic phenotype. Decreased bone mineral density is evident by 1 month of age with the occurrence of multiple fractures. Gross morphological abnormalities are present in older mice. An increase in numbers of both osteoclasts and osteoblasts has been noted by researchers, indicating a high bone turnover state which is consistent with osteoporosis (Bucay et al., 1998).

## 1.2 Death Receptor 3

Death receptor 3 is member 25 of the TNFRSF and like other members of the family is capable of bringing about a wide range of responses from apoptosis to proliferation. It is the study of this receptor that forms the principle component of this thesis.

### 1.2.1 Human DR3

The human Death Receptor 3 (Wsl-1, APO-3, TRAMP, LARD, TR3, TNFRSF25) gene was originally cloned in 1996. Multiple research groups identified the gene at the same time resulting in its various names (Chinnaiyan et al., 1996, Kitson et al., 1996, Screaton et al., 1997, Marsters et al., 1996, Bodmer et al., 1997). The discovery of DR3 was principally achieved through searching expressed sequence tag (EST)

databases for genes with homology to TNFR1 or FAS (Bodmer et al., 1997, Chinnaiyan et al., 1996, Marsters et al., 1996, Screaton et al., 1997). Kitson et al. (1996), however, used a combination of a yeast two-hybrid system, utilizing the death domain of TNFR1, and PCR to identify the gene (Kitson et al., 1996). The chromosomal location of human DR3 was assigned to chromosome 1p36.2 via fluorescence in situ hybridization (FISH) (Bodmer et al., 1997). It is currently entered into the NCBI database as TNFRSF25 and comprises 1665 base pairs. It has a genomic structure of 10 exons, 6 of which are leader sequence and extracellular domain, 1 is transmembrane domain and the remaining 3 make up the cytoplasmic domain (Screaton et al., 1997).

DR3, like other members of the receptor superfamily, is a type I transmembrane protein. The originally discovered DR3 gene was predicted to contain 417 amino acids (Screaton et al., 1997) maintaining a high level of sequence homology with TNFR1, displaying 28% overall sequence identity, rising to 45% in the death domain (Kitson et al., 1996). Analysis of the hydrophobicity profile of the protein indicated the existence of a signal sequence, followed by an extracellular domain containing the characteristic cysteine-rich repeats of which there were 4, a transmembrane domain and a cytoplasmic portion comprising the death domain (Marsters et al., 1996). Two potential N-linked glycosylation sites were also identified (Screaton et al., 1997).

### 1.2.2 Murine DR3

The murine DR3 gene was cloned in 2001 by Wang et al. By screening a 129Sv mouse genomic library using the full length human DR3 gene, they isolated and sequenced a single clone of the gene. RT-PCR of mouse thymic cDNA was used to determine the intron:exon boundaries (Wang et al., 2001a). Murine DR3 was found to be 55% homologous to the human DR3 gene. It comprises 1619 base pairs and like human DR3 is composed of 10 exons (Wang et al., 2001a).

The murine DR3 protein is 63% homologous to its human counterpart with conservation of 52% sequence identity in the extracellular domain and 94% in the death domain (Wang et al., 2001a). Like human DR3, it contains 2 putative N-glycosylation sites and 25 of the 28 cysteines found in the human gene are present. The 3$^{rd}$ cysteine rich domain in murine DR3, however, was found to differ significantly from that in the human gene. In the 2$^{nd}$ half of this region, 2 cysteine residues present in human DR3, are absent due to a 9 amino acid deletion. Additionally, 2 amino acid substitutions are present, with the replacement of a cysteine and a phenylalanine with threonine and a cysteine respectively. These differences are not predicted to alter ligand binding properties compared to the human gene, as the first half of the 3$^{rd}$ cysteine-rich region is essentially conserved between the 2 genes and it is this region, along with cysteine-rich domain II that are involved in ligand interactions (Wang et al., 2001a).

### 1.2.3 Expression

Northern blot analysis of human DR3 transcript expression originally indicated a restricted expression pattern. Transcripts of 3.4 - 4Kb were identified in spleen, thymus and peripheral blood leukocytes (Kitson et al., 1996, Screaton et al., 1997) leading researchers to believe that DR3 was the first member of the TNFRSF with lymphoid-organ restricted expression. However, further analysis identified DR3 transcript expression in the colon and small intestine in addition to fetal lung, brain and kidney (Marsters et al., 1996, Chinnaiyan et al., 1996, Bodmer et al., 1997). Expression of murine DR3 by Northern blot analysis revealed signals in the brain, heart, kidney, spleen, liver, thymus and skin with transcripts ranging in size from 1.8 – 7Kb, which was thought to result from the presence of untranslated sequence at the 5' end (Wang et al., 2001a).

Both human and murine DR3 have multiple splice variants, further complicating its pattern of expression. There are at least 13 human DR3 splice variants (Screaton et al., 1997, Warzocha et al., 1998), and 3 murine DR3 splice variants (Wang et al., 2001a). The majority of the human DR3 splice variants produce truncated forms of the receptor, with a stop codon introduced before the trans-membrane domain (Screaton et al., 1997). In most cases this is achieved by the removal of 1 or more complete exons although 2 of the splice variants (-2 and -10) contain 101 and 200 base pair insertions respectively and splice variant -1b contains an additional 3 nucleotides (CAG) (Screaton et al., 1997). The 13$^{th}$ variant was discovered later and was originally named DR3β. This is the longest of the variants containing 2 insertions of 20 and 7 bases at position 612 and 667 respectively, generating a 426 amino acid protein compared to 417 amino acids of the second longest isoform

(variant 1) (Warzocha et al., 1998). These 2 proteins are identical apart from 28 amino acids in the extracellular domain and DR3β expression is more restricted (Warzocha et al., 1998). Interestingly, both T and B cells were found to predominantly express the truncated isoforms. However, following PHA blasting, variant 1 expression predominates (Screaton et al., 1997). Western blot analysis has revealed proteins ranging in size from 47 KDa to 59 KDa which may result from differing degrees of glycosylation (Marsters et al., 1996, Kitson et al., 1996, Bodmer et al., 1997).

Murine DR3 has 3 identified splice variants (Wang et al., 2001a), the longest of which encodes a 55 KDa protein. Variant 2 is a soluble form of the receptor in which exon 6 is absent, result in a stop site prior to the trans-membrane domain. Variant 3 lacks both exon 5 and exon 6 resulting in the absence of cysteine-rich domain 4 (Wang et al., 2001a).

### 1.2.4 Signalling

DR3 shares a similar signalling pathway to that of TNFR1. Chinnaiyan et al. (1996) investigated the signalling pathway of DR3 by studying the interactions of a glutathione-S-transferase (GST) -DR3 fusion protein with GST fusion proteins of TRADD, FADD and RIP. DR3 was found to specifically associate with TRADD but not with FADD or RIP. However, when DR3 was expressed in 293 cells in the presence of TRADD, there was an enhanced association with RIP, FADD and TRAF2 (Chinnaiyan et al., 1996). Through the recruitment of these signalling molecules, DR3 is able to initiate both apoptosis and NFκB activation. Overexpression of DR3 in 293 cells

resulted in apoptosis, with cells displaying the associated characteristic morphology (Kitson et al., 1996, Bodmer et al., 1997, Chinnaiyan et al., 1996). Expression of a truncated form of the gene, lacking the death domain, did not result in apoptosis (Kitson et al., 1996). This DR3 mediated apoptosis could also be prevented by the use of 2 inhibitors of the ICE-like proteases and through the presence of dominant negative forms of FADD (Chinnaiyan et al., 1996). Therefore, DR3 is capable of signalling for apoptosis via the recruitment of TRADD, FADD and TRAF2, mirroring those pathways utilised by TNFR1. Although the signalling pathways employed by both TNFR1 and DR3 appear very similar, there have been reports of divergent downstream signalling pathways, notably in the regulation of IL-8 expression where separate kinase cascades are thought to be utilised (Su et al., 2006).

DR3 expression has also been shown to induce NFκB activation. In an NFκB luciferase reporter gene assay, DR3 expression dose-dependently induced reporter gene activity (Bodmer et al., 1997). In the presence of dominant negative forms of the signalling molecules RIP and TRAF2 but not FADD, NFκB activation was blocked (Chinnaiyan et al., 1996). The signalling pathways employed by DR3 are shown in figure 1.2.

In an attempt to clarify the effects of DR3 signalling in more physiologically relevant systems Wen et al (2003) tested the effect of adding the natural DR3 ligand, TL1A, to cultures of the erythroleukaemic cell line TF-1. TL1A stimulation preferentially caused the formation of a TRADD, TRAF-2 and RIP signalling complex rather than one containing FADD or procaspase 8 (Wen et al., 2003). NFκB activation was

detected in addition to the induction of other downstream signalling molecules including JNK, p38 and ERK1,2 MAPK, resulting in gene expression (Wen et al., 2003). Apoptosis could only be initiated following blockade of NFκB signalling which was hypothesised to be due to NFκB-induced expression of the anti-apoptotic factor c-IAP2 (Wen et al., 2003). Thus DR3 may be capable of initiating both cell survival and cell death mechanisms but this is likely to be due to the environment in which DR3 is expressed.

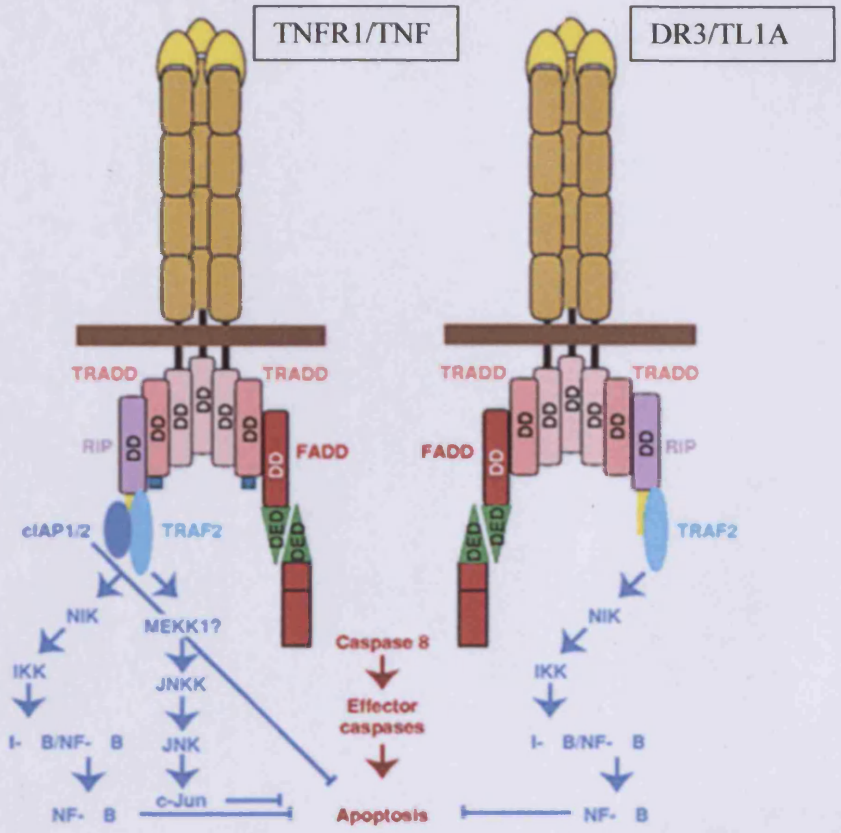


**Figure 1.2. Signalling via DR3 and TL1A**. Like TNFR1, DR3 initiates downstream effects via the recruitment of TRADD, FADD and TRAF2. Reproduced from (Ashkenazi and Dixit, 1998)

### 1.2.5 The DR3 Ligand

Identification of a ligand for DR3 has proven difficult and multiple candidates have been suggested. The first proposed ligand for DR3 was Apo3L. This ligand was identified through expressed sequence tag database searching. Northern blot analysis revealed a broad pattern of expression with positive detection in human blood, gut, reproductive organs, thymus, spleen, pancreas, kidney, liver, lung, brain and heart (Marsters et al., 1998). This ligand was shown to induce apoptosis through a FADD mediated signalling pathway and was capable of activating NFκB. Using a FLAG-epitope tagged version of the ligand, Apo3L was shown to specifically bind DR3 but not TNFR1, TNFR2, FAS or DR4 (Marsters et al., 1996). However, in 2000, Kaptein et al. published the first report suggesting that Apo3L, which is also named TWEAK, was not the true ligand for DR3. In this study, DR3 did not bind a whole panel of TNF family ligands including FASL, RANKL and TWEAK using an ELISA based assay. Additionally, cells which were transfected with a DR3 expression vector resulting in both NFκB and apoptosis induction, were not affected by the addition of TWEAK nor were there any differences in the ability of TWEAK to bind peripheral blood lymphocytes from DR3 deficient and sufficient mice (Kaptein et al., 2000). Thus Apo3L/TWEAK could no longer be considered the ligand for DR3. In 2002, TNF-like protein 1A (TL1A) was discovered and this is the currently accepted ligand for DR3. TL1A was identified by searching expressed sequence tag sequences and was discovered to be a longer variant of the already cloned vascular endothelial growth inhibitor (VEGI) (Migone et al., 2002). It is produced as a membrane bound protein which is also capable of generation into a soluble form (Kim and Zhang, 2005). Analysis of mRNA expression of this protein is not reported to be as broad as

that of TWEAK, being predominantly detected on endothelial cells although low levels have also be seen in the human kidney, placenta, stomach, intestine, lung, spleen and thymus (Migone et al., 2002). TL1A was found to specifically bind to Fc-fusion proteins of DR3 and DcR3, a human decoy receptor, but not to any other TNFRSF members. This was further established by coimmunoprecipitation studies (Migone et al., 2002) and has more recently been confirmed in an extensive evaluation of the interations between ligands and receptors belonging to the TNF superfamily (Bossen et al., 2006). An equivalent protein to the DcR3 found in humans has yet to be identified in the mouse.

TL1A has been described as a T cell co-stimulator, increasing T cell responsiveness to IL-2 and inducing secretion of other cytokines including IFNγ and GM-CSF (Migone et al., 2002). Additionally it has been shown to be expressed on monocytes and dendritic cells following FcγR stimulation (Prehn et al., 2007). TL1A also has a reported role in the upregulation of OX40L on a novel subset of cells akin to $CD4^+CD3^-$ cells found in fetal lymphoid tissue (Kim et al., 2006). These cells are thought to play a role in the generation of antibody responses to protein antigens and have been localised to B cell areas and the B cell : T cell interface, where they interact with antigen-specific T cells within the spleen. They have been shown to upregulate their expression of 2 TNF family ligands, namely CD30L and OX40L in culture, and their interaction with OX40 on $CD4^+$ T cells, enhances survival of these T cells. *In vivo* studies have suggested that this signalling through OX40 on T cells is imperative for maintaining T cell memory and antibody responses (Kim et al., 2003). DR3 is expressed on both adult and neonatal $CD4^+CD3^-$ cells (Kim et al., 2006). The

addition of TL1A to these cells is reported to upregulate OX40L expression (Kim et al., 2006), implicating a role for TL1A via DR3 signalling in antibody responses.

### 1.2.6 DR3 knockout ($DR3^{-/-}$) mouse model

Mice deficient in DR3 were generated by Wang et al. in 2001. In order to generate these mice, the entire coding region of the DR3 gene was replaced with a construct containing an internal ribosomal entry site (iRES), the β galactosidase (LacZ) gene and the neo gene flanked by 2 lox P sites. By replacing the entire coding region, no DR3 protein, including any splice variants could be expressed. Instead, β galactosidase expression in the $DR3^{-/-}$ mice would act as a useful tool for reporting wild-type DR3 expression. Embryonic stem cells containing the targeting construct were used to generate heterozygous mice on a C57BL/6 background, which could then be bred for the generation of DR3 null animals (Wang et al., 2001b).

Characterisation of the $DR3^{-/-}$ mice revealed normal development in all of the major organs including the brain, heart, kidney, thymus, spleen, lymph nodes and peyer's patches (Wang et al., 2001b). An increased thymus size compared to the $DR3^{+/-}$ mice was reported with 10% larger thymuses in $DR3^{-/-}$ animals at 2 to 5 weeks of age. Using bromodeoxyuridine (BrdU), which is incorporated into proliferating cells, this was shown not to be due to thymocyte turnover, as thymocytes from both $DR3^{+/-}$ and $DR3^{-/-}$ mice did not differ significantly in BrdU incorporation (Wang et al., 2001b). As a result of this observation, DR3 was shown to have a regulatory role in thymocyte development with impaired negative selection in $DR3^{-/-}$, H-Y transgenic mice. Additionally, cross-linking of CD3 on thymocytes using low concentrations of

antibody, resulted in reduced apoptosis in $DR3^{-/-}$ mice compared to $DR3^{+/-}$ mice (Wang et al., 2001b). Despite this role in negative selection during thymocyte development, $DR3^{-/-}$ mice do not show signs of autoimmunity.

### 1.2.7 *In vivo* Functions of DR3

The *in vivo* functions of DR3 have yet to be fully elucidated and similar to other TNFRSF members, are likely to be extremely diverse. DR3 is capable of initiating both cell death and cell survival signals through the activation of caspases and NFκB respectively (Chinnaiyan et al., 1996) but what the significance is of this in disease is poorly understood. $DR3^{-/-}$ mice do progress normally into adulthood and do not show signs of spontaneous disease development. However, data is beginning to emerge which suggests that DR3 might play an important role in a number of diseases including cancer, neurological and inflammatory disease states.

#### 1.2.7.1 DR3 and Cancer

DR3 expression has been identified in non-Hodgkin's lymphoma (Warzocha et al., 1998) and colon carcinoma patient samples (Gout et al., 2006). In colon cancer, it has been proposed that DR3 contributes to cancer metastasis through interactions with the endothelial adhesion receptor, E-selectin. This interaction may trigger pro-survival and pro-migratory signals via the activation of protein kinases (Gout et al., 2006). However, an analysis of E-selectin ligands expressed on G-CSF mobilized peripheral blood leukocytes did not identify DR3 as a novel ligand (Dagia et al., 2006) thus this requires further investigation. Researchers studying the role of DR3 in neuroblastoma have reported the presence of a DR3 gene duplication which is

tandemly linked to the DR3 gene on chromosome 1p36.2-1p36.3 and both of which are either deleted or translocated in certain neuroblastoma cell lines. In addition, low DR3 protein expression has been reported in 7 of 17 neuroblastoma cell lines (Grenet et al., 1998). Thus DR3 has been linked to a number of cancer types but its role in cancer development is unclear and complicated by duplications in the DR3 gene.

#### 1.2.7.2 DR3 and Inflammatory Diseases

An important role for DR3 in inflammatory disease states is beginning to emerge with links being made with inflammatory bowel disease (IBD) (Bamias et al., 2003, Bamias et al., 2006), Rheumatoid Arthritis (Osawa et al., 2004, Takami et al., 2006, Cassatella et al., 2007), atherosclerosis (Kang et al., 2005, Kim et al., 2008), allergic lung inflammation (Fang et al., 2008) and in renal inflammation (Al-Lamki et al., 2008). Following the identification of TL1A as a T cell co-stimulator capable of inducing the expression of IFNγ (Migone et al., 2002), Bamias et al (2003) sought to investigate the role of DR3/TL1A in inflammatory bowel disease which is typically described as a Th1-mediated disease. Via analysis of samples from Crohn's disease and ulcerative colitis patients, the authors reported an upregulation of TL1A protein expression in association with the degree of inflammation observed. This expression was associated with both $CD4^+$ and $CD8^+$ T cells in addition to tissue macrophages in Crohn's disease patients but appeared to be expressed on plasma cells in ulcerative colitis. Additionally, DR3 expression was upregulated in both disease states and was localised to $CD4^+$ and $CD8^+$ lymphocytes in inflamed areas (Bamias et al., 2003). When lamina propria mononuclear cells were incubated with

TL1A, an upregulation of IFNγ was detected which was more pronounced when cells were isolated from Crohn's disease patients rather than controls (Bamias et al., 2003). DR3 and TL1A upregulation has also been confirmed in mouse models of Crohn's disease (Bamias et al., 2006). By examining DR3 expression in the terminal ileum of mice in a model of chronic ileitis, a specific upregulation of full length DR3 expression as opposed to other DR3 splice variants was observed (Bamias et al., 2006). This upregulation of the full length DR3 splice variant was also illustrated upon T cell activation and may represent a control mechanism for DR3 signalling under normal physiological conditions. In the murine model of chronic ileitis, TL1A expression appeared to be restricted to lamina propria dendritic cells (Bamias et al., 2006). Upregulation of IFNγ by TL1A occurs in synergy with IL-12 and IL-18 stimulation in $CD4^+$ T cells, $CD8^+$ T cells and NK cells (Papadakis et al., 2004). A specific subset of T cells which are located in the lamina propria of the small intestine and are associated with IBD is a $CCR9^+$ memory T cell subset. TL1A addition to these cells enhanced IFNγ production following activation via CD3 and CD28 or CD2 and CD28 (Papadakis et al., 2005). IFNγ production following TL1A administration was further enhanced when $CCR9^+$ T cells were stimulated with IL-12 and IL-18 and this was associated with upregulation of DR3 expression specifically on this cell subset (Papadakis et al., 2005). Thus the DR3/TL1A pathway may play a prominent role in the pathogenesis of IBD via its ability to enhance IFNγ in synergy with IL-12 and IL-18 thus contributing to the inflammatory response.

In atherosclerosis, DR3 and TL1A expression has been reported in foam cell-rich regions of atherosclerotic plaques obtained from patients (Kim et al., 2008). Foam

cells are derived from macrophages thus researchers have used the human monocytic THP-1 cell line as a model. Activation of the DR3 receptor on THP-1 cells via cross-linking with an immobilized antibody, in conjunction with IFN treatment resulted in the induction of TNFα, MCP-1 and IL-8 (Kang et al., 2005). Similar experiments have also shown that DR3 activation in THP-1 cells can induce the release of MMP-1, MMP-9 and MMP-13 which are proposed to contribute to the destabilization of the atherosclerotic plaques (Kim et al., 2001). Treatment of THP-1 cells with TL1A also stimulated MMP-9 expression (Kang et al., 2005). Therefore, DR3 and TL1A appear to have an important role in the pathogenesis of atherosclerosis.

DR3 has also recently been linked with the inflammatory joint disease Rheumatoid Arthritis (RA) and much of the focus of this thesis will concentrate on this relationship. Prior to reviewing the current literature concerning the role of DR3 in RA, some background theory of the disease and the pathological joint changes with which it is associated will now be discussed.

### 1.3 The Normal Synovial Joint

In order to appreciate the pathological changes associated with RA, it is important to understand the anatomy and physiology of a normal synovial joint. The synovial joints (diarthrodial) are the most common joints in the human body, classified both by their ability to move and their encapsulation in a joint cavity lined with synovial tissue. These joints are capable of a wide range of movements and have 4 common features: synovial capsule; synovial membrane; articular cartilage and synovial fluid.

Under normal physiological conditions, these function to produce a smooth frictionless movement (Wooley et al., 2005).

### 1.3.1 The Synovial Capsule

The outer layer of the synovial capsule is composed of dense connective tissue which provides support and stability to the joint (Ralphs and Benjamin, 1994). Ligaments form a component of this connective tissue, connecting 2 bones together and limiting the extent of joint motion. The inner layer of the synovial capsule is the synovial membrane.

### 1.3.2 The Synovium

The synovial membrane consists of 2 distinct layers, namely the intimal lining layer and the synovial sublining, which function both to provide nutritional support to the joint and to generate the synovial fluid necessary for smooth joint movements (Wooley et al., 2005). Under normal conditions, the intimal lining layer is only 1-2 cells thick. It is generally accepted that this intimal lining layer is composed of 2 principle cell types: Type A synoviocytes and type B synoviocytes (Iwanaga et al., 2000). Type A synoviocytes, which are also termed macrophage-like synoviocytes, may function to absorb material from within the joint such as cell debris, bacteria and antigens (Iwanaga et al., 2000). Type B synoviocytes, also known as fibroblast-like synoviocytes, function to secrete a number of factors into the synovial fluid including cytokines, matrix metalloproteinases (MMPs), hyaluronan and proteoglycans (Knedla et al., 2007). The synovial sublining is relatively acellular, consisting principally of blood vessels, fat cells and fibroblasts (Smith et al., 2003).

The synovium has 3 membrane types: Areolar; adipose and fibrous. Areolar tissue has a folded surface with projections which are often termed synovial villi. Here the intimal lining layer is relatively thick. The adipose tissue has a single cell thick intimal layer and finally, the fibrous tissue contains a thin intimal layer in direct contact with dense collagenous tissue (Iwanaga et al., 2000).

### 1.3.3 Articular Cartilage

Articular cartilage is a mesenchymal tissue which overlies subchondral bone, functioning to provide smooth, low resistance surfaces within the joint that are capable of withstanding compression (Saxne and Bengt, 2000). The extracellular matrix of articular cartilage is organised into 4 layers namely the superficial, intermediate, deep and calcified layers (Eyre, 2002) which comprise collagens, proteoglycans and the sole cell type of articular cartilage, the chondrocyte (Hall et al., 1996). Collagen is an exceptionally strong structure due to its extensive network of cross-linking fibres. However, if it becomes disrupted or damaged it is not capable of efficient repair. The principle collagens of articular cartilage are types II, IX and XI (Eyre, 2002). The principle proteoglycan of articular cartilage is aggrecan. Other minor proteoglycans such as decorin and fibromodulin are also present within articular cartilage (Roughley, 2001). Chondrocytes are the only cell type present within articular cartilage and are capable of both the synthesis and the degradation of all the components of cartilage (Saxne and Bengt, 2000). The relative composition of the different components of cartilage varies throughout the layers. The superficial layers are relatively acellular and chondrocytes display a flattened shape lying in parallel with the surface. Within this layer, collagen fibres

run in parallel with the surface. Conversely, in the deep layers, chondrocytes are quite abundant and display more of a rounded shape, with collagen fibres adopting a more vertical orientation (Saxne and Bengt, 2000). The properties of each of the components of articular cartilage enable its efficient functioning throughout the majority of an individual's life, providing that its physiological state is not compromised. However, cartilage is susceptible to degradation by multiple proteases that can be produced by chondrocytes and synovial fibroblasts during states of inflammation. Of these proteases, the matrix metalloproteases (MMPs) and the ADAMTSs (a disintegrin and a metalloprotease with thrombospondin motifs) are responsible for the degradation of collagen and aggrecan respectively (Mort and Billington, 2001).

### 1.3.4 Bone

Bone is a vital structure in the human body serving as a support frame, providing a protective shield for internal organs, generating blood cells and acting as a store for minerals and ions. It is a dynamic structure which is constantly undergoing a highly coordinated and complex remodeling process with approximately 10% of total bone content of adults being replaced per year (Takayanagi, 2007). Bone contains 2 principle cell types namely the osteoblast and the osteoclast. Osteoblasts are bone forming cells of mesenchymal origin which are capable of secreting bone matrix proteins and of promoting bone mineralization (Harada and Rodan, 2003). Osteoclasts are the only cells capable of resorbing bone, specifically functioning to dissolve the crystalline hydroxyapatite of bone via hydrochloric acid secretion and to degrade the organic bone matrix through the release of enzymes (Schett, 2007).

### 1.3.5 Physiological Bone Remodelling

Physiological bone remodelling (depicted in figure 1.3) can be divided into 5 stages (Fernandez-Tresguerres-Hernandez-Gil et al., 2006). During the quiescent phase, no processes of bone remodelling are occurring. The first processes occur during the activation phase when bone lining cells retract and the mineralized bone surface is exposed through the action of collagenases. Osteoclast precursors are subsequently recruited to the site and differentiate into functional osteoclasts, permitting the degradation of the mineralized matrix. This is termed the resorption phase. Pre-osteoblasts then generate a cementing substance during the formation phase which enables the attachment of new osteoid material generated by osteoblasts within a few days. Finally, the material becomes mineralized to form new bone during the mineralization phase (Fernandez-Tresguerres-Hernandez-Gil et al., 2006).

### 1.3.6 Osteoclasts

Osteoclasts are terminally differentiated cells derived from pluripotent hematopoietic stem cells and are considered to be of the monocyte-macrophage lineage. Osteoclasts can be recognized by their multinuclear appearance and characteristic expression of tartrate resistant acid phosphatase (TRAP) and calcitonin receptor (Fujikawa et al., 1996). *In vitro* studies have illustrated that multiple cell types have the capacity to differentiate into osteoclasts when provided with the right signals and that ascertaining the stage at which a precursor cell is committed to becoming an osteoclast has proven difficult to establish. The earliest osteoclast precursor is reported to be the colony forming unit-granulocyte

macrophage (Kurihara et al., 1990). Husheem et al (2005) have shown that purified monocytes from human peripheral blood mononuclear cells can differentiate into osteoclasts when cultured on bovine bone cultures in the presence of RANKL, M-CSF, TNFα and dexamethasone. Furthermore, the authors illustrated that various subpopulations of monocytes had differing capacities to differentiate, with osteoclast formation being 90, 30 and 20 times higher in $CD14^+$, $CD11b^+$ and $CD61^+$ purified monocyte cell cultures respectively when compared to controls (Husheem et al., 2005). $F4/80^+$ macrophages have also been shown to have the capacity to differentiate into functional osteoclasts. By culturing murine bone marrow cells with the viral supernantant from cells infected with a RANKL expressing retroviral vector, Lean and colleagues were able to generate multinucleated osteoclasts from mononuclear cells that strongly expressed the macrophage marker F4/80 (Lean et al., 2000).

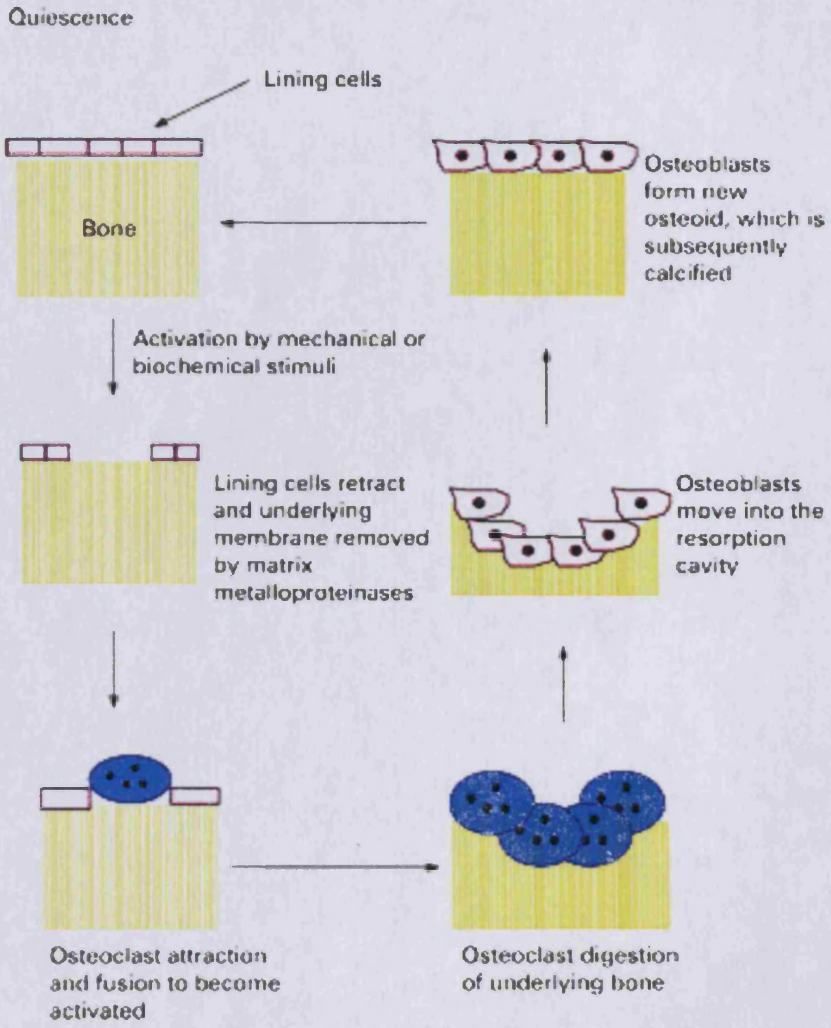


**Figure 1.3. Physiological bone remodelling**. The cycle of bone removal and replacement via the action of osteoclasts and osteoblasts. Reproduced from (Datta et al., 2008)

The process of osteoclast differentiation from osteoclast precursor cells has been well documented. Early *in vitro* studies using co-cultures of murine spleen cells and osteoblasts in the presence of 1 alpha-dihydroxyvitamin D3 revealed that in order to develop functional bone resorbing osteoclasts, the presence of osteoblasts is essential (Takahashi et al., 1988). Using the murine osteopetrotic *op/op* model, it was further determined that the osteoblast/stromal cell derived factor macrophage colony-stimulating factor (M-CSF), through binding its receptor c-Fms, is central to osteoclast differentiation. *Op/op* mice are unable to generate functional M-CSF and therefore suffer from impaired bone resorption which can be recovered by the administration of recombinant M-CSF (Felix et al., 1990). Osteoblasts were determined to play a further role in the development of osteoclasts following the discovery of osteoprotegerin (OPG) and consequently osteoprotegerin ligand (OPGL) more commonly termed receptor activator of NFκB ligand (RANKL). In 1997, OPG was identified as a TNFRSF member, which is expressed as a secreted protein with mRNA transcripts detected within the bone of a 15 day old mouse embryo (Simonet et al., 1997). Transgenic mice expressing rat OPG developed an osteopetrotic phenotype and OPG administration in *in vitro* spleen cell cultures was capable of inhibiting osteoclastogenesis. Furthermore, the authors illustrated that administration of OPG to normal mice resulted in an excess accumulation of bone and cartilage indicating that OPG acts as a circulating factor which inhibits the bone resorbing properties of osteoclasts (Simonet et al., 1997). Investigators speculated from this study that OPG might be a receptor for a ligand molecule that had the capability of directing osteoclastogenesis and in 1998 such a ligand, named OPGL was identified. OPGL was found to be a member of the type II membrane bound

TNF family of cytokines and was discovered by screening various cell lines with an OPG-Fc fusion protein. The identified protein was found to be identical to 2 previously reported proteins TRANCE (Wong et al., 1999) and RANKL (Anderson et al., 1997) and occurred in both membrane bound and soluble forms, both interacting specifically with OPG (Lacey et al., 1998). In *in vitro* cultures of stromal cells and osteoclast precursors, OPGL treatment was capable of enhancing osteoclastogenesis and acted synergistically with M-CSF to produce functional bone resorbing osteoclasts (Lacey et al., 1998). Cell binding studies using a fluorescein conjugated OPGL revealed that OPGL binds directly to osteoclast precursors in order to promote osteoclastogenesis. When OPGL was injected directly into mice, a reduction in bone volume in the proximal tibia was reported. Interestingly, osteoclast numbers in these mice were not different to those of controls but the size and multinuclearity of osteoclasts was significantly greater (Lacey et al., 1998). The receptor for OPGL or RANKL as it will now be termed is RANK. RANK was originally described in dendritic cells, along with its ligand RANKL, as having a role in T-cell proliferation following dendritic cell interaction (Anderson et al., 1997). It was subsequently found to be expressed by osteoclast precursor cells and through binding RANKL, could initiate osteoclastogenesis (Hsu et al., 1999). Taken together, this data has resulted in the generation of the current model of osteoclast differentiation and is depicted in figure 1.4. Osteoclast precursors from the bone marrow are mobilized and recruited to sites where bone turnover is occurring. Here, precursor cells receive signals from osteoblasts via interaction of RANKL, expressed on the osteoblast and its receptor RANK, expressed on the osteoclast precursor cell to differentiate into osteoclasts. Additionally, osteoblasts and stromal

cells secrete M-CSF to enhance osteoclast differentiation. The soluble receptor OPG competes with RANK for RANKL binding thus acting as an osteoclast differentiation control mechanism. Although this is a heavily simplified model which does not take into account the effects of other factors, such as cytokines, it highlights the crucial factors involved in osteoclast differentiation.

Following osteoclast differentiation, the mature osteoclast is capable of active bone resorption. During this process, an osteoclast displays 4 distinct membrane domains as a result of polarization of the cell and reorganization of microtubules and microfilaments. The sealing zone attaches to the bone matrix and the ruffled border membrane forms, representing the resorption organ. A functional secretory domain also forms within the basolateral membrane (Vaananen and Laitala-Leinonen, 2008). A vascular ATPase proton pump within the ruffled border membrane permits the release of hydrochloric acid from vesicles within the osteoclast into the resorption lacuna, ultimately resulting in the dissolution of bone (Schett, 2007). Additionally osteoclasts release matrix degrading enzymes such as matrix metalloproteinases and cathepsins which are capable of degrading molecules such as collagen. Normally this process occurs at sites where old bone is removed and replaced by new bone such as at the trabecular surface and within thin bone channels of cortical bone.

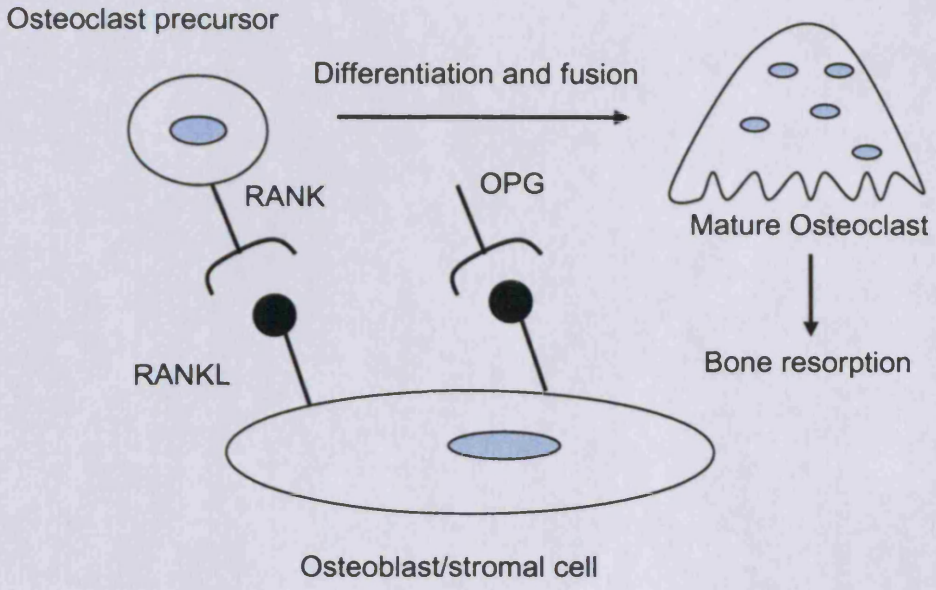


**Figure 1.4. The process of osteoclast differentiation.** Osteoclast precursor cells interact with osteoblasts/stromal cells via RANK/RANKL in order to drive differentiation into mature osteoclasts. Adapted from (Yasuda et al., 1998).

### 1.3.7 Osteoblasts

Osteoblasts are derived from mesenchymal stem cells in the bone marrow (Kassem et al., 2008). They are cuboid cells which resemble fibroblasts in morphology and which function to synthesise bone matrix proteins and enhance mineralization (Harada and Rodan, 2003). Their differentiation, like that of osteoclasts, is complex and highly coordinated involving numerous factors such as hormones and growth factors (Datta et al., 2008). Terminally differentiated osteoblasts that become encased within the matrix are termed osteocytes. These no longer function to generate new bone but are thought to play a role in sensing mechanical stress and regulating bone turnover (Datta et al., 2008).

## 1.4 Rheumatoid Arthritis – Historical origin

Rheumatoid Arthritis (RA) was first described in Europe by Landre-Beauvais in his doctoral thesis in 1800. He named the disease "primary aesthenic gout", listing it as a disease of people with a "feeble constitution" and described its characteristic features in a number of female patients. These features are recognisable today as RA and included swelling, pain, stiffness and distortion of the joints, recurrence of disease and its polyarticular nature (Landre-Beauvais, 2001). Prior to this description, there is little historical evidence of the disease. However, suggestions of it can be traced as far as ancient Egypt, although the precise origin of the disease is a matter for debate (Short, 1974). Following the Landre-Beauvais's description in 1800, RA was given its current name by Alfred Baring Garrod in 1859, differentiating it from rheumatism and rheumatic gout (Short, 1974). It is currently described as a systemic chronic inflammatory disease, typically characterised by inflammation,

pain and stiffness of the synovial joints (Majithia and Geraci, 2007). RA currently has a 1% worldwide prevalence and is more commonly suffered by women in a 3:1 ratio (Alamanos and Drosos, 2005). RA is an idiopathic autoimmune disease in which both auto-antibodies, such as rheumatoid factor, anti-collagen antibodies and anti-citrullinated antibodies, and auto-reactive T cells may play a role. Although the cause of RA is unknown, many theories have been proposed. Studies investigating a genetic cause of RA susceptibility identified alleles in the HLA-DRB1 locus as being responsible, at least in part, for the disease (Wordsworth et al., 1989). These are now known most commonly to be the HLA-DRB1*04 group of alleles which are identifiable by the existence of a shared epitope (QKRAA, GRRAA, RRRAA) in the 3$^{rd}$ hypervariable region of DRB1 (Orozco et al., 2006). In addition to a genetic component of the disease, environmental factors including the contraction of certain viruses and also several hormonal factors have been associated with the disease. However, it is likely that RA results from a combination of environmental and genetically predisposing factors.

### 1.4.1 Clinical Manifestations of Rheumatoid Arthritis

RA can affect both the small and large joints and is usually polyarticular. Those joints most commonly affected are the wrists, proximal interphalangeal (PIP) and metacarpophalangeal (MCP) joints of the hand (Rindfleisch and Muller, 2005). Extra-articular manifestations of disease may also be present such as the development of rheumatoid nodules and vasculitis (Akil and Amos, 1995). RA is diagnosed according to the criteria of the American Rheumatism Association (ARA). In 1987 the ARA revised the criteria for the classification of RA. Patients who met 4

of the 7 criteria indicated in table 1.2 are diagnosed as having RA. If left untreated, RA can affect an increasing number of joints resulting in damage, deformity and severe disability.

| Criterion | Definition |
|---|---|
| 1. Morning stiffness | Morning stiffness in and around the joints, lasting at least one hour before maximal improvement. |
| 2. Arthritis of 3 or more joint areas | At least 3 joint areas simultaneously have had soft tissue swelling or fluid observed by a physician. The 14 possible areas are right or left PIP, MCP, wrist, elbow, knee, ankle and MTP joints. |
| 3. Arthritis of hand joints | At least 1 area swollen in a wrist, MCP or PIP joint. |
| 4. Symmetric arthritis | Simultaneous involvement of the same joint areas on both sides of the body. |
| 5. Rheumatoid nodules | Subcutaneous nodules, over bony prominences, or extensor surfaces, or in juxtaarticular regions observed by a physician. |
| 6. Serum rheumatoid factor | Demonstration of abnormal amounts of serum rheumatoid factor by any method for which the result has been positive in <5% of normal control subjects. |

| | |
|---|---|
| 7. Radiographic changes | Radiographic changes typical of Rheumatoid Arthritis on posteroanterior hand and wrist radiographs, which must include erosions or unequivocal bony decalcification localised in or most marked adjacent to the involved joints (osteoarthritis changes alone do not qualify). |

**Table 1.2. The ARA 1987 Revised Criteria for the Classification of RA.**

PIP = proximal interphalangeal, MCP = metacarpophalageal, MTP = metatarsophalangeal
Reproduced from (Arnett et al., 1988)

### 1.4.2 The Rheumatoid Joint

Numerous characteristic pathological changes occur within the joints of RA patients, resulting in the clinical symptoms associated with the disease and the eventual destabilization and destruction of the joints. A diagram illustrating an RA joint compared to a normal joint is shown in figure 1.5.

#### 1.4.2.1 The Joint Capsule

Swelling is one of the earliest symptoms of RA and can be attributed to oedema and fibrin deposition occurring within the joints (Weinberg et al., 1991). This causes distention of the joint capsule resulting in pain. Ligament damage may also arise.

#### 1.4.2.2 The Synovium

Following oedema, the synovial lining layer proliferates, with both cell number and size increasing. The thickness of the synovium increases from 1-2 cells to 3-7 cells thick and displays an increased number of villi (Henderson et al., 1988). Endothelial cell swelling and vascular proliferation occurs resulting in an increase in the number of blood vessels present within the joint. Marked mononuclear cell infiltration is evident, displaying both a diffuse and nodular pattern and consisting primarily of neutrophils, lymphocytes, principally of the CD4+ memory cell phenotype with smaller numbers of CD8+ T cells, macrophages and plasma cells (Cush and Lipsky, 1988). Synovial fibroblast cells become invasive and form the pannus at the synovium-cartilage interface.

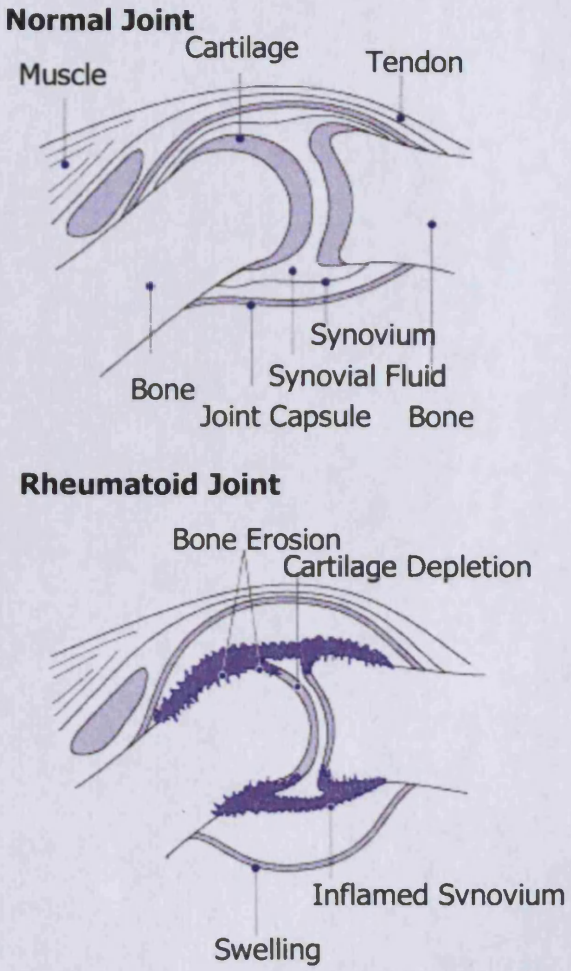


**Figure 1.5 Comparison of a normal and a rheumatoid joint.** Compared with a normal joint, the rheumatoid joint appears inflamed, displays synovial hyperplasia and develops bone erosion and cartilage depletion. Image modified from (National Institute of Health, 2004)

Although the trigger which results in the initial synovial infiltration is unclear, the importance of the infiltrating cells and the molecules they secrete is beginning to be understood and the central mediators of the disease are emerging. These are principally being revealed to be cytokines and more specifically interleukins and TNF superfamily members. TNFα and IL-1 are two such mediators. In 1988, Buchan et al. demonstrated that IL-1, TNFα and lymphotoxin mRNA levels were all elevated in monocytes cultured from rheumatoid synovial fluid and synovial membrane compared with control PBMC (Buchan et al., 1988). In 1989, Brennan et al. extracted and cultured mononuclear cells from rheumatoid synovium and found that TNFα was produced by all samples in the absence of external stimuli and that this could be blocked by anti-TNFα treatment but not by anti-lymphotoxin. IL-1 was also detected in the cultures and interestingly, anti-TNFα treatment was shown to significantly inhibit IL-1 activity (Brennan et al., 1989). Anti-TNFα treatment in rheumatoid synovial cultures has since been shown to reduce the production of other pro-inflammatory cytokines including IL-6, IL-8 and GM-CSF (Feldmann et al., 1996), which has led to the hypothesis that TNFα regulates a cytokine cascade within the rheumatoid joint, and that blocking its activity, and thus the activity of other pro-inflammatory cytokines, may alter the pathological outcome of the disease.

#### 1.4.2.3 Articular Cartilage

Destruction of articular cartilage results from both the physical invasiveness of the pannus and the generation of enzymes such as MMPs. Further invasion into tissues such as the menisci, undermine the physical integrity of the joint and causes

instability. Those mediators already considered central to the inflammation associated with RA are also likely culprits in the destruction of cartilage. TNFα has been shown to increase the expression of certain MMPs, the enzymes responsible for cartilage degradation. In 1985, Dayer et al. illustrated that the addition of TNFα to cultured synovial fibroblasts resulted in increased production of collagenase (Dayer et al., 1985). More specifically, treatment of cultured synovial fibroblasts with TNFα was shown to increase production of the active form of MMP-2, a gelatinase responsible for the degradation of types IV and V collagen (Migita et al., 1996). IL-1 has also been linked with cartilage degradation as monocytes taken from IL-1 deficient mice were noted to have impaired expression of MMPs -3 and -13 (Zwerina et al., 2007). Similarly, in the absence of IL-6, cartilage structure according to positive safranin-O staining, is preserved following antigen-induced arthritis, whereas in IL-$6^{+/+}$ mice, marked cartilage destruction has been noted (Ohshima et al., 1998).

#### 1.4.2.4 Bone

Bone erosion is present both at areas adjacent to and distant from pannus development in the rheumatoid joint resulting in deformity and disability (Goldring, 2003). The mechanisms of bone erosion in the joint arise from a disruption in the physiological balance between bone formation and destruction, through the bone-producing activity of osteoblasts and bone-resorbing activity of osteoclasts. A number of cytokines are reportedly involved in this process. Mice genetically designed to over-express TNFα develop severe bone erosions by 6-8 weeks of age (Zwerina et al., 2007). The mechanisms by which TNFα causes this are complex and

discussed in further detail in chapter 6. However, it should be mentioned that TNFα is proposed to induce osteoclastogenesis both directly, by increasing the size of the osteoclast precursor pool, and indirectly by inducing RANKL expression on synovial cells and osteoblasts to enhance osteoclast maturation (Boyce et al., 2005). In an attempt to uncouple the functions of TNFα and IL-1 in bone erosion, Zwerina et al. crossed mice genetically over-expressing TNFα (hTNFtg) with IL-1 deficient mice. These mice developed the characteristic synovial inflammation seen in hTNFtg mice but erosion of the bone was reduced by approximately 50%. This was attributed to a reduction in osteoclastogenesis and responsiveness of monocytes to RANKL but not to reduced osteoclast functionality (Zwerina et al., 2007). RANKL, via interaction with its receptor RANK on the surface of osteoclast precursor cells, is fundamental in the process of osteoclastogenesis. It is a member of the TNF family of cytokines and is normally produced by osteoblasts and stromal cells. Romas et al. investigated the expression of RANKL in the collagen-induced arthritis model using both in-situ hybridization in inflamed joints and by staining for the osteoclast specific markers TRAP and calcitonin receptor. Multinucleated TRAP positive cells were identified at all sites of focal bone erosion and these cells also stained positive for calcitonin receptor. Normal rat joints did not display any positive staining for these markers. RANKL mRNA expression was detected in all of the actively eroding joints, in most of the mononuclear cells contained in the synovial infiltrate and particularly at the point where bone and synovium form an interface. Osteoclasts and chondrocytes also expressed RANKL mRNA (Romas et al., 2000). Thus RANKL is highly expressed within the rheumatoid joint permitting the differentiation of osteoclasts and therefore the degradation of bone. The increased expression of RANKL may be

attributed to the aforementioned cytokines which are highly expressed within the rheumatoid joint. The role of the novel cytokine IL-17 in bone destruction has recently been of particular interest. Sato et al. used a co-culture system containing murine osteoblasts and bone marrow cells and illustrated that the addition of IL-17 producing Th17 cells resulted in the generation of TRAP+ cells. The addition of IL-17 in this co-culture system had the same effect. Addition of IL-17 was, however, unable to generate TRAP+ cells in a system containing bone marrow cells in the presence of RANKL and M-CSF, thus implying that IL-17 regulates osteoclastogenesis via an effect on osteoblasts (Sato et al., 2006). This has been supported in a separate study using an osteoblast and bone marrow co-culture system where IL-17 was only able to induce osteoclast formation when the osteoclast and bone marrow cells were in direct contact with each other (Kotake et al., 1999). Thus IL-17 may exert its effect on osteoclastogenesis via the positive regulation of RANKL expression on osteoblasts.

### 1.5 Experimental Models for Adverse Joint Pathologies

Both cell culture models and animal models of arthritis have been fundamental to furthering our understanding of the causes and pathological processes of RA. *In vitro* models have provided insight into the mediators involved in the processes of inflammation and joint destruction. Those cytokines which are currently considered centrally involved in these processes, such as TNFα and IL-1, were identified through synovial cell cultures (Buchan et al., 1988). Similarly, cultures of bone marrow cells with either osteoblasts or RANKL/M-CSF, have been used to study the process of osteoclastogenesis (Sato et al., 2006). *In vivo* models of RA are routinely

used to investigate the pathological changes occurring during RA. Numerous models exist in multiple species and a comparison of the 3 most commonly used murine models of the disease are shown in table 1.3. Each model has its own merits in terms of similarity with the human disease and ease of induction and replication in available strains of mice. The collagen-induced arthritis (CIA) model is often considered as the benchmark model for RA and has been used to assess the efficacy of novel therapeutics. As a systemic model which relies on both immune and genetic components and displaying the histopathological features which are highly associated with the disease, it bears close resemblance to human RA. However, it is not easily inducible in all available strains of mice and therefore it is often not suitable for use. The antigen-induced arthritis model (AIA) is easily inducible in available mice strains. Its histopathological features mirror those of both human RA and CIA, however, it is only a local model of disease and thus does not mimic the systemic nature of RA.

### 1.6 Current RA Therapies

Multiple classes of drugs are currently used in the treatment of RA. Many of these drugs such as non-steroidal anti-inflammatory drugs (NSAIDs), steroids and analgesics are used in the daily control of pain. However, the principle aim of RA therapy is to prevent the progression of disease and preserve joint architecture. The development of novel anti-TNF therapies has made significant improvements in the treatment of RA. Etanercept and Infliximab are 2 such anti-TNF agents which have been licensed for use in treatment of this disease (Jobanputra et al., 2002). Etanercept is a TNFR2-IgG Fc fusion protein that binds soluble and cell bound TNFα,

and Infliximab is an anti-TNFα monoclonal antibody. Both of these function to block signalling via TNFα thus preventing the detrimental activities of TNFα in RA patients (Feldmann and Maini, 2001). Efficacy of anti-TNF treatment is evaluated using the American College of Rheumatology (ACR) response criteria which takes into account the number of affected joints, pain and the general assessment of the disease. Responses of ACR 20, ACR 50 and ACR 70 can be achieved, representing reductions of 20 %, 50 % and 70 % of the disease criteria respectively (Jobanputra et al., 2002). In the most successful clinical trials with Etanercept and Infliximab, 79% and 75% of patients achieved an ACR 20 response (Jobanputra et al., 2002). Although this represents substantial clinical improvement, approximately 30 % of patients do not show beneficial responses to this drug therapy. Furthermore, radiographic analysis of joint damage following treatment with these therapies illustrates that progression of destruction is not completely prevented (Bathon et al., 2000, Lipsky et al., 2000). Thus, there is certainly scope for the development of novel RA therapies which better preserve the architecture of the joint.

**Table 1.3. A comparison of the 3 principle murine models for RA with the human disease.**

| Rheumatoid Arthritis Characteristics | Antigen-induced Arthritis<br>Induction via mBSA Administration | Collagen-induced Arthritis<br>Induction via Type II Collagen Administration | Adjuvant-induced Arthritis<br>Induced via Mycobacterium Administration |
|---|---|---|---|
| **Polyarticular** | No | Yes | Yes |
| **Cellular Infiltration** | Yes | Yes | Yes |
| **Synovial Hyperplasia and Pannus Formation** | Yes | Yes | Yes |
| **Bone and Cartilage Erosion** | Yes | Yes | Yes |
| **Genetic Susceptibility** | No | Yes | Yes |
| **T cell Involvement** | Yes | Yes | Yes |
| **Autoantibody Involvement** | No | Yes | No |
| **Alleviated Via Anti-cytokine Therapy** | Yes | Yes | Yes |

### 1.7 The Role of DR3 in Rheumatoid Arthritis

DR3 has been identified as a candidate gene for association with RA. Using fluorescence-based microsatellite marker analysis and affected sib-pair linkage analysis in RA patients Shiozawa et al. (2000) identified the region D1S214/252 on chromosome 1 as having a genetic link with the disease. As DR3 resides very close to this region, they investigated the expression of DR3 mRNA in affected individuals. An increase in mRNA in RA patients for the transmembrane portion of DR3 compared with controls was discovered. However, no such difference was observed in mRNA for the death domain portion of DR3, suggesting a complex role for DR3 in RA (Shiozawa et al., 2000). In 2004, the same group further implicated a role for DR3 in RA by using fluorescence in situ hybridisation to identify a duplication of the DR3 gene approximately 200kb upstream of the original. This duplication occurred in 78% of RA patients examined compared to only 39% of controls (Osawa et al., 2004). In a separate study based on comparative modeling of DR3, mutations in the DR3 gene thought to be associated with RA were predicted to cause reduced stability in the ligand binding domain of the receptor, potentially reducing its activation during the disease. However, as this is only a predicted model and because DR3 signalling is complicated by the existence of both soluble and membrane bound forms (Kitson et al., 1996), the effect this would have is uncertain (Borysenko et al., 2005). Most recently, the only known ligand for DR3, TL1A, has been linked with RA. Having determined that soluble TL1A release by human monocytes could be induced *in vitro* by stimulation with insoluble immune complexes, Cassatella et al. (2007) investigated the expression of soluble TL1A in RA patients. Those patients that were rheumatoid factor positive displayed strong TL1A

expression in their synovium. The cells displaying this staining had monocyte-macrophage morphology and expressed CD68 and CD14. This staining was less intense in rheumatoid factor negative patients. Additionally, monocytes from healthy donors which were cultured with purified insoluble immune complexes and PEG precipitates from rheumatoid factor positive patients, released high amounts of soluble TL1A (Cassatella et al., 2007). Thus increased TL1A expression in RA may increase DR3 activation and contribute to the progression of the disease. Interestingly, it was also determined in this study that monocyte production of soluble TL1A by immune complex stimulation, occurred with slower kinetics than that of either TNFα or IL-1 production and was not affected by the addition of anti-TNFα neutralising antibodies (Cassatella et al., 2007). Therefore, soluble TL1A production by monocytes may occur via a distinct pathway to TNFα providing a potentially important function for DR3 in RA. The mechanism by which DR3 and TL1A might contribute to the pathogenesis of RA is unknown. Recent data has implicated a role for DR3 in osteoblast regulation. Both soluble and full length versions of DR3 are expressed on human osteoblasts and the human osteosarcoma cell line MG63. The latter represents a model of mid-differentiation osteoblasts (Borysenko et al., 2006). At low density cultures of MG63 cells, DR3 activation via receptor cross-linking has been shown to result in apoptosis and reduced bone matrix synthesis. This could be blocked via the addition of media containing soluble DR3 (Borysenko et al., 2006). However, to date neither expression of DR3 on osteoclasts nor a potential role for DR3 in osteoclast differentiation and function has been identified.

### 1.8 Aims of the thesis

DR3 has been implicated in multiple inflammatory diseases, however, few *in vivo* studies have been carried out in order to fully elucidate the role of DR3 in inflammatory disease states. This is in part due to a lack of available reagents with which to study DR3 function.

The aims of this thesis are to address the issue of reagent availability, by carrying out gene cloning and antibody generation for use in scientific research, and to determine the *in vivo* role of DR3 in an inflammatory disease state namely, RA, using a murine model for the disease. The *in vivo* study should also be complimented by the generation of reagents. The specific aims of this thesis are:

- **To clone DR3 genes and express them in eukaryotic systems.** Both murine and human DR3 genes will be cloned by PCR and subcloned into eukaryotic expression vectors for the generation of soluble proteins and stable cell lines.
- **To generate antibodies to murine and human DR3.** Soluble proteins and stable cell lines will be used to immunize mice for the generation of antibodies via the Kohler and Milstein hybridoma method of antibody generation.
- **To investigate the role of DR3 in the murine antigen-induced arthritis (AIA) model of Rheumatoid Arthritis.** Mice genetically deficient in DR3 will be induced to develop AIA and the resulting inflammatory response will be evaluated via measurement of joint swelling and histological analysis.

# Materials and Methods

## 2. Materials and Methods

### 2.1 Solutions

Unless otherwise indicated, all reagents given below were supplied by Sigma-Aldrich (Poole, Dorset).

Acetate Buffer:

35.2ml 0.2M sodium acetate (Fisher Scientific, Loughborough, UK) 14.8ml 0.2M acetic acid solution, 50ml $dH_2O$.

Ampicillin Solution:

Ampicillin (Roche, Germany) was dissolved in $dH_2O$ at a concentration of 50mg/ml before being sterilised through a 0.22μm filter and stored at -20°C.

DABCO:

2% (w/v) 1,4-Diazabicyclo[2.2.2]octane (DABCO), 10% (v/v) phosphate buffered saline (PBS) (Oxoid, Hampshire) in glycerol.

Disodium Hydrogen Orthophosphate Solution (Fisher Scientific):

28.4mg/ml dissolved in $dH_2O$.

DNA Loading Buffer-Orange G:

2.5mg/ml Orange G loading dye in 2X TBE containing 30% glycerol.

EDTA Decalcification Solution:

70g EDTA was dissolved in 140ml of sodium dihydrogen orthophosphate solution and 340ml disodium hydrogen orthophosphate which was then made up to 1L with $dH_2O$.

Eosin Solution:

10mg/ml Eosin (Fisher Scientific) dissolved in $dH_2O$.

Fast Green Staining Solution:

0.5mg/ml dissolved in $dH_2O$.

Formic Acid Decalcification Solution:

100ml formic acid and 50ml formaldehyde (Fisher Scientific) mixed with 850ml of $dH_2O$.

Freezing Media:

Foetal Calf Serum (FCS) 90% (v/v) (Invitrogen, Netherlands) mixed with 10% dimethyl sulphoxide (DMSO) and filtered through a 0.22μm filter.

Kanamycin Solution:

Kanamycin (Roche) was dissolved in $dH_2O$ at a concentration of 50mg/ml before being sterilised through a 0.22μm filter and stored at -20°C.

Lauria Bertani (LB) Agar:

1.5% agar (w/v) (Oxoid) was added to LB broth. Ampicillin or Kanamycin (50μg/ml) was added if required when the broth had cooled to 50°C.

LB Broth:

20g LB broth low salt powder (Melford, Suffolk, UK) was dissolved in 1L $H_2O$ and autoclaved. Ampicillin or Kanamycin was added at 100μg/ml if required when the broth had cooled to 50°C.

LB X-gal Plates:

40μl of X-gal solution was spread on pre-warmed LB agar plates.

Lysis Buffer:

0.5ml TRIS-HCl (pH 8.0), 1 ml 10% SDS, 2ml 0.5M EDTA, 1ml 1M NaCl, 100μl proteinase K, 5ml $dH_2O$.

PBS:

8% (w/v) sodium chloride, 0.2% (w/v) potassium chloride, 0.12% (v/v) anhydrous sodium hydrogen phosphate at pH 7.4.

PBS-T:

PBS containing 0.1% (v/v) Tween-20.

RIPA Buffer:

0.5% NP40, 0.1% SDS, 0.5% deoxycholic acid, 150mM NaCl, 10mM Tris pH 8.0, 5mM EDTA made up to 50ml with $dH_2O$.

Safranin O Staining Solution:

1mg/ml safranin O dissolved in $dH_2O$.

SOC:

2% (w/v) tryptone, 0.5% (w/v) yeast extract, 0.05% (w/v) NaCl and 2.5mM KCl was autoclaved. Filter sterilised 2M $MgCl_2$ and 1M glucose was then added to a final concentration of 10mM and 20mM, respectively.

Sodium Dihydrogen Orthophosphate Solution:

31.2mg/ml sodium dihydrogen orthophosphate (Fisher Scientific) dissolved in $dH_2O$.

TBE (10x):

54g Tris, 27.5g boric acid dissolved in $dH_2O$ to a final volume of 990ml and then 10ml 1M EDTA pH 8.0 added.

TBE Agarose Gels:

1 x TBE containing 1% (w/v) agarose.

TBS Solution:

1L $dH_2O$ containing 61g Tris and 90g NaCl pH 7.6.

Towbin Buffer:

28.8g glycine, 6g TRIS, 400ml methanol, made up to 2L with $dH_2O$.

TRAP Staining Solution:

50ml 0.1M acetate buffer, 10ml 0.3M sodium tartrate, 1ml 10mg/ml naphtol AS-MX phosphate, 100µl Triton X-100, 38.9ml $dH_2O$, 0.3mg/ml Fast Red Violet LB salt.

X-gal Solution:

40mg/ml 5-bromo-4-chloro-3-indolyl-β-D-galactopyranoside in 100ml N, N-dimethyl formamide (DMF).

## 2.2 Molecular Cloning

### 2.2.1 Agarose Gel Electrophoresis

DNA fragments were separated according to size by electrophoresis on a 1% (v/v) TBE agarose gel containing 10% ethidium bromide (Sigma-Aldrich). Gels were set in trays for 1 hour prior to placing them into gel tanks and submerging them in TBE buffer. Samples were mixed with gel loading solution (Sigma-Aldrich) or Orange G DNA loading buffer and pipetted into wells alongside a wide range DNA marker (Sigma-Aldrich). Electrophoresis was carried out at a constant voltage of 100 volts for 40 minutes to 1 hour. Bands were then visualised by ultraviolet (UV) illumination at 365nm.

### 2.2.2 Plasmid Vectors

Signal pIgplus was a commercial vector made originally by R&D systems. pDR2δEF1α was a gift from Dr. I. Anegon (INSERM U437, Nantes, France) (Charreau et al., 1994). pAL190 (pEGFP-N1, Clontech) was a gift from Dr Richard Stanton (Medical Microbiology, Cardiff University). hDR3 in pcDNA3.1 was a gift from Stuart Farrow (Glaxo Wellcome, Herts, UK).

### 2.2.3 Polymerase Chain Reaction for human DR3 and murine DR3 from plasmid DNA

All PCR reactions were carried out using a PX2 Thermal Cycler (Thermo Electron Corp., USA). PCR reactions using plasmid DNA as the template were carried out using Taq DNA polymerase (NEB, USA). Reaction mixtures contained the manufacturer's supplied buffer, dNTPs (1mM) (NEB), forward and reverse primers

(10pmol of each) and DMSO (5%) (Sigma-Aldrich). For human DR3 cloning, plasmids were linearized via restriction enzyme digest prior to PCR reaction. The following thermocycling reaction was used:

| | | | |
|---|---|---|---|
| Initial Denaturation: | 94°C | 5 minutes | |
| Denaturation: | 94°C | 1 minute | x 35 |
| Annealing: | 50°C | 1 minute | |
| Extension: | 72°C | 1 minute | |
| Final Extension: | 72°C | 10 minutes | |
| Hold: | 4°C | | |

| Product | Primer Sequence | Predicted Size (bp) |
|---|---|---|
| Dominant negative (DN) hDR3 | 5' gga cta gta acc acg acg ggc aga gag c 3'<br>5' cgg atc ctt att ttt cga act gcg ggt ggc tcc aag cgc tcc cag ctt cat ctg cag taa c 3' | 812 |
| Soluble (Sol) hDR3 | 5' gga cta gta acc acg acg ggc aga gag c 3'<br>5' cgg atc ctg cca gaa cat ctg cct cca gcc 3' | 663 |
| Sol hDR3 + streptag | 5' gga cta gta acc acg acg ggc aga gag c 3'<br>5' cgg atc ctg tta ttt ttc gaa ctg cgg gtg gct cca agc gct cca gaa cat ctg cct cca gcc 3' | 696 |
| Sol hDR3 + streptag (no stop codon) | 5' gga cta gta acc acg acg ggc aga gag c 3'<br>5' cgg atc ctg ttt ttc gaa ctg cgg gtg gct cca agc gct cca gaa cat ctg cct cca gcc 3' | 693 |

Table 2.1: List of primers used in hDR3 cloning. All forward primers contain an Spe1 enzyme site and all reverse primers contain a BamHI enzyme site.

### 2.2.4 Polymerase Chain Reaction for Cloning Soluble Human and Murine DR3 from Signal Pigplus into pDR2δEF1α

Reactions were carried out using Platinum Pfx DNA polymerase (Invitrogen) with the manufacturer's supplied buffer, dNTPs (1mM) (NEB), forward and reverse primers (10pmol of each) and DMSO (5%) (Sigma-Aldrich). The following thermocycling reaction was used:

| | | | |
|---|---|---|---|
| Initial Denaturation: | 94°C | 5 minutes | |
| Denaturation: | 94°C | 1 minute | x 35 |
| Annealing: | 50°C | 1 minute | |
| Extension: | 72°C | 2 minutes | |
| Final Extension: | 72°C | 10 minutes | |
| Hold: | 4°C | | |

Forward primers were designed for human and murine soluble DR3 including XbaI and SpeI restriction enzyme sites respectively. The same reverse primer was used in both reactions and contained an EcoRV restriction enzyme site.

Table 2.2: Primers used in cloning soluble hDR3 and mDR3 from Signal pIgplus into pDR2δEF1α

| Product | Primer Sequences | Predicted Size (bp) |
|---|---|---|
| Soluble hDR3 | 5′ cga tct aga taa cta gag aac cca ctg 3′ | 1523 |
| | 5′ cga gat atc gca ttt agg tga cac tat 3′ | |
| Soluble mDR3 | 5′ cga act agt taa cta gag aac cca ctg 3′ | 1547 |
| | 5′ cga gat atc gca ttt agg tga cac tat | |
| | 3′ | |

### 2.2.5 Reverse Transcription – Polymerase Chain Reaction for murine DR3

#### 2.2.5.1 RNA extraction

Prior to all RNA work, plasticware, benches and pipettes were treated with RNase Away (Invitrogen, Groningen, Netherlands). All centrifuge steps were carried out at 10000 x g. Total RNA was extracted from murine thymus tissue using an RNeasy Midi Kit (Qiagen, West Sussex, UK) according to manufacturer's instructions. Briefly, freshly removed and flash frozen tissue was ground under liquid nitrogen in a mortar and pestle. Following transfer to a 15ml falcon, 2ml of buffer RLT containing 20µl 2-mercaptoethanol (Sigma-Aldrich) was added and vortexed. A 21 gauge needle was then used to homogenize the tissue. Samples were centrifuged and supernatant discarded. Ethanol (70%) (2ml) was added and samples were vigorously shaken. Samples were then added to an RNeasy column and centrifuged and the flow through was discarded. RW1 (4ml) was added and columns were centrifuged again, followed by 2.5ml of RPE and another centrifugation step. All flow throughs were discarded. The column was transferred to a collection tube and RNA was eluted into 300µl of RNAse free water (Invitrogen), allowing a minute to stand following the addition of the water, prior to centrifugation. If storage was necessary, RNA was stored at -70°C.

#### 2.2.5.2 Reverse Transcription

cDNA was generated via a reverse transcription reaction using Superscript II Reverse Transcriptase (Invitrogen). RNA (1µg) was used in each reaction and its concentration was determined by measuring absorbance at 260nm. Reaction mixtures also contained the manufacturer's supplied buffer, random primers

(250ng) (Invitrogen), dNTPs (1mM) (NEB), DTTs (0.1M) (Invitrogen) and RNase Out (40U) (Invitrogen). Following addition of the random primers and dNTPs to the RNA, the reaction was heated to 65°C for 5 minutes and then placed on ice. Buffer, DTTs and RNase out were then added and the reaction held at 25°C for 2 minutes prior to the addition of Superscript II reverse transcriptase. The thermocycling reaction then proceeded at 25°C for 10 minutes, 42°C for 50 minutes and 70°C for 50 minutes. cDNA was stored at -70°C.

#### 2.2.5.3 Polymerase chain reaction

Murine DR3 was cloned via PCR reaction from cDNA using a version of the "slowdown PCR" technique adapted from Bachmann et al (2003). Reactions were carried out using Platinum Pfx DNA polymerase (Invitrogen) with the manufacturer's supplied buffer, dNTPs (1mM) (NEB), forward and reverse primers (10pmol of each) and DMSO (5%) (Sigma-Aldrich). The following thermocycling reaction was used:

| | | |
|---|---|---|
| Initial denaturation: | 95°C | 5 minutes |
| 48 cycles of: | | |
| Denaturation: | 95°C | 30 seconds |
| | | Ramp Rate 2.5°C |
| Annealing: | 70°C – 1°C every 3rd cycle | 30 seconds |
| | | Ramp Rate 1.5°C |
| Extension: | 68°C | 1 minute 45 s |
| | | Ramp Rate 2.5°C |
| 15 cycles of: | | |
| Denaturation: | 95°C | 30 seconds |
| | | Ramp Rate 2.5°C |
| Annealing: | 58°C | 30 seconds |
| | | Ramp Rate 1.5°C |
| Extension: | 68°C | 1 minute 45 seconds |
| | | Ramp Rate 2.5°C |
| Final Extension: | 68°C | 5 minutes |
| | | Ramp Rate 2.5°C |
| Hold | 4°C | |

**Table 2.3: Primers used in cloning mDR3.**

| Product | Primer Sequences | Predicted Size (bp) |
|---|---|---|
| Full length mDR3 | 5' gga cta gta ccg caa tgg agg cac ggc tg 3'<br>5' cgg atc cgc aga taa gca aaa gtg agg 3' | 1392 |
| DN mDR3 for pal190 | 5' ctc gag acc gca atg gag gca cgg 3'<br>5' gga tcc gcc aga gga gtt cca aga gtt c 3' | 925 |
| DN mDR3 for pDR2δEF1α | 5' ctc gag acc gca atg gag gca cgg 3'<br>5' gga tcc tta ttt ttc gaa ctg cgg gtg gct cca agc gct tgc cag agg agt tcc aag agt tc 3' | 958 |
| Sol mDR3 | 5' ctc gag acc gca atg gag gca cgg 3'<br>5' ggt cta gac aag gct gcc atc gac aa 3' | 632 |
| Sol mDR3 + ct streptag | 5' ctc gag acc gca atg gag gca cgg 3'<br>5' tct aga ttt ttc gaa ctg cgg gtg gct cca caa ggc tgc cat cga caa 3' | 703 |
| Sol mDR3 + nt streptag | 5' ctc gag tgg agc cac ccg cag ttc gaa aaa acc gca atg gag gca cgg 3'<br>5' ggt cta gac aag gct gcc atc gac aa 3' | 703 |
| mDR3 – exon 5 and 6 | 5' gta cta gta cgc gac cga cca gag cc 3'<br>5' cgg atc cgc aga taa gca aaa gtg agg 3' | 1326 |
| mDR3 exon 3 | 5' gcg cag aac cct gtg gc 3'<br>5' cat cac aga ctt ggc agc 3' | 107 |
| mDR3 exon 10 | 5' ccg cag ctc tac gat gtg 3'<br>5' cct cgg cac agc ctt cc 3' | 225 |

A variety of enzyme sites were included into the primers including: Spe1; BamHI; Xho1 and Xba1.

### 2.2.6 Strep-Tag

A strep-tag II (IBA, USA) DNA sequence was incorporated into a number of PCR primers for use in protein detection and purification. The DNA sequence corresponds to an 8 amino acid sequence (WSHPQFEK).

### 2.2.7 PCR DNA and Gel Band Purification Using GFX Columns (Amersham, Buckinghamshire, UK)

This kit was used for the purification of DNA from solution or gel bands, via the use of a chaotropic agent and a glass fibre matrix column. Gel bands were weighed and dissolved at 65°C in an equivalent volume of capture buffer and centrifuged at 10000 x g in the column. DNA in solution was mixed with 500µl of capture buffer before following the same protocol as the gel bands. Columns were then washed in wash buffer containing 80% ethanol. DNA was eluted into 50µl of distilled water following a 1 minute incubation step at room temperature and stored at -20°C.

### 2.2.8 Topo TA Cloning Kit (Invitrogen)

All DNA generated by PCR reaction was immediately cloned into the TOPO TA vector pCR2.1-TOPO vector (Invitrogen). This vector is provided linearised with 3' T overhangs, which enables efficient ligation to the single deoxyadenosine overhang on PCR products generated with Taq DNA polymerase. Briefly, PCR products were incubated at room temperature with the vector in the presence of a salt solution provided by the manufacturer for 30 minutes. TOP10 chemically competent E.Coli, also provided with the kit, were thawed on ice and 3µl of the cloning reaction added to it. This was incubated on ice for 30 minutes. E.Coli was then transformed

via a 30 second heat shock reaction at 42°C and recovered in an orbital shaker in 200µl LB at 37°C for one hour. The transformation reaction (200µl) was spread onto prewarmed ampicillin or kanamycin selective LB plates containing 40mg/ml X-gal. Plates were incubated overnight at 37°C and white colonies selected the following day for analysis and selection.

### 2.2.9 Plasmid DNA Miniprep

The QIAprep Spin Miniprep kit (Qiagen) was used for the small scale production of plasmid DNA. Bacterial cultures were cultured overnight in 5ml of LB medium containing a 1/1000 dilution of antibiotic (50mg/ml) corresponding to the resistance of the plasmid. This culture was then used to generate plasmid DNA. The QIAprep Spin Miniprep kit is based on an alkaline lysis of bacterial cells followed by the adsorption of DNA to the silica membrane column in the presence of high salt. All centrifugation steps were carried out at 10000 x g. The centrifuged bacterial culture was resuspended in buffer P1 (250µl) containing RNaseA and mixed by pipetting. Bacteria were then lysed by the addition of buffer P2 (250µl) and mixed by inversion. The reaction was not allowed to proceed beyond 5 minutes before the addition of neutralization buffer (350µl) and mixture by inversion. The colourless precipitate was centrifuged and the supernatant decanted into the columns provided. Centrifugation of the columns permitted the adsorption of DNA to the silica membrane and the flow through was discarded. Salts were removed by a washing step in buffer PE (750µl) before DNA was eluted into a low salt buffer (buffer EB or distilled water) (50µl).

### 2.2.10 Restriction Enzyme Digest

DNA was digested via the use of restriction enzymes (NEB). All digestions were carried out in a volume of 20µl containing supplied enzyme buffer (2µl), restriction enzyme (20 units) and DNA. BSA (Sigma-Aldrich) was also used in reactions requiring its presence. Double digestions were carried out in the recommended compatible buffer or by sequential digestion. Reaction mixtures were incubated at 37°C for 1-2 hours prior to separation by agarose gel electrophoresis. DNA bands of the desired size were gel purified using Amersham GFX columns.

### 2.2.11 Production of Competent E.Coli

A sample of XL1-Blue E.Coli was provided by Dr Richard Stanton (Medical Microbiology, Cardiff University) and grown overnight on a tetracycline resistant LB plate. A single colony was selected and grown in LB (5ml) media containing tetracycline (0.1%) overnight at 37°C in an orbital shaker (Weiss-Gallenkamp, Loughborough, UK). The overnight culture (2.5ml) was inoculated into LB media (500ml) in a conical flask containing 20% glucose (10ml) and 1 M $MgCl_2$ (5ml). This was incubated at 37°C in an orbital shaker until the optical density at 600nm was equal to 0.7-0.8, as measured on an Ultrospec 3000 spectrophotometer (Pharmacia Biotech, Cambridge, UK). The culture was then chilled on ice before washing twice in 10% glycerol (250ml) and centrifuging at 6000 x g for 20 minutes at 4°C. A third washing step in 10% glycerol (25ml) was carried out before resuspending the culture in 10% glycerol (5ml) and snap freezing in 100µl volumes. E.Coli was stored at -80°C.

### 2.2.12 Transformation of E.Coli

Bacterial cells were transformed via an electroporation method. Approximately 50ng of plasmid were pipetted into competent E.Coli on ice in an electroporation cuvette (Bio-Rad, USA). After 5 minutes, bacteria were electroporated at 2.5 volts and recovered via the addition of SOC media (950µl) in an orbital shaker at 37°C for 1 hour. Cultures (50-250µl) were grown overnight on a selective LB plate at 37°C.

### 2.2.13 Ligation Reactions

Both vector and insert DNA were digested with appropriate restriction enzymes and vector DNA was subsequently dephosphorylated with 5 units Antarctic Phosphatase (NEB) in the manufacturer's supplied buffer. Vector DNA (100ng) was mixed with insert DNA in a molar ration of 3:1 to give a total reaction volume of 30µl containing T4 DNA ligase (1 unit) (Roche), supplied buffer (3µl) and water. The reaction was incubated at 16°C overnight prior to use in transformation reactions.

### 2.2.14 DNA Concentration Estimation

DNA concentration was analysed by a spectrophotometer, which measures the absorbance of a DNA solution at 260nm compared to a control solution containing no DNA. In situations where DNA concentration was too low to accurately determine using the spectrophotometer, it was run on a TBE agarose gel alongside a smart ladder marker (Eurogentec, Southampton) which contains DNA fragments of defined size and concentration.

### 2.2.15 Removal of Single Stranded Extensions

Out of frame soluble hDR3 Signal Pigplus constructs were treated with mung bean nuclease (NEB) in order to put the hDR3 sequence in frame with the CD33 signal peptide. Constructs were digested with the restriction enzyme Hind III, as described in 2.2.10. The linear DNA (10μg) was then incubated with 10 units of mung bean nuclease in the manufacturer's supplied buffer for 30 minutes at 30°C. Following DNA purification as described in 2.2.7, constructs were blunt end ligated as described in 2.2.13.

### 2.2.16 BigDye Sequencing

All constructs were sequenced using the "BigDye" terminator v3.1 cycle sequencing kit (Perkin-Elmer, USA). A 10μl reaction mixture was prepared containing DNA (50ng), BigDye ready reaction mixture (4μl), primer (3.2pm) and water. The following thermocycling program was used:

| | | |
|---|---|---|
| Denaturation: | 96°C for 30 seconds | ⎫ |
| Annealing: | 50°C for 15 seconds | ⎬ 25 cycles |
| Extension: | 60°C for 4 minutes | |

DNA was subsequently precipitated (see section 2.2.17) and analysed on an ABI PRIZM 377 DNA sequencer (Applied Biosystems, USA).

### 2.2.17 Precipitation of DNA

DNA for sequencing was precipitated via the addition of 10% (v/v) sodium acetate

and 100% (v/v) ethanol (2.5 x total volume) and mixed by pipetting. The sample was centrifuged at 4°C for 20 minutes at 10000 x g. The supernatant was removed and 2 washing steps were carried out in 70% (v/v) ethanol (750µl) and spun for 10 minutes at 10000 x g between each wash. Supernatant was removed and the DNA was air dried.

### 2.2.18 Glycerol Stocks

In addition to purified plasmid DNA, plasmids were stored as glycerol stocks. Overnight cultures (500µl) were mixed well with an equal volume of 65% (v/v) glycerol and stored at -80°C in cryovials (Greiner, Gloucestershire, UK).

### 2.2.19 Genes Ordered Commercially

In addition to cloning mDR3 by RT-PCR, two of the mDR3 splice variants were also synthesized commercially by Genscript (USA). Full length mDR3 and soluble mDR3 (lacking exon 6) were ordered flanked by SpeI and BamHI enzyme sites. Both genes had been cloned into the vector pUC57 upon receipt.

### 2.2.20 Peptide Design

Peptides to mDR3 were designed with the aid of the online Peptide Select tool (Invitrogen) and assistance from Professor B. Paul Morgan (Medical Biochemistry and Immunology, Cardiff University). This is further described in chapter 4.

### 2.2.21 Genotyping

Tail samples measuring approximately 2mm were lysed overnight at 56°C in lysis buffer. Genomic DNA was phenol-chloroform extracted in an equal volume of phenol:chloroform:isoamyl alcohol (Fisher), shaken for 10 minutes and centrifuged at 10000 x g for 10 minutes. An equal volume of ice cold isopropanol was added to the aqueous layer and inverted 20 times to clot the DNA. This was centrifuged at 10000 x g for 10 minutes and the supernatant poured off. Ethanol (70%) (0.5ml) was added and left to stand for 30 minutes at room temperature prior to centrifugation. Ethanol was carefully removed and the DNA was air dried before being resuspended in 10mM Tris. Genomic DNA (2µl) was used in a PCR reaction containing Taq DNA polymerase (2.5 units) (Invitrogen), supplied buffer (4µl), $MgCl_2$ (1.2µl), 1mM dNTPs (5µl) (NEB) primer F8 (0.2µl), primer 4f (0.2µl), primer 2r (0.4µl) and water. The following thermocycling reaction was used:

| | | |
|---|---|---|
| Denaturation: | 94°C for 5 miuntes | |
| Annealing: | 62.5°C for 30 seconds | 1 cycle |
| Extension: | 72°C for 40 seconds | |

| | | |
|---|---|---|
| Denaturation: | 94°C for 30 seconds | |
| Annealing: | 62.5°C for 30 seconds | 33 cycles |
| Extension: | 72°C for 40 seconds | |

| | | |
|---|---|---|
| Denaturation: | 95°C for 30 seconds | |
| Annealing: | 62.5°C for 30 seconds | 1 cycle |
| Extension: | 72°C for 5 minutes | |

Primers F8 (5' tct cct gtc atc tca cct tgc 3'), 4F (5' aga agg aga aag tca gta gga ccg 3') and 2R (5' gaa agg atg aaa ctt gcc tgt tgg 3') were used for genotyping.

## 2.3 Cell Culture

### 2.3.1 Cell Lines

Chinese Hamster Ovary (CHO) cells, HEK-293 cells and NIH-3T3 cells (provided by Sian Llewellyn-Lacey, MRC Tissue Culture Technician, Cellular and Viral Immunology Resource, Cardiff), were grown in 175cm$^2$ tissue culture flasks. X63.Ag8.653 mouse myeloma cells (provided by Sian Llewellyn-Lacey, MRC Tissue Culture Technician, Cardiff) were maintained in 75cm$^2$ tissue culture flasks. All cells were cultured at 37°C in 5% $CO_2$ in humidified incubators. All tissue culture plasticware was provided by Corning, USA. CHO cells were maintained in Roswell Park Memorial Institute (RPMI) 1640 (Invitrogen) supplemented with L-glutamine (2 mM) (Invitrogen), penicillin (1 x $10^5$ IU/ml) (Invitrogen) and 10% (v/v) FCS (Invitrogen). FCS-free RPMI was also used in the generation of soluble proteins. 293 cells and NIH-3T3 cells were maintained in Dulbecco's Modified Eagle Medium (DMEM) (Invitrogen) supplemented with penicillin (1 x $10^5$ IU/ml) and 10% (v/v) FCS. Mouse myeloma cells were maintained in DMEM supplemented with L-glutamine (2mM) (Invitrogen), penicillin (1 x $10^5$ IU/ml) (Invitrogen), 10% (v/v) FCS (Invitrogen), glucose (4.5g/L) (Sigma-Aldrich), sodium pyruvate (2mM) (Invitrogen), HEPES (10mM) (Sigma-Aldrich) and sodium bicarbonate (1.5g/L) (Sigma-Aldrich). FCS-free DMEM and complete selective medium, supplemented as for myeloma cell maintainance, was also used in hybridoma generation. Selective medium additionally contained azaserine-hypoxanthine (1 vial) (Sigma-Aldrich) and BM-Condimed H1 (10% v/v) (Roche). Upon reaching confluence, adherent cells were passaged and divided 1:10 by removing medium, washing the cells with PBS and

incubating the cells with 8ml of Trypsin/EDTA (Invitrogen) until the cells were no longer adherent. Suspension cells were divided 1:5.

### 2.3.2 Cell Counting

100µl of cell suspension was diluted 1:1 with Trypan Blue (Sigma-Aldrich) and applied to a haemocytometer (Reichert, USA). Viable cells were identified under white light by the exclusion of blue dye and the total number of cells present was calculated using the following equation:

Total no. cells/ml = (No cells/no of squares counted) x 2 x ($1 \times 10^4$)

### 2.3.3 Cryopreservation of Cells

Cells were washed in PBS prior to the addition of Trypsin/EDTA to put the cells into suspension. Cells were centrifuged at 4°C for 5 minutes at 300 x g and the Trypsin/EDTA poured off. Cells were then re-suspended in 1ml of freezing media for each confluent $25cm^2$ tissue culture flask. Each 1ml aliquot of cells was transferred to a cryovial (Greiner) and placed in a Nalgene 5100 Cryo 1°C freezing container (Merck, West Drayton) containing isopropanol at room temperature. This was then placed in a -70°C freezer overnight before the cryovials were stored in liquid nitrogen. Cells were recovered from liquid nitrogen by rapidly thawing in a 37°C $H_2O$ bath. Cells were then transferred to a 15ml falcon tube (Greiner) and 10ml of 37°C media was added. The cells were centrifuged at 300 x g for 5 minutes and resuspended in media for counting prior to seeding in an appropriate tissue culture flask at the required density.

### 2.3.4 Transfection Methods

Two methods were used for the transfection of plasmid DNA constructs into mammalian cell lines: calcium phosphate transfection using the Calcium Phosphate Transfection Kit (Invitrogen) and a non-liposomal lipid method using Effectene Transfection Reagent (Qiagen). For both methods, cells were seeded at a density of $0.5 \times 10^6$ cells per $25cm^2$ tissue culture flask on day 0. Fresh media was placed onto the cells 3 hours prior to transfection on day 1. The calcium phosphate transfection method is based on the formation of a calcium phosphate - DNA precipitate, which binds DNA to the cell surface and enters the cells by endocytosis. Plasmid DNA (10μg) was mixed with calcium chloride (18μl) and made up to 150μl with distilled water. This mixture was added dropwise to Hepes buffered saline (150μl) whilst vortexing and incubated at room temperature for 30 minutes in order for a precipitate to form. The precipitate was added dropwise to the media of the cells. 16 hours post transfection, the media was removed from the cells and they were washed twice in PBS. Glycerol (5ml of 15% (v/v)) was added to the cells for precisely 2 minutes before 2 further washes in PBS. Normal media was returned to the cells. 48 hours post - transfection, cells were split 1:3 and placed in selective media. The Effectene method is based upon the condensation of DNA by interaction with the manufacturer's supplied enhancer which then complexes with Effectene and can be taken up by the cells. Plasmid DNA (2μg) was added to the manufacturer's supplied buffer (298μl) and mixed with the enhancer (16μl) before vortexing and incubating for 5 minutes at room temperature. Effectene reagent (50μl) was added to the mixture and vortexed before incubation at room temperature for 10 minutes. Normal media (1ml) was added and the mixture placed dropwise onto the media of

the cells. After 24 hours, the media was replaced with normal growth media and after 48 hours, cells were passaged 1:3 into selective media.

### 2.3.5 Cell Selection

Transfected cells were selected in media containing the appropriate drug for the resistance gene contained within the plasmid in order to generate stably selected cell lines. In order to determine the concentration of drug required, a "kill curve" was generated. Untransfected cells were seeded in a 24-well tissue culture plate at a concentration of 1 x $10^5$ cells per well. After 24 hours, doubling dilutions of either G418 (Autogen Bioclear, Wiltshire, UK) or Hygromycin (Autogen Bioclear) were added to the wells. Cells were observed for 14 days and the extent of cell killing was measured. It was determined that 300μg/ml G418 be used on transfected CHO cells and 200μg/ml hygromycin be used on transfected NIH-3T3 cells and 293 cells.

### 2.3.6 Isolation of GFP expressing cells

Transfected cells expressing GFP were isolated from bulk cultures as follows. Adherent cells in 25$cm^2$ tissue culture flasks were washed in PBS and then put into solution via the addition of 2ml Trypsin/EDTA. Cells were filtered with a 40μm cell strainer and re-suspended at a final concentration of 1 x $10^6$ cells per ml in the appropriate culture media. Cells were sorted using a MoFlo cell sorter (Beckman Coulter) into a 15ml falcon containing culture media.

### 2.3.7 Hybridoma Generation

The day prior to spleen and myeloma cell fusion, all vessels and media were pre-warmed to 37°C and 100µl of complete selective medium was dispensed into each well of 12 x 96-well plates and allowed to equilibrate overnight at 37°C. Mouse myeloma cells (X63.Ag8.653) were cultured for 2 weeks prior to fusion and 1 x $10^7$ cells were used for each mouse spleen fusion. Myeloma cells were centrifuged at 300 x g for 5 minutes and resuspended in 10ml of serum-free media. Spleen cells were released from the intact spleen into 5ml DMEM by gently teasing it apart with two needles in a Petri dish and transferring the cells to a 15ml falcon tube. A further 5ml DMEM was used to rinse the Petri dish and this was added to the falcon tube. Both spleen cells and myeloma cells were then centrifuged at 300 x g for 5 minutes and resuspended in 5ml of serum-free DMEM. Both cell preparations were then mixed with each other and centrifuged for 10 minutes at 300 x g to give a pellet containing both cell types. 300µl of Hybri-max PEG (Sigma-Aldrich) was added to the pellet which was gently resuspended by flicking the tube. Cells were left in the PEG for at least 3 minutes but no more than 8 minutes so following a 3 minute incubation, cells were centrifuged for 5 minutes at 300 x g and the PEG was removed using a Pasteur pipette. Cells were resuspended in complete selective media (5ml) and then added to 95ml of selective media in a pre-warmed glass bottle. Cells were left to stand at 37°C for 30 minutes prior to adding 100µl of cells to each well of the previously prepared 96 well plates and culturing at 37°C in 5% $CO_2$. One control well per plate contained myeloma cells only. Cells were cultured for approximately 8-10 days changing the media regularly until clones were easily visible. Screening of wells via ELISA was then undertaken as described in 2.4.3.

Positive clones were transferred to 24 well plates and re-screened. Any positive clones were then grown in 25cm$^2$ flasks for further analysis and freezing.

## 2.4 Immunodetection Methods

### 2.4.1 SDS-Page and Western Blotting

#### 2.4.1.1 Production of Cell Lysate

Confluent cells in 25cm$^2$ tissue culture flasks were removed from the incubator and washed twice in ice cold PBS. A further 5ml of ice cold PBS was added to the flasks and cells were scraped off using a cell scraper (Greiner). Suspensions of cells were then transferred to 15ml falcons and centrifuged at 4°C for 5 minutes at 300 x g. PBS was poured off and 200µl RIPA buffer containing 5µl 2-mercaptoethanol was added. Cells were lysed on ice for 10 minutes and 100µl NuPage (Invitrogen) buffer was added and mixed by pipetting. Samples were transferred to 0.5ml eppendorfs and heated to 99°C for 10 minutes. Samples were used immediately or stored at -20°C.

#### 2.4.1.2 SDS - Polyacrylamide Gel Electrophoresis (PAGE)

Proteins were resolved by SDS-PAGE in NuPAGE MOPS SDS running buffer (Invitrogen) using the NuPAGE Novex 4-12% Bis-Tris pre-cast gel system (Invitrogen). Each sample (15µl) was loaded into the wells of a gel alongside a SeeBlue Plus2 pre-stained protein marker (10µl) (Invitrogen) and resolved at a constant voltage of 200V for 1 hour.

#### 2.4.1.3 Western Blotting

Proteins were transferred to a PVDF membrane (Invitrogen) in Towbin buffer using the XCell II Blot Module (Invitrogen) at a constant voltage of 30 volts for 1 hour. The transfer membrane was pre-soaked in methanol and the filter paper and blotting pads in transfer buffer prior to transfer. The gel, membrane and blotting pads were placed into the XCell II Blot Module according to the manufacturer's instructions, which was then filled with transfer buffer. The module was then surrounded with distilled water in order to keep it cool during transfer. Immediately after transfer, the pre-stained protein marker was marked with an antigen-antibody pen for mouse (Alpha Diagnostics International, USA) in order to visualize the bands. The membrane was then blocked in PBS-T containing 5% Marvel milk powder (w/v) overnight at 4°C. Membranes were incubated in primary antibody diluted 1/1000 in PBS-T 5% milk for 1 hour at room temperature and then washed in 3 changes of PBS-T 5% milk powder for an hour. The appropriate horse-radish peroxidase conjugated secondary antibody was then added to the membrane diluted to the required concentration in PBS-T 5% milk for 1 hour at room temperature. A further 1 hour wash as described above was then carried out. Proteins were visualized via the addition of ECL Western Blotting Substrate (Perbio Pierce, Belgium) according to the manufacturer's instructions.

**Table 2.4: Antibodies used in Western Blotting**

| Antibody | Supplier | Raised in | Dilution |
|---|---|---|---|
| IgG1 Fc | Chemicon | Mouse | 1/1000 |
| GFP | Santa Cruz | Rabbit | 1/2000 |
| Actin | Sigma | Rabbit | 1/5000 |
| DR3 | R and D | Goat | 1/500 |
| Streptag II | IBA | Mouse | 1/1000 |

| Antibody | Supplier | Dilution |
|---|---|---|
| Anti-mouse HRP | Biorad | 1/1000 |
| Anti-rabbit HRP | Biorad | 1/5000 |

### 2.4.2 Fluorescence Microscopy

Cells which had been seeded onto glass coverslips were washed twice in PBS and then fixed in paraformaldehyde (2%) for 20 minutes at room temperature. Following washing in PBS, cells were permeabilised in Triton X-100 (0.1%) and then incubated with anti-streptag II (1/100) (IBA) primary antibody for 1 hour at 37°C in a humidifying chamber. Cells were washed 6 times in PBS and then incubated with anti-mouse Alexafluor 594 (1/1000) (Invitrogen) secondary antibody (1/1000) at 37°C as previously described. Cells were again washed 6 times in PBS and finally mounted under the coverslip in 2% (w/v) DABCO. All slides were visualised using a Leica DM IRBE microscope (Leica, Germany) attached to a Hamamatsu ORCA-ER camera (Hamamatsu, Japan) and Improvision Openlab 3 software (Improvision, Coventry).

### 2.4.3 ELISA

#### 2.4.3.1 Hybridoma Screening

Peptide antigens (10μg/ml) were coated onto Nunc-Immuno Maxisorp 96 well plates and incubated overnight at 4°C. Blocking media (5mg/ml BSA in PBS) (100μl) was then added to each well and incubated a room temperature for 1 hour. Plates were washed 3 times in PBS-Tween 20 (0.1%) and left inverted to dry for 30 minutes. Either 50μl of hybridoma supernatant or 100μl of mouse serum was added to the appropriate wells. Mouse serum from immunised animals or a non-immunised control was diluted in 5mg/ml BSA in PBS-Tween 20 and added to the wells at doubling dilutions in duplicate. A row of wells containing no serum was also left as a blank control. Serum and supernatant were incubated at room

temperature for 1 hour and then plates were again washed as described. Secondary HRP conjugated anti-mouse antibody (Biorad) was diluted in 5mg/ml BSA in PBS-Tween 20 (1/1000) and added to each well (100µl). This was incubated at room temperature for 1 hour before a final wash as described. ABTS substrate (Sigma) (100µl) was added to each well and allowed to develop for 10 minutes at room temperature before the reaction was stopped via the addition of 1% (w/v) SDS. Plates were read in a plate reader at 405nm.

#### 2.4.3.2 Anti-mBSA Titre Analysis

Methylated BSA was coated onto Nunc-Immuno Maxisorp 96 well plates and incubated overnight at 4°C. Blocking media (PBS-5% milk) (100µl) was then added to each well and incubated at room temperature for 1 hour. Plates were washed 3 times in PBS-Tween 20 (0.1%) and left inverted to dry for 30 minutes. 50µl of mouse serum from immunised or non-immunised control mice was added to the appropriate wells at doubling dilutions in duplicate. Mouse serum was diluted in blocking media. A row of wells containing no serum was also left as a blank control. Serum was incubated at room temperature for 1 hour and then plates were again washed as described. Secondary HRP conjugated anti-mouse antibody (Biorad) was diluted in blocking media (1/1000) and added to each well (100µl). This was incubated at room temperature for 1 hour before a final wash as described. ABTS substrate (Sigma) (100µl) was added to each well and allowed to develop for 10 minutes at room temperature before the reaction was stopped via the addition of 1% (w/v) SDS. Plates were read in a plate reader at 405nm.

## 2.5 Animals

### 2.5.1 Housing and Home Office Approval

Animals were housed in the Joint Biological Services Unit (Cardiff University) at constant temperature and humidity on a 12 hour light/dark cycle. All animals were kept in filter top containers until they were entered into the antigen-induced arthritis study when they were transferred to conventional housing. Food and water was available to the animals *ad libitum*. $DR3^{-/-}$ animals were bred in house on a C57/BL6J background. All experimental procedures were consistent with Home Office approved license 30/1999.

### 2.5.2 Peptide Immunisation Protocol

Peptides were dissolved in water and emulsified in either complete Freund's adjuvant (CFA) (Sigma-Aldrich) or incomplete Freund's adjuvant (IFA) (Sigma-Aldrich) to a final concentration of 1mg/ml. $DR3^{-/-}$ mice were immunised initially with peptide in CFA and subsequently with peptide in IFA no less than 2 weeks between each immunisation. Injections were administered subcutaneously at 2 distinct sites per immunisation in 50µl volumes. Immunisations continued until positive screening results were observed and mice were selected for hybridoma generation. Mice were culled via schedule 1 three days after a booster immunisation was administered and spleens were removed and placed into DMEM media. A serum sample was also taken via cardiac puncture.

### 2.5.3 Tail Bleeds for Analysis of Antibody Production

Mice were test bled by venesection after the 3rd peptide immunisation and again 4 weeks later to assess antibody titres. No more than 10% of total blood volume was taken at any one time.

### 2.5.4 Murine Antigen-Induced Arthritis

Mice were immunised on 2 occasions, 1 week apart, with methylated bovine serum albumin (mBSA) (1mg/ml) (Sigma-Aldrich) dissolved in distilled water and emulsified with CFA. Injections were given subcutaneously in two 50µl volumes. An intra-peritoneal injection of heat killed bordetella pertussis toxin (40µg/ml) (Sigma-Aldrich) was given as an additional adjuvant with the first mBSA injection. This was administered as a single 100µl injection. Fourteen days after the second mBSA immunisation (day 0), following baseline measurements of knee joint diameters, mice received a 6µl intra-articular injection of mBSA in distilled water (10mgs/ml) into the hind right knee joint. Knee joint diameters were then measured on days, 1, 2, 3, 5, 7, 14 and 21 as the difference between right knee joint and control left knee joint, using a POCO 2T analogue micrometer (Kroeplin, Germany). Mice were sacrificed on days 3 or 21 and joints were retained for analysis. A serum sample was also taken via cardiac puncture. In experiments conducted in order to assess the effect of TL1A on the model, increasing concentrations of TL1A protein (1ng, 10ng, 100ng) (R and D Systems) diluted in PBS-BSA (0.1%) were also administered into the joint in the intra-articular mBSA injection on day 0.

## 2.6 Histological Techniques

### 2.6.1 Joint Harvest and Processing

#### 2.6.1.1 Joint Harvest

Murine knee joints were harvested, placed into tissue biopsy cassettes (Thermo Electron) and immediately fixed in neutral buffered formal saline (Sigma-Aldrich) at 4°C for 1 week. Joints were then decalcified for 2 weeks via one of two methods: formic acid decalcification or EDTA decalcification using appropriate decalcification solutions. Both methods were carried out at 4°C.

#### 2.6.1.2 Determination of Endpoint of Decalcification

A sample of decalcifying solution was neutralized with concentrated sodium hydroxide. An equal volume of saturated ammonium oxalate solution (Fisher) was then added and allowed to stand for 30 minutes. The formation of a white precipitate indicated the presence of calcium ions in the solution as calcium oxalate is formed. Decalcification was continued until no precipitate was seen.

#### 2.6.1.3 Shandon Tissue Processor Cycle

Joint tissues were infiltrated with paraffin wax via the following processing cycle: 70 % alcohol (30 minutes), 90% alcohol (1 hour), 5 x 100% alcohol (1 hour each), 2 x xylene (1 hour each at 37°C), xylene (1 hour at 45°C), 4 x wax (1 hour each at 60°C). Following processing, joints were embedded in paraffin wax blocks using a Shandon Histocentre.

### 2.6.2 Paraffin Wax Sections

Mouse knee joints were harvested and processed. Serial sections (7μm) were cut on a microtome and floated onto distilled water (50°C) prior to collection on pre-cleaned X-tra adhesive microslides (Surgipath, USA). Slides were incubated overnight at 60°C and then stored at room temperature until required.

### 2.6.3 Haematoxylin and Eosin (H+E) Staining

Paraffin wax sections on glass slides were deparaffinised through 3 rinses in xylene (5 minutes) followed by 3 minutes in each descending grade of methanol (2 x 100%, 1 x 90% and 1 x 70%). Sections were then rinsed in running water for 5 minutes and dipped into distilled water prior to immersing in Harris's Haematoxylin solution (BDH, Poole, UK) for 1 minute and 30 seconds. Sections were again washed in running water and dipped in distilled water as described above before placing in Scott's tap water (30 seconds) to blue. After another wash step in water, sections were immersed in Eosin solution for 1 minute and washed quickly in running tap water. Sections were dehydrated through an ascending series of methanol as described above but omitting the first 70% wash and including a third 100% wash, and immersed in 3 changes of xylene. Slides were mounted in Ralmounts (BDH, UK) or DPX (Sigma-Aldrich) mounting media and left to set overnight at 60°C.

### 2.6.4 Histological Analysis

Following haematoxylin and eosin staining, two blinded independent observers scored sections for the arthritis index. The arthritis index is a sum of 4 parameters which reflect the degree of arthritis severity in the joint. These are cellular exudate,

synovial hyperplasia and bone erosion, all scored from 0 (normal) to 3 (severe) and cellular infiltrate scored from 0 to 5. As histological sections were scored relative to the other sections in each experimental group, this data could not be normally distributed.

### 2.6.5 Tartrate Resistant Acid Phosphatase (TRAP) Staining

EDTA decalcified sections were deparaffinised as described in section 2.6.3 and washed in running water for 5 minutes. Sections were then incubated in pre-warmed TRAP staining solution at 37°C for 3 hours. Sections were washed in running water for 5 minutes, counterstained in Haematoxylin and "blued" in Scott's Tap water as described in section 2.6.3. After washing in running tap water for 5 minutes and dipping in distilled water, sections were air dried and mounted in Ralmounts or DPX medium and set overnight at 60°C. Images were captured using an Olympus N457 digital camera. Randomly selected areas were assessed for TRAP positive staining using Adobe Photoshop CS3.

### 2.6.6 Safranin O/Fast Green Staining for Cartilage Depletion

EDTA decalcified sections were deparaffinised as described in section 2.6.3 and washed in running water for 5 minutes before a brief immersion in distilled water. Sections were then stained in Harris's Haematoxylin solution (2 minutes) and again washed in running tap water before placing in Scott's tap water (30 seconds) to blue. After washing in distilled water (2 minutes), sections were placed into Fast Green staining solution (0.2mg/ml) for 10 minutes, acetic acid (1%) for 10 seconds, and finally into Safranin-O staining solution (1mg/ml) for 5 minutes. Sections were

washed in distilled water for 2 minutes and dehydrated in 90% methanol, 100% methanol and xylene for 1 minute each. Sections were mounted using DPX mounting media. Cartilage depletion was measured as a percentage of total cartilage (safranin O positive) under x40 magnification using an eye piece with a line-graduated scale.

### 2.6.7 F4/80 Staining

F4/80 is used as a marker for macrophages. Staining of processed and paraffin wax embedded joint sections was carried out using anti-mouse F4/80 (Invitrogen) and an anti-rat HRP-DAB cell and tissue staining kit (R&D Systems). Sections were deparaffinised as described in section 2.6.3 and rinsed in running tap water for 5 minutes. Sections were then placed into TBS solution for 30 minutes before being encircled with a hydrophobic barrier from a Pap pen (Sigma-Aldrich). A peroxidase blocking step using reagents supplied in the kit was carried out as described in the manufacturer's instructions. Antigen unmasking was achieved by incubating the sections in pre-warmed Trypsin/EDTA (0.1%) in TBS for 30 minutes at 37°C. Sections were washed twice in TBS for 5 minutes and then serum, avidin and biotin blocking steps were carried out as described in the manufacturer's instructions. Following rinsing in TBS, either anti-mouse F4/80 antibody (1/50) or isotype control (1/400) were added to the sections and incubated at 4°C overnight. Sections were washed in TBS 3 times for 15 minutes each and the biotinylated secondary antibody was then applied and incubated at room temperature for 1 hour. Sections were again washed 3 times for 15 minutes each in TBS and HSS-HRP from the kit was then applied for 30 minutes at room temperature. DAB chromogen and DAB chromogen

buffer were mixed as described in the manufacturer's instructions and 3 drops were applied to each section and incubated for 20 minutes before washing in distilled water. Sections were counterstained in Haematoxylin and "blued" in Scott's Tap water before dehydrating in an ascending series of alcohol and xylene and mounting in Ralmounts or DPX medium as described in section 2.6.3. Images were captured using an Olympus N457 digital camera. Randomly selected areas were assessed for F4/80 positive staining using Adobe Photoshop CS3.

**2.7 Statistical Analysis**

All results were graphically illustrated as the mean ± standard error of the mean (SEM) and were statistically analysed using GraphPad Prizm v4. p values of $\leq 0.05$ were considered significant and those of $\leq 0.01$ were considered highly significant. The statistical tests used in this study were the Mann-Whitney-U test, which was used when comparing the means of two unpaired groups of non-normally distributed data and the one-way and two-way ANOVAs were used when comparing more than 2 groups or variables respectively.

# Results

# Chapter 3

## 3. Results – Molecular Cloning of Murine and Human DR3 Genes

### 3.1 Introduction

Prior to the commencement of this work, there were no commercially available antibodies with which to study mDR3 function and only 1 polyclonal anti-human DR3 antibody. Therefore, a principle aim of this study was the generation of reagents for use in DR3 research. In order to facilitate this work, human DR3 and murine DR3 were both amplified via PCR reaction and cloned into suitable eukaryotic expression vectors. They were subsequently transfected into mammalian cells, which were then analysed for protein expression via Western blot and immunofluorescence.

### 3.2 PCR Amplification of hDR3

The strategy employed to generate the hDR3 gene is illustrated in Figure 3.1. Human DR3 was obtained via PCR amplification from a pcDNA3.1 construct containing the full length human gene. A dominant negative form of the gene, in which the death domain was absent was amplified using primer pairs described in section 2.2. The primers were engineered to insert 2 restriction enzyme sites into the PCR product which were Spe1 and BamHI in the forward and reverse positions respectively. A streptag sequence was also included in the reverse primer in order to facilitate protein detection. Due to the lack of antibodies against DR3, adding a tag sequence was the only method available for detecting protein. The resulting PCR product was 826 base pairs in size. The gene was subsequently Topo cloned into the pCR2.1 Topo vector and sequenced to confirm that it matched the published sequence (Figure 3.2).

**Figure 3.1**



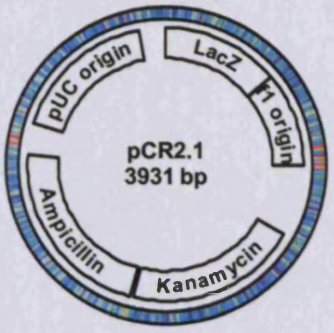


The hDR3 gene was PCR amplified from vector DNA and TOPO cloned into the pCR2.1 TOPO vector.

hDR3 was isolated from the TOPO vector by restriction digest using enzyme sites Spe1 and BamHI

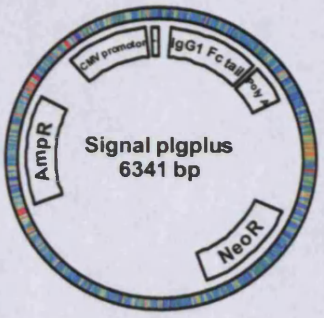


Digested with Nhe1 and BamHI

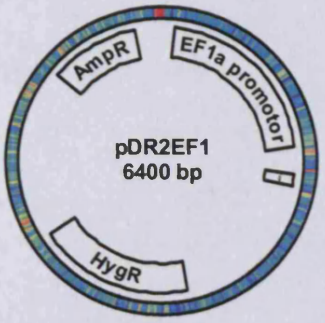


Digested with Xba1 and BamHI

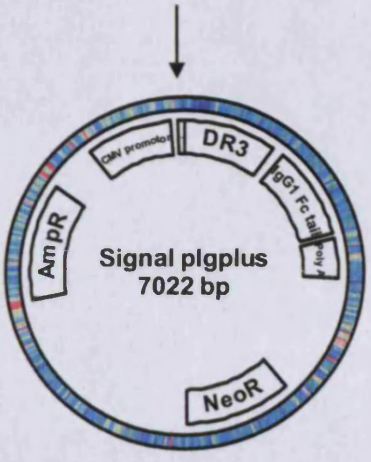


Soluble hDR3 with or without a streptag was ligated into signal plgplus

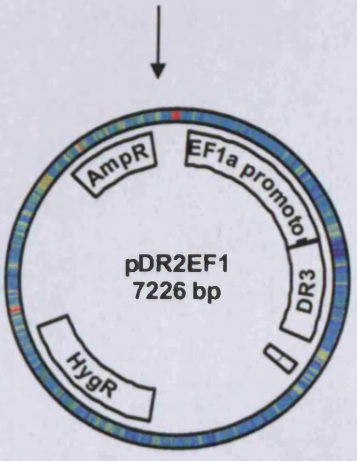


Dominant negative hDR3 with a streptag was ligated into pDR2δEF1α

**Figure 3.1. Cloning strategy for hDR3 construct generation.** Human DR3 was PCR amplified from vector DNA in both dominant negative (no death domain) and soluble (no transmembrane domain) forms. The genes were TOPO-TA cloned into the pCR2.1 vector. The genes were then cut from this vector using Spe1 and BamHI restriction enzyme sites which were engineered in the primers. Genes were then ligated into pDR2δEF1α and Signal pIgplus vectors.

A soluble form of the gene in which the transmembrane domain was absent was also PCR amplified. Three versions of the soluble gene were generated either with a Streptag sequence included or not. The third version of the soluble gene contained a Streptag sequence in which a stop codon was included after the Streptag sequence (primer sequences described in section 2.2). The 3 resulting PCR products were 711 base pairs, 681 base pairs and 714 base pairs in size respectively. The soluble versions of the gene were Topo cloned into the pCR2.1 Topo vector and sequenced to confirm they matched the published sequence (Figure 3.2).

### 3.3 Subcloning hDR3 into Eukaryotc Expression Vectors

In order to facilitate protein expression in an eukaryotic system, the PCR amplified hDR3 genes were subcloned into appropriate eukaryotic expression vectors. Dominant negative hDR3 was excised from the pCR2.1 Topo vector using Spe1 and BamHI restriction enzymes. The pDR2δEF1α vector was digested using Xba1 and BamHI (Spe1 and Xba1 produce compatible ends) restriction enzymes. The dominant negative hDR3 gene was then ligated into the pDR2δEF1α vector and re-sequenced to confirm that it still matched the published sequence (Figure 3.3).

Soluble hDR3 was excised from the pCR2.1 Topo vector using Spe1 and BamHI restriction enzymes and ligated into the Nhe1 and BamHI (Spe1 and Nhe1 produce compatible ends) enzyme sites in the Signal Pigplus vector. Soluble hDR3 was re-sequenced to confirm that it matched the published sequence (Figure 3.3).

**Figure 3.3**

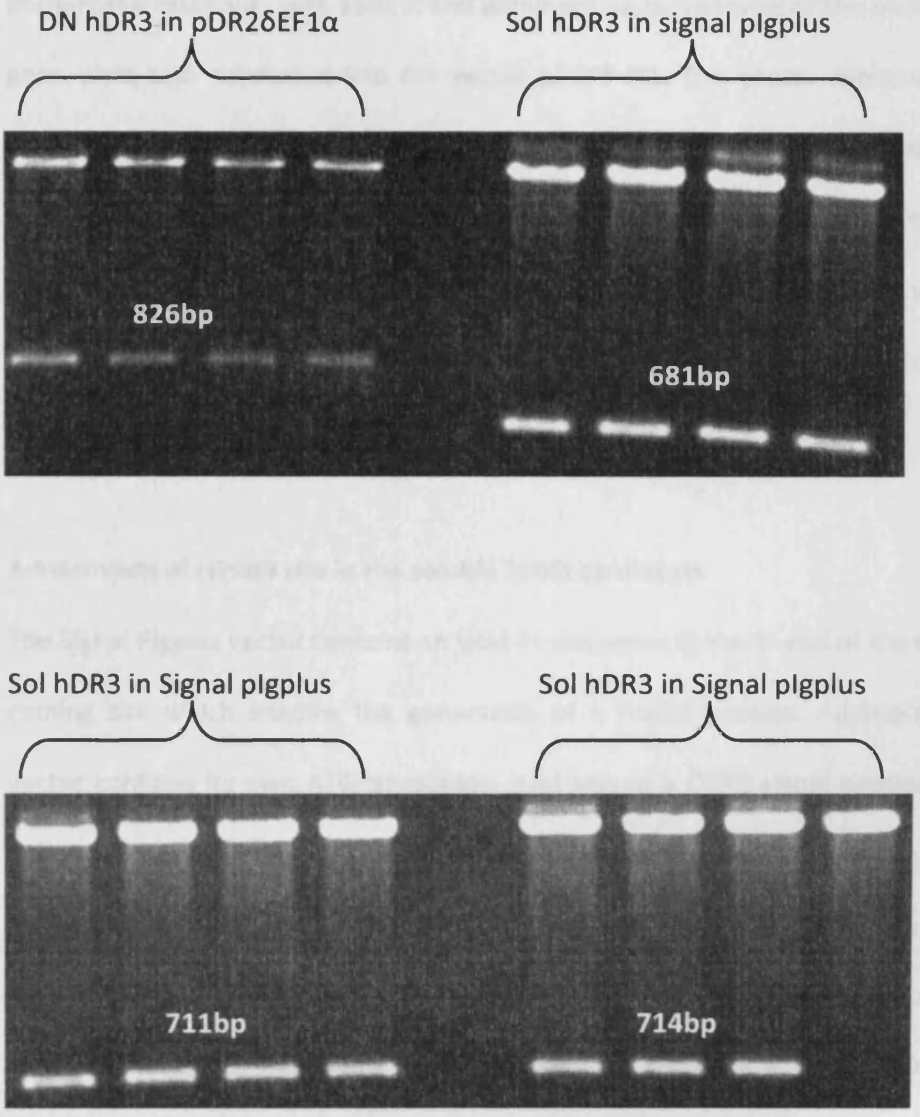


**Figure 3.3 Subcloning of hDR3 into eukaryotic expression vectors.** Agarose gel electrophoresis on 1% (v/v) TBE agarose gel. The successful cloning of dominant negative and soluble hDR3 into eukaryotic expression vectors is illustrated via restriction digest analysis. Upper bands show the vector and lower bands show the excised DR3 genes. Vectors analysed from 4 colonies for each gene insert. DN hDR3 was excised using BamHI/Xho1 and sol hDR3 was excised using BamHI/HindIII.

Due to the difficulties in detecting protein expression via Western blot and immunofluorescence, both soluble and dominant negative forms of the human DR3 gene were also subcloned into the vector pEGFP-N1. This vector contains a GFP sequence which enables the expression of GFP in an eukaryotic system and allows easy visualization of transfected cells using a fluorescence microscope. GFP is a large protein that may affect the folding or solubility of the protein of interest. However, it does enable confirmation of both a successful transfection protocol and a correctly inserted in frame sequence.

**3.4 Removal of HindIII site in the soluble hDR3 constructs**

The Signal Pigplus vector contains an IgG1 Fc sequence at the 3' end of the multiple cloning site which enables the generation of a fusion protein. Additionally the vector contains its own ATG translation start site in a CD33 signal peptide which enhances the secretion of soluble proteins. In order to generate a soluble protein with an IgG1 Fc tail, the amplified hDR3 PCR products must be cloned "in frame" with both the CD33 signal peptide and the IgG1 Fc tail. When the primers were originally designed, they were only engineered to generate a soluble hDR3 PCR product that would be "in frame" with the IgG1 Fc tail and not with the CD33 signal peptide. In order to correct this over sight, 1 or 4 bases needed to be removed from the sequence. A HindIII site was selected which was 5' of the hDR3 sequence and an unused enzyme site in the multiple cloning site. The HindIII site was digested with HindIII to generate a linear vector which was subsequently treated with Mung Bean nuclease which removes "sticky ends". The vector was then relegated via blunt end ligation and analysed for HindIII site removal by enzymatic digest with HindIII and

NotI. Those vectors in which HindIII had successfully been removed produced a linearised vector and those in which the HindIII site was retained produced an excised band of DNA which was 87bp in size. The successful removal of the HindIII site from all soluble hDR3 Signal Pigplus vectors is illustrated in Figure 3.4.

Figure 3.4

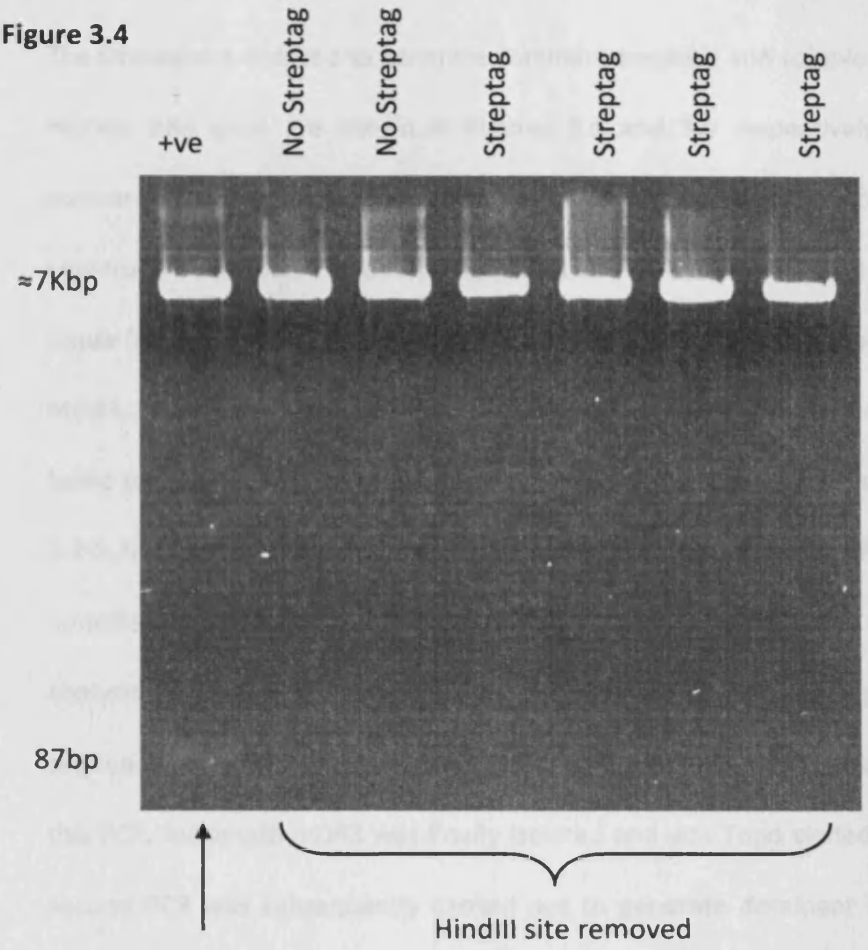


**Figure 3.4 Removal of HindIII sites from soluble hDR3 in signal pIgplus vectors.** Agarose gel electrophoresis on 1% (v/v) TBE agarose gel. In order to produce a DR3 gene sequence which was 'in frame' with the CD33 signal sequence in Signal pIgplus, the HindIII site in the vectors was digested and blunt ended via mung bean nuclease treatment prior to religation. Confirmation of removal of this enzyme site is illustrated via restriction digest analysis with HindIII and NotI.

### 3.5 PCR amplification of mDR3

The strategies employed to generate dominant negative and soluble versions of the murine DR3 gene are shown in Figures 3.5 and 3.6 respectively. Prior to the commencement of this work, the mDR3 gene was not available to us in a vector construct. Therefore, it had to be amplified via RT-PCR from murine tissue. Thymus tissue from C57BL/6 mice was chosen for RT-PCR as it has confirmed expression of mDR3. Despite multiple attempts at RT-PCR using many primer combinations, we failed to clone mDR3. Upon employment of the "slow-down" PCR method (Section 2.2.5.3) using primers described in Section 2.2, full length mDR3 was RT-PCR amplified and Topo cloned into the pCR2.1 Topo vector. However, upon sequence analysis, both exons 5 and 6 were found to be absent, corresponding to the sequence for mDR3 splice variant 3 (Wang et al., 2001a). Following 26 repeats of this PCR, full length mDR3 was finally isolated and was Topo cloned into pCR2.1. A second PCR was subsequently carried out to generate dominant negative mDR3 using the full length mDR3 gene in the Topo vector as a template. Xho1 and a BamHI restriction enzyme sites were engineered into the sequence. The resulting dominant negative mDR3 PCR product was 938bp in size and was Topo cloned into the pCR3.1 Topo vector (Figure 3.7). It was subsequently analysed to confirm that it matched the published sequence.

A naturally occurring soluble form of mDR3 exists as a splice variant of the full length receptor. This splice variant is termed variant 2 and is missing exon 6, which results in an early stop codon just upstream of the transmembrane domain. In order to investigate the role of this splice variant, the gene which encodes it was commercially manufactured by Genscript (USA) and used as a template to PCR amplify 3 versions of the gene either containing a c terminal streptag, an n terminal streptag or no streptag at all. Both n terminal and c terminal streptag constructs were generated in case one permitted greater protein detection than the other. All 3 genes were also engineered to contain an Xho1 and an Xba1 restriction enzyme site. The 3 resulting PCR products were 654bp, 656bp and 633bp in size and were Topo cloned into the PCR3.1 Topo vector (Figure 3.7). They were subsequently analysed to confirm that they matched the published sequence.

**Figure 3.5**

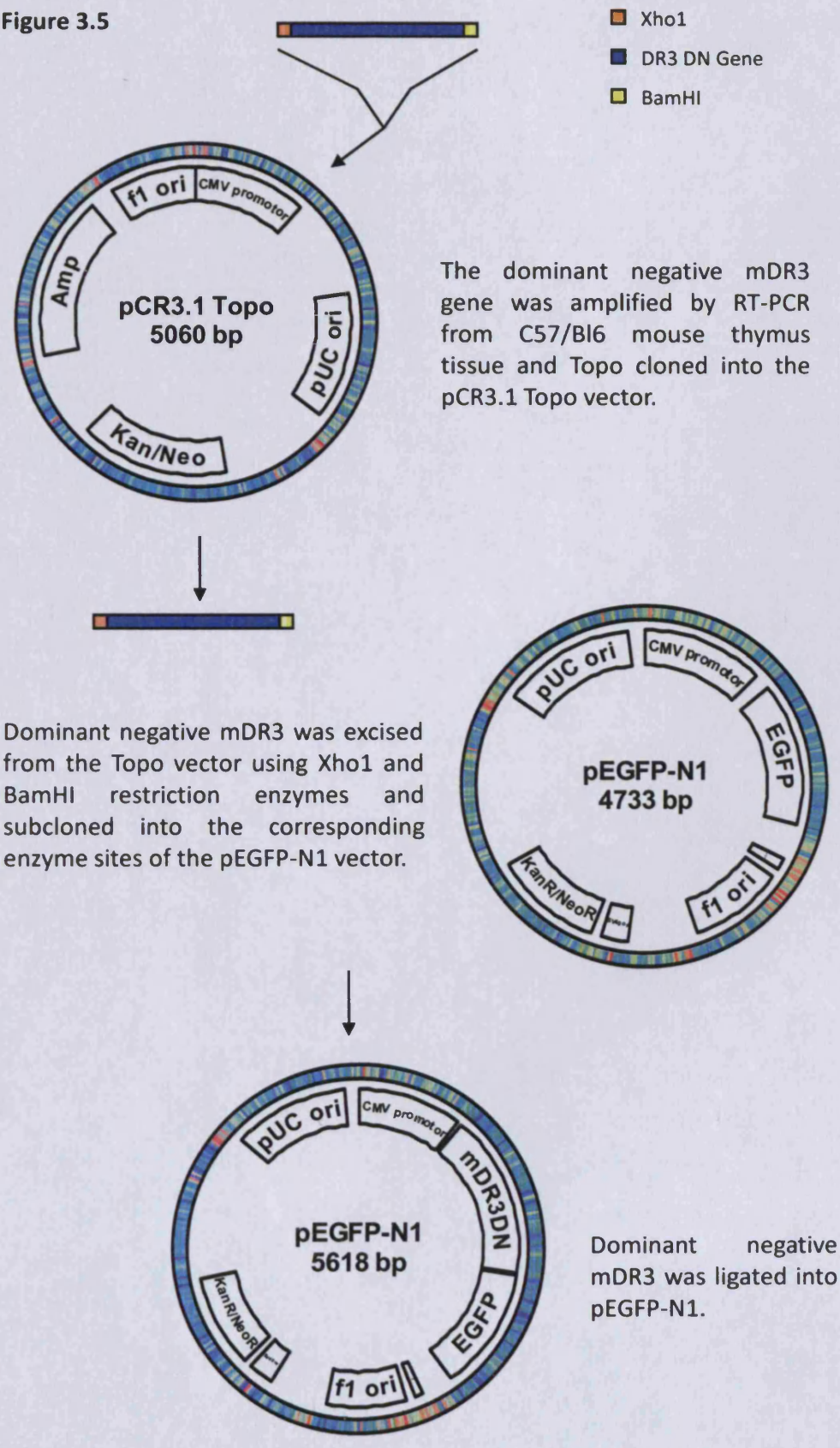


The dominant negative mDR3 gene was amplified by RT-PCR from C57/Bl6 mouse thymus tissue and Topo cloned into the pCR3.1 Topo vector.

Dominant negative mDR3 was excised from the Topo vector using Xho1 and BamHI restriction enzymes and subcloned into the corresponding enzyme sites of the pEGFP-N1 vector.

Dominant negative mDR3 was ligated into pEGFP-N1.

**Figure 3.5. Cloning strategy for mDR3 dominant negative construct generation.** Dominant negative murine DR3 was RT-PCR amplified from thymus tissue. The gene was TOPO-TA cloned into the pCR3.1 vector. The gene was then cut from this vector using Xho1 and BamHI restriction enzyme sites which were engineered in the primers and was then ligated into the Xho1 and BamHI sites of pEGFP-N1.

**Figure 3.6**

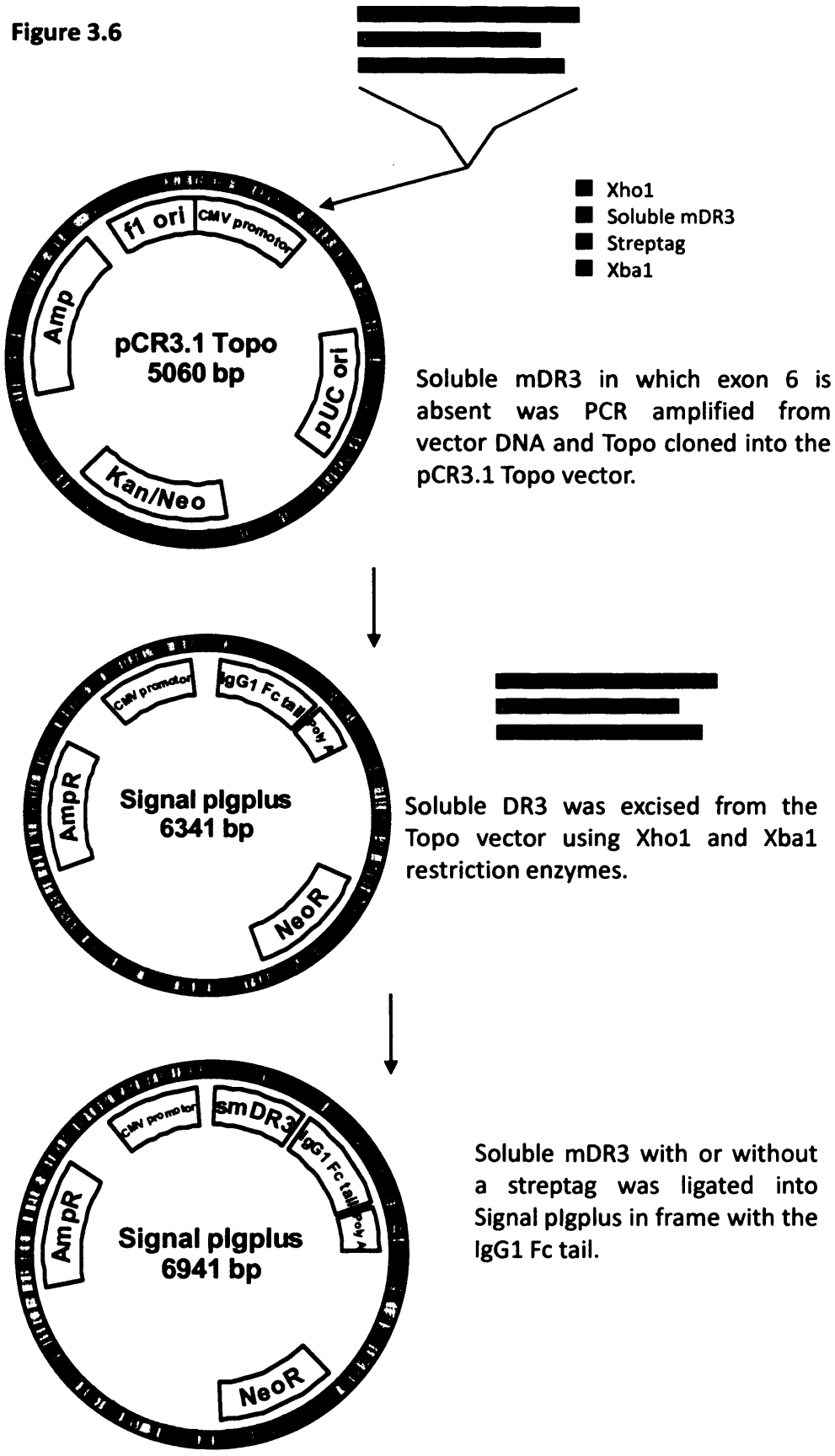


Soluble mDR3 in which exon 6 is absent was PCR amplified from vector DNA and Topo cloned into the pCR3.1 Topo vector.

Soluble DR3 was excised from the Topo vector using Xho1 and Xba1 restriction enzymes.

Soluble mDR3 with or without a streptag was ligated into Signal pIgplus in frame with the IgG1 Fc tail.

**Figure 3.6. Cloning strategy for soluble mDR3 construct generation.** Soluble murine DR3 was PCR amplified from vector DNA which included the complete mDR3 gene minus exon 6. Three products were generated either with no streptag, a c terminus streptag or an n terminus streptag. The genes were TOPO-TA cloned into the pCR3.1 vector. They were then cut from this vector using Xho1 and Xba1 restriction enzyme sites which were engineered in the primers and were then ligated into the Xho1 and Xba1 sites of signal plgplus.

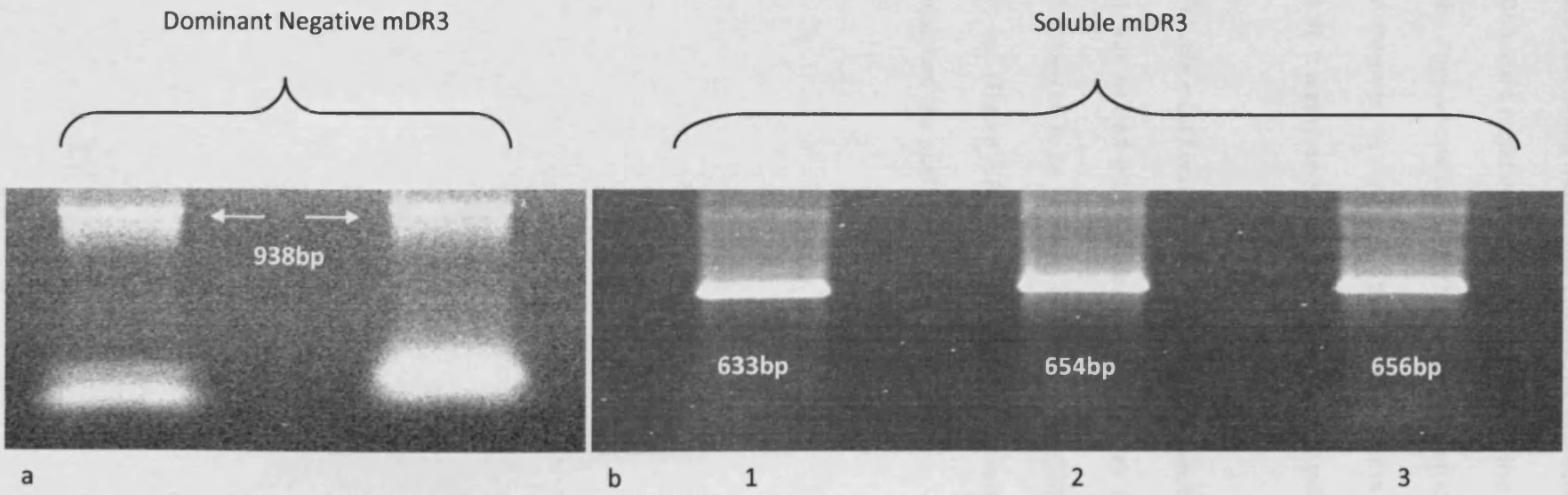


**Figure 3.7. RT-PCR and PCR amplification of dominant negative and soluble murine DR3.** Agarose gel electrophoresis on 1% (v/v) TBE agarose gel. The original amplification of mDR3 is illustrated. a) Dominant negative mDR3 shown at 938bp. b) Soluble mDR3 without (1) and with (2 and 3) streptag sequence included.

### 3.6 Subcloning mDR3 into Eukaryotic expression vectors

Dominant negative mDR3 was cloned into the pEGFP-N1 vector. It was excised from the Topo vector using Xho1 and BamHI restriction enzymes and subcloned into the corresponding sites in the pEGFP-N1 vector in frame with the GFP sequence (Figure 3.8). It was re-sequenced to confirm that it still matched the published sequence.

Soluble mDR3 was excised from the Topo vector using Xho1 and Xba1 enzyme sites. It was ligated into the corresponding sites in the Signal Pigplus vector and was engineered to be in frame with both the CD33 signal sequence and the human IgG1 Fc tail (Figure 3.8). The constructs were re-sequenced to ensure that mDR3 still matched the published sequence.

### 3.7 *In vitro* expression of human and murine DR3 constructs

The soluble and dominant negative hDR3 constructs were expressed in eukaryotic cell lines for the purpose of soluble protein production and antibody generation. Both NIH-3T3 cells (murine fibroblast cells) and CHO cells (Chinese hamster ovary cells) were used due to their ease of handling. Initially the Effectene method of transfection was used. However, when this resulted in a low transfection efficiency, the calcium phosphate method was used instead. Following this protocol, transfected cells grew well under selective media. A table indicating the hDR3 constructs that were transfected into mammalian cells is shown in table 3.1. Dominant negative hDR3 in the pDR2δEF1α was transfected into NIH-3T3 cells and protein expression via immunofluorescence against the streptag was achieved (Figure 3.9). However, the streptag protein was never detected via Western blot analysis. The soluble hDR3 constructs that were originally created were out of frame with the CD33 signal peptide and therefore no expression was detected. Following repair of these constructs, protein expression was detected via immunofluorescence against the streptag protein (Figure 3.9). Diffuse cytoplasmic staining was evident. The empty vector control also displayed a low level of background staining. However, Western blot detection of this protein was never achieved. Expression of soluble hDR3 in the pEGFP-N1 vector was also achieved (Figure 3.10) with transfected cells fluorescing green. From the cell lysate of these cells, both GFP and streptag could be detected by Western blot analysis (Figure 3.11). However, the soluble protein was never detected in the supernatant from the cells.

**Figure 3.8**

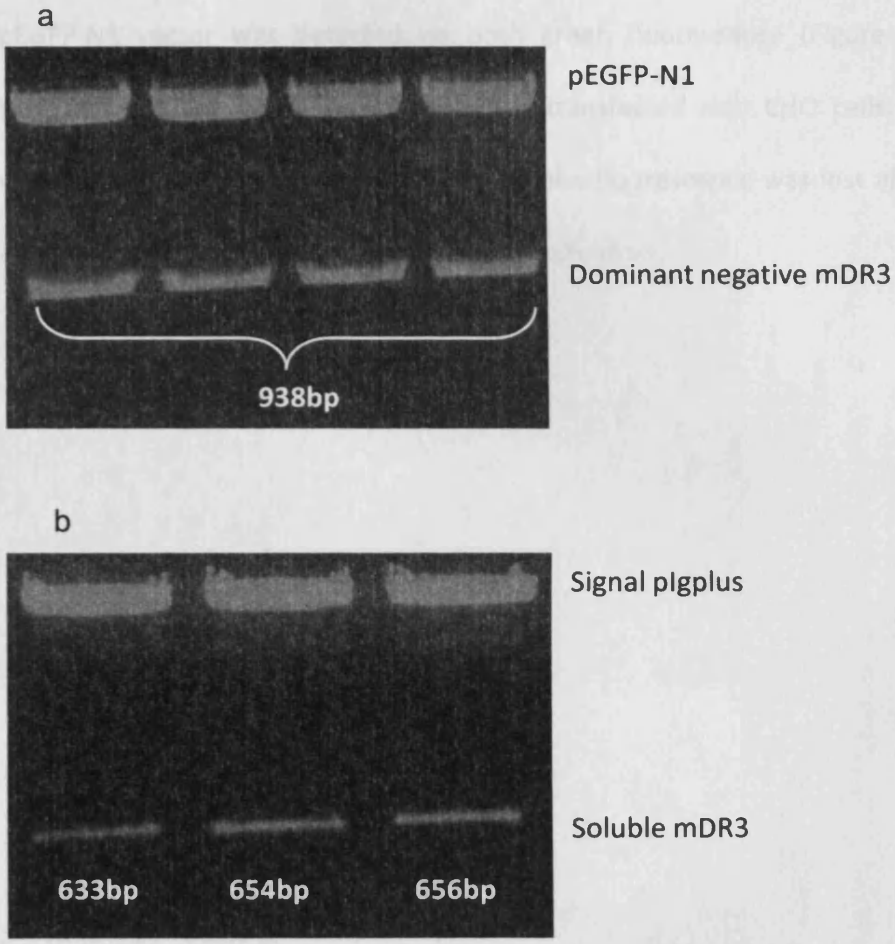


**Figure 3.8 Subcloning of mDR3 into eukaryotic expression vectors.** Agarose gel electrophoresis on 1% (v/v) TBE agarose gel. The successful cloning of (a) dominant negative and (b) soluble mDR3 (containing either no streptag, n terminal streptag or c terminal streptag) into eukaryotic expression vectors is illustrated via restriction digest analysis. Upper bands show vectors and lower bands show mDR3 gene inserts. DN mDR3 was excised using Xho1/BamHI and soluble mDR3 was excised using Xho1/Xba1.

A summary of the transfected murine DR3 constructs is shown in table 3.2. Soluble mDR3 with either an n terminal or a c terminal streptag transfected into CHO cells could not be detected via Western blot analysis. Dominant negative mDR3 in the pEGFP-N1 vector was detected via both green fluorescence (Figure 3.10) and Western blot analysis (Figure 3.11) when transfected into CHO cells. However, when transfected into NIH-3T3 cells, the green fluorescence was lost after 5 days and GFP was never detected via Western blot analysis.

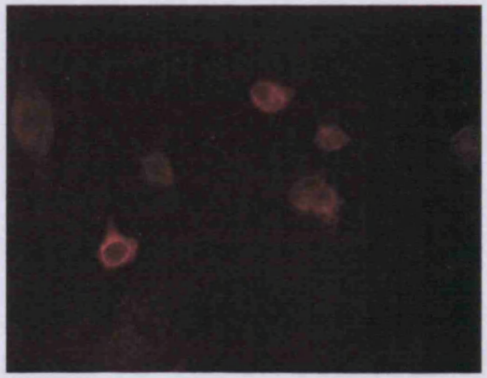

Dominant negative hDR3

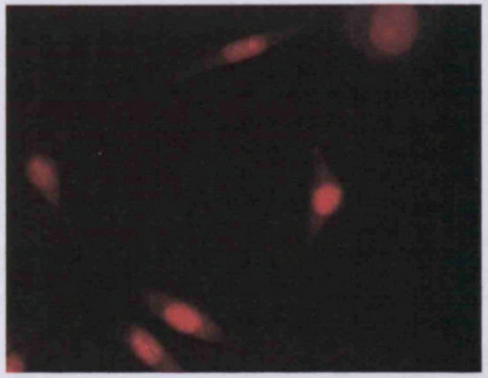

Soluble hDR3 + streptag

Soluble hDR3 + streptag + Fc

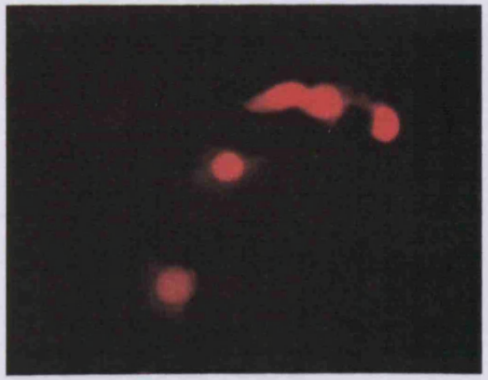

Empty vector control

**Figure 3.9. Detection of hDR3 constructs in 3T3 cells via anti-streptag immunofluorescence.** 3T3 cells transfected with hDR3 constructs exhibited positive staining for anti-streptage immunofluorescence. However, a low level of background fluorescence was also seen in the empty vector control.

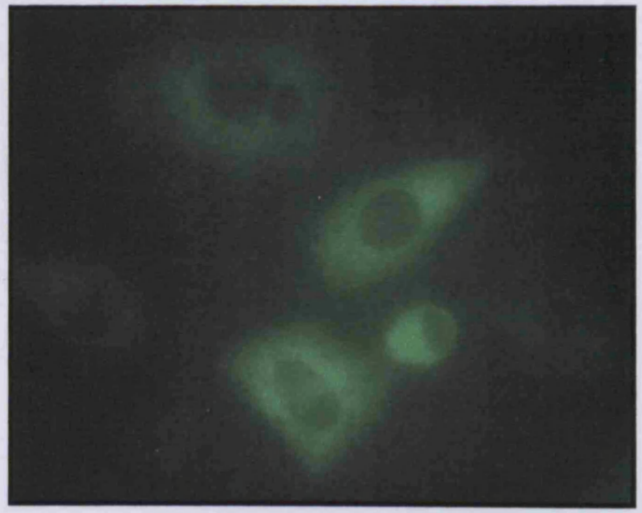

Sol hDR3 + streptag + GFP in pEGFP-N1

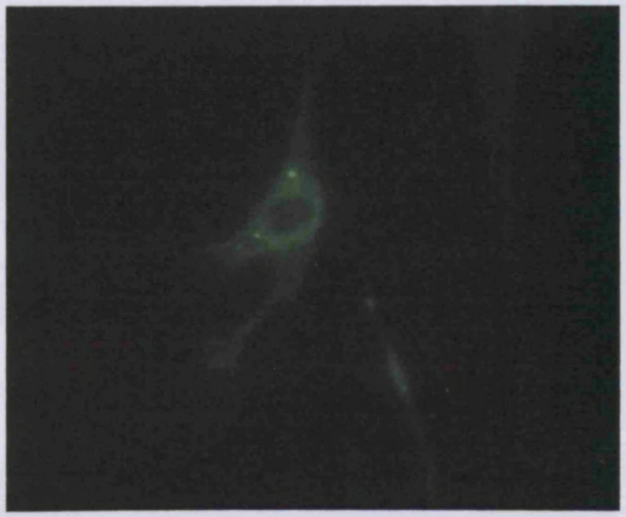

DN mDR3 + GFP in pEGFP-N1

**Figure 3.10. GFP expression from soluble hDR3 and dominant negative mDR3 pEGFP-N1 vector constructs in CHO cells.** CHO cells were transfected with pEGFP-N1 containing either sol hDR3 or DN mDR3. Transfected cells fluoresced green.

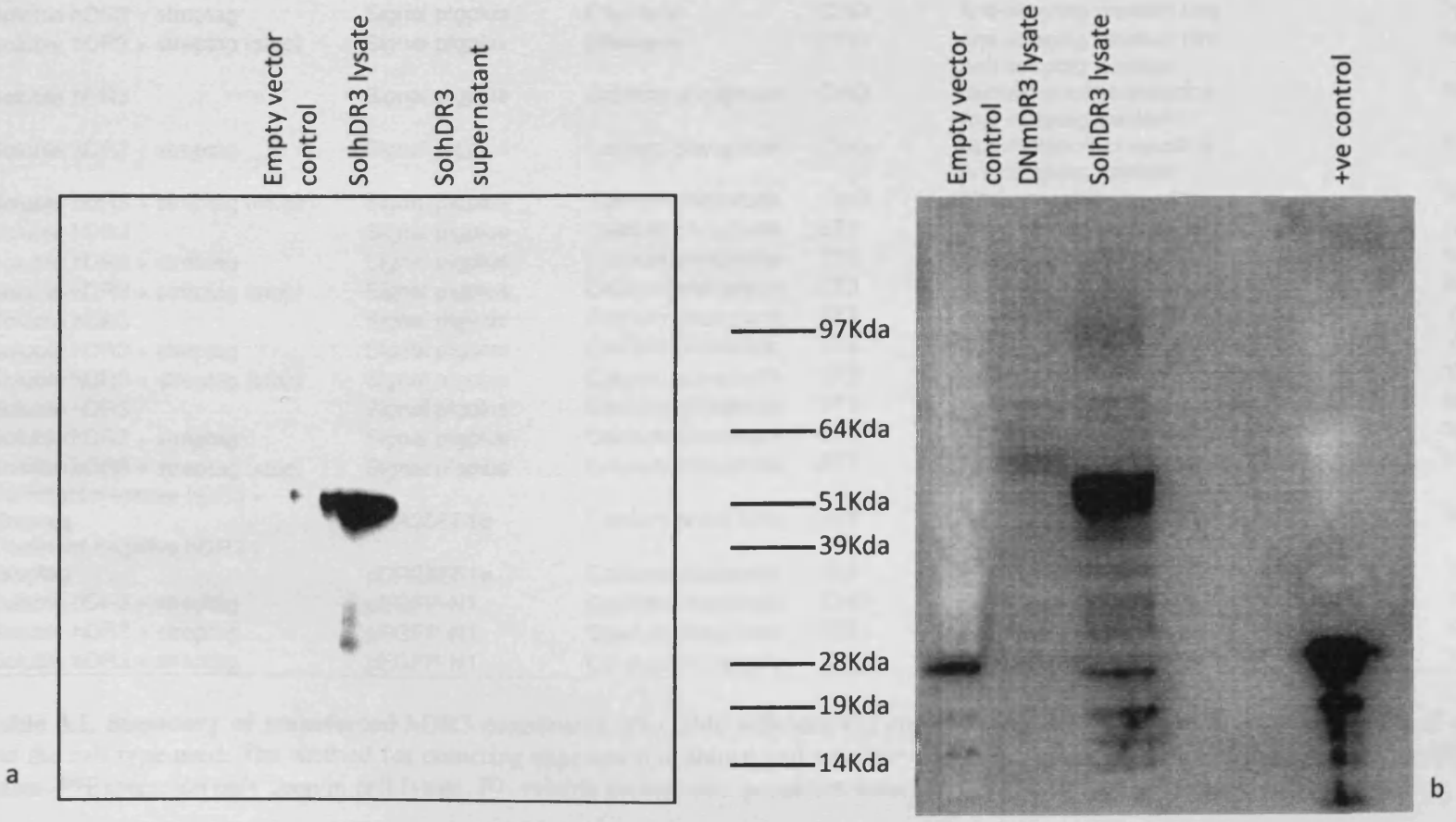


**Figure 3.11. Western blot detection of human and murine DR3.** Proteins were resolved by SDS-PAGE and subsequently transferred to a PVDF membrane. Soluble human DR3 containing a streptag in pEGFP-N1(49KDa) was detected with antibodies against both streptag (a) and GFP (b). Dominant negative murine DR3 in pEGFP-N1(61KDa) could only be detected with antibodies against GFP. All cell lysates were generated from 3T3 cells as described in section 2.4.1.1.

| Construct | Vector | Transfection Method | Cell type | Method of detection of expression | Expression |
|---|---|---|---|---|---|
| Soluble hDR3 | Signal plgplus | Effectene | CHO | Anti-streptag western blot | No* |
| Soluble hDR3 + streptag | Signal plgplus | Effectene | CHO | Anti-streptag western blot | No* |
| Soluble hDR3 + streptag (stop) | Signal plgplus | Effectene | CHO | Anti-streptag western blot | No* |
| Soluble hDR3 | Signal plgplus | Calcium phosphate | CHO | Anti-streptag western blot/immunofluorescence | No |
| Soluble hDR3 + streptag | Signal plgplus | Calcium phosphate | CHO | Anti-streptag western blot/immunofluorescence | No |
| Soluble hDR3 + streptag (stop) | Signal plgplus | Calcium phosphate | CHO | Anti-streptag western blot/immunofluorescence | No |
| Soluble hDR3 | Signal plgplus | Calcium phosphate | 3T3 | Anti-streptag western blot | No |
| Soluble hDR3 + streptag | Signal plgplus | Calcium phosphate | 3T3 | Anti-streptag western blot | No |
| Soluble hDR3 + streptag (stop) | Signal plgplus | Calcium phosphate | 3T3 | Anti-streptag western blot | No |
| Soluble hDR3 | Signal plgplus | Calcium phosphate | 3T3 | Anti-streptag immunofluorescence | Yes |
| Soluble hDR3 + streptag | Signal plgplus | Calcium phosphate | 3T3 | Anti-streptag immunofluorescence | Yes |
| Soluble hDR3 + streptag (stop) | Signal plgplus | Calcium phosphate | 3T3 | Anti-streptag immunofluorescence | Yes |
| Soluble hDR3 | Signal plgplus | Calcium phosphate | 3T3 | Anti-hDR3 polyclonal western blot | No |
| Soluble hDR3 + streptag | Signal plgplus | Calcium phosphate | 3T3 | Anti-hDR3 polyclonal western blot | No |
| Soluble hDR3 + streptag (stop) | Signal plgplus | Calcium phosphate | 3T3 | Anti-hDR3 polyclonal western blot | No |
| Dominant negative hDR3 + streptag | pDR2δEF1α | Calcium phosphate | 3T3 | Anti-streptag western blot | No |
| Dominant negative hDR3 + streptag | pDR2δEF1α | Calcium phosphate | 3T3 | Anti-streptag immunofluorescence | Yes |
| Soluble hDR3 + streptag | pEGFP-N1 | Calcium phosphate | CHO | Anti-streptag western blot | Yes** |
| Soluble hDR3 + streptag | pEGFP-N1 | Calcium phosphate | CHO | Anti-GFP western blot | Yes** |
| Soluble hDR3 + streptag | pEGFP-N1 | Calcium phosphate | CHO | GFP fluorescence | Yes |

**Table 3.1. Summary of transfected hDR3 constructs.** The table indicates the constructs which were transfected, the method of transfection and the cell type used. The method for detecting expression is shown and whether or not expression is achieved is indicated. *Sequence not in frame. **Expression only seen in cell lysate. No soluble protein in supernatant detected.

| Construct | Vector | Transfection Method | Cell type | Method of detection of expression | Expression |
|---|---|---|---|---|---|
| Soluble mDR3 + nt streptag | Signal plgplus | Effectene | CHO | Anti-streptag western blot | No |
| Soluble mDR3 + ct streptag | Signal plgplus | Effectene | CHO | Anti-streptag western blot | No |
| Dominant negative mDR3 | pEGFP-N1 | Effectene | 3T3 | Anti-GFP western blot | No |
| Dominant negative mDR3 | pEGFP-N1 | Effectene | 3T3 | GFP fluorescence | Yes* |
| Dominant negative mDR3 | pEGFP-N1 | Calcium phosphate | CHO | Anti-GFP western blot | Yes |
| Dominant negative mDR3 | pEGFP-N1 | Calcium phosphate | CHO | GFP fluorescence | Yes |
| Soluble mDR3 +CD33+Fc | pDR2δEF1α | Calcium phosphate | CHO | Anti-IgG1 Fc western blot | No |

**Table 3.2. Summary of transfected mDR3 constructs.** The table indicates the constructs which were transfected, the method of transfection and the cell type used. The method for detecting expression is shown and whether or not expression is achieved is indicated. *Green fluorescence was lost after 5 days.

### 3.8. Subcloning of human and murine soluble DR3 from the Signal Pigplus vector into pDR2δEF1α

Due to the difficulties in detecting expression of both human and murine DR3 in cell lines, soluble versions of the gene containing no streptag were re-amplified from the already generated genes in the Signal Pigplus vector. PCR primers were engineered to amplify the entire region in the Signal Pigplus vector that contained the CD33 signal sequence, the DR3 gene and the IgG1 Fc tail. A summary of this is shown in Figure 3.12. Restriction enzyme sites were also engineered in the primer sequences to enable ligation of the human and murine PCR products into Xba1/EcoRV and Spe1/EcoRV of pDR2δEF1α respectively. The EF1a promoter in the pDR2δEF1α vector is a very powerful promoter which coupled with the CD33 signal sequence from the Signal Pigplus vector should drive high expression of the soluble DR3 genes. Retaining the IgG1 Fc tail also permits the detection and purification of the protein. The PCR products containing soluble human (1523bp) or murine (1517bp) DR3 with the CD33 signal sequence and IgG1 Fc tail are shown in Figure 3.13.

The soluble murine DR3 containing the CD33 signal peptide and Fc tail in pDR2δEF1α was transfected into CHO cells and analysed for expression of the IgG1 Fc tail via Western blot analysis. Protein expression was not detected.

**Figure 3.12**

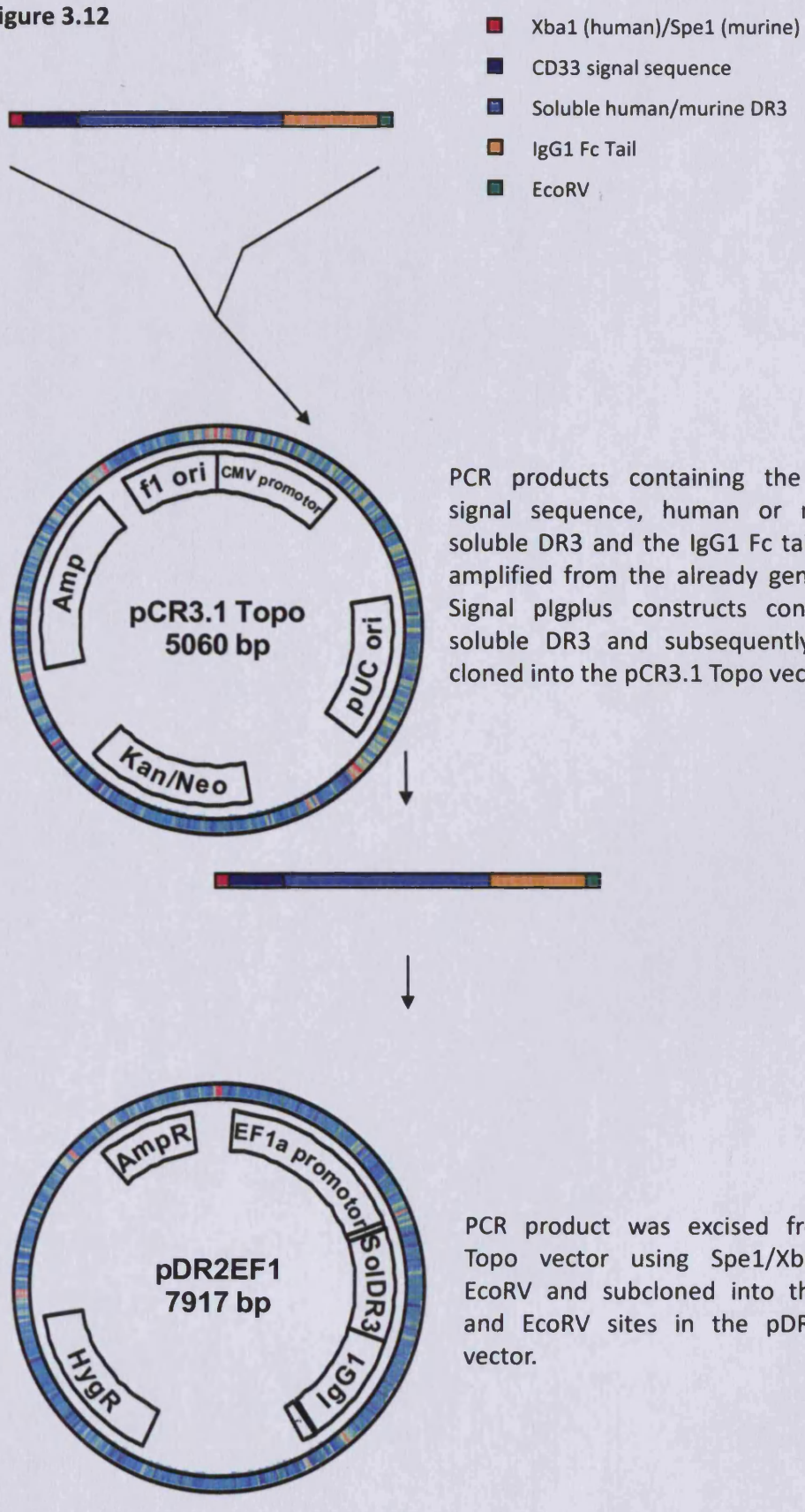


PCR products containing the CD33 signal sequence, human or murine soluble DR3 and the IgG1 Fc tail were amplified from the already generated Signal pIgplus constructs containing soluble DR3 and subsequently Topo cloned into the pCR3.1 Topo vector

PCR product was excised from the Topo vector using Spe1/Xba1 and EcoRV and subcloned into the Spe1 and EcoRV sites in the pDR2δEF1α vector.

**Figure 3.12. Cloning of soluble human and murine DR3 from Signal pIgplus to pDR2δEF1α.** Both human and murine soluble DR3 were re-amplified from the Signal pIgplus constructs using primers designed to include the CD33 signal sequence and IgG1 Fc tail in the PCR product. These were subsequently Topo cloned into the pCR3.1 vector and then subcloned into pDR2δEF1α in an attempt to increase soluble protein production.

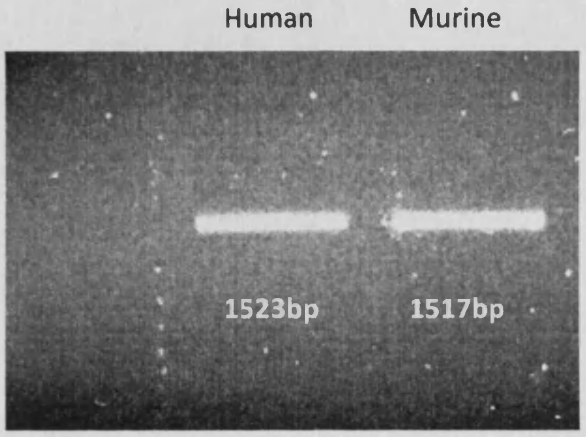


**Figure 3.13. PCR amplification of soluble human and murine DR3 from signal pIgplus.** Agarose gel electrophoresis on 1% (v/v) TBE agarose gel. Human and murine soluble DR3 were re-amplified from the signal pIgplus vector including the CD33 signal sequence and the IgG1 Fc tail.

# Results
# Chapter 4

## 4. Results – Generation of Antibodies

### 4.1 Introduction

At the commencement of this PhD there were no antibodies available against murine DR3 and there was only one polyclonal antibody available against human DR3. Therefore, in order to progress research in the DR3 field, the ultimate goal of DR3 reagent generation was the production of antibodies.

Initially, the strategy employed to generate antibodies involved the production of vector constructs containing human or murine DR3 genes in both soluble and dominant negative forms. These were used to transfect mammalian cells either to produce stable cell lines containing the dominant negative gene constructs or cells lines which produced soluble proteins. Using this strategy, animals could be immunised with either cell suspensions or soluble proteins in order to generate antibodies. However, as was highlighted in the previous chapter, difficulties were encountered in detecting successful transfections. As such, neither stable cell lines nor soluble proteins were generated.

A second strategy was employed to generate antibodies against murine DR3. Synthetic peptides based on the murine DR3 sequence were designed and ordered from an in-house supplier and used to immunise $DR3^{-/-}$ mice, in which normal antibody responses are unimpaired. Spleen cells from immunised mice were subsequently removed and fused with mouse myeloma cells in order to generate a continuous culture of antibody producing cells. This is based on the method of Kohler and Milstein (1975) who described the production of a sheep red blood cell

antibody producing cell line via the fusion of immunised mouse spleen cells and mouse myeloma cells (Kohler and Milstein, 2005). This method is now commonly employed in the process of antibody generation.

The aims of this chapter were:

1. To design immunoreactive peptides based on various regions of the murine DR3 protein sequence.
2. To immunise $DR3^{-/-}$ mice with the peptides in order to generate an antibody response within those mice.
3. To generate continuous antibody secreting cell lines via the fusion of spleen cells from immunised mice and a mouse myeloma cell line.

**4.2 Peptide Design**

Peptide sequences which were predicted to be antigenic were selected with the assistance of the online Peptide Select Tool (http://peptideselect.invitrogen.com) (Invitrogen), which aids in identification of peptides with high solubility and antigenicity and those which are likely to produce antibodies capable of recognising native protein. Due to time and cost restraints only peptides for mDR3 were generated, as antibodies against murine DR3 are more valuable to our current research than those against human DR3 as human DR3 reagents are now more widely available. Four peptide sequences were identified. Peptide 1 (casesqkrygpfccrgcpkghy) was located at amino acid position 40 – 61 in cysteine-rich domain 1. Using a structural analysis model, this region has previously been

predicted to be located on an exposed face of the native receptor (Newman et al., 2000) and thus represented a good sequence for generating antibodies capable of recognising native protein. Peptide 2 (gattpvheaptprpc) is located at position 147 – 167 in cysteine-rich domain 3. Cystein-rich domain 3 is the region which differs most significantly from the same region of other TNFRSF members including TNFR1 and FAS (Wang et al., 2001a) and is thus most likely to generate antibodies which are only specific for mDR3. Peptide 3 (lpgfyirgndc) is located at position 162 – 172 in cysteine-rich domain 4. This domain is absent from mDR3 splice variant 3 (Newman et al., 2000) and thus should generate antibodies which only recognise the remaining 2 splice variants. Peptide 4 (qpaglgalyaalermgleg) is located at position 380 – 398 in the death domain and thus should generate antibodies capable of detecting the full length receptor and variant 3 but not the soluble receptor. Peptides were generated by an in-house facility (Central Biotechnology Services, Cardiff University). The original synthesis of peptide 3 was not successful and therefore it was not used for immunisations. The selected peptide sequences are depicted in Figure 4.1. The peptides were generated on a poly-lysine core in order to avoid the use of a carrier protein and yet due to the high molecular weight of these molecules, still obtain a peptide with strong antigenic properties.

### 4.3 Immunisation of DR3$^{-/-}$ mice

DR3$^{-/-}$ mice were used for immunisation as they are devoid of DR3 and should generate immune responses against the peptides which shouldn't be recognised as self. DR3$^{-/-}$ mice received 2 initial sub-cutaneous injections containing a total of 100µg peptide emulsified in complete Freund's adjuvant. For each peptide, 2

separate mice were immunised. Mice received 2 booster immunisations of 100μg peptide emulsified in incomplete Freund's adjuvant and were subsequently tested for antibody production via tail bleed and an enzyme-linked immunosorbent assay (ELISA) analysis was performed to detect the presence of antibodies. Figure 4.2 illustrates the results of the first ELISA screen using blood plasma obtained from the tail bleed.

**Figure 4.1. mDR3 peptide sequences.** Peptide sequences are shown in red or blue type. The 4 cysteine-rich domains are labelled. The trans-membrane domain is higlighted in red and the death domain is highlighted in yellow.

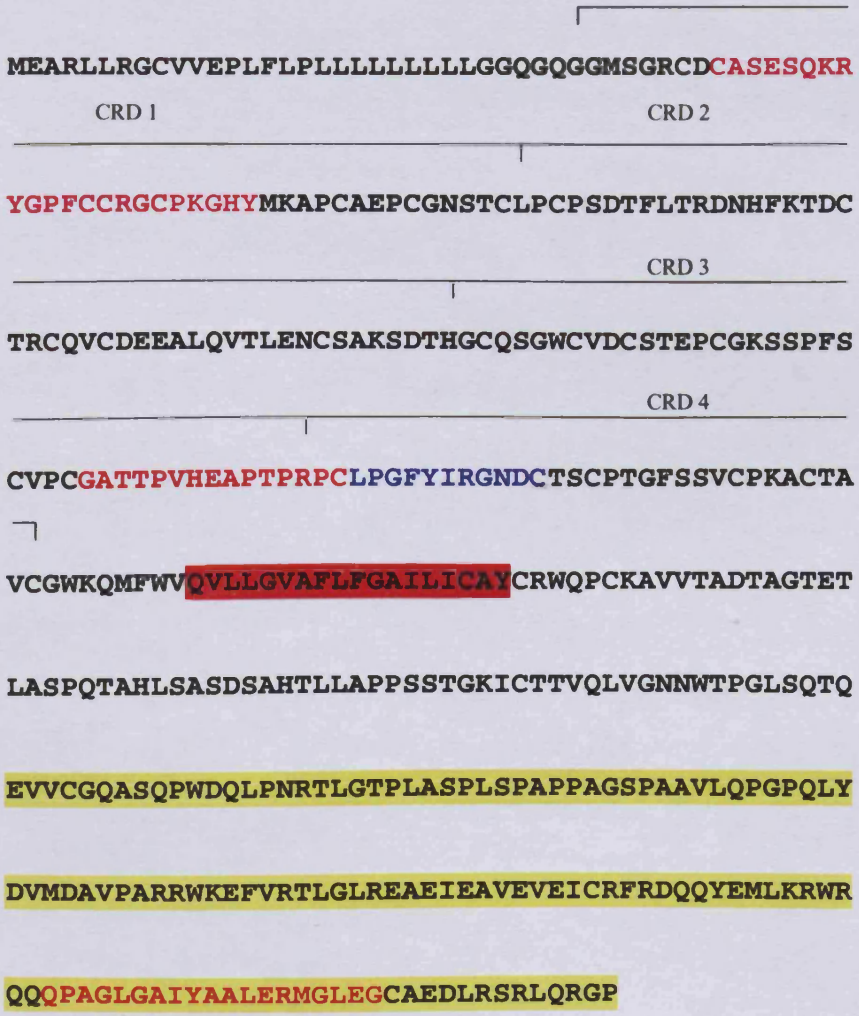

**Figure 4.2. Tail Bleed Screening 1**

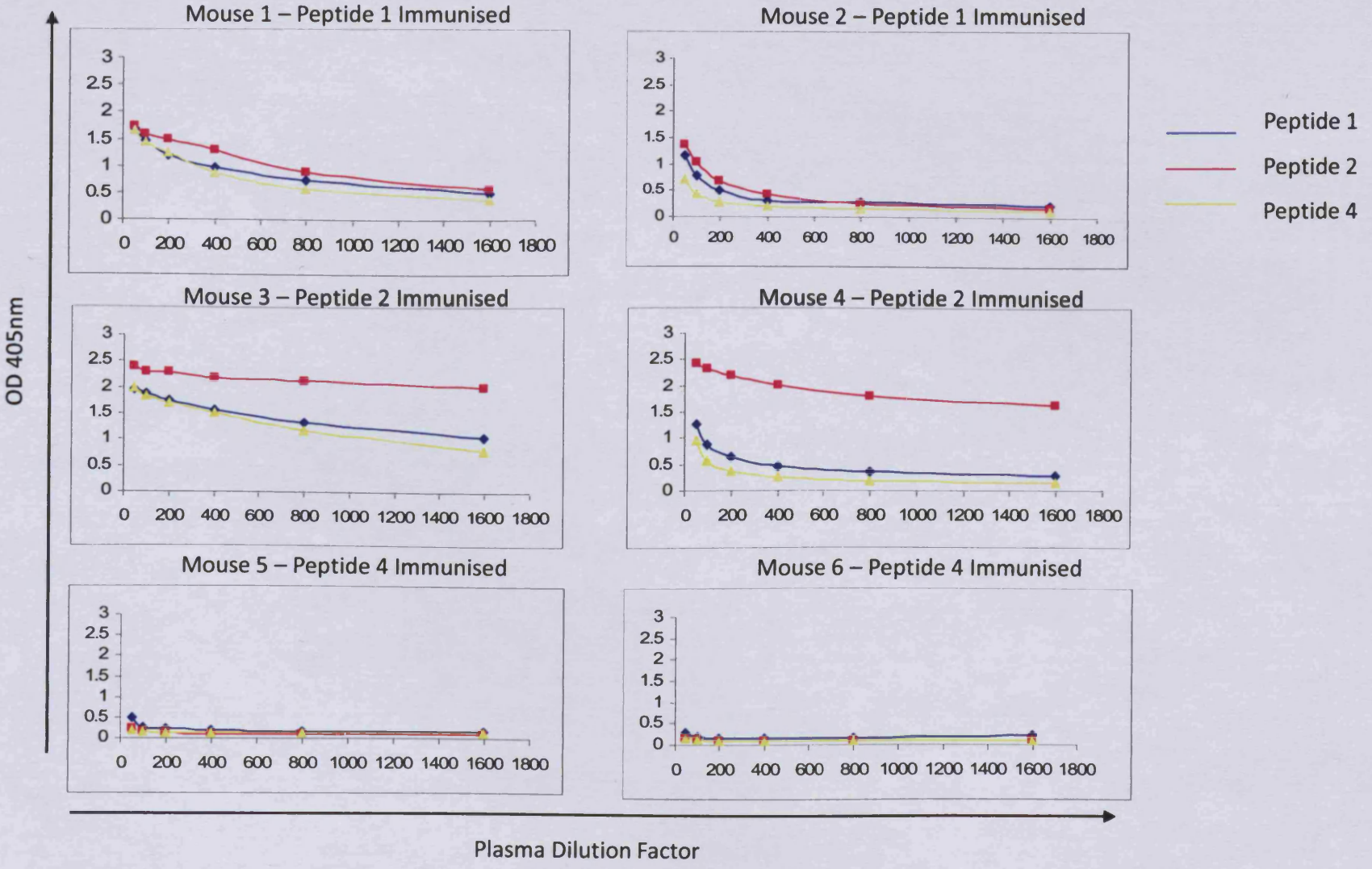

**Figure 4.2. Tail Bleed Screening 1.**

Results of the first plasma screening are shown. Peptide antigens were coated onto ELISA plates at a concentration of 10 μg/ml and were used to screen serially diluted tail bleed plasma samples from the immunised mice. Plasma from each mouse was screened against both the immunising peptide and the other 2 non-immunising peptides. Plasma from mice 1 and 2 generated similar reactions against all 3 peptides. Plasma from mice 3 and 4 appeared to react specifically with the immunising peptide. Plasma from mice 5 and 6 did not react with any of the peptides.

The original peptides were coated onto ELISA plates and then serially diluted plasma samples were incubated with the peptides in order to assess if any antibodies that reacted with the peptides were present. All plasma samples were screened against all peptides to give an indication as to whether any positive results were specific for the immunising antigen or a non-specific response. Mice 1 and 2, which were immunised with peptide 1, produced a comparable O.D.405nm against all 3 peptides and did not appear to be specifically generating antibodies against peptide 1. Mice 3 and 4, which were immunised with peptide 2, generated a higher O.D.405nm against peptide 2 than they did against peptides 1 and 4 and thus appeared to be producing peptide specific antibodies. Mice 5 and 6, which were immunised with peptide 4, did not appear to be producing any DR3 antibodies. Consistently low O.D.405nm values when screened against all peptides were observed. All mice were given two further booster immunisations over a 4 week period and were reassessed for antibody generation. The results of the second ELISA screen are shown in Figure 4.3. Mice 1 and 2 continued to fail to produce specific antibodies against peptide 1. Mice 5 and 6 similarly failed to produce antibodies against peptide 4. Mice 3 and 4 however appeared to be generating antibodies specific for peptide 2 and received 1 single final booster injection prior to sacrifice and spleen removal.

**4.4 Hybridoma Production**

Spleen cells obtained from mouse number 3 were fused with murine myeloma cells and cultured in selective media. Once visible clones had appeared in the wells, supernatant was removed and analysed for the presence of antibody. The

supernatants were screened against the immunising peptide (peptide 2) and also against a peptide which the mouse was not immunised with (peptide 1) to help determine specificity. Of the 720 wells in which the hybridomas cells were cultured, visible clones appeared in only 54.

**Figure 4.3. Tail Bleed Screening 2**

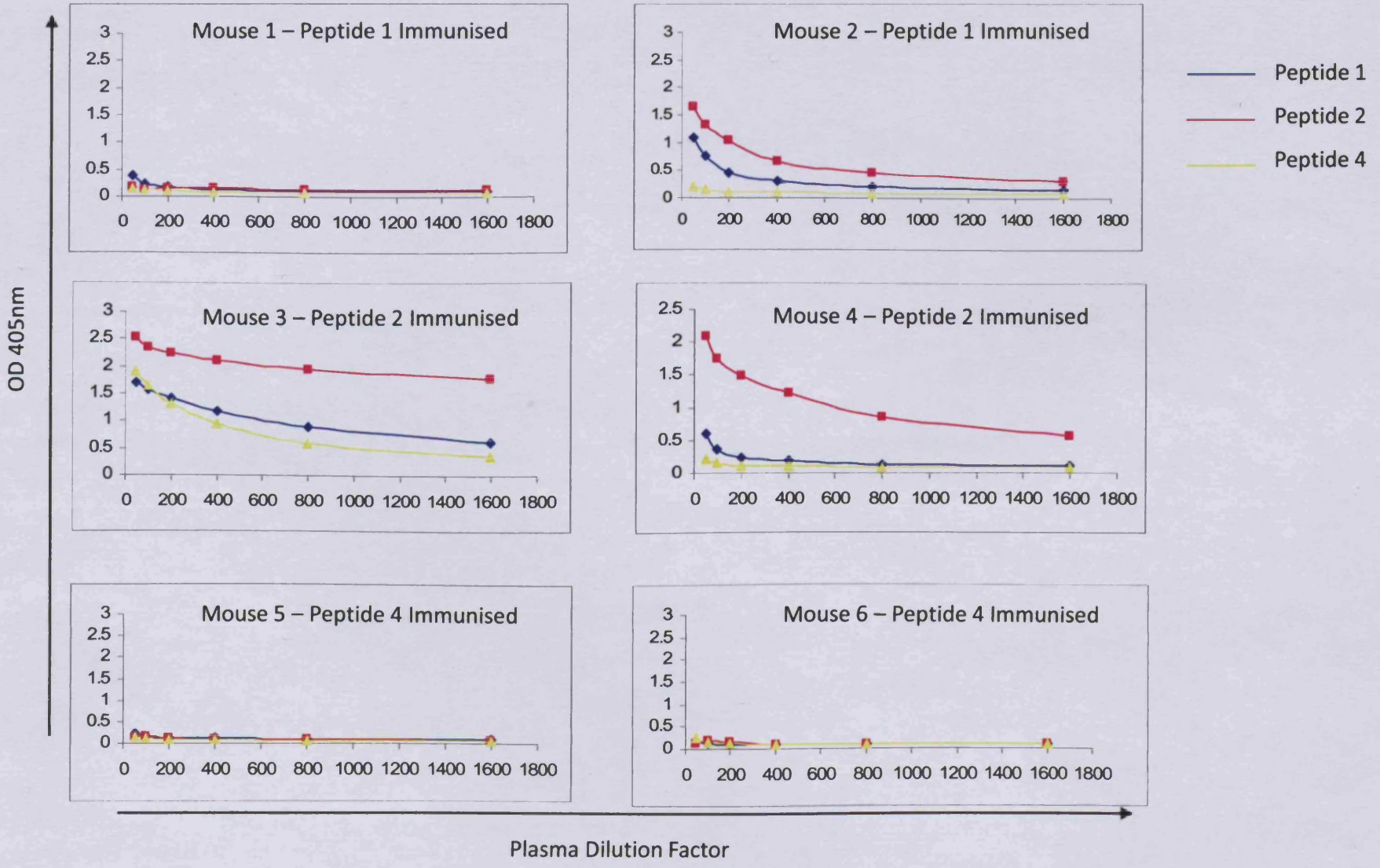

**Figure 4.3. Tail Bleed Screening 2.**

Results of the second plasma screening are shown. Peptide antigens were coated onto ELISA plates at a concentration of 10 μg/ml and were used to screen serially diluted tail bleed plasma samples from the immunised mice. Plasma from each mouse was screened against both the immunising peptide and the other 2 non-immunising peptides. Plasma from mice 1, 5 and 6 failed to react with any of the peptides. Plasma from mice 3 and 4 continued to react specifically with the immunising peptide. Plasma from mouse 2 did not react specifically with the immunising peptide.

Supernatants from all 54 clones were screened via ELISA against the immunising peptide (Figure 4.4). Of these, only 6 clones gave a positive result. These clones were cultured up into larger flasks and subsequently re-screened against the immunising (peptide 2) and non-immunising (peptide 1) peptides (Figure 4.5). All 6 clones displayed a non-specific affinity for the non-immunising peptide. Additionally, the O.D.405nm values were lower than had been seen before growing the clones up into larger cultures implying the presence of an over-growing non-antibody producing cell within the cultures. All clones apart from number 13 were discarded. As clone number 13 displayed the greatest specificity for the immunising peptide, it was maintained in culture for further analysis. However, these cells subsequently died.

**Figure 4.4. Hybridoma Screen via ELISA.** Supernatants from the hybridoma clones were screened against the immunising peptide (peptide 2). Samples in red were considered positive. Serum obtained from the immunised mouse was used as a positive control. Media from non-hybridoma cells was used as a negative control.

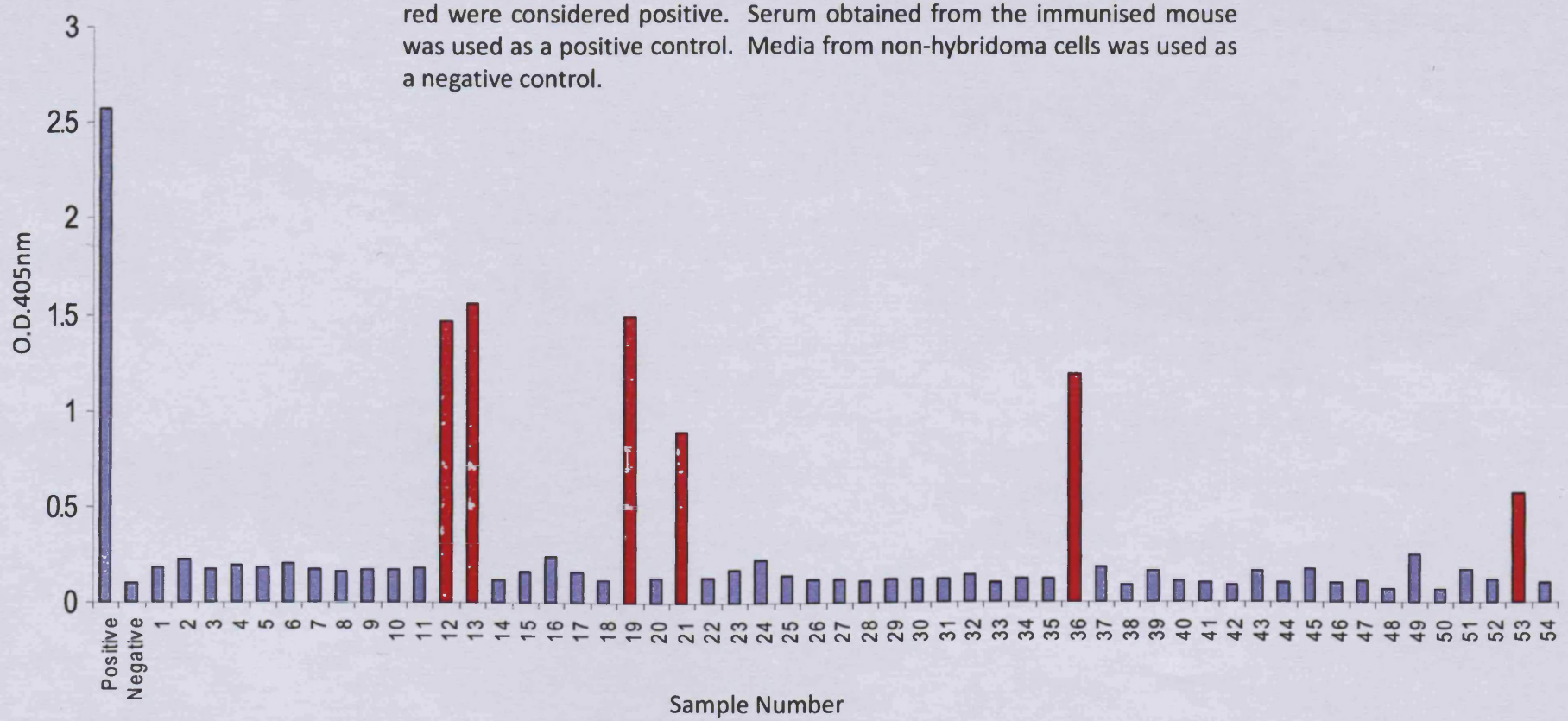

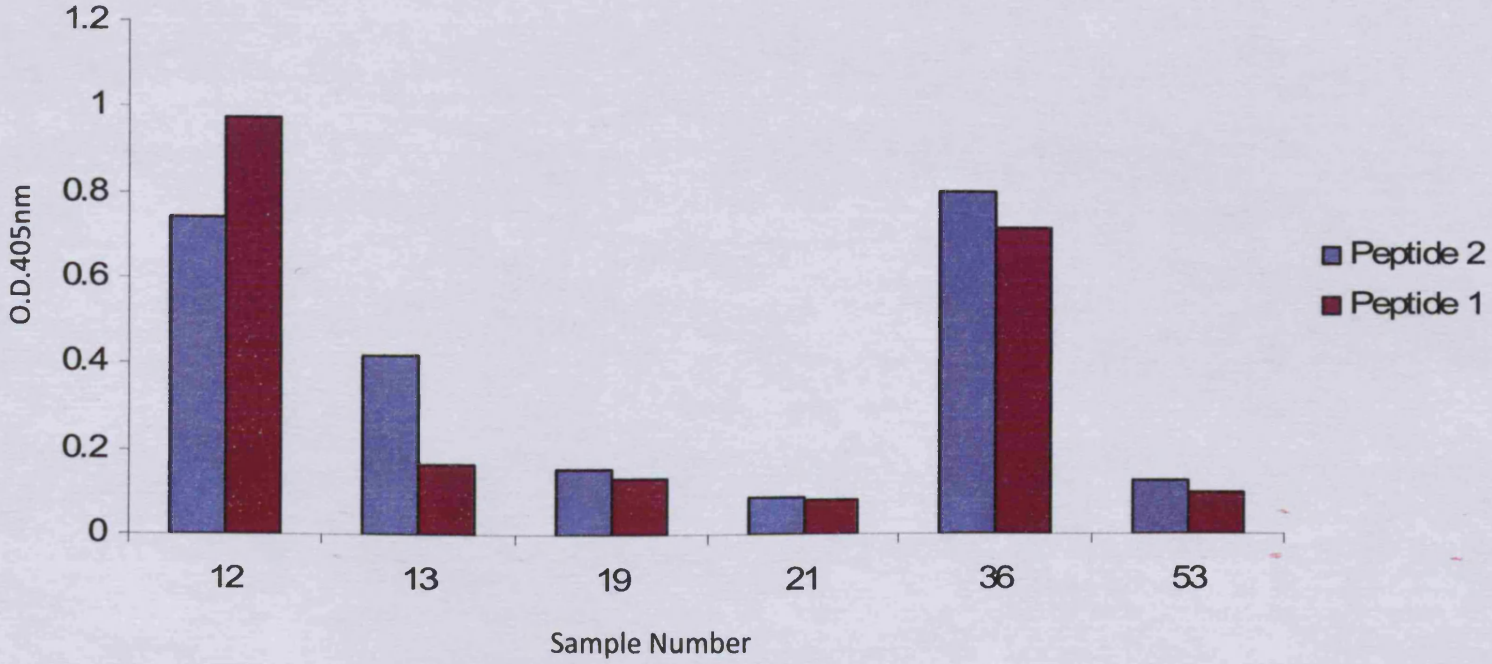


**Figure 4.5.** ELISA screen of positive samples against both immunising (peptide 2) and non-immunising (peptide 1) peptides. Supernatants from all clones were reactive against both peptides.

# Results
# Chapter 5

## 5. Characterisation of the susceptibility of DR3$^{-/-}$ mice to antigen-induced arthritis

### 5.1 Introduction

Rheumatoid Arthritis is a complex disease which, despite recent advances, is still poorly understood. Much focus and attention in the development of therapies for the treatment of RA has concentrated on blocking the TNFα/TNFR1 pathway. TNFα, via its interaction with TNFR1, is widely accepted as a central mediator in the pathogenesis of RA. Drugs such as Etanercept, a TNFR2-IgG Fc fusion protein that binds soluble and cell bound TNFα, and Infliximab, an anti-TNFα monoclonal antibody, are classed as disease modifying antirheumatic drugs (DMARDs) and are currently available for treatment of patients with RA (Jobanputra et al., 2002). In the most successful clinical trials, only 79% and 75% of patients achieved an ACR20 response with Infliximab and Etanercept respectively. Additionally, adverse reactions such as infections were also observed (Jobanputra et al., 2002). These studies indicate a need to develop novel therapies for Rheumatoid Arthritis which have a higher rate of success and lower incidence of infection.

The development of the aforementioned drugs was in large part permitted via the employment of *in vivo* models, which have been one of the most useful tools in enhancing our understanding of the disease. In 1992, a number of groups employed the CIA model for Rheumatoid Arthritis in order to support the rationale for anti-TNF therapy in treatment of the disease and to support already known *in vitro* data. In a study by Williams et al. (1992), the CIA model was induced in male DBA/1 mice to assess the effect of administering neutralizing antibodies against TNFα/β both before and after the onset of clinical disease. When treated weekly for four weeks

prior to the development of disease, mice displayed significantly reduced paw swelling and only 19% of joints were considered to have severe histopathological features compared with 71% of joints from control mice. Severely affected joints were defined as having extensive synovial hyperplasia and bone erosions with disruption of the overall joint architecture. Similarly, when mice were treated with the anti-TNF antibody after arthritic disease was established, a significant reduction in paw swelling was again observed, as well as a significant reduction in severely affected joints. There were, however, significantly more mildly affected joints in the treatment group, displaying minimal evidence of synovial hyperplasia and cartilage and bone loss (Williams et al., 1992). This study in an animal model therefore highlighted the potential use of anti-TNF agents not only in reducing the symptoms of swelling but also in preserving overall joint architecture and preventing bone destruction. The same group again used the CIA model in 1994 to illustrate a synergy between TNFα and CD4+ T cells in the progression of disease. It was found that both paw swelling and erosions of the joint were significantly reduced when mice were treated after the onset of disease with a combination of an anti-TNFα/β antibody and an anti-CD4 antibody when compared to either of these agents administered alone. Joint erosions were evident in 70-80% of joints analysed from mice receiving sub-optimal anti-TNF alone or anti-CD4 alone compared to only 22% of joints from mice receiving a combination of sub-optimal anti-TNF and anti-CD4 (Williams et al., 1994). This provided further important insight into the mechanisms of joint destruction during CIA and the possibility that this debilitating consequence of the disease might be treatable. The antigen-induced arthritis model has also been used to illustrate the role of TNF in Rheumatoid Arthritis. Lewthwaite et al.

(1995) employed the rabbit AIA model to induce arthritis via the use of the antigen ovalbumin. Over the 21 day timecourse, TNFα was detected in the joint fluid on day 1 post-arthritis induction and was detectable in the articular cartilage by day 3. Treatment of these animals with anti-TNFα neutralising antibodies over the first 3 days post-arthritis induction resulted in a dose-dependent reduction in swelling and leukocyte infiltration. Reduction in cartilage proteoglycan depletion however was not achieved at any antibody dose examined (Lewthwaite et al., 1995). Thus animal models of Rheumatoid Arthritis have been instrumental in enhancing our understanding of the disease, allowing an insight into the mechanisms of joint destruction and the evaluation of anti-TNF therapies which now have human benefit.

The antigen-induced arthritis (AIA) model is a local model of disease, which was first described in rabbits (Dumonde and Glynn, 1962) and later in rodents (Brackertz et al., 1977). In the first rabbit model, animals were immunised with the antigen fibrin emulsified in complete Freund's adjuvant, prior to intra-articular injection of the antigen in order to initiate an inflammatory response. Description of the changes observed in the joint tissue over a sixteen week period revealed a chronic inflammatory process, initiating in the first 48 hours with an infiltration of inflammatory cells and the development of cellular exudate. This was proceeded by the thickening of synovial tissue, which developed into pannus and the appearance of bone erosions within four weeks. Evidence of inflammation continued to be present within the joint throughout the period of the study. This investigation highlighted the similarities between the model and the human disease in terms of

chronicity, infiltration of immune cells and hyperplasia of the synovium (Dumonde and Glynn, 1962). The antigen-induced arthritis model in rabbits was further developed in 1971 using ovalbumin as the antigen, which was injected intra-articularly into pre-immunised rabbits. This study by Consden et al. (1971) sought to investigate the conditions necessary to generate a chronic experimental arthritis in terms of retention of antigen in the joint, the use of complete Freund's adjuvant during immunisations and the minimal dose of antigen required. Retention of antigen within the joint, as determined via radiolabelling, was greater in the immunised compared to the non-immunised animal. It took 7 days for the initial injection of 8mg ovalbumin to fall below 1μg in the non-immunised animal compared to over 100 days in the immunised animal. Antigen retention was also enhanced by the use of complete Freund's adjuvant compared to incomplete Freund's adjuvant corresponding with a greater degree of chronic arthritis. A minimal dose of 10μg of antigen injected intra-articularly was not sufficient for arthritis to develop (Consden et al., 1971). Using the evaluation of the ovalbumin model in rabbits, a similar model in rats and mice was developed.

The AIA model in mice was described in 1977. In this model the antigen methylated bovine serum albumin (mBSA) was used in mouse strains found to be susceptible (C57Bl and Balb/c). Mice were immunised on days 0 and 7 with 100μg mBSA in complete Freund's adjuvant prior to the induction of arthritis on day 21 via an intra-articular injection of 100μg aqueous mBSA. Pertussis toxin was also administered on day 0. This protocol generated a chronic arthritis with characteristic infiltration of immune cells, synovial hyperplasia and cartilage and bone erosion. This persisted

for up to 3 months before gradually subsiding. The arthritic response was specific to the antigen used for immunisation as intra-articular injection with a different antigen, namely methylated human gabba globulin, to mBSA immunised mice only elicited a minor reaction (Brackertz et al., 1977). Unlike CIA, AIA is not a systemic model of inflammation and thus has more limited similarities with the human disease. However, many of its features are consistent with human RA. Experimental AIA joints display a chronic inflammatory disease with marked cellular infiltration, synovial hyperplasia and the destruction of both bone and cartilage (Dumonde and Glynn, 1962). The pathogenesis of AIA is also dependent on both T cell and B cell responses. Transfer of T cells from mBSA immunised mice to severe combined immunodeficient (SCID) mice rendered SCID mice susceptible to antigen-induced arthritis, implying a central role for T cells in the pathogenesis of the disease (Petrow et al 1996). Reduction in anti-mBSA titres are also correlated with a reduced severity of disease indicating an important role for B cells and antibody production. Since the development of this model in mice, it has been utilised in a number of studies to aid progression in the Rheumatoid Arthritis field.

The aim of this chapter was to evaluate the role of DR3 in RA using $DR3^{-/-}$ mice in the antigen-induced arthritis model. The availability of $DR3^{-/-}$ mice has provided a sound opportunity to investigate the role of DR3 signalling in a murine model of inflammatory joint disease. The susceptibility of $DR3^{-/-}$ mice and littermate controls to the AIA model is described, as assessed by routine methods. Animals were monitored for joint swelling and histopathological changes within the joint.

Additionally, the effect of administering the ligand TL1A into the joint on day 0 of the model was analysed. Specifically the aims of this chapter were:

- To induce the AIA model for Rheumatoid Arthritis in DR3 deficient mice.
- To analyse the pathological changes resulting from this model in $DR3^{-/-}$ mice using histological techniques.
- To determine if the pathological response to the model in $DR3^{-/-}$ mice is DR3 specific using the ligand TL1A.

## 5.2 Results

### 5.2.1 Anti-mBSA antibody responses were comparable between $DR3^{+/+}$ and $DR3^{-/-}$ mice

A positive correlation between serum antibody titres and severity of arthritis in the AIA model has been reported (Cooke and Jasin, 1972). The anti-mBSA antibody titres were therefore analysed in both $DR3^{+/+}$ and $DR3^{-/-}$ mice via ELISA. At day 21 post-arthritis induction, serum anti-mBSA levels were not found to be significantly different between $DR3^{+/+}$ and $DR3^{-/-}$ mice ($p>0.05$ Unpaired t-test) (Figure 5.1). It was therefore assumed that AIA could be successfully induced in both groups of mice.

### 5.2.2 AIA was induced in $DR3^{+/+}$ and $DR3^{-/-}$ mice with 100% incidence but joint swelling decreased at a faster rate in DR3 deficient animals

To investigate the degree of joint swelling in DR3 sufficient and DR3 deficient mice, AIA was induced in the right knee joints of these animals. Prior to the induction of disease on day 0, baseline knee diameter measurements were taken using a micrometer. Average baseline knee joint diameters of DR3 sufficient mice measured 4.75mm and 4.72mm for right and left knee joints respectively. Those for DR3 deficient mice measured 4.89mm and 4.94mm and were not significantly different from $DR3^{+/+}$ mice. $DR3^{+/+}$ mice and $DR3^{-/-}$ mice pre-immunised with mBSA in CFA, were given an intra-articular injection of mBSA into the hind right knee joint on day 0 of the experiment. Post-arthritis induction, joint swelling was measured (using a micrometer) as the difference between hind right and hind left knee joint

diameters. Swelling of the AIA knee joint gave an indication of the successful induction of disease.

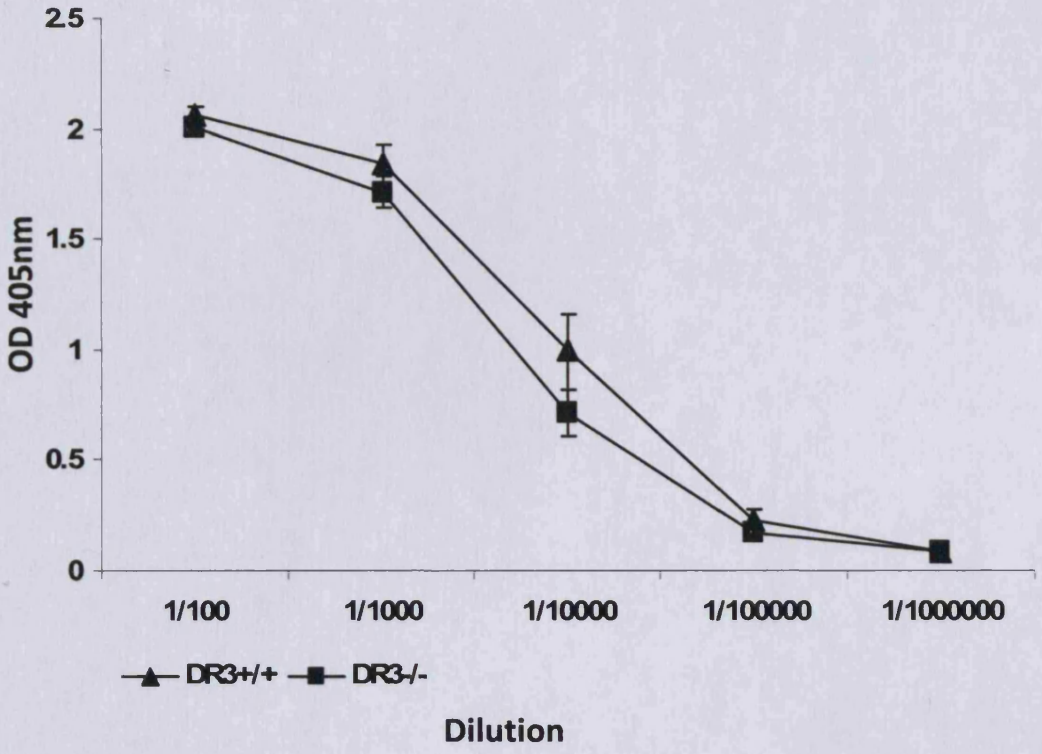


**Figure 5.1. Anti-mBSA antibody concentrations.** Serum concentrations of anti-mBSA antibodies were analysed via ELISA using mice sacrificed on day 21 post-arthritis induction. 5μg/ml mBSA was coated onto ELISA plates for 24 hours. Sera was diluted as indicated in 5% (w/v) milk extract in PBS containing 0.1% Tween 20. Data are mean ± SEM, n = 6. Levels of antibodies in $DR3^{-/-}$ mice were found to be normal when compared to $DR3^{+/+}$ mice when analysed using a t-test.

All $DR3^{+/+}$ mice responded to intra-articular injection of antigen (mBSA) and exhibited joint swelling. A peak of inflammation was observed on day 1 post-arthritis induction, with joint size increasing from average baseline diameters of 4.7mm up to a maximum of 6.8mm. Mean peak joint swelling measured as the difference between right and left knee joints, was 1.72mm. Following this peak, inflammation subsequently decreased over the course of the experiment returning to baseline levels on day 14.

All $DR3^{-/-}$ mice similarly responded to AIA induction and reached a peak joint swelling on day 1 post-arthritis induction. The maximum joint diameter observed reached 6.9mm. Mean peak joint swelling in DR3 deficient animals was 1.67mm. Inflammation decreased over subsequent days returning to baseline levels on day 7 post-arthritis induction.

The pattern of joint swelling over the 21 day experiment was comparable between $DR3^{+/+}$ and $DR3^{-/-}$ mice, both reaching a peak on day 1 and subsequently decreasing (Figure 5.2). Peak swelling was also comparable in $DR3^{+/+}$ (1.72mm) and $DR3^{-/-}$ (1.67mm) mice. However, swelling decreased at a faster rate in the absence of DR3, returning to baseline levels on day 7 post-arthritis induction compared to day 14 in DR3 sufficient mice. Joint swelling over the 21 day time period was significantly lower in $DR3^{-/-}$ mice compared with controls when analysed using a Two-Way Anova. Therefore, although $DR3^{-/-}$ mice exhibited a similar pattern of joint swelling in response to AIA induction, swelling decreased at a faster rate than in control mice over the course of the experiment.

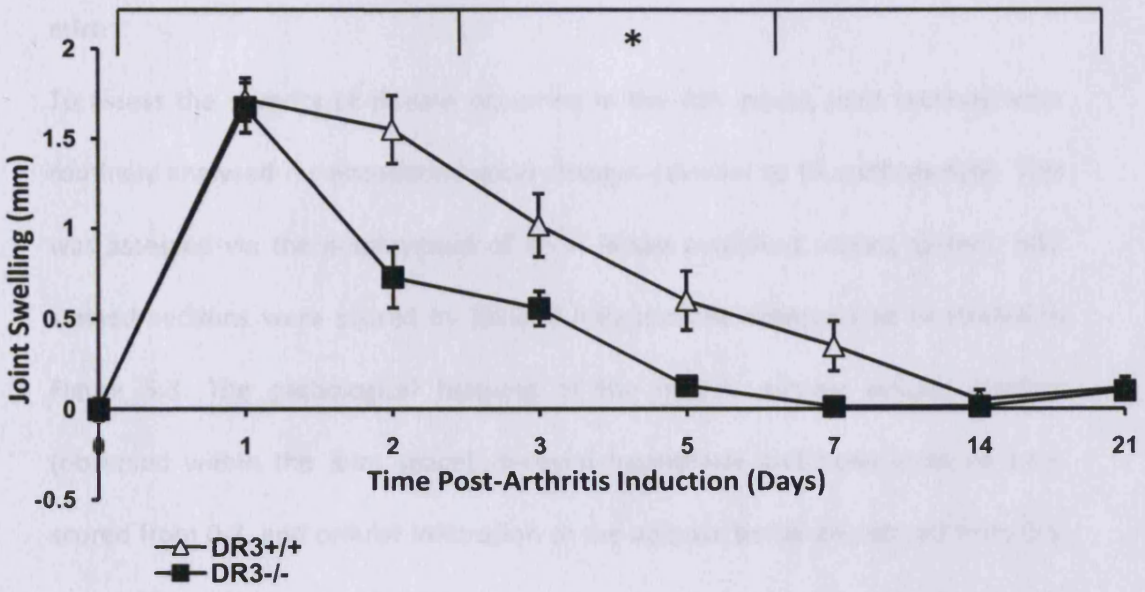


**Figure 5.2. Joint Swelling in Response to intra-articular mBSA injection.** Joint swelling, measured using a digital micrometer as a comparison between AIA joint (right knee) and normal joint (left knee), was measured over a 21 day time period in mice induced with AIA. Data are mean ± SEM, n = 6. Statistical analysis was performed using a two-way ANOVA. Joint swelling curves were significantly different between $DR3^{-/-}$ and $DR3^{+/+}$mice over the 21 day timecourse , as indicated by the upper bar. * $p<0.05$.

### 5.2.3 Early joint pathology does not differ significantly between DR3$^{-/-}$ and control mice

To assess the severity of disease occurring in the AIA model, joint sections were routinely analysed for histopathological changes relevant to RA pathogenesis. This was assessed via the employment of an in house published scoring system. H&E stained sections were scored by blinded independent observers as illustrated in Figure 5.3. The pathological features of the model, namely cellular exudate (observed within the joint space), synovial hyperplasia and bone erosions were scored from 0-3, and cellular infiltration of the adipose tissue was scored from 0-5, with 0 representing a normal joint. Total scores were summed to give the arthritis index (AI).

H&E stained sections taken from joints of mice sacrificed on day 3 post-arthritis induction were assessed for severity of arthritic disease according to the arthritis index. DR3$^{+/+}$ mice displayed cellular exudate within the joint space and had significant infiltration of inflammatory cells into the adipose tissue (Figure 5.4a). At this time point, only minor synovial hyperplasia and bone erosions were evident.

Joint sections from DR3$^{-/-}$ mice on day 3 post-arthritis induction displayed cellular exudate within the joint space and infiltration of cells into the adipose tissue (Figure 5.4b). There was only very minor synovial hyperplasia and no bone erosions. Comparison of the arthritis index between DR3 sufficient and deficient animals at this stage showed no significant difference using a Mann-Whitney U test ($p>0.05$)

(Figure 5.5a). All individual parameters of the arthritis index were comparable and also showed no significant differences ($p>0.05$) (Figure 5.5b).

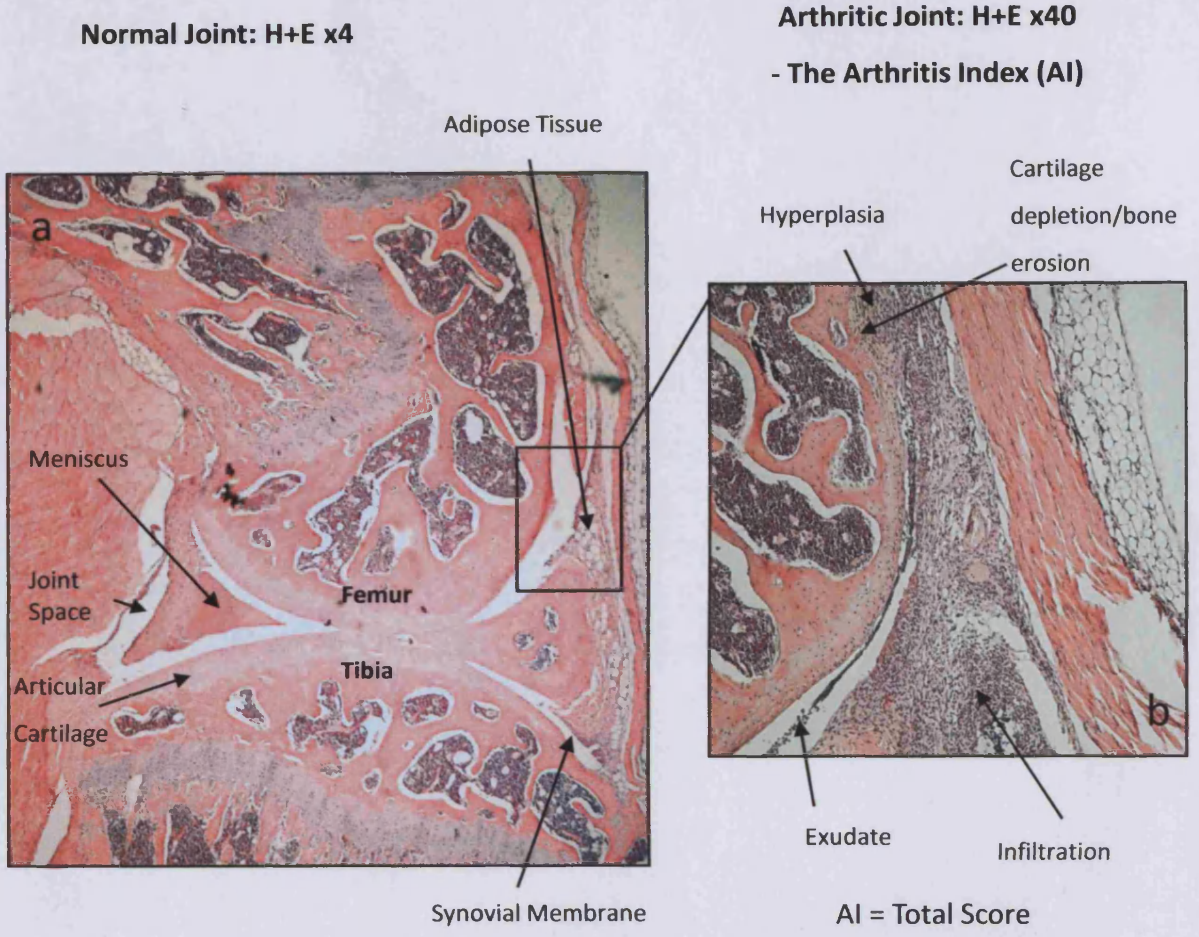


**Figure 5.3. The arthritis index.** H&E stained joint sections illustrating the method of analysis of the arthritis index (AI). a) A normal non-diseased joint illustrating the overall anatomy of the murine knee joint (x4). b) A diseased joint illustrating the parameters that were assessed in determining the AI (x20). Individual features of arthritic disease were scored (cellular exudate (0-3), cellular infiltration (0-5), synovial hyperplasia (0-3), bone erosions (0-3)) and summed to give the arthritis index. This method of assessment was used routinely in analysis of joint pathology within AIA and control joints. Sections were assessed by 2 blinded independent observers.

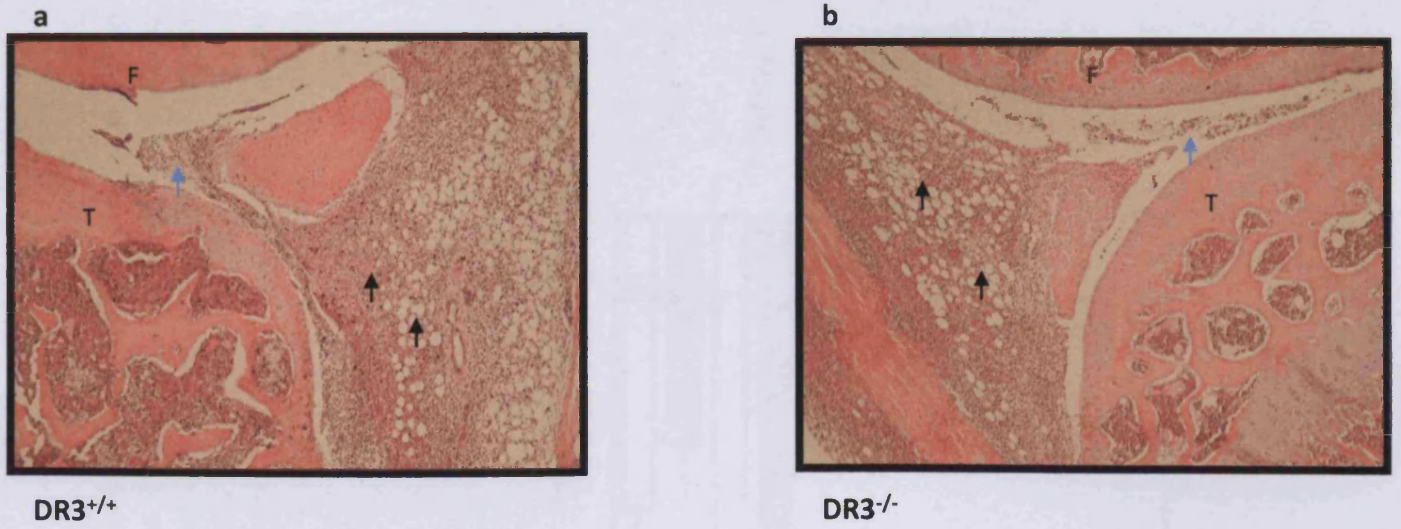


**Figure 5.4. H&E Stained Joint Sections from Animals Sacrificed on Day 3.** Joint sections were H&E stained and analysed for AI. Images were captured at x20 magnification. Cellular infiltration (black arrows) and cellular exudate (blue arrows) were evident in both $DR3^{+/+}$ (a) and $DR3^{-/-}$ (b) mice. F = femur, T = tibia.

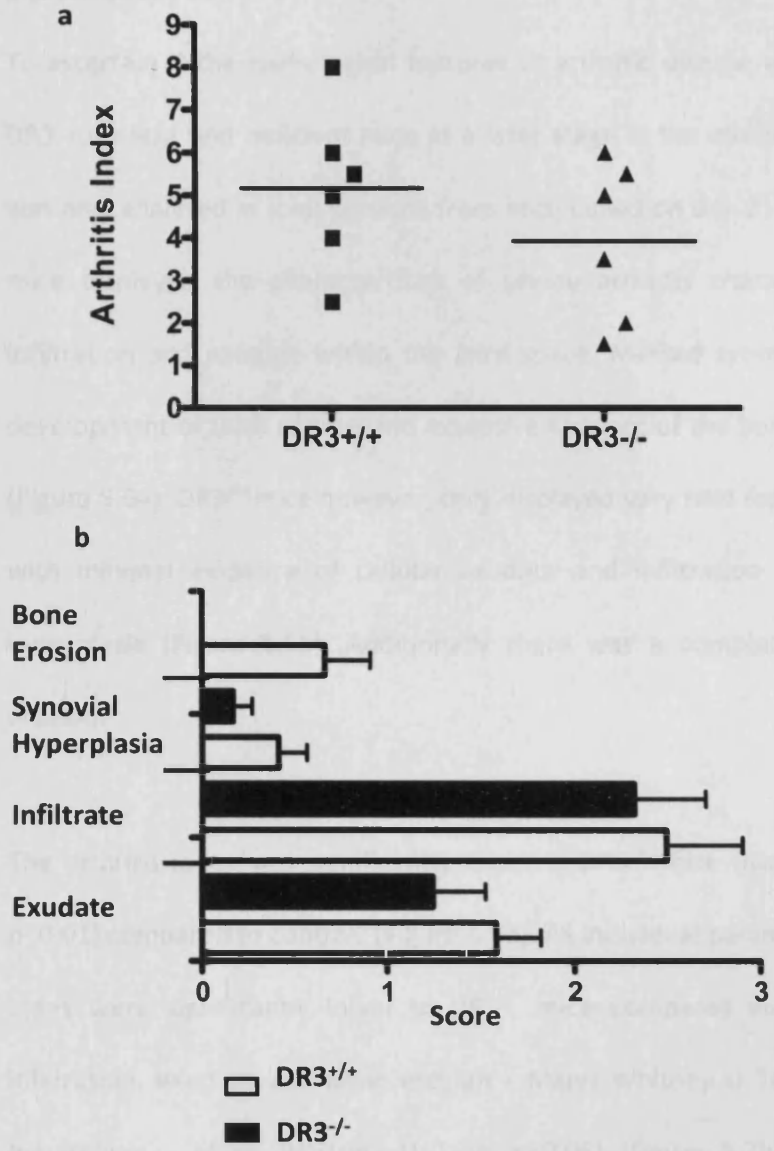


**Figure 5.5. Arthritis Index at Day 3 Post-arthritis Induction.** Joint sections taken at day 3 post-arthritis induction were assessed for arthritis index. (a) A comparison of the AI between $DR3^{+/+}$ and $DR3^{-/-}$ mice indicates no significant difference in disease severity. Horizontal lines depict means. (b) Comparison of the individual parameters of the AI. Data are mean ± SEM. Data was analysed using a Mann-Whitney U test, n = 6.

### 5.2.4 DR3$^{-/-}$ mice displayed resistance to the pathological features of arthritic disease at day 21

To ascertain if the pathological features of arthritic disease were more severe in DR3 sufficient and deficient mice at a later stage in the model, the arthritis index was also analysed in joint sections from mice culled on day 21 of the study. DR3$^{+/+}$ mice displayed the characteristics of severe arthritis characterised by cellular infiltration and exudate within the joint space. Marked synovial hyperplasia, the development of thick pannus and extensive erosions of the bone were also evident (Figure 5.6a). DR3$^{-/-}$ mice however, only displayed very mild features of the disease with minimal evidence of cellular exudate and infiltration and minor synovial hyperplasia (Figure 5.6b). Additionally there was a complete absence of bone erosion.

The arthritis index was significantly lower in DR3$^{-/-}$ mice (Mann Whitney U Test; $p<0.01$) compared to controls (Figure 5.7a). All individual parameters of the arthritis index were significantly lower in DR3$^{-/-}$ mice compared with controls (cellular infiltration, exudate and bone erosion - Mann Whitney U Test; $p<0.01$; synovial hyperplasia - Mann Whitney U Test; $p<0.05$) (Figure 5.7b). DR3$^{-/-}$ mice were therefore resistant to the development of the histopathological hallmarks of AIA at day 21 of the model.

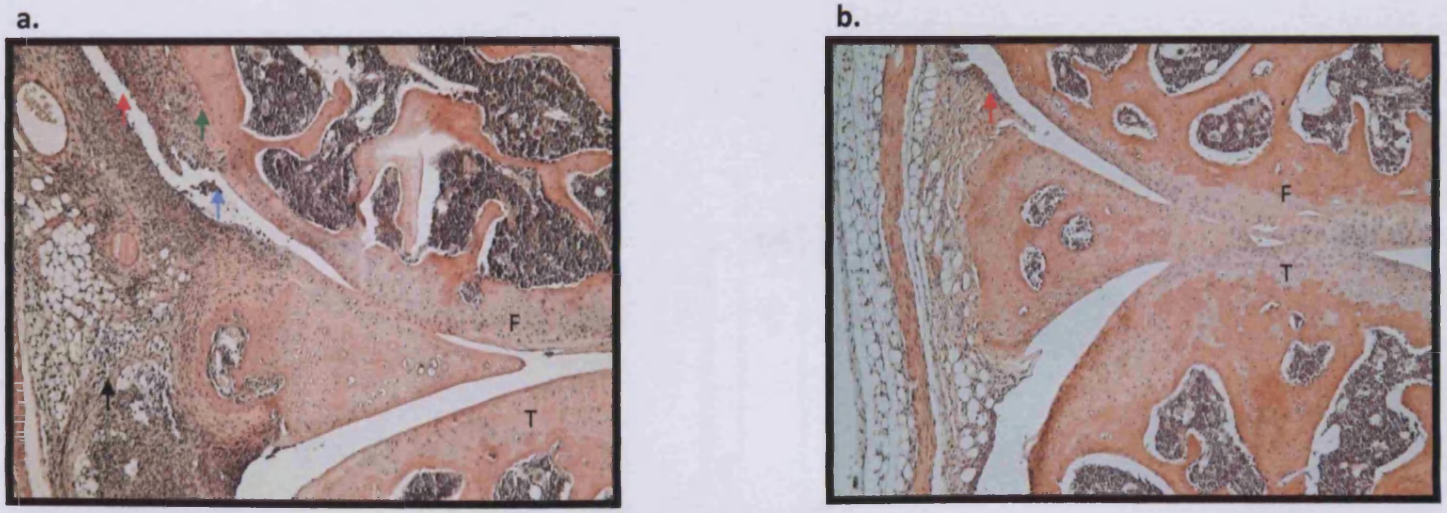


**Figure 5.6. H&E Stained Joint Sections from Animals Sacrificed on Day 21.** Joint sections were H&E stained and analysed. Images were captured at x20 magnification. $DR3^{+/+}$ mice (a) displayed features of cellular infiltration (black arrows), cellular exudate (blue arrows), synovial hyperplasia (red arrows) and bone erosion (green arrows). $DR3^{-/-}$ mice (b) showed only very mild features of disease with some minor synovial hyperplasia (red arrows). F = femur, T = tibia.

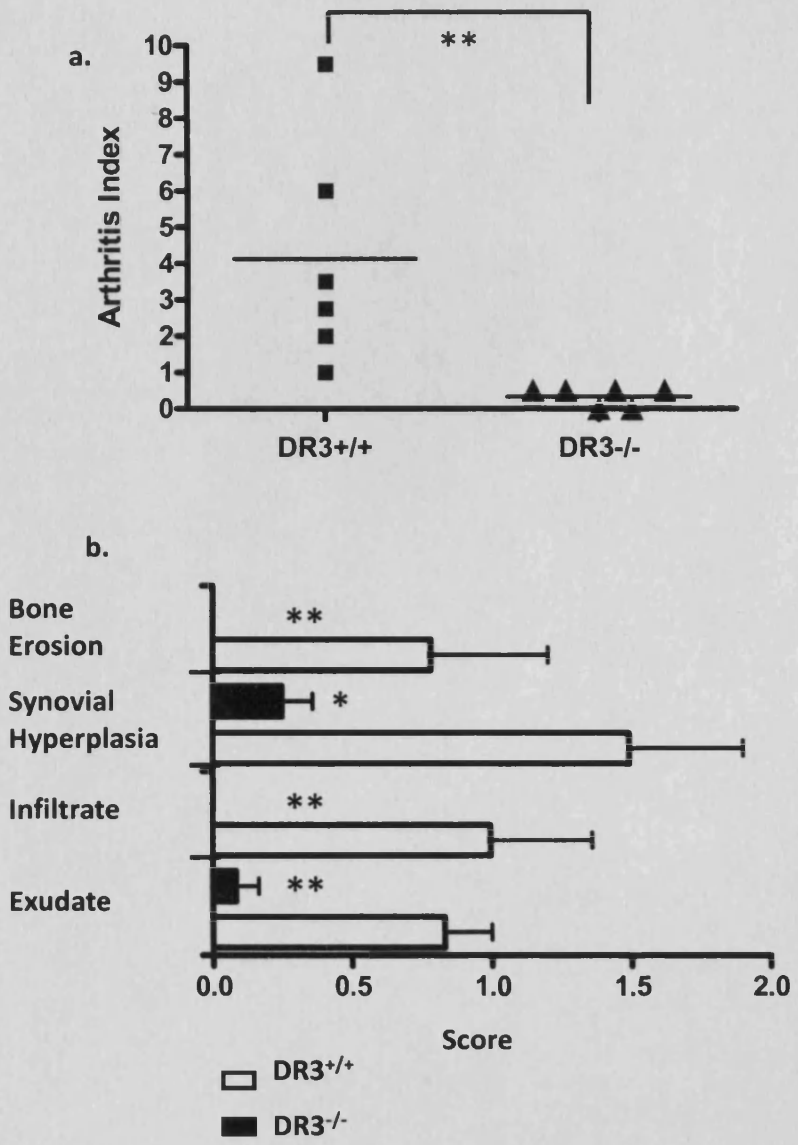


**Figure 5.7. Arthritis Index at Day 21 Post-arthritis Induction.** (a) A comparison of the AI between $DR3^{+/+}$ and $DR3^{-/-}$ mice indicates a significant difference (** $p<0.01$) in disease severity. Horizontal lines depict means. (b) Comparison of the individual parameters of the AI indicates a reduction in all features in $DR3^{-/-}$ mice. There is a significant difference between cellular exudate (** $p<0.01$), infiltrate (** $p<0.01$), synovial hyperplasia (* $p<0.05$) and bone erosion (** $p<0.01$). Data are mean ± SEM. Statistical analysis was performed using a Mann-Whitney U test. n = 6.

### 5.2.5 Articular cartilage is preserved in the absence of the DR3 gene

Articular cartilage is a dynamic structure which functions to provide a protective low resistance tissue, covering the surface of diarthrodial joints (Saxne and Bengt, 2000). Under normal conditions, it acts to withstand compression upon load bearing. However, during the course of diseases such as RA, it can become depleted and degenerative joint disease may occur. Articular cartilage is principally composed of water, collagen and proteoglycans. Its depletion can be determined histologically via the use of Safranin O staining. This is a sensitive method used to illustrate the concentration and distribution of cartilage proteoglycans, via its binding to glycosaminoglycans (Rosenberg, 1971). Fast green is used as a counterstain to aid visualisation and analysis of the red Safranin O staining, producing a visible tidemark. To assess the effect of DR3 on articular cartilage during AIA, articular cartilage depletion in the femoral head was analysed at both day 3 and day 21 post-arthritis induction, in both DR3 sufficient and deficient animals. This was achieved by measuring the depth of depletion and expressing it as a percentage of the total cartilage depth.

At day 3 post-arthritis induction, $DR3^{+/+}$ mice displayed evidence of cartilage depletion with the presence of an obvious tidemark (Figure 5.8a), corresponding to approximately 40% depletion. In $DR3^{-/-}$ mice however, cartilage was generally preserved (Figure 5.8b) with less than 20% depletion. Thus although the AI did not differ significantly between the 2 groups of mice at day 3, cartilage depletion was significantly affected, and was substantially greater in $DR3^{+/+}$ mice (Figure 5.9) (Mann Whitney U test; $p<0.01$).

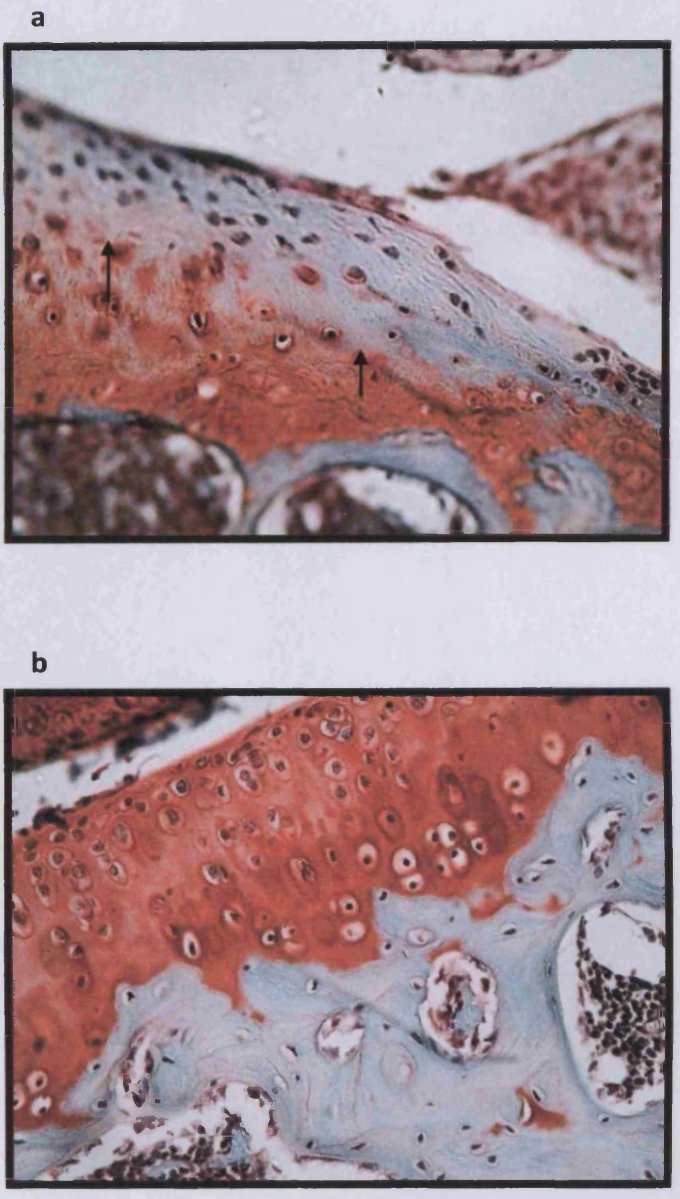


**Figure 5.8. Day 3 Cartilage Depletion in $DR3^{+/+}$ and $DR3^{-/-}$ Mice.** Representative Safranin O/ Fast Green stained sections (x40) are shown. Cartilage depletion was measured as a percentage of total cartilage using an eye piece with a line-graduated scale. Articular cartilage in the femoral head was significantly more depleted in $DR3^{+/+}$ mice (a) than in $DR3^{-/-}$ mice (b) at day 3 post-arthritis induction. Depth of depletion is shown by the tidemark (black arrows).

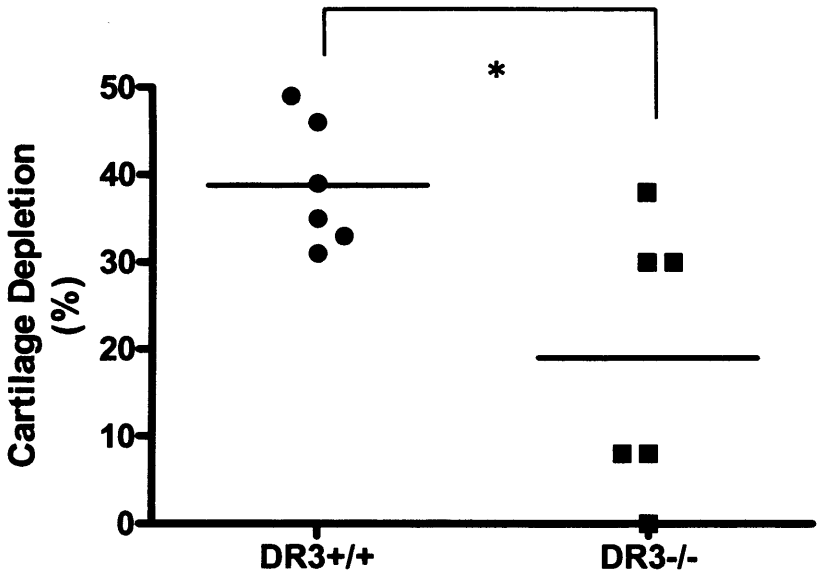


**Figure 5.9. Cartilage Depletion on Day 3 Post-arthritis Induction.** Cartilage depletion in the femoral head, measured as a percentage of total cartilage, was significantly lower in $DR3^{-/-}$ mice (* $p<0.05$) as determined using a Mann-Whitney U test. Horizontal lines depict mean. n = 6.

At day 21 post-arthritis induction, cartilage continued to be depleted in the $DR3^{+/+}$ mice, increasing to approximately 45% (Figure 5.10a). Depletion in the absence of DR3 however, did not increase and remained below 20% (Figure 5.10b). This corresponded with a significantly higher depletion of cartilage in DR3 control mice compared with $DR3^{-/-}$ mice at day 21 ($p<0.05$) (Figure 5.11) implying an important role for DR3 in the destruction of articular cartilage during AIA.

a

b

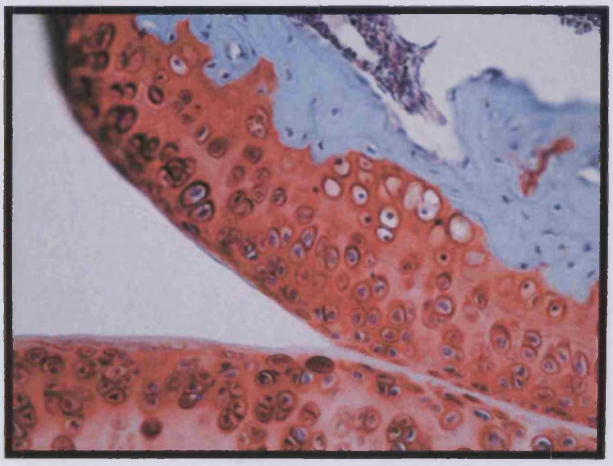

**Figure 5.10. Day 21 Cartilage Depletion in $DR3^{+/+}$ and $DR3^{-/-}$ Mice.** Representative Safranin O/ Fast Green stained sections (x40) are shown. Cartilage depletion was measured as a percentage of total cartilage using an eye piece with a line-graduated scale. Articular cartilage in the femoral head was significantly more depleted in $DR3^{+/+}$ mice (a) than in $DR3^{-/-}$ mice (b) at day 21 post-arthritis induction. Depth of depletion is shown by the tidemark (black arrows).

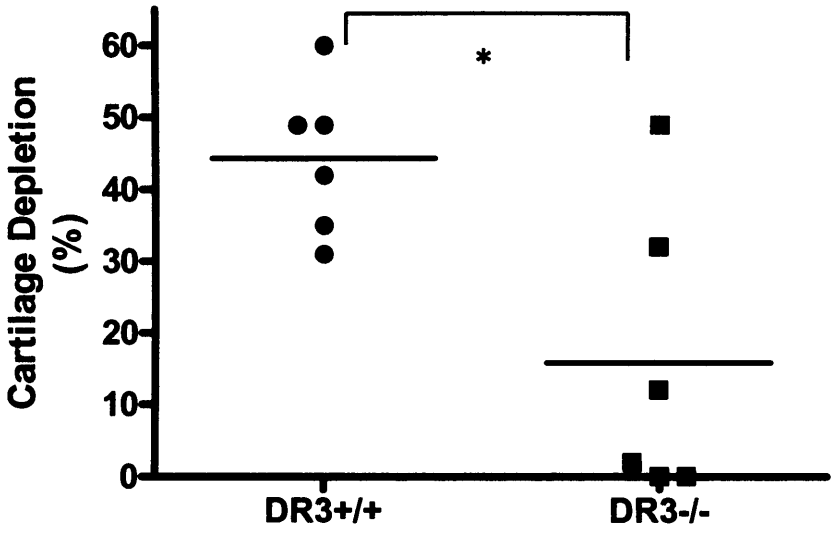


**Figure 5.11. Cartilage Depletion on Day 21 Post-arthritis Induction.** Cartilage depletion in the femoral head, measured as a percentage of total cartilage, is significantly higher in $DR3^{+/+}$ mice than in $DR3^{-/-}$ mice (*$p<0.05$) as determined using a Mann-Whitney U test. Horizontal lines depict means. n =6.

### 5.2.6 Characterisation of DR3$^{+/-}$ mice in the AIA model

DR3$^{+/-}$ mice contain 1 copy of the DR3 gene and are bred in abundance within the colony due to the heterozygote breeding pattern employed. AIA was characterised in these mice to assess their potential use in the model and to assess whether a significant gene-dosage effect occurs.

### 5.2.7 AIA was induced in DR3$^{+/-}$ mice with 100% incidence and joint swelling followed a pattern similar to that of DR3$^{+/+}$ mice

Pre-immunised animals were induced with AIA on day 0 of the experimental protocol in the same manner as used for both DR3$^{+/+}$ mice and DR3$^{-/-}$ mice. As previously described, the pattern of joint swelling was assessed using a micrometer. DR3$^{+/-}$ mice exhibited a peak in joint swelling on day 1 post-arthritis induction, with joint diameters rising from an average of 4.9mm on day 0 (pre-arthritis induction) to 6.3mm on day 1. Joint swelling decreased over subsequent days returning to baseline levels on day 14 post-arthritis induction (Figure 5.12). This pattern in joint swelling was comparable to those of both DR3$^{+/+}$ mice and DR3$^{-/-}$ mice and did not differ significantly from either at any individual time point. However, on days 2, 3, 5 and 7, joint swelling in DR3$^{+/-}$ mice appeared to be intermediate of those of DR3$^{+/+}$ and DR3$^{-/-}$ mice. Similar to DR3$^{+/+}$ mice however, baseline swelling did not return until day 14. Therefore, AIA can be induced in DR3$^{+/-}$ mice with 100% incidence with joint swelling following a similar pattern to DR3 sufficient mice.

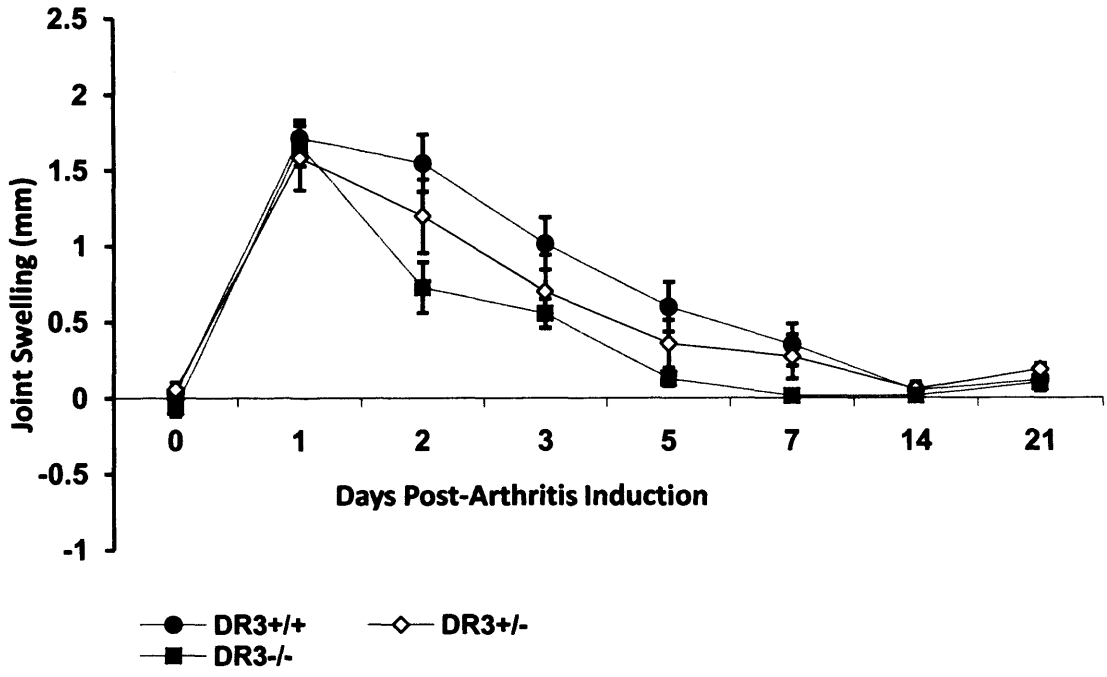


**Figure 5.12. $DR3^{+/-}$ mice joint swelling post-AIA induction.** Joint swelling was analysed in $DR3^{+/-}$ mice for 21 days post-arthritis induction using a digital micrometer. Joint swelling of $DR3^{+/-}$ mice (solid line) follows the same pattern as that of $DR3^{+/+}$ and $DR3^{-/-}$ mice (broken lines) and is not significantly different from either. Data are mean ± SEM, n = 6.

### 5.2.8 The AI of DR3$^{+/-}$ mice was less severe than that of DR3$^{+/+}$ mice but did not differ significantly on either day 3 or day 21

To investigate whether DR3$^{+/-}$ mice displayed the histopathological hallmarks of arthritic disease, at days 3 and 21 post-arthritis induction, DR3$^{+/-}$ mice were analysed for the AI in the same manner as the analysis carried out on DR3$^{+/+}$ and DR3$^{-/-}$ mice. At day 3 post-arthritis induction, DR3$^{+/-}$ mice showed evidence of joint pathology with infiltration of inflammatory cells into the adipose tissue and cellular exudate within the joint space. Synovial hyperplasia and bone erosion was minimal (Figure 5.13a). There was no significant difference in AI at day 3 between DR3$^{+/-}$ mice (mean AI 4.9) and either DR3$^{+/+}$ (mean AI 5.2) or DR3$^{-/-}$ mice (mean AI 3.9) (Figure 5.13b). At day 21 post-arthritis induction, DR3$^{+/-}$ mice displayed degenerative joint pathologies with both bone erosions and pannus development and a mean AI of 2.3 (Figure 5.14a). This was not as severe as that seen within the joint of DR3$^{+/+}$ mice (mean AI 4.1) however, there was not complete protection from bone erosion as seen in DR3 deficient animals (mean AI 0.3). There was no significant difference in AI between DR3$^{+/-}$ mice and DR3$^{+/+}$, however AI in the DR3$^{+/-}$ mice was significantly greater than that seen in DR3 deficient animals (Mann-Whitney U test; $p<0.01$) (Figure 5.14b). Therefore, DR3$^{+/-}$ mice are susceptible to AIA displaying the characteristic histopathological features of disease at day 21 post-arthritis induction, however, this is not as severe as that seen in DR3$^{+/+}$ mice.

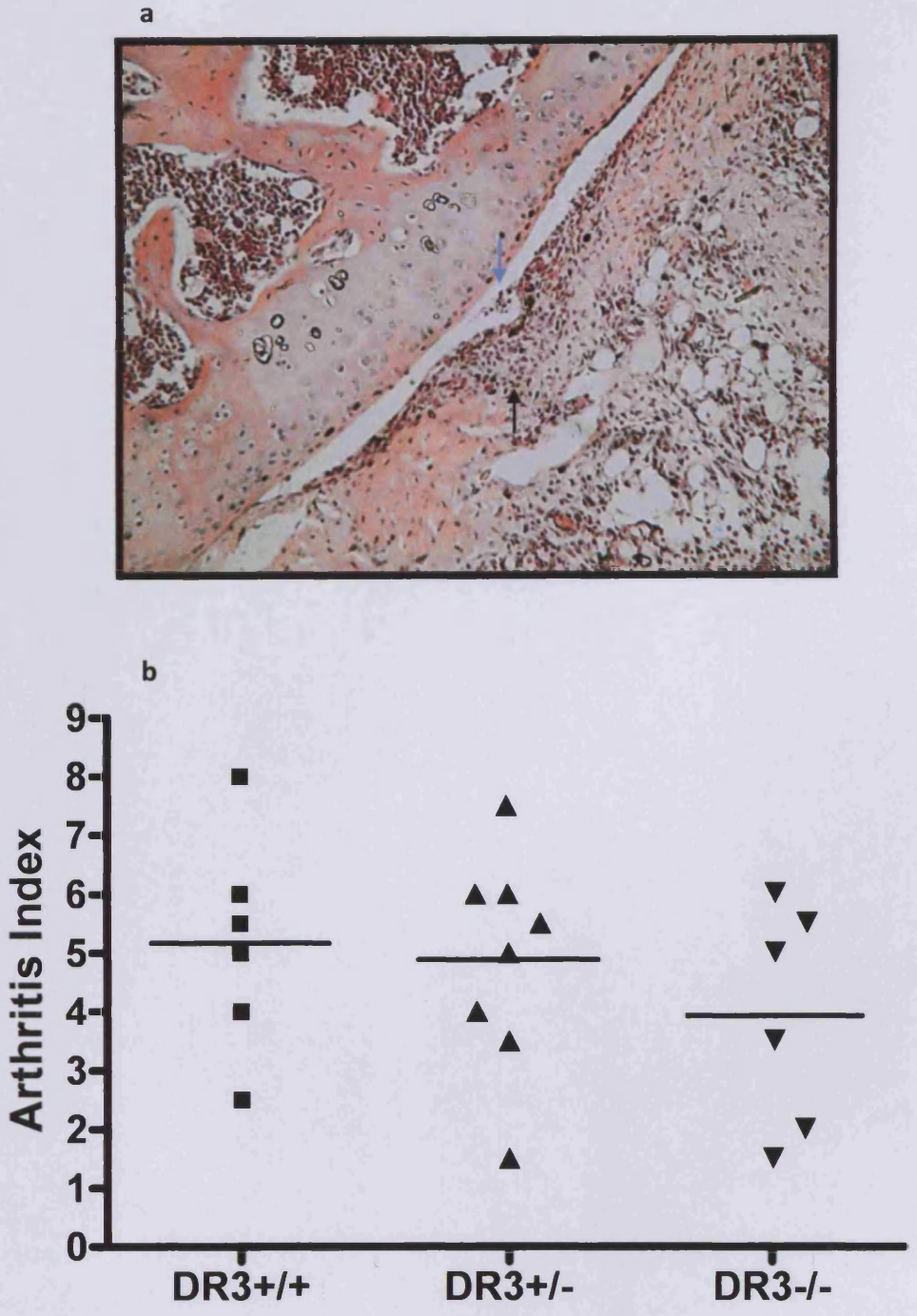


**Figure 5.13. Arthritis Index of DR3$^{+/-}$ Mice on Day 3 Post-Arthritis Induction.** a) A representative H and E stained joint section (x40) from a DR3$^{+/-}$ mouse on day 3 post-arthritis induction. DR3$^{+/-}$ mice display cellular exudate (blue arrows) and infiltration (black arrows) on day 3 post-arthritis induction. b) A comparison of the AI between DR3$^{+/+}$, DR3$^{+/-}$ and DR3$^{-/-}$. AI of DR3$^{+/-}$ mice does not differ significantly from either DR3$^{+/+}$ or DR3$^{-/-}$ mice. Horizontal lines depict means, n = 6. Data was analysed using a Mann-Whitney U test.

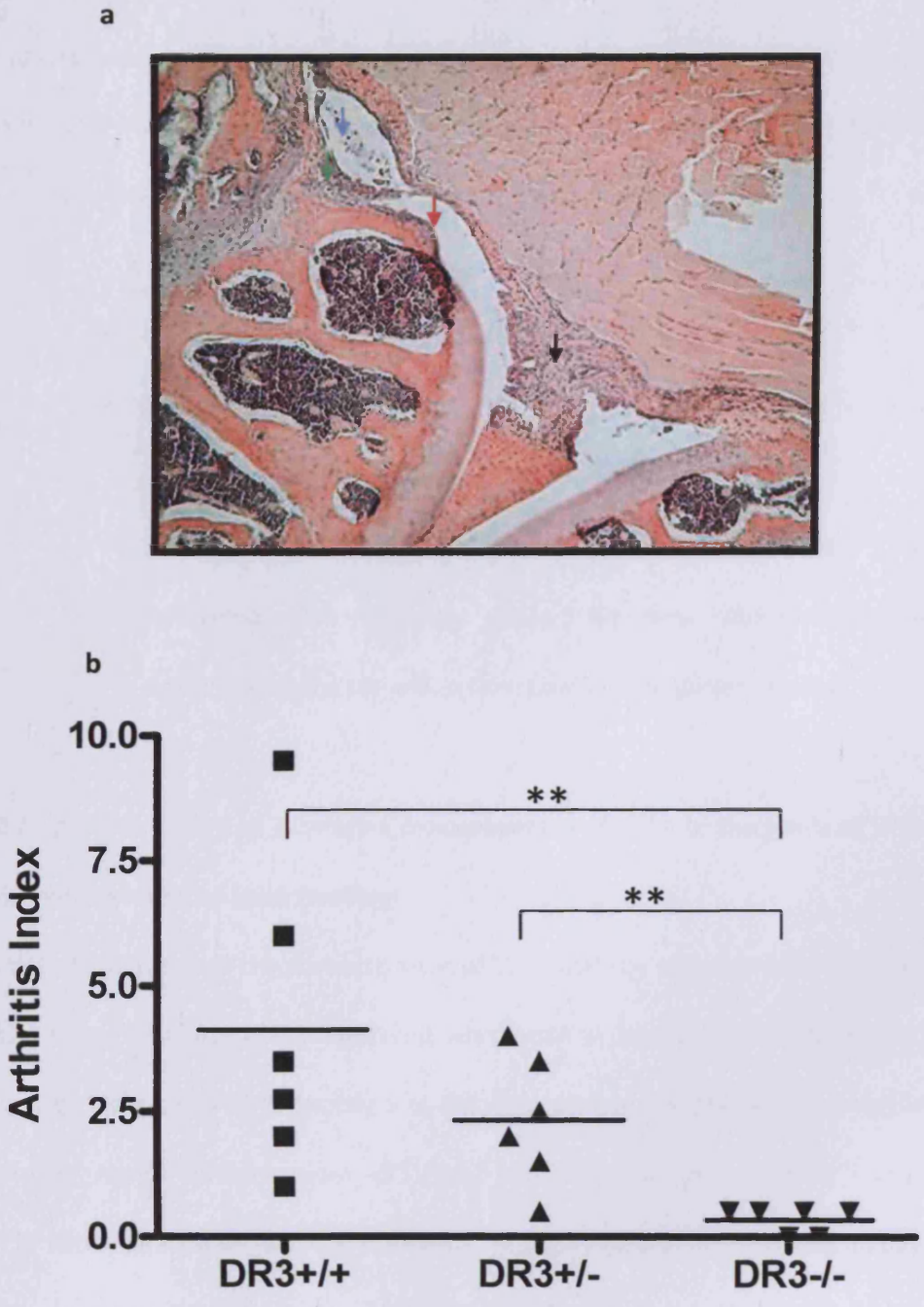


**Figure 5.14. Arthritis Index of DR3$^{+/-}$ Mice on Day 21 Post-Arthritis Induction.** a) A representative H and E stained joint section (x20) from a DR3$^{+/-}$ mouse on day 21 post-arthritis induction. DR3$^{+/-}$ mice display all features of the AI on day 21 post-arthritis induction. Cellular infiltration (black arrows), cellular exudate (blue arrows), synovial hyperplasia (red arrows), bone erosion (green arrows). b) AI of DR3$^{+/-}$ mice does not differ significantly from DR3$^{+/+}$ but is significantly higher than DR3$^{-/-}$ mice. ** $p<0.01$ (Mann-Whitney U test). Horizontal lines depict means. n = 6.

one-way Anova ($p>0.05$) (Figure 5.15). Therefore, TL1A has no significant effect on joint swelling in $DR3^{+/-}$ mice when administered into the joint on day 0 of the AIA model at any of the concentrations that were assessed.

### 5.2.11 Administration of increasing concentrations of TL1A to the joints of $DR3^{+/-}$ mice results in an increase in AI in a dose-dependent manner

To discover if there was an effect of TL1A administration on joint pathology, the arthritis index of $DR3^{+/-}$ mice receiving TL1A was analysed at day 21 post-arthritis induction. Mice receiving no TL1A displayed all histopathological features of arthritic disease, namely cellular infiltration and exudate, synovial hyperplasia and bone erosions, as previously determined in $DR3^{+/-}$ mice. The addition of 1ng of TL1A into the joint resulted in a similar histopathological outcome with evidence of cellular exudate, infiltration, synovial hyperplasia and bone erosion. A mean AI of 3.3 was observed. Raising the concentration of TL1A to 10ng resulted in an increase in AI to a mean value of 4.6 as a result of an increase in cellular exudate, synovial hyperplasia, cellular infiltration and bone erosion. Further increasing the concentration of TL1A to 100ng resulted in an increase in synovial hyperplasia and erosions of the bone. However, cellular exudate and infiltration did not increase (Figure 5.16). When comparing the significance of the AI at different concentrations of TL1A, it was found to increase in a dose-dependent manner with increasing concentration of TL1A (One-Way ANOVA; $p<0.05$) (Figure 5.17). When comparing the individual parameters of the AI at the different concentrations of TL1A, there was no significant difference in cellular infiltration or cellular exudate at any of the concentrations despite a dose-dependent increase in these parameters with TL1A

administration. However, both synovial hyperplasia (One-Way ANOVA; $p<0.05$) and bone erosion (One-Way ANOVA; $p<0.05$) became significantly more severe with increasing concentration of TL1A (Figure 5.18). The increasing size of bone erosions was particularly striking.

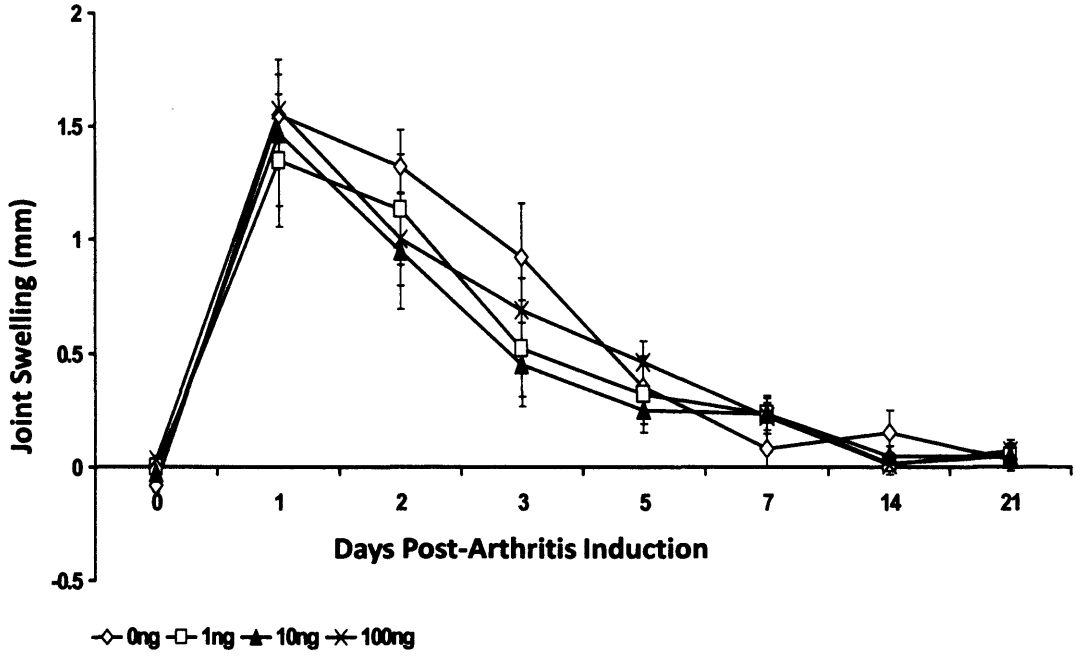


**Figure 5.15. The Administration of Increasing Concentrations of TL1A to DR3$^{+/-}$ Mice has no Effect on Joint Swelling.** TL1A was administered to DR3$^{+/-}$ mice in increasing concentrations on day 0 of the AIA protocol. Joint swelling was analysed over 21 days post-arthritis induction using a digital micrometer. Data are mean ± SEM. 6 mice were analysed at each concentration of TL1A. Administering TL1A into the joints of DR3$^{+/-}$ mice did not effect joint swelling in response to mBSA injection across the 21 day timecourse.

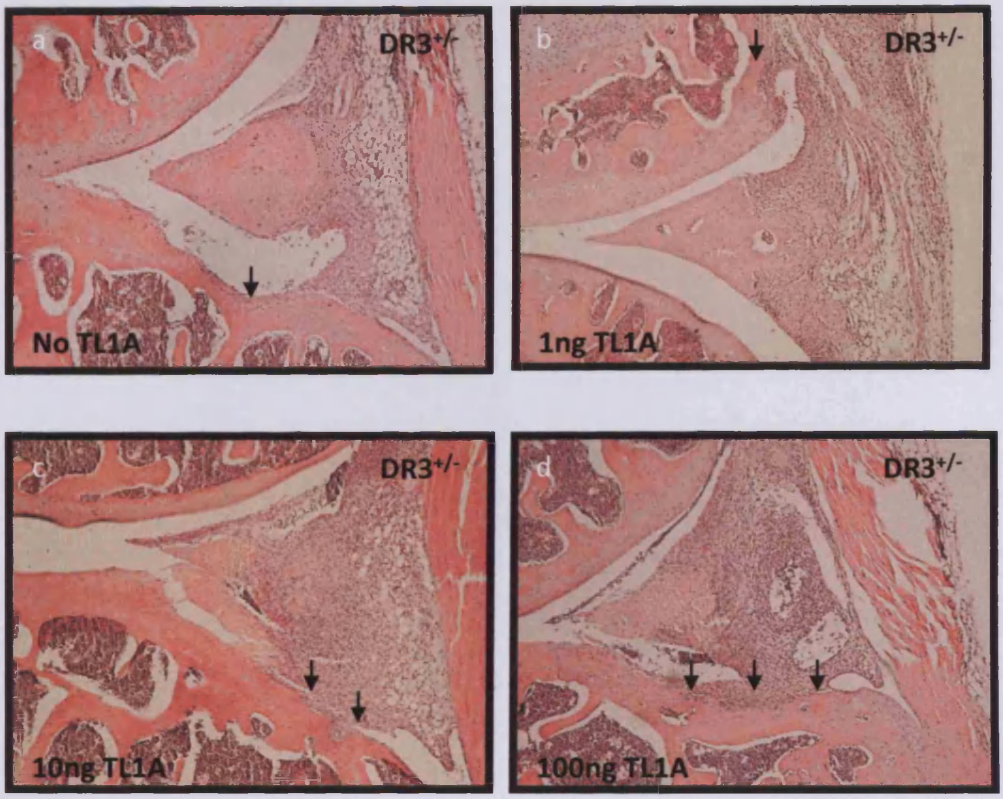


**Figure 5.16. Administration of Increasing Concentrations of TL1A to DR3$^{+/-}$ Mice Results in a Dose-Dependent Increase in AI.** H and E stained representative images (x20) of DR3$^{+/-}$ mouse knee joints on day 21 post-arthritis induction are shown. (a) no TL1A (b), 1ng TL1A (c), 10ng TL1A (d) and 100ng TL1A . Bone erosions are indicated with black arrows.

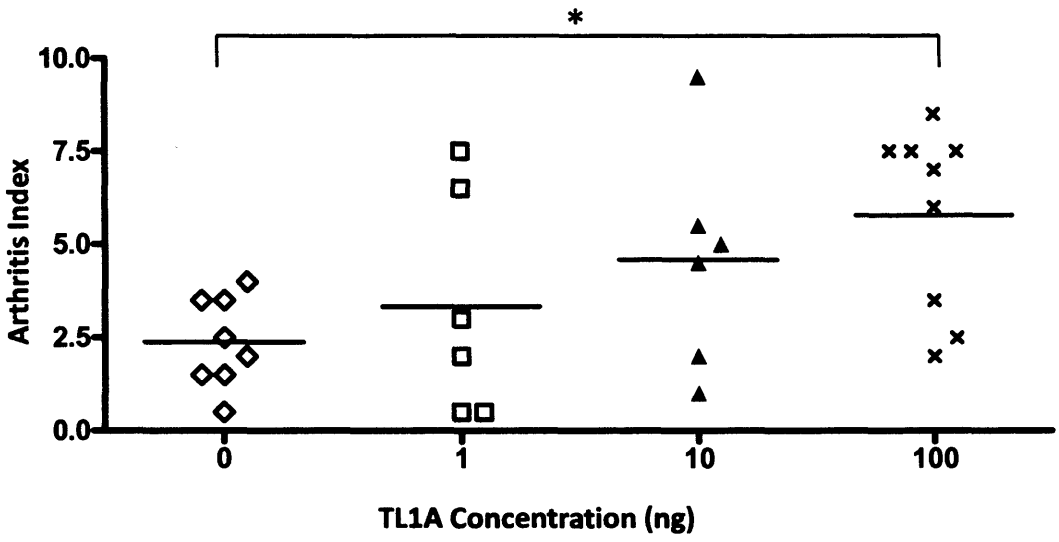


**Figure 5.17. Administration of TL1A to DR3$^{+/-}$ Mice Results in a Dose-Dependent Increase in AI.** AI at day 21 post-arthritis induction increases with concentration of TL1A. *p<0.05 (One-Way ANOVA). Horizontal lines depict means. Each symbol represents one mouse.

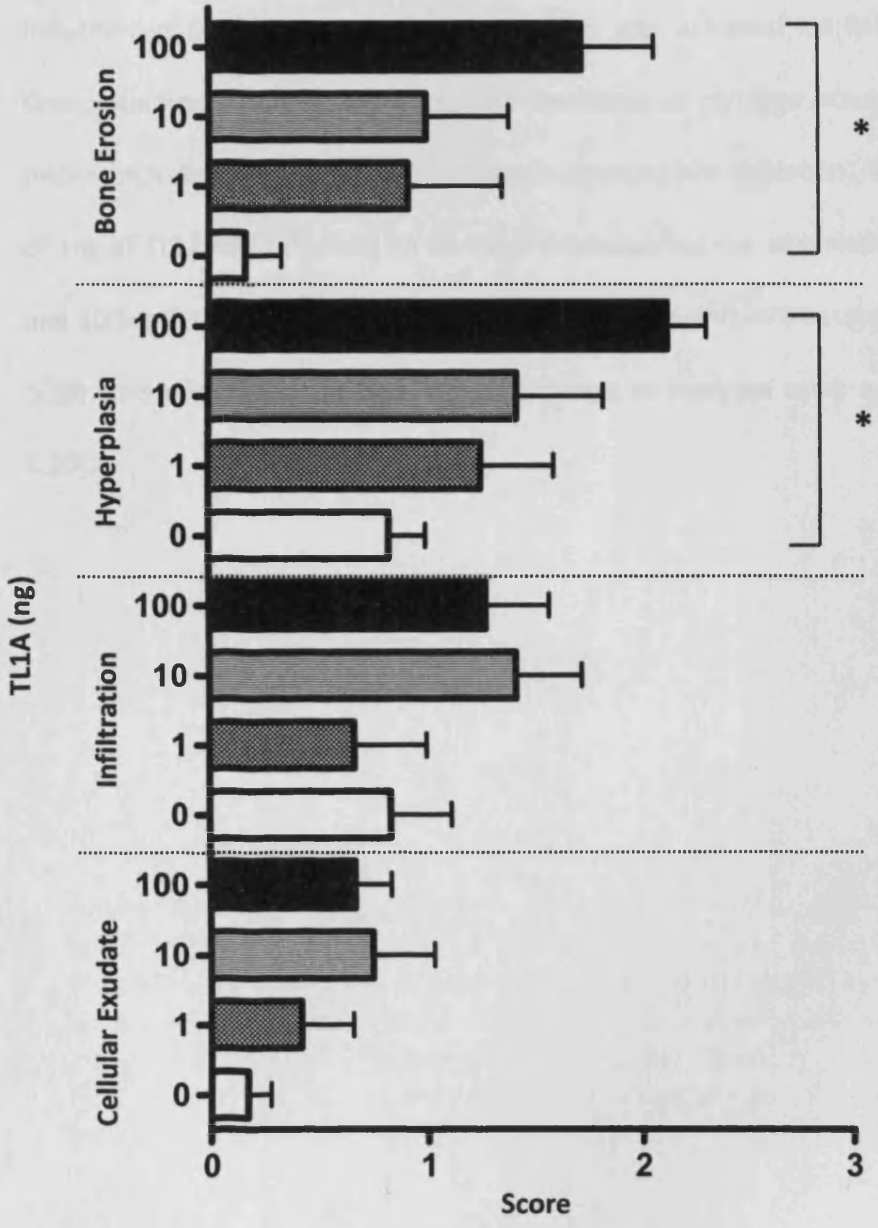


**Figure 5.18. A Comparison of the Individual Features of the AI for DR3$^{+/-}$ Mice Receiving Increasing Concentrations of TL1A.** Administration of increasing concentration of TL1A generally results in a dose-dependent increase in the individual features of the AI. Both synovial hyperplasia and bone erosion become significantly more severe with increasing concentration of TL1A as analysed using a one-way ANOVA (* $p<0.05$). Date are mean ± SEM.

### 5.2.12 TL1A administration to DR3$^{+/-}$ mice caused a trend towards exacerbation of cartilage depletion at 100ng

Cartilage depletion in the femoral head was analysed at day 21 post-arthritis induction in DR3$^{+/-}$ mice receiving TL1A. This was achieved via Safranin O/Fast Green staining as previously described. Depletion of cartilage occurred in DR3$^{+/-}$ mice which did not receive TL1A with approximately 30% depletion. Administration of 1ng of TL1A had no effect on cartilage depletion but the administration of 10ng and 100ng TL1A increased cartilage depletion to 34% and 45% respectively (Figure 5.19). This effect was not significantly different as analysed using a t-test (Figure 5.20).

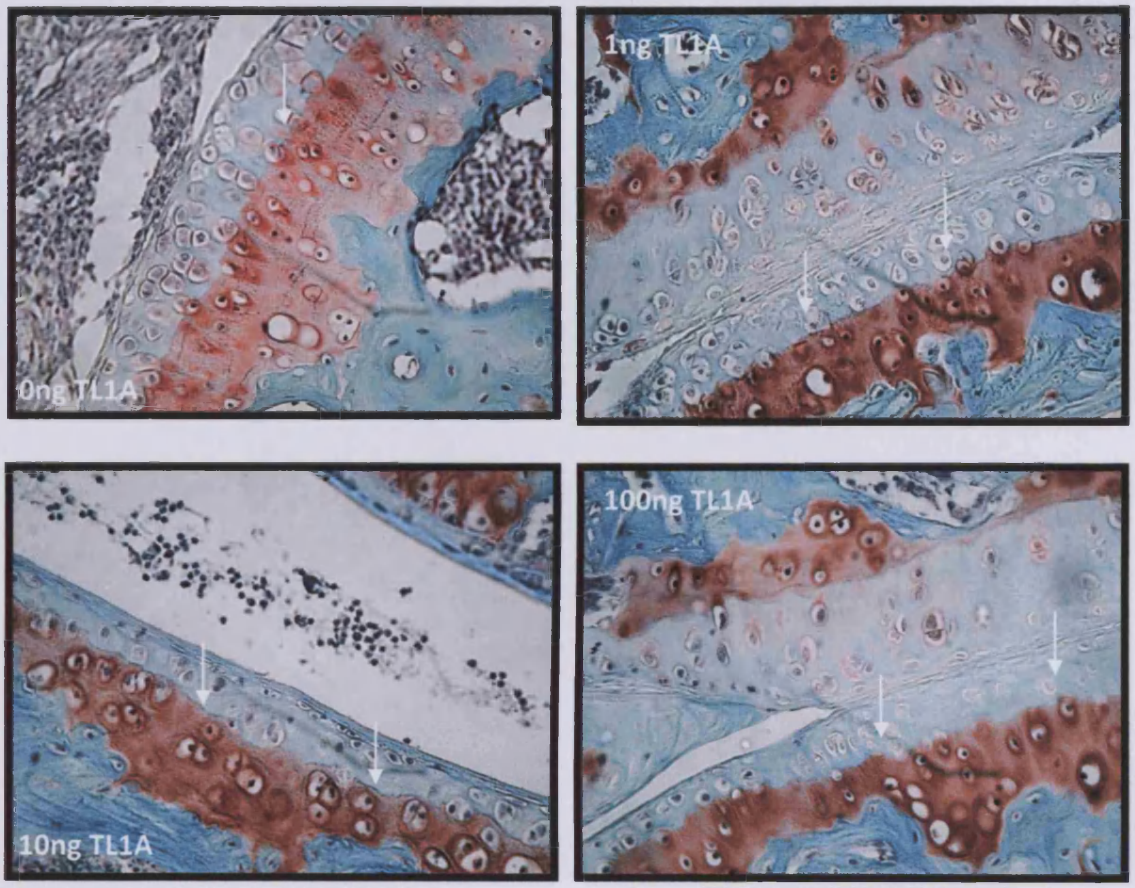


**Figure 5.19. Cartilage Depletion Increases in a Dose-Dependent Manner with Administration of TL1A to DR3$^{+/-}$ mice on day 21 post-arthritis induction.** Representative Safranin O/ Fast Green stained sections (x40) are shown. Cartilage depletion was measured as a percentage of total cartilage using an eye piece with a line-graduated scale. Depletion of articular cartilage is illustrated by the visible tidemark (white arrows). Depth of depletion increases with increasing concentration of TL1A.

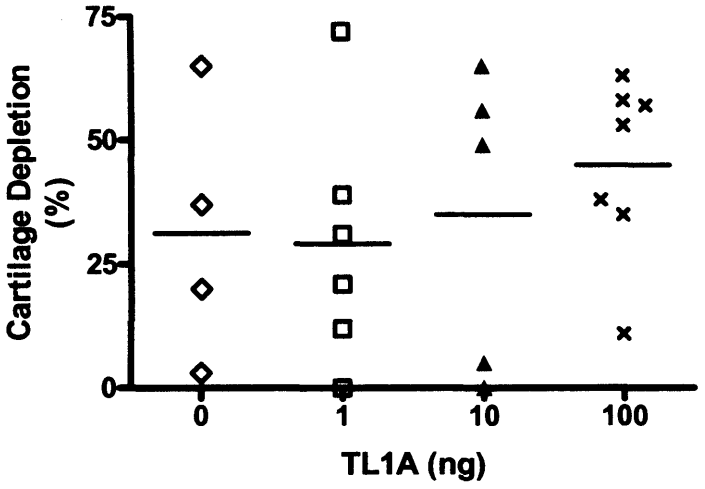


**Figure 5.20. Cartilage Depletion in DR3$^{+/-}$ Mice Receiving Increasing Concentrations of TL1A.** Cartilage depletion in the femoral head, measured as a percentage of total cartilage was analysed. Safranin O/Fast Green staining of joint sections from DR3$^{+/-}$ mice receiving TL1A revealed a trend towards exacerbation of proteoglycan loss at 100ng TL1A. Horizontal lines depict means. Each individual symbol represents one mouse.

### 5.2.13 Administration of increasing concentrations of TL1A to the joints of $DR3^{-/-}$ mice had no significant effect on swelling or AI

As TL1A is reported to be the only known specific ligand for DR3, the fact that it was able to exacerbate arthritic disease in a dose-dependent manner in $DR3^{+/-}$ mice implies that it is a DR3-dependent effect. To further clarify this, TL1A was administered to the joint of DR3 deficient mice where no effect should be observed. Concentrations of 0ng, 1ng, 10ng and 100ng of TL1A were examined. Joint swelling occurred at all concentrations of TL1A following the typical pattern of peaking on day 1 post-arthritis induction and subsequently decreasing, returning to baseline levels on day 7 post-arthritis induction. Peak swelling of joints on day 1 reached 1.67mm with no TL1A, 1.17mm with 1ng TL1A, 1.6mm with 10ng TL1A and 1.7mm with 100ng TL1A. There was no significant difference in joint swelling at the different concentrations of TL1A (Figure 5.21). AI was also assessed at day 21 post-arthritis induction. As previously determined, $DR3^{-/-}$ mice did not show the histopathological features associated with arthritis, in particular, they have a complete absence of bone erosions. The addition of TL1A did not have a dose-dependent effect on AI (Figure 5.22). However, mean AI did increase from normal $DR3^{-/-}$ values (mean AI without TL1A = 0.3) to 1.5 with 1ng TL1A, 2.2 with 10ng TL1A and 2.1 with 100ng TL1A (Figure 5.23). These increases were not significantly different from normal $DR3^{-/-}$ AI values when analysed via One-way ANOVA. When examining the individual parameters of the AI (Figure 5.24), administration of TL1A did result in an increase in these features although when statistically analysed, these did not reach significant levels. Cellular exudate rose from an average of 0.08 without the administration of TL1A to 0.17 at 10ng and 0.42 at 100ng TL1A.

Increase in cellular infiltrate was quite uniform regardless of TL1A concentration administered. No infiltration was seen in the absence of TL1A but an average of 0.58, 0.55 and 0.42 was observed at 1ng, 10ng and 100ng TL1A respectively. Synovial hyperplasia appeared to increase in a dose-dependent manner with TL1A administration, rising from an average of 0.25 without TL1A to 0.83 with 100ng TL1A. The most notable effect was that of TL1A in $DR3^{-/-}$ mice on bone erosion. Previously it was noted that there was a complete absence of bone erosion in DR3 deficient mice with antigen-induced arthritis. However, the administration of TL1A resulted in the emergence of bone erosions. An average score of 0 for bone erosion was observed without the administration of TL1A but this increased to 0.5, 0.92 and 0.42 with the addition of 1ng, 10ng and 100ng TL1A respectively. It must be noted that these increases in the individual features of the AI upon administration of TL1A to DR3 deficient mice, did not restore wildtype phenotype or achieve scores as high as those observed when administering TL1A to $DR3^{+/-}$ mice.

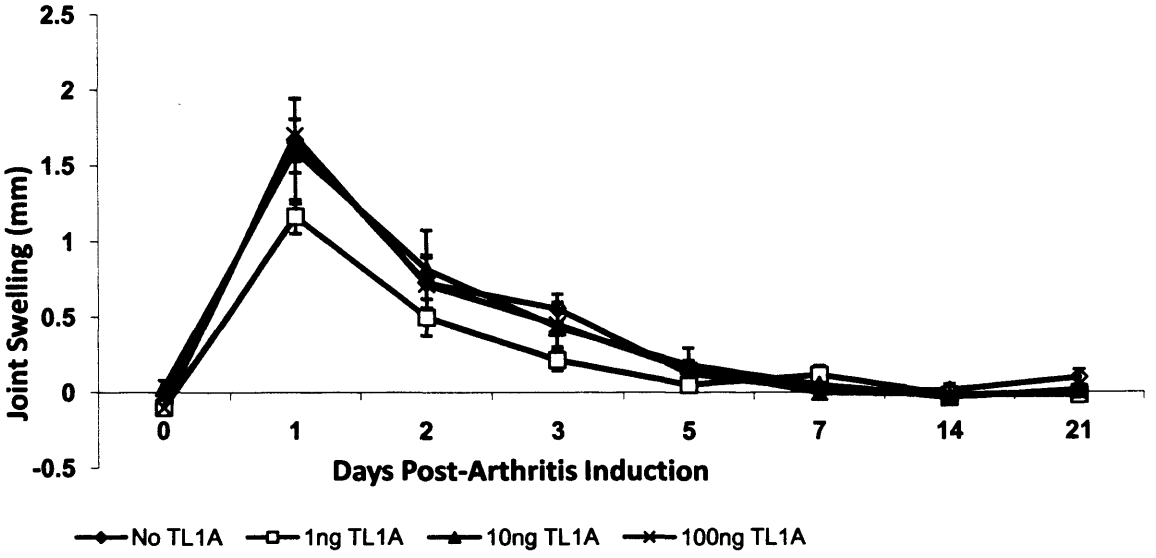


**Figure 5.21. The Administration of Increasing Concentrations of TL1A to DR3$^{-/-}$ Mice has no Effect on Joint Swelling.** Joint swelling in DR3$^{-/-}$ mice which received TL1A on day 0 of the AIA protocol was assessed using a digital micrometer. Administering TL1A into the joints of DR3$^{-/-}$ mice did not effect joint swelling in response to mBSA injection. Data are mean ± SEM. n = 6.

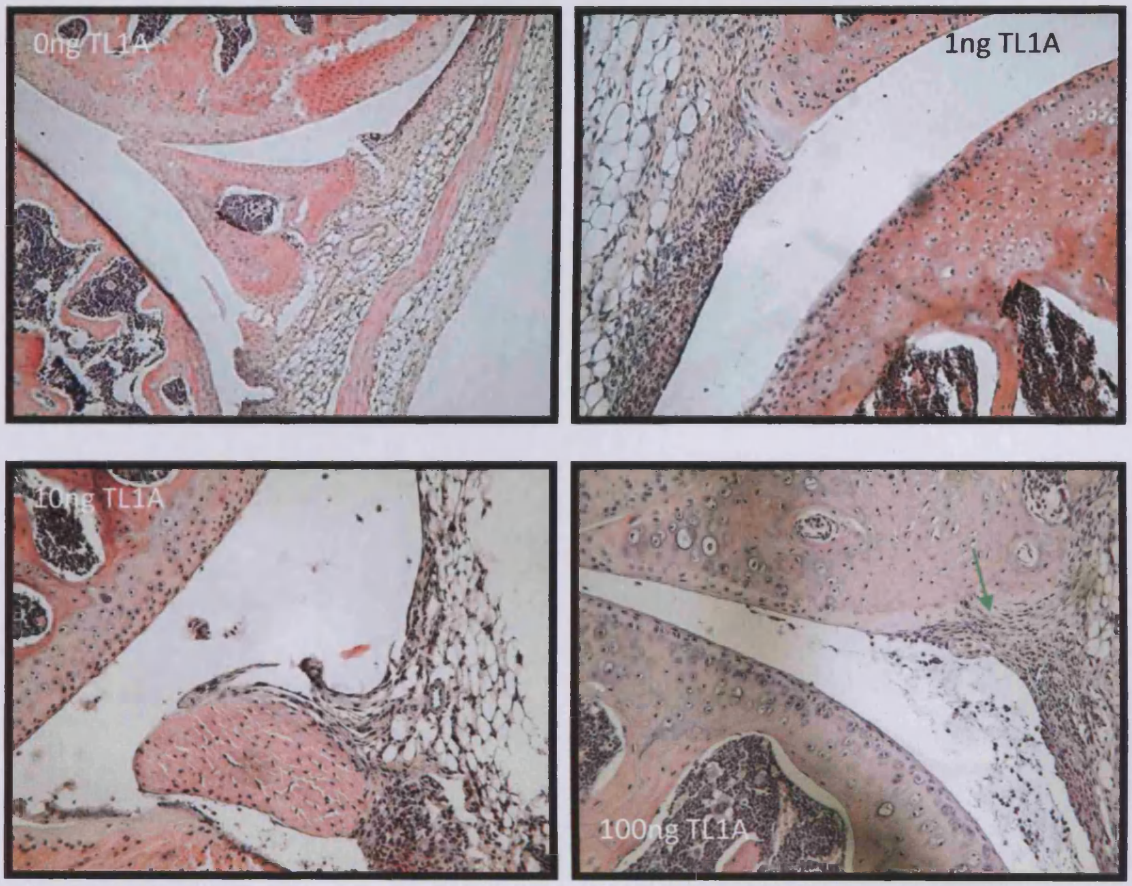


**Figure 5.22. Arthritis Index of DR3$^{-/-}$ Mice Receiving TL1A.** Increasing concentrations of TL1A were administered to DR3$^{-/-}$ mice on day 0 of the AIA protocol. Images show representative H and E stained sections from DR3$^{-/-}$ mice receiving a) no TL1A (x10), b) 1ng TL1A (x20), c 10ng TL1A (x20) and d) 100ng TL1A (x20). Administration of TL1A to DR3$^{-/-}$ mice did not have a dose-dependent nor significant effect on AI. However, there was a greater emergence of features of the AI including bone erosion (green arrows).

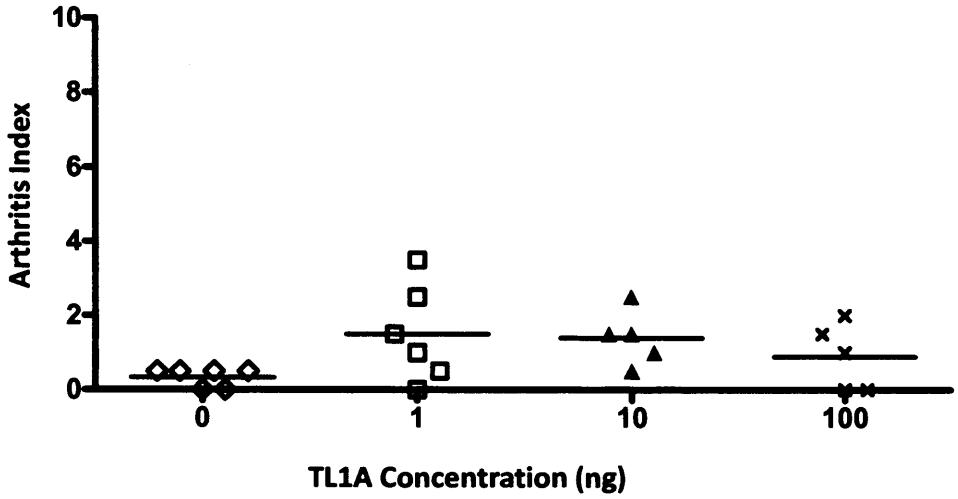


**Figure 5.23. Administration of Increasing Concentrations of TL1A to DR3$^{-/-}$ Mice Has no Effect on AI Score.** AI was analysed from DR3$^{-/-}$ mice receiving increasing concentrations of TL1A as shown, on day 0 of the AIA protocol and sacrificed on day 21 post-arthritis induction. There was no significant effect of administering increasing concentrations of TL1A to DR3 deficient mice in terms of AI. Horizontal lines depict means. n = 6.

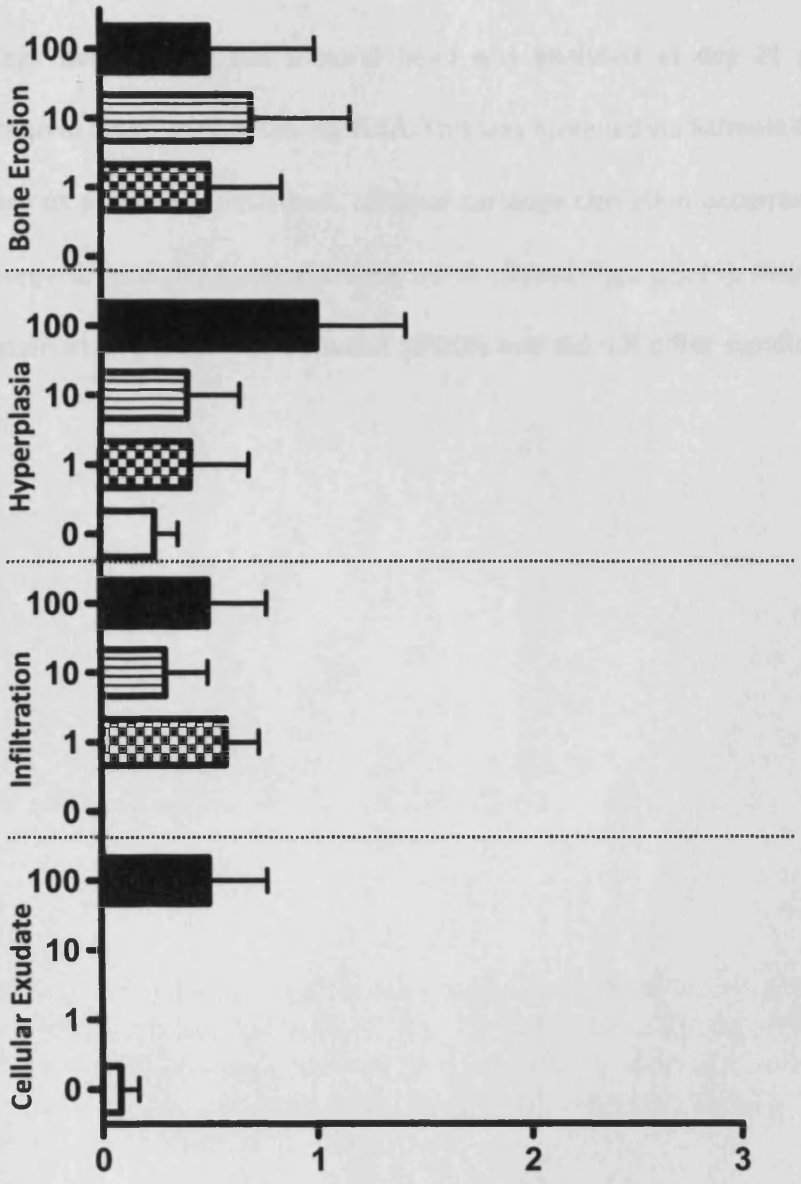


**Figure 5.24. A Comparison of the Individual Features of the AI for DR3$^{-/-}$ Mice Receiving Increasing Concentrations of TL1A.** Administration of increasing concentration of TL1A had no significant effect on any individual features of the AI (one-way ANOVA). However, there was an increased emergence of cellular exudate, infiltration, synovial hyperplasia and bone erosion. Data are mean ± SEM. n = 6.

### 5.2.14 Administration of increasing concentrations of TL1A to the joints of DR3$^{-/-}$ mice had no significant effect on cartilage depletion

Cartilage depletion in the femoral head was analysed at day 21 post-arthritis induction in DR3$^{-/-}$ mice receiving TL1A. This was achieved via Safranin O/Fast Green staining as previously described. Minimal cartilage depletion occurred in all DR3$^{-/-}$ mice regardless of TL1A concentration administered (Figure 5.25). Average cartilage depletion in all groups was between 10-20% and did not differ significantly (Figure 5.26).

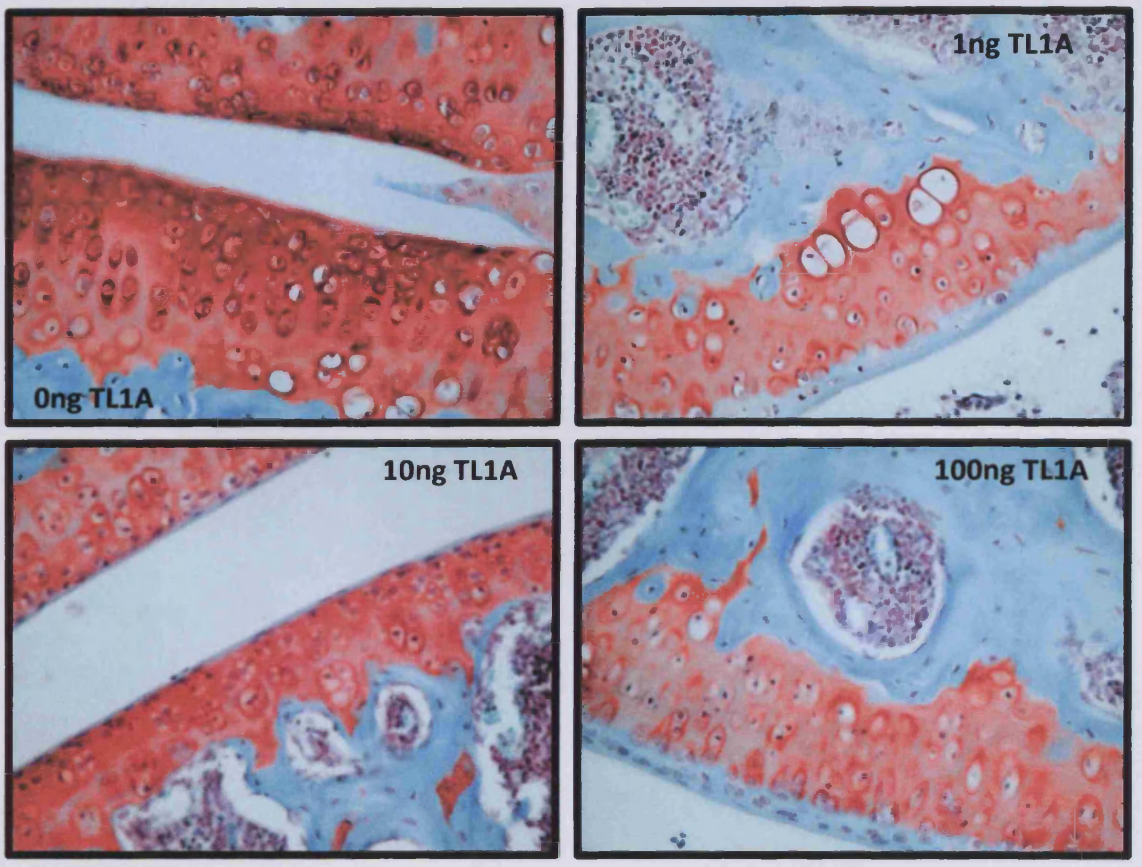


**Figure 5.25. TL1A does not affect cartilage depletion when administered to DR3$^{-/-}$ mice.** Representative Safranin O/ Fast Green stained sections (x40) are shown. Cartilage depletion was measured as a percentage of total cartilage using an eye piece with a line-graduated scale. Depth of depletion does not increase with increasing concentration of TL1A.

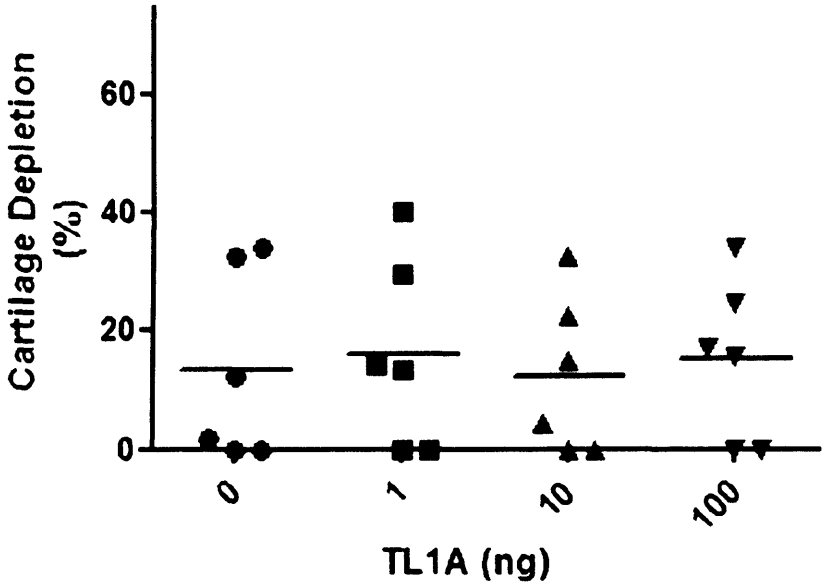


**Figure 5.26. Cartilage depletion on day 21 post-arthritis induction in DR3$^{-/-}$ mice receiving increasing doses of TL1A.** Cartilage depletion in the femoral head, measured as a percentage of total cartilage was analysed. TL1A had no effect on cartilage depletion in DR3$^{-/-}$ mice. Horizontal lines depict means. n = 6.

# Results
# Chapter 6

## 6. Adverse Joint Pathology is Reduced in DR3$^{-/-}$ mice in the AIA Model

### 6.1 Introduction

One of the most debilitating consequences of RA is the eventual destruction of joints resulting in deformity and disability. This is a costly result of the disease both for the patient and for society, with approximately 50% lower work force participation amongst sufferers and increased medical costs from hospitalisation and drug treatments (March and Lapsley, 2001). Furthermore, the pain and suffering associated with the disease and the eventual mortality is highly distressing for all of those involved. It has become accepted that in order to prevent joint damage, RA must be treated early using DMARDs, such as those mentioned in the previous chapter, before joint destruction becomes established. The long-term goal of this sort of therapy is not only to control the symptoms associated with RA but also to slow or ideally stop the progression of disease, allowing joint architecture to be protected.

Anti-TNF therapy has proven successful to a certain extent in controlling joint destruction. In clinical trials, both Infliximab and Etanercept have been shown to halt or at least slow the progression of joint erosion. In a study by Lipsky et al (2000), the effect of administering Infliximab in a combined therapy with another DMARD, Methotrexate, was examined over a one year period in patients with persistently active arthritis. By evaluating joints for radiographic scores according to the degree of destruction, it was found that the combined therapy of Infliximab and Methotrexate resulted in significantly less progression of joint damage compared to treatment with Methotrexate alone. In fact, between 39% and 55% of those

receiving the combined therapy actually resulted in improved radiographic scores compared with 14% of those receiving Methotrexate (Lipsky et al., 2000). In an Etanercept trial in patients with early arthritis, joints were again analysed for radiographic scores and it was found that twice weekly administration of 25mg of Etanercept resulted in a mean increase in erosion score of 0.47 at 12 months compared with 1.03 when treated with Methotrexate alone. Those in the Methotrexate group were also more likely to discontinue treatment due to adverse effects (Bathon et al., 2000). Adverse effects were experienced by a proportion of all experimental groups in both of the aforementioned trials and regardless of treatment group, a proportion of patients did not see any improvement in the progression of joint damage. Thus although these results provide promising data, Infliximab, Etanercept and Methotrexate cannot be described as a "cure" for the joint destruction associated with Rheumatoid Arthritis.

The mechanisms of normal bone turnover and the proposed processes of pathological bone resorption during RA have been discussed in setions 1.3 and 1.4. Why blocking TNFα results in a certain degree of protection from joint destruction is still a matter for debate. In a review article by Boyce et al (2005), a mechanism for TNFα mediated bone destruction is proposed. It is suggested that TNFα influences the formation of osteoclasts, the priniciple bone resorbing cells, by both RANK dependent and independent mechanisms. Independent of RANK, TNFα is suggested to promote the differentiation and proliferation of osteoclast precursors in the bone marrow by stimulating c-Fms expression. In this respect an increase in the osteoclast precursor pool size is achieved. In the later stages of osteoclast

development, TNFα is suggested to work in concert with RANK/RANKL to enhance osteoclast maturation by both inducing RANKL expression on synovial cells, T cells and osteoblasts and also by binding directly to the osteoclast precursors in order to induce their differentiation (Boyce et al., 2005). Numerous conflicting studies have led to the proposal of this model, with authors producing conflicting arguments for the mechanism of TNFα induced osteoclastogenesis. Lam et al. (2000) suggested that "permissive" levels of RANKL are required for TNFα induced osteoclastogenesis and that TNFα induced osteoclastogenesis cannot be achieved independently of RANKL. In a population of osteoclast precursors, the authors were unable to induce osteoclastogenesis in the presence of TNFα and M-CSF. However, when treated with both TNFα and low doses of RANKL, TNFα was capable of increasing osteoclastogenesis in a dose-dependent manner. Interestingly, this effect was only seen when TNFα was administered 2-4 days after RANKL and not when administered at the same time (Lam et al., 2000). Nakao et al (2007) have also shown a synergistic effect of TNFα and RANK signalling on osteoclastogenesis. In co-cultures of osteoclast precursor cells with osteoblasts from wildtype, TNFα or TNFR1 deficient mice, osteoclastogenesis was always reduced in the absence of TNF signalling. Furthermore, blockade of RANKL signalling via OPG administration in this system completely inhibited osteoclastogenesis thus implying that TNF promotes osteoclastogenesis in the presence of RANKL (Nakao et al., 2007). Additionally, when osteoclast precursor cells were cultured with RANKL itself in the presence of M-CSF and anti-TNFα or anti-TNFR1 neutralising antibodies, osteoclastogenesis was inhibited in a dose-dependent manner. RANKL treatment of the osteoclast precursor cells was also shown to increase TNFα mRNA expression implying that

TNFα may act as an autocrine agent in osteoclastogenesis (Nakao et al., 2007). In a conflicting study, using a murine bone marrow macrophage culture system, Kobayashi et al. (2000) demonstrated the generation of TRAP positive cells induced by TNFα during the blockade of RANK activity (Kobayashi et al., 2000). This implies a RANK independent mechanism for osteoclastogenesis in this system. However, when Boyce et al. (2000) crossed mice expressing chronic low levels of TNFα with RANK knockout mice they found that although the mice exhibited an increase in CD11b+ osteoclast precursor cells compared to control animals, they were unable to generate mature bone resorbing osteoclasts (Boyce et al., 2005). This data, taken together with the results from the clinical trials, confirms an important but complex role for the TNF signalling pathway in pathological bone resorption and that TNFα is capable of influencing osteoclastogenesis.

Like DR3 TNFR1, RANK and OPG are also members of the tumour necrosis factor receptor superfamily, and thus this family of receptors appears to play an important role in bone destruction due to their role in osteoclastogenesis. In the previous chapter, we identified that $DR3^{-/-}$ mice which were induced to develop AIA had not developed erosions of the bone within the knee joint at the end point of the experiment. This was in stark comparison to the wildtype littermate controls which displayed extensive erosions. These results suggest that DR3 plays a role in bone degradation during the AIA model for Rheumatoid Arthritis and that its blockade may be an effective therapy for protecting joint architecture during the disease. For these reasons we decided to examine the numbers of osteoclasts evident at different sites within the AIA joints of experimental animals. Additionally, osteoclast

precursor numbers within the joint were also examined via F4/80 staining to detect cells of the monocyte/macrophage lineage. These cells have been shown to have the potential to differentiate into osteoclasts and their accumulation within the joint is required for osteoclastogenesis. The specific aims of this chapter were:

- To assess the numbers of osteoclasts present within the AIA joints of DR3 sufficient and deficient mice at day 3 post-arthritis induction at 3 distinct sites namely: growth plate; femoral head and sites of focal erosion.
- To assess the numbers of osteoclasts present within the AIA joints of DR3 sufficient and deficient mice at day 21 post-arthritis induction at 3 distinct sites namely: growth plate; femoral head and sites of focal erosion.
- To assess the numbers of monocyte/macrophages within the AIA joints of DR3 sufficient and deficient mice at day 3 post-arthritis induction at 2 distinct sites namely: growth plate and within the cellular infiltration.
- To assess the numbers of monocyte/macrophages within the AIA joints of DR3 sufficient and deficient mice at day 21 post-arthritis induction at 2 distinct sites namely: growth plate and within the cellular infiltration.

## 6.2 Results

### 6.2.1 Osteoclast expression at day 3 and day 21 post-arthritis induction

Osteoclast expression was assessed in knee joint sections from $DR3^{+/+}$ and $DR3^{-/-}$ mice on day 3 and day 21 post-arthritis induction. This was achieved via tartrate resistant acid phosphatase (TRAP) staining which results in osteoclasts staining red. TRAP is a metallophosphoesterase which catalyses the hydrolysis of phosphate monoesters (Brehme et al., 1999). In histology, TRAP is used as a routine marker for osteoclasts, acting as an early differentiation marker for osteoclastogenesis (Schett, 2007) and being secreted into the resorptive bone area during the resorptive phase of mature osteoclasts (Ek-Rylander et al., 1991). Osteoclast expression was examined at 3 separate sites. Under normal physiological conditions, osteoclasts are located within the growth plate, where they are involved in the normal turnover of chondrocytes within the maturation zone (Tsuboi et al., 2003). Additionally they are located within the cortical bone where remodeling occurs within microchannels (Schett, 2007). In RA, osteoclasts are additionally located at the bone:pannus interface resulting in local bone erosions (Schett, 2007). The 3 sites within the joint that were selected for analysis at day 3 were the femoral head, the growth plate and in the absence of bone erosions at this early time-point, in the infiltrating cells of the adipose tissue. At day 21, sites of active bone erosion were additionally examined.

### 6.2.2 Osteoclast expression at day 3 post-arthritis induction in the growth plate

Multinucleated TRAP+ cells were evident in the growth plate of both DR3 sufficient and deficient mice on day 3 post-arthritis induction (Figure 6.1). The average TRAP+

area in the growth plate of DR3 sufficient animals was 8.7%. In $DR3^{-/-}$ mice this value was slightly lower at 6.5%. The reduction in TRAP+ staining in DR3 deficient animals compared with controls was not statistically significant (Figure 6.2).

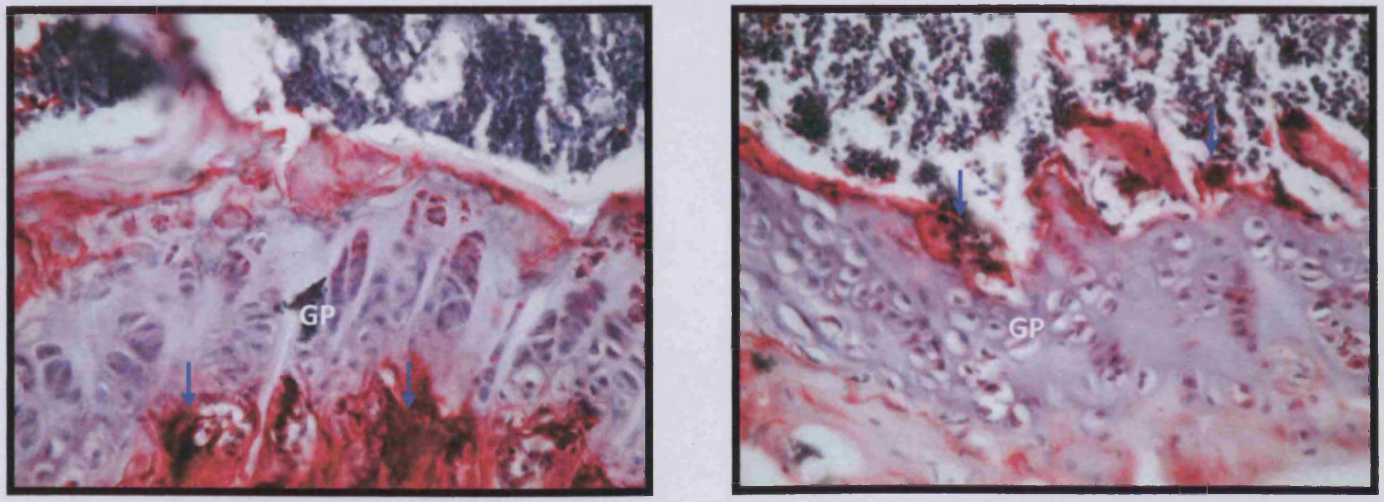


**Figure 6.1 TRAP Expression in the Growth Plate at Day 3 Post-Arthritis Induction**. Representative TRAP/Haemotoxylin stained knee joint sections from DR3 sufficient and deficient mice induced with AIA and sacrificed on day 3 post-arthritis induction. Sections were maintained in TRAP staining solution for 3 hours at 37°C as described in section 2.6.5. Osteoclasts (blue arrows) are expressed in the growth plate of $DR3^{+/+}$ and $DR3^{-/-}$ mice at comparable levels. GP = growth plate.

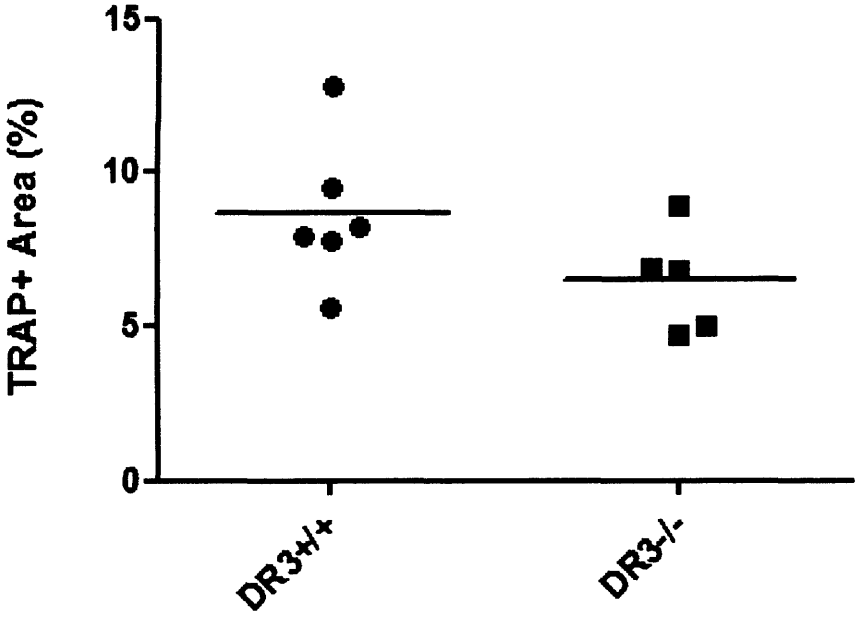


**Figure 6.2. Osteoclast Expression in the Growth Plate at day 3 Post-Arthritis Induction.** TRAP+ area was analysed in five randomly selected areas in the growth plate. In each area, the TRAP+ area in square pixels was determined using Adobe Photoshop CS3 and expressed as a percentage of the total area in view. TRAP+ area in the growth plate at day 3 post-arthritis induction is comparable in both DR3 sufficient and deficient mice. No statistical difference was observed (Mann-Whitney U test). Horizontal lines depict means. Each symbol represents one mouse.

### 6.2.3 Osteoclast expression at day 3 post-arthritis induction in the femoral head

TRAP+ staining was evident in the femoral head of both DR3 sufficient and deficient mice at day 3 post-arthritis induction (Figure 6.3). Control mice displayed an average TRAP+ area of 8.5% compared to 6.8% in $DR3^{-/-}$ animals. This was not a significant difference when assessed statistically (Figure 6.4).

### 6.2.4 Osteoclast expression at day 3 post-arthritis induction in the adipose tissue

As erosion of the bone is not typically evident at day 3 post-arthritis induction, this was not assessed. However, when analyzing the histological sections, TRAP+ cells were noted in the infiltrate of the adipose tissue of some of the mice (Figure 6.5). Therefore, TRAP expression in this area was instead examined. TRAP+ cells were generally only seen in DR3 sufficient animals within the adipose tissue. These cells did not display multinuclearity. Mean TRAP+ expression in this area in $DR3^{+/+}$ animals was 0.08% whilst only an average area of 0.005% in $DR3^{-/-}$ mice was TRAP+. This difference was statistically different when analysed using a Mann Whitney-U test ($p<0.05$) (Figure 6.6).

### 6.2.5 Osteoclast Expression at Day 21 Post-Arthritis Induction in the Growth Plate

Osteoclast expression at day 21 post-arthritis induction was assessed in the same manner as those analysed on day 3 post-arthritis induction. Infiltrating cells of the adipose tissue were not assessed. Instead, points of focal erosion at the bone-pannus interface or equivalent anatomical areas were analysed. Multinucleated TRAP+ cells were evident in the growth plate of both DR3 sufficient and deficient mice on day 21 post-arthritis induction (Figure 6.7). When analysed for TRAP+

percentage area as described in Materials and Methods, $DR3^{+/+}$ mice had an average TRAP+ percentage area of 3% in the growth plate.

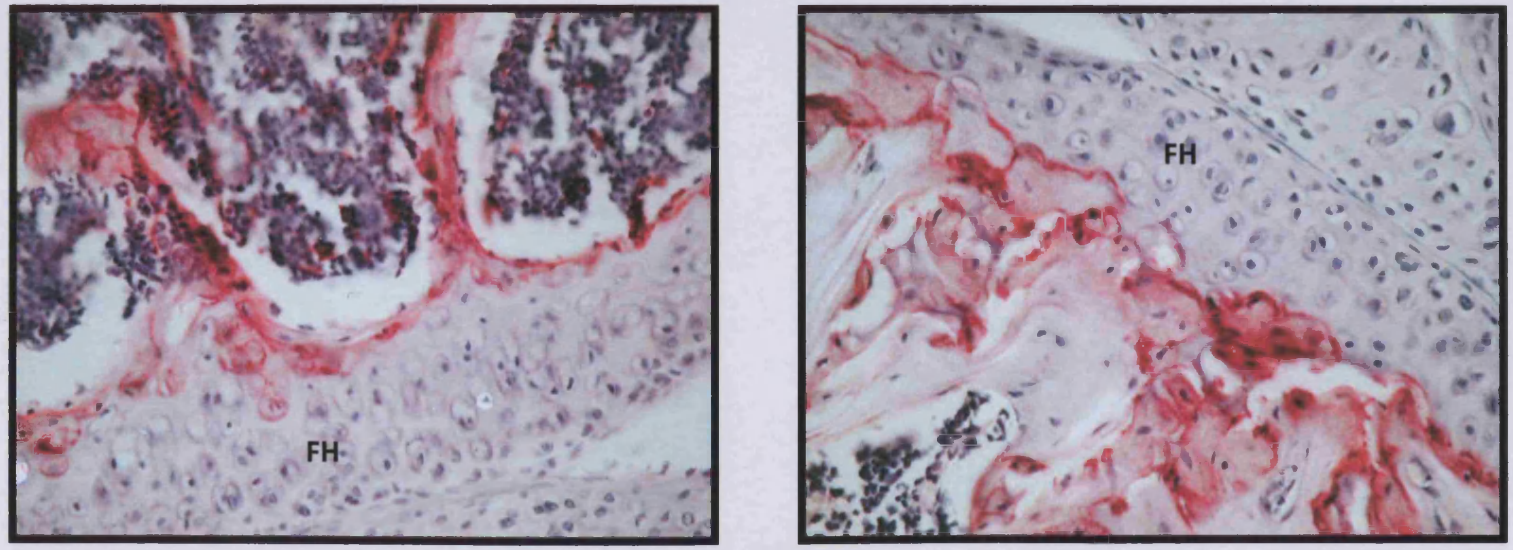


**Figure 6.3 TRAP Expression in the Femoral Head at Day 3 Post-Arthritis Induction.** Representative TRAP/Haemotoxylin stained knee joint sections from DR3 sufficient and deficient mice induced with AIA and sacrificed on day 3 post-arthritis induction. Sections were maintained in TRAP staining solution for 3 hours at 37°C as described in section 2.6.5. Osteoclast expression is not significantly different in the femoral head of $DR3^{-/-}$ mice compared to $DR3^{+/+}$ mice at day 3 post-arthritis induction. FH = femoral head.

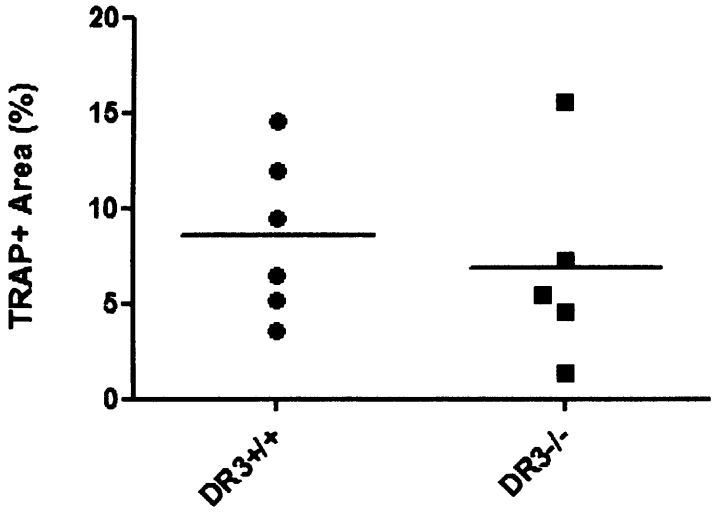


**Figure 6.4. TRAP Expression in the Femoral Head at Day 3 Post-Arthritis Induction.** TRAP+ area was analysed in five randomly selected areas in the femoral head. In each area, the TRAP+ area in square pixels was determined using Adobe Photoshop CS3 and expressed as a percentage of the total area in view. Osteoclast expression in the femoral head, as visualised by TRAP+ staining, is not significantly altered in $DR3^{-/-}$ mice at day 3 post-arthritis induction (Mann-Whitney U test). Horizontal lines depict means. n = 6.

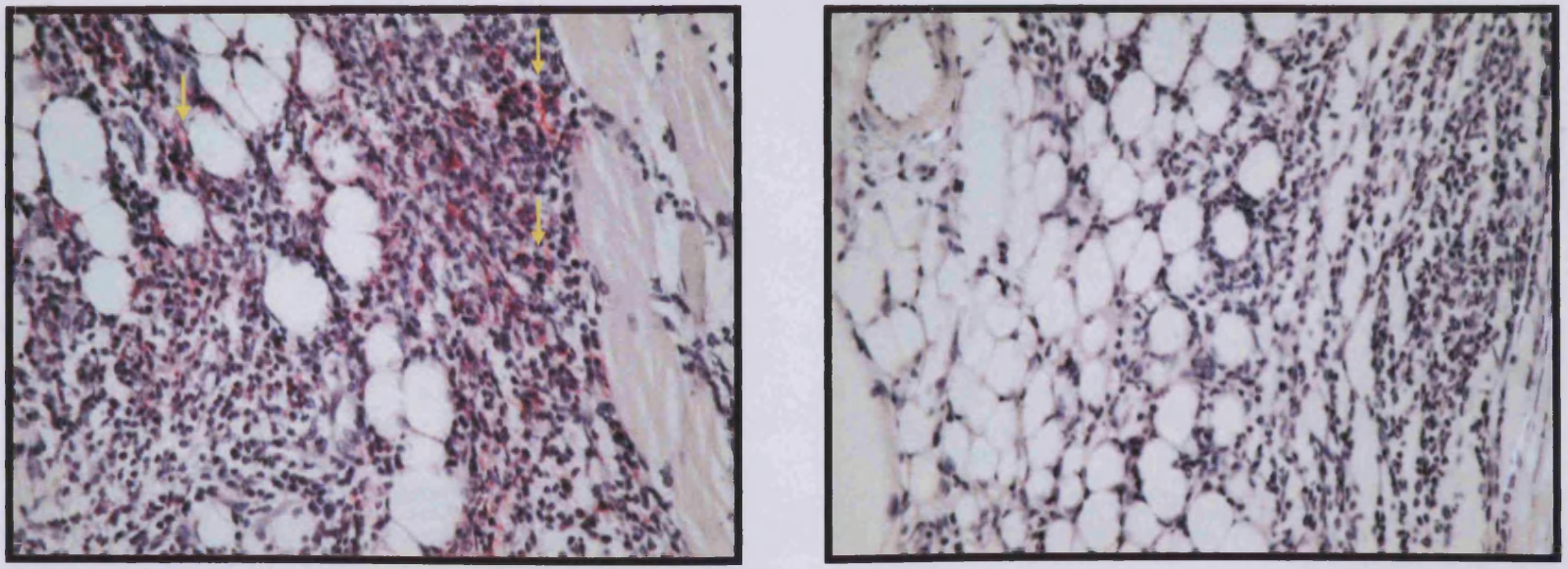


**Figure 6.5 TRAP Expression in the Infiltrating cells of the Adipose Tissue at day 3 Post-Arthritis Induction.** Representative TRAP/Haemotoxylin stained knee joint sections from DR3 sufficient and deficient mice induced with AIA and sacrificed on day 3 post-arthritis induction. Sections were maintained in TRAP staining solution for 3 hours at 37°C as described in section 2.6.5. TRAP positive cells (yellow arrows) are clearly visible within the adipose tissue in $DR3^{+/+}$ mice but not in $DR3^{-/-}$ mice. Red staining is significantly greater in $DR3^{+/+}$ mice.

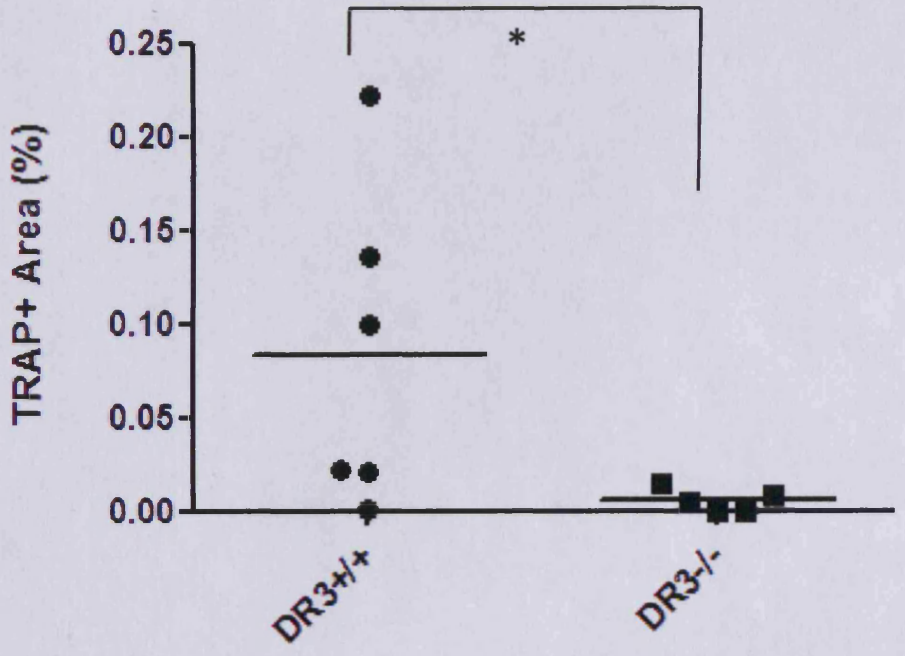


**Figure 6.6. TRAP Expression within the Infiltrating Cells in the Adipose Tissue at Day 3 Post-Arthritis Induction.** TRAP+ area was analysed in five randomly selected areas in the infiltrate. In each area, the TRAP+ area in square pixels was determined using Adobe Photoshop CS3 and expressed as a percentage of the total area in view. TRAP expression in the adipose tissue is significantly greater in $DR3^{+/+}$ mice at day 3 post-arthritis induction when analysed using a Mann-Whitney U test. * $p = <0.05$. Horizontal lines depict means. Each symbol represents one mouse.

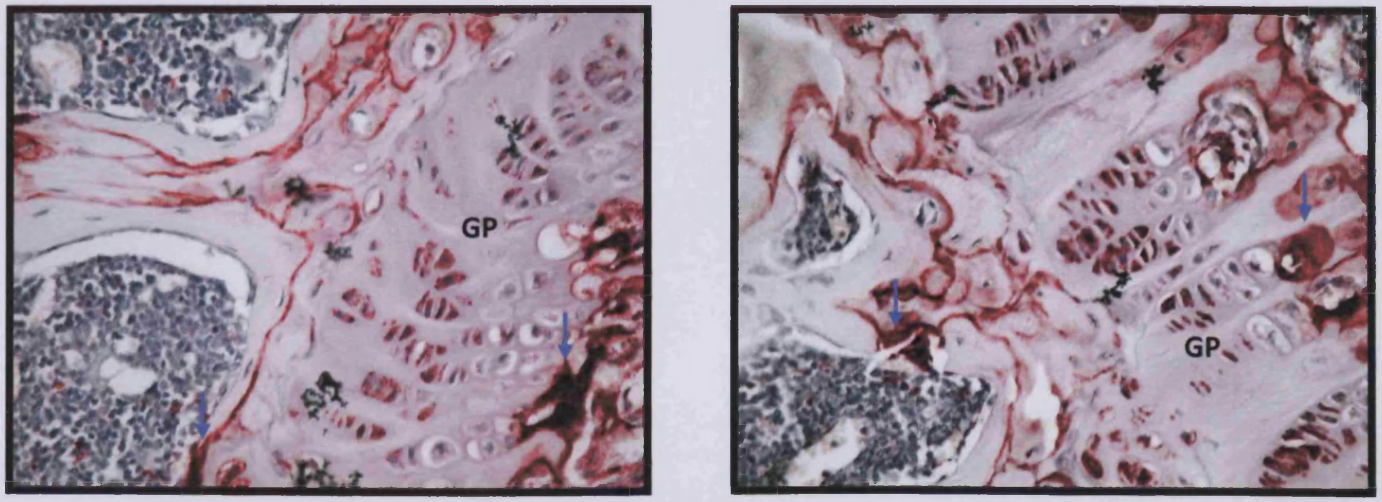


**Figure 6.7 TRAP Expression in the Growth Plate at Day 21 Post-Arthritis Induction.** Representative TRAP/Haemotoxylin stained knee joint sections from DR3 sufficient and deficient mice induced with AIA and sacrificed on day 21 post-arthritis induction. Sections were maintained in TRAP staining solution for 3 hours at 37°C as described in section 2.6.5. Osteoclasts (blue arrows) are expressed in the growth plate of $DR3^{+/+}$ and $DR3^{-/-}$ mice at comparable levels. GP = growth plate.

$DR3^{-/-}$ mice exhibited an average TRAP+ percentage area of 3.5%. When the average values were analysed statistically using a Mann-Whitney U test, no statistical significance was observed in TRAP+ area in the growth plate of $DR3^{+/+}$ and $DR3^{-/-}$ mice (Figure 6.8).

### 6.2.6 Osteoclast Expression at Day 21 Post-Arthritis Induction in the Femoral Head

TRAP+ cells in the femoral head of $DR3^{+/+}$ and $DR3^{-/-}$ mice were evident (Figure 6.9). DR3 sufficient mice had an average TRAP+ area of 0.6%. DR3 deficient mice had a lower TRAP+ area in the femoral head displaying an average of 0.4%. When compared statistically using a Mann-Whitney U test, the TRAP+ area in the femoral head of $DR3^{+/+}$ and $DR3^{-/-}$ mice at day 21 post-arthritis induction did not differ significantly (Figure 6.10).

### 6.2.7 Osteoclast Expression at day 21 Post-Arthritis Induction at sites of Erosion

Sites of bone erosion adjacent to areas of pannus development were not evident in $DR3^{-/-}$ mice. However, in order to statistically compare the areas of bone erosion in $DR3^{+/+}$ mice and $DR3^{-/-}$ mice, it was necessary to analyse those areas in the DR3 sufficient mice for TRAP+ cells and compare them to equivalent areas in the DR3 deficient mice. Thus, bone erosions in the DR3 sufficient animals were viewed under high magnification and anatomically equivalent areas in the $DR3^{-/-}$ mice were located and both were analysed for TRAP+ percentage area. In $DR3^{+/+}$ mice, areas of focal erosion were clearly evident adjacent to a thick layer of pannus development. TRAP+ multinucleated cells were present at these sites of erosion (Figure 6.11). Equivalent areas in the DR3 deficient mice did not display any evidence of TRAP+

staining. The mean TRAP+ area at sites of focal erosion in $DR3^{+/+}$ mice was 0.7%. The corresponding average value in the DR3 deficient mice was 0.2% (Figure 6.12). When analysed statistically using a Mann Whitney U test, a significant difference was identified between TRAP expression at sites of focal erosion between DR3 sufficient and deficient mice ($p<0.05$).

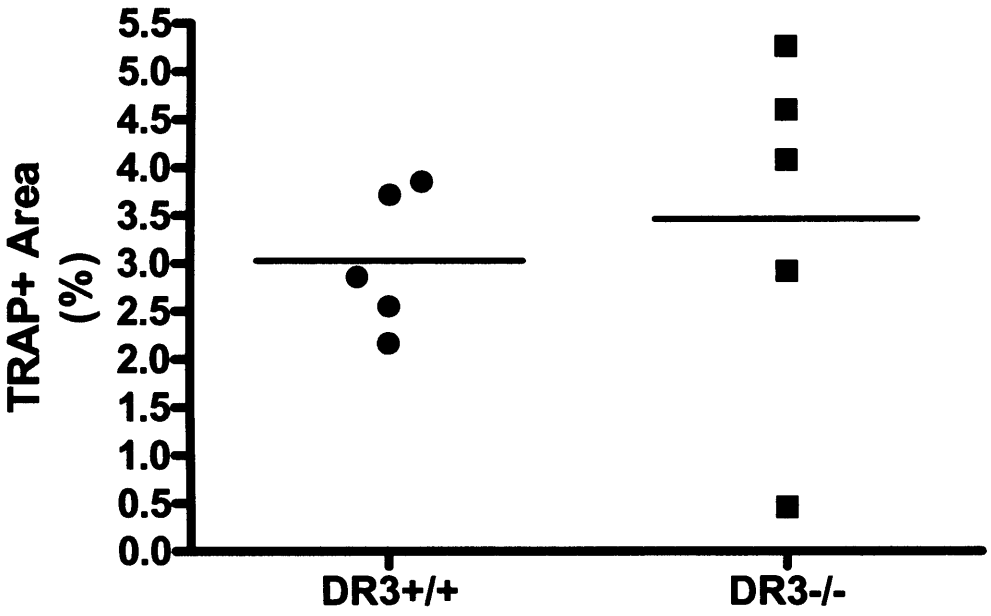


**Figure 6.8. Osteoclast Expression in the Growth Plate at day 21 Post-Arthritis Induction.** TRAP+ area was analysed in five randomly selected areas in the growth plate. In each area, the TRAP+ area in square pixels was determined using Adobe Photoshop CS3 and expressed as a percentage of the total area in view. TRAP+ osteoclast numbers in the growth plate at day 21 post-arthritis induction are comparable in both DR3 sufficient and deficient mice. No statistical difference was observed (Mann-Whitney U test). Horizontal lines depict means. n = 5.

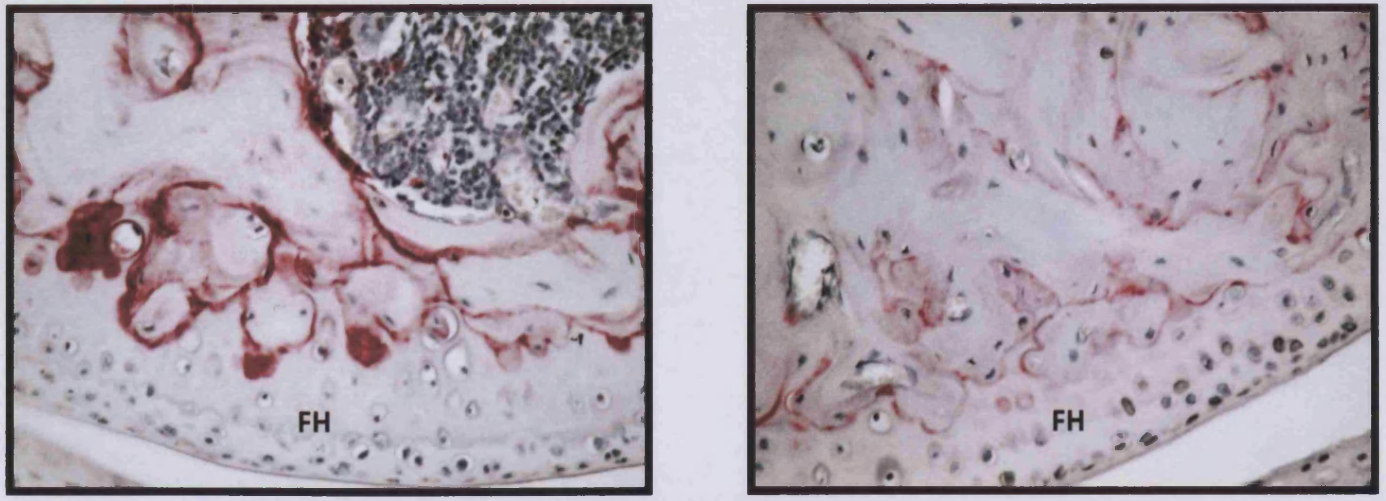


**Figure 6.9 TRAP Expression in the Femoral Head at Day 21 Post-Arthritis Induction.** Representative TRAP/Haemotoxylin stained knee joint sections from DR3 sufficient and deficient mice induced with AIA and sacrificed on day 21 post-arthritis induction. Sections were maintained in TRAP staining solution for 3 hours at 37°C as described in section 2.6.5. Osteoclast expression is reduced in the femoral head of $DR3^{-/-}$ mice compared to $DR3^{+/+}$ mice, however, this reduction in expression is not significant.

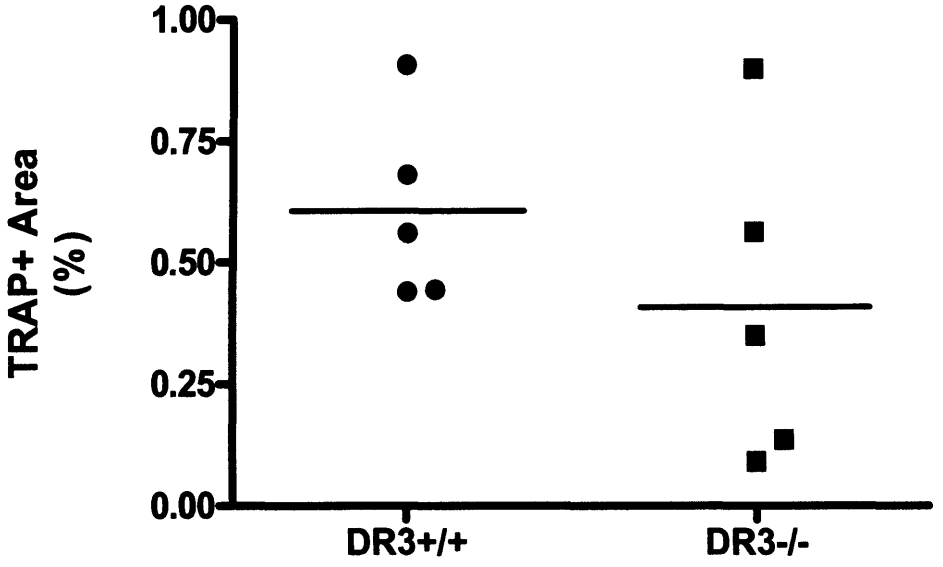


**Figure 6.10. TRAP Expression in the Femoral Head at Day 21 Post-Arthritis Induction.** TRAP+ area was analysed in five randomly selected areas in the femoral head. In each area, the TRAP+ area in square pixels was determined using Adobe Photoshop CS3 and expressed as a percentage of the total area in view. Osteoclast expression in the femoral head, as visualised by TRAP staining, is reduced in DR3$^{-/-}$ mice at day 21 post-arthritis induction although not significantly so (Mann-Whitney U test). Horizontal lines depict means. n = 5.

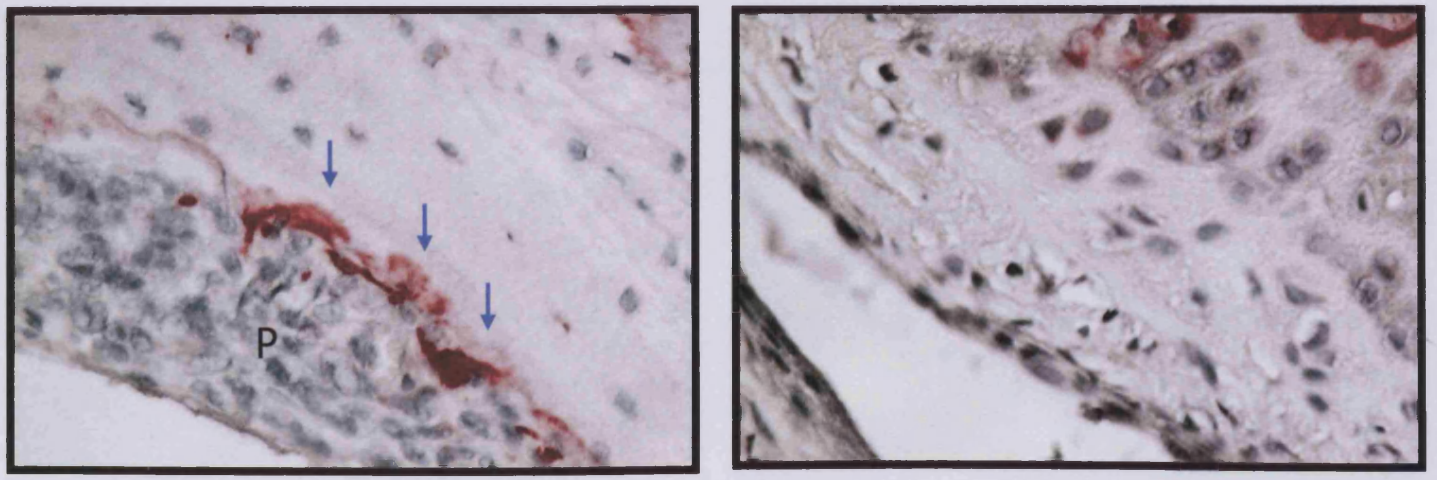


**Figure 6.11 TRAP Expression in Areas of Focal Bone Erosion at Day 21 Post-Arthritis Induction.** Representative TRAP/Haemotoxylin stained knee joint sections from DR3 sufficient and deficient mice induced with AIA and sacrificed on day 21 post-arthritis induction. Sections were maintained in TRAP staining solution for 3 hours at 37°C as described in section 2.6.5. Multinucleated osteoclasts (blue arrows) are clearly visible adjacent to pannus formation at areas of focal bone erosion in $DR3^{+/+}$ mice. Comparable areas in $DR3^{-/-}$ mice do not display positive staining for osteoclasts nor pannus formation. P = pannus.

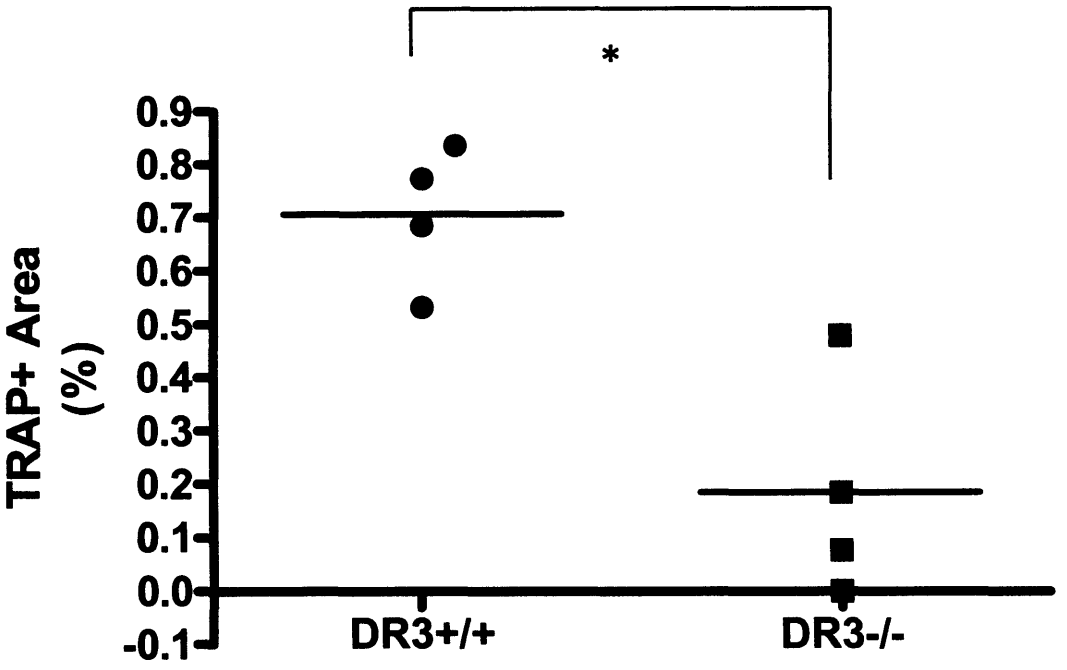


**Figure 6.12. TRAP Expression in Areas of Focal Bone Erosion at Day 21 Post-Arthritis Induction.** TRAP+ area was analysed at sites of active bone erosion. In each area, the TRAP+ area in square pixels was determined using Adobe Photoshop CS3 and expressed as a percentage of the total area in view. Areas of focal bone erosion in $DR3^{+/+}$ mice displayed significantly more TRAP+ expression than anatomically equivalent areas in $DR3^{-/-}$ mice. * $p = <0.05$ (Mann-Whitney U test). Horizontal lines depict means. $n = 4$.

### 6.2.8 Expression of F4/80+ cells in the AIA joint at day 3 post-arthritis induction

Osteoclast precursors are derived from cells of the monocyte/macrophage lineage, as discussed in section 1.3.6. Thus, in order for bone resorbing osteoclasts to be present within the joint, it is necessary for osteoclast precursor cells to first be recruited to the joint before they can differentiate into mature functional osteoclasts. In order to assess whether $DR3^{-/-}$ mice displayed dysfunctional recruitment of cells of the monocyte/macrophage lineage into the joint, the expression of F4/80 at both day 3 and day 21 post-arthritis induction was analysed. F4/80 is a monoclonal antibody that recognises a mouse macrophage-restricted glycoprotein which is routinely used in macrophage research (McKnight et al., 1996). Although macrophages are not necessarily destined to become osteoclasts, they do share a common progenitor cell. As such, the recruitment of the precursor cells of both macrophages and osteoclasts to the joint likely share common mobilisation and recruitment processes. Thus, in the absence of a specific marker for osteoclast precursor cells, F4/80 expression was studied instead. F4/80+ cells residing within the growth plate, where physiological bone remodeling occurs, and those which entered the joint in the inflammatory cell infiltrate were both examined.

At day 3 post-arthritis induction, F4/80+ cells are clearly visible in the growth plate of both DR3 sufficient and deficient mice (Figure 6.13). $DR3^{+/+}$ mice had a mean F4/80 positive area in the growth plate of 0.07%. The corresponding mean F4/80+ percentage area in the growth plate of DR3 deficient mice was 0.11%. When compared statistically using a Mann-Whitney U test, no significant difference was

found between the F4/80+ area in the growth plate of $DR3^{+/+}$ and $DR3^{-/-}$ mice at day 3 post-arthritis induction (Figure 6.14).

Infiltration of F4/80+ cells into the adipose tissue of the joint was examined. Both $DR3^{+/+}$ and $DR3^{-/-}$ mice displayed very little F4/80+ staining within the adipose tissue at day 3 post-arthritis induction (Figure 6.15). $DR3^{+/+}$ mice had a mean F4/80+ area of 0.002% compared to a corresponding value of 0.002% in the $DR3^{-/-}$ animals. There was no significant difference when compared statistically (Figure 6.16).

### 6.2.9 Expression of F4/80+ cells in the AIA joint at day 21 post-arthritis induction

At day 21 post-arthritis induction, F4/80+ cells were present in the growth plate of both DR3 sufficient and deficient mice (Figure 6.17). $DR3^{+/+}$ mice displayed an average F4/80+ area within the growth plate of 0.22%. $DR3^{-/-}$ mice displayed a mean F4/80+ area of 0.21%. When analysed statistically using a Mann Whitney U test, there was no significant difference in F4/80+ area within the growth plate of $DR3^{+/+}$ and $DR3^{-/-}$ at day 21 post-arthritis induction (Figure 6.18).

Within the cell infiltrate in the adipose tissue, F4/80+ cells were quite abundant in both $DR3^{+/+}$ and $DR3^{-/-}$ mice by day 21 post-arthritis induction (Figure 6.19). DR3 sufficient animals had an average F4/80+ area of 0.07%. The corresponding mean value in $DR3^{-/-}$ mice was 0.03%. These values did not differ significantly when testing statistically (Figure 6.20).

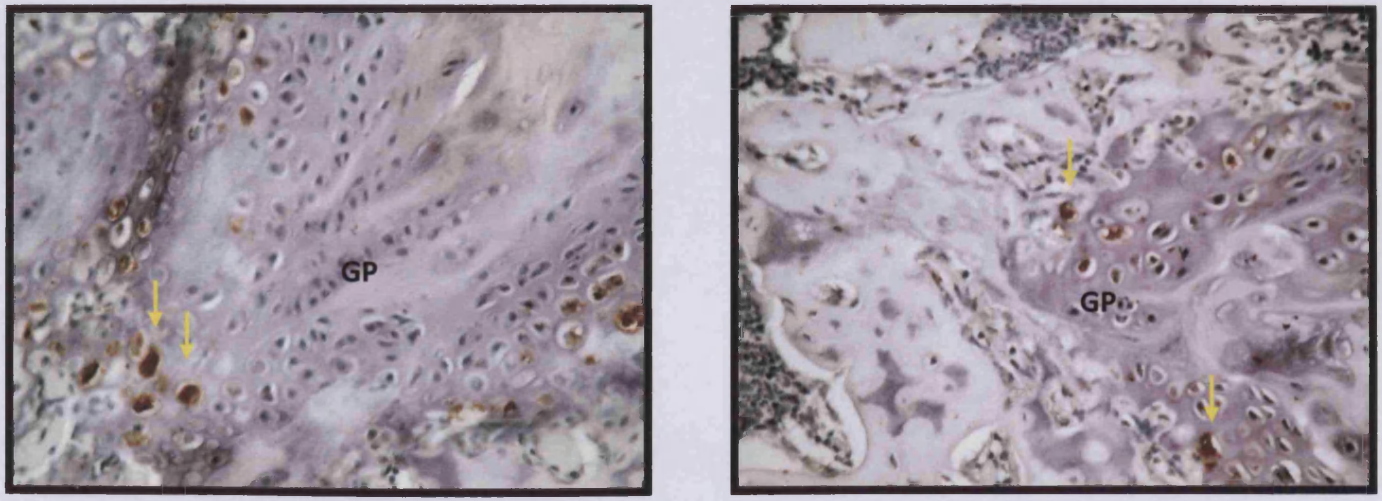


**Figure 6.13 F4/80 Expression in the Growth Plate at Day 3 Post-Arthritis Induction.** Representative F4/80/Haemotoxylin stained knee joint sections from DR3 sufficient and deficient mice induced with AIA and sacrificed on day 3 post-arthritis induction. Sections were incubated with anti-mouse F4/80 monoclonal antibody overnight at 4°C, as described in section 2.6.7. F4/80+ mononuclear cell expression (yellow arrows) in the growth plate, as indicated by positive F4/80 staining, was comparable between $DR3^{+/+}$ and $DR3^{-/-}$ mice at day 3 post-arthritis induction. GP = growth plate.

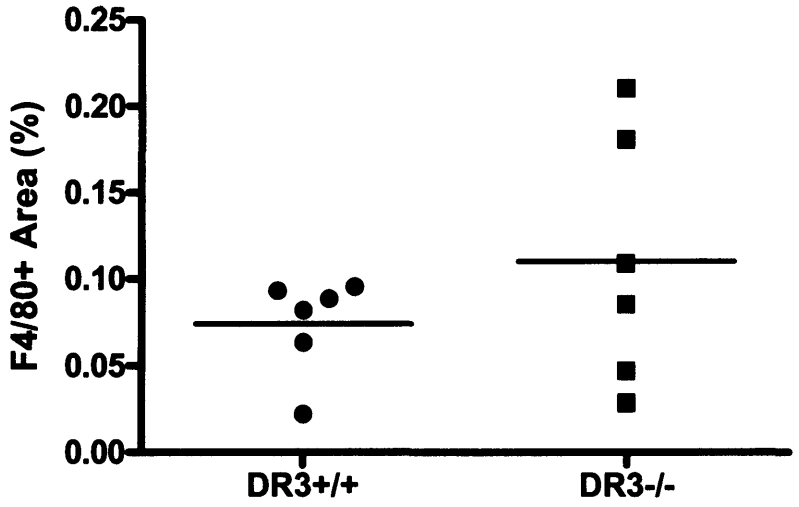


**Figure 6.14. F4/80 Expression in the Growth Plate at day 3 Post-Arthritis Induction.** F4/80+ area was analysed in five randomly selected areas in the growth plate. In each area, the F4/80+ area in square pixels was determined using Adobe Photoshop CS3 and expressed as a percentage of the total area in view. Comparable levels of F4/80+ staining was evident in the growth plate on day 3 post-arthritis induction (Mann-Whitney U test). Horizontal lines depict means. n = 6.

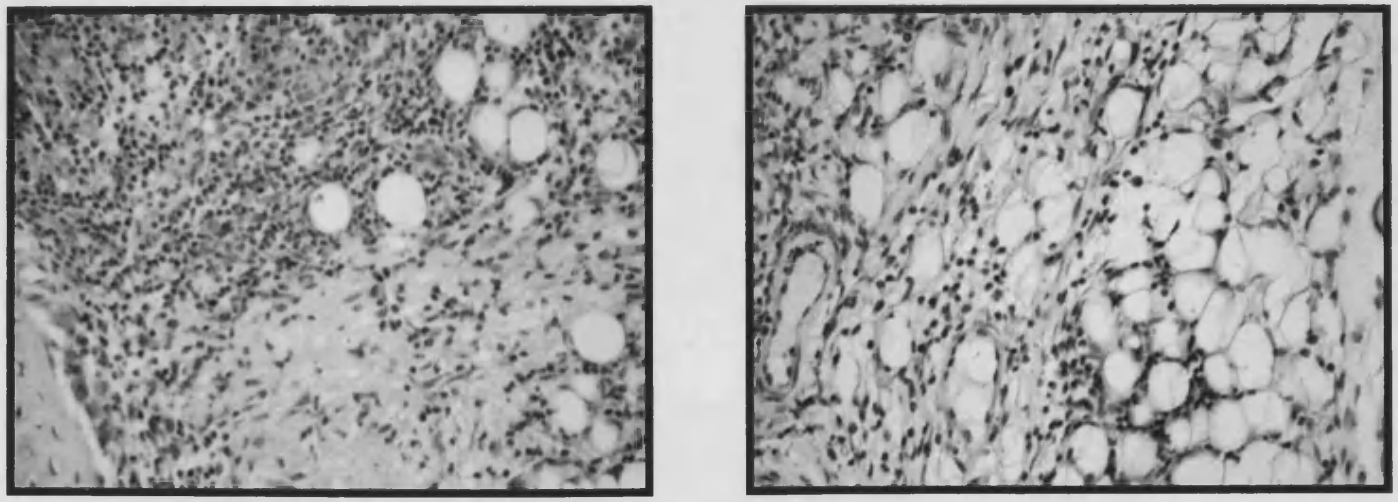

$DR3^{+/+}$ $DR3^{-/-}$ x40

**Figure 6.15. F4/80 Expression in Adipose Tissue on Day 3 Post-arthritis Induction.** Representative F4/80/Haemotoxylin stained knee joint sections from DR3 sufficient and deficient mice induced with AIA and sacrificed on day 3 post-arthritis induction. Sections were incubated with anti-mouse F4/80 monoclonal antibody overnight at 4°C, as described in section 2.6.7. F4/80+ mononuclear cell infiltration into the adipose tissue was comparable between $DR3^{+/+}$ and $DR3^{-/-}$ mice at day 3 post-arthritis induction.

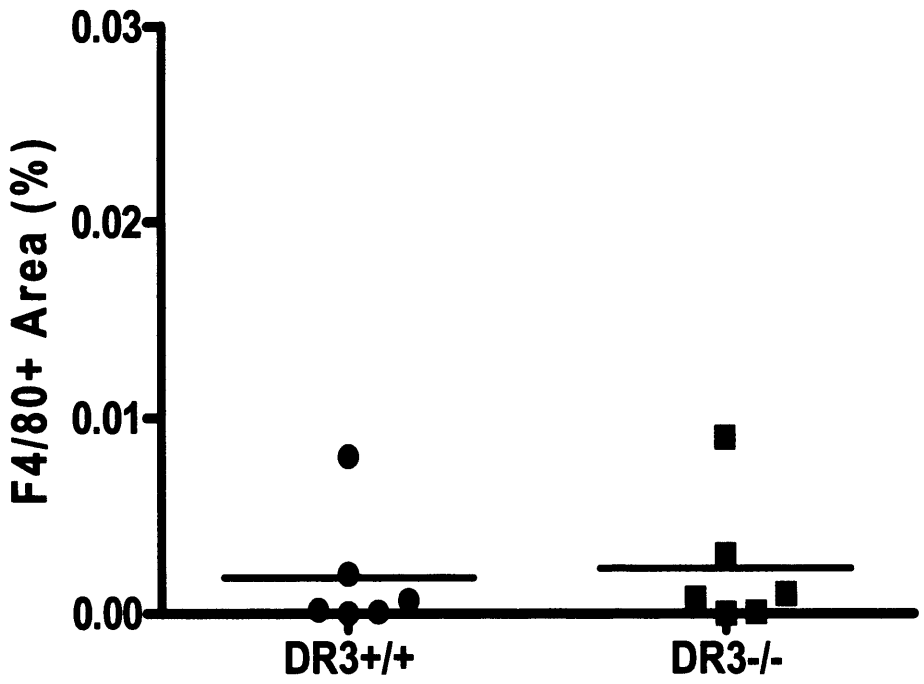


**Figure 6.16. Statistical Analysis of F4/80+ Mononuclear Cell Infiltration into the Adipose Tissue on Day 3 Post-Arthritis Induction.** F4/80+ area was analysed in five randomly selected areas in the infiltration. In each area, the F4/80+ area in square pixels was determined using Adobe Photoshop CS3 and expressed as a percentage of the total area in view. No statistical difference was observed in mononuclear cell infiltration into the adipose tissue of the joint on day 3 post-arthritis induction when analysed using a Mann-Whitney U test. Horizontal lines depict means. n = 6.

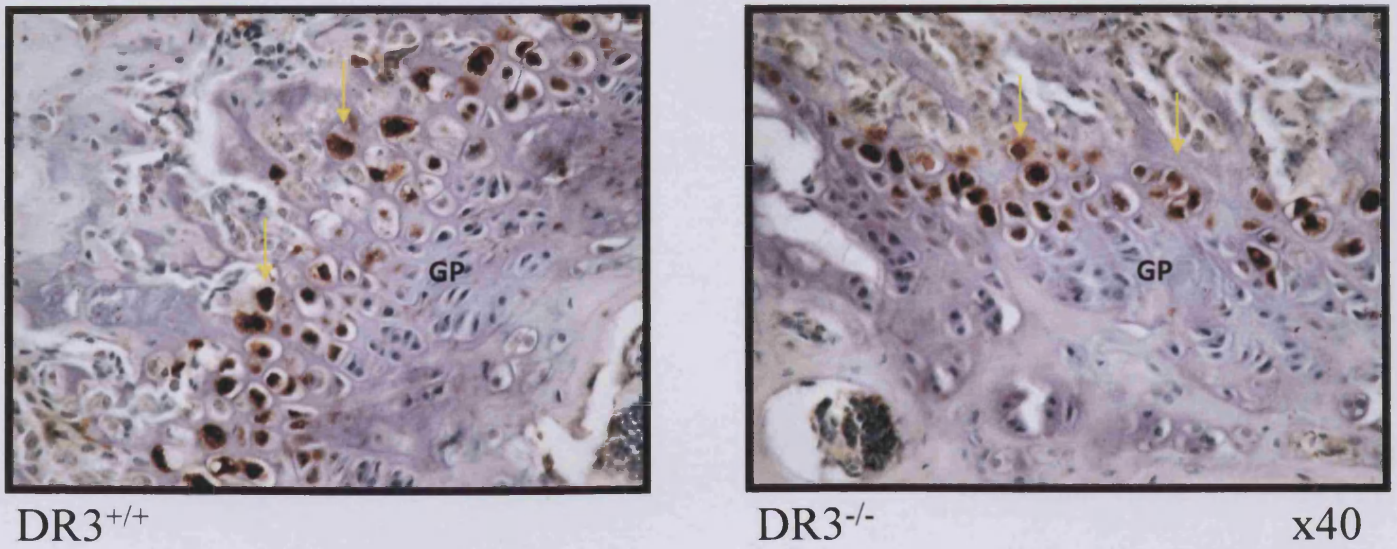


**Figure 6.17. F4/80 Expression in the Growth Plate at Day 21 Post-Arthritis Induction.** Representative F4/80/Haemotoxylin stained knee joint sections from DR3 sufficient and deficient mice induced with AIA and sacrificed on day 21 post-arthritis induction. Sections were incubated with anti-mouse F4/80 monoclonal antibody overnight at 4°C, as described in section 2.6.7. F4/80+ mononuclear cell expression (yellow arrows) in the growth plate, as indicated by positive F4/80 staining, was comparable between $DR3^{+/+}$ and $DR3^{-/-}$ mice at day 21 post-arthritis induction. GP = growth plate.

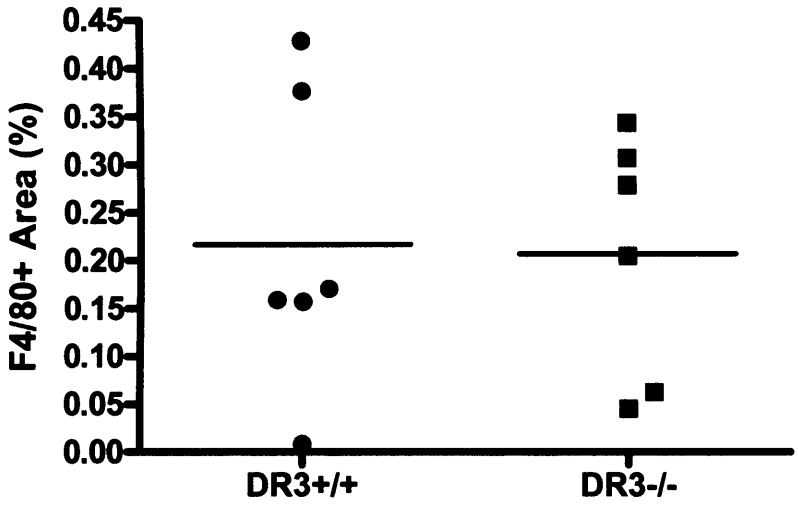


**Figure 6.18. F4/80 Expression in the Growth Plate at day 21 Post-Arthritis Induction.** F4/80+ area was analysed in five randomly selected areas in the growth plate. In each area, the F4/80+ area in square pixels was determined using Adobe Photoshop CS3 and expressed as a percentage of the total area in view. Comparable levels of F4/80+ cells were present in the growth plate at day 21 post-arthritis induction (Mann-Whitney U test). Horizontal lines depict means. n = 6.

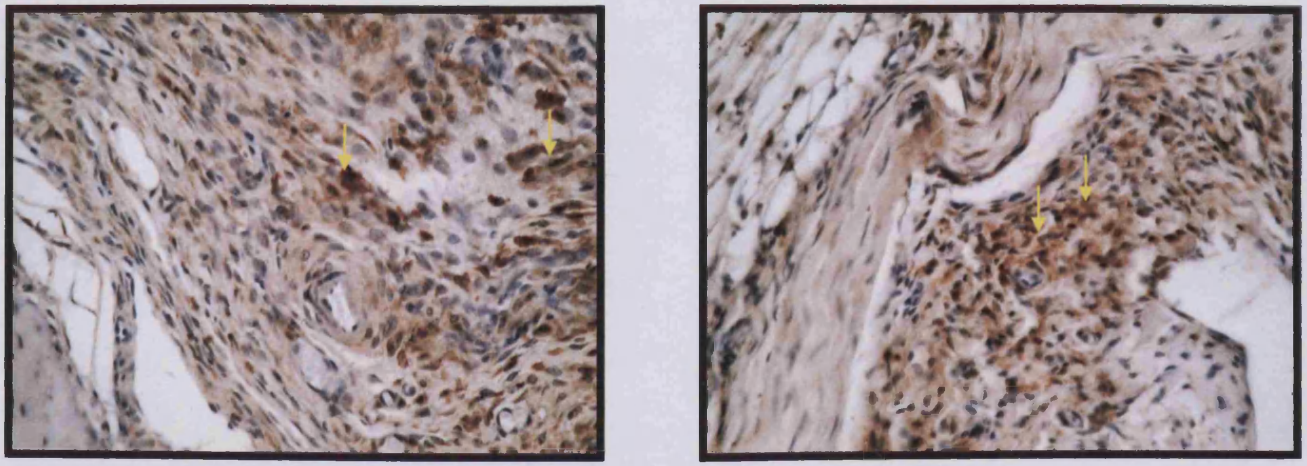

$DR3^{+/+}$ $DR3^{-/-}$ x40

**Figure 6.19. F4/80 Expression in Adipose Tissue on Day 21 Post-arthritis Induction.** Representative F4/80/Haemotoxylin stained knee joint sections from DR3 sufficient and deficient mice induced with AIA and sacrificed on day 21 post-arthritis induction. Sections were incubated with anti-mouse F4/80 monoclonal antibody overnight at 4°C, as described in section 2.6.7. F4/80+ mononuclear cell infiltration (yellow arrows) into the adipose tissue, as indicated by positive F4/80 staining, was comparable between $DR3^{+/+}$ and $DR3^{-/-}$ mice at day 21 post-arthritis induction.

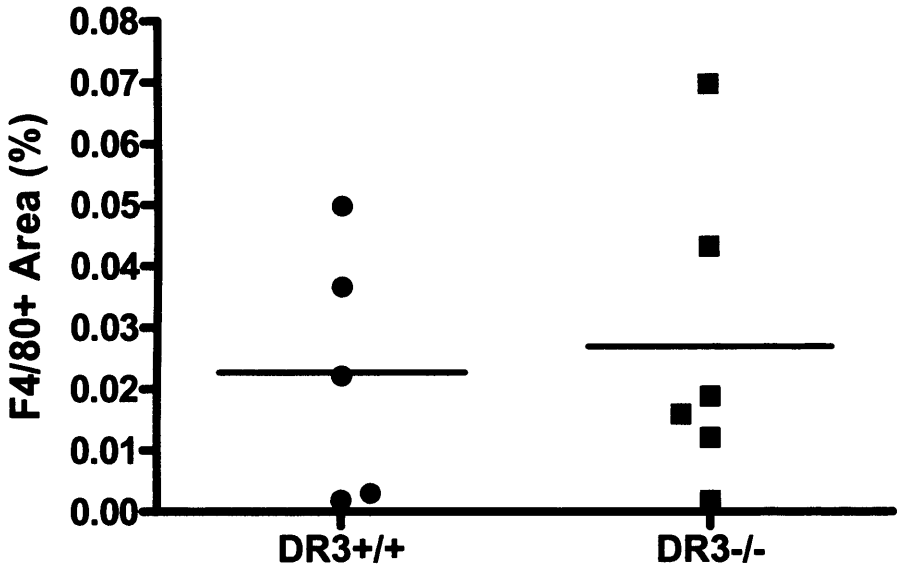


**Figure 6.20. Statistical Analysis of F4/80+ Mononuclear Cell Infiltration into the Adipose Tissue on Day 21 Post-Arthritis Induction.** F4/80+ area was analysed in five randomly selected areas in the infiltrate. In each area, the F4/80+ area in square pixels was determined using Adobe Photoshop CS3 and expressed as a percentage of the total area in view. No statistical difference was observed in mononuclear cell infiltration into the adipose tissue of the joint on day 21 post-arthritis induction when analysed using a Mann-Whitney U test. Horizontal lines depict means. Each symbol represents one mouse.

# Discussion

## 7. Discussion

### 7.1 DR3 Reagent Generation

A general lack of DR3 reagents, including antibodies and soluble proteins, has hampered progression in the DR3 field. As such, an aim of this project was to attempt to generate a number of reagents for use in DR3 research and particularly to help confirm any of our *in vivo* observations in the AIA model.

#### 7.1.1 Summary of Findings from Chapter 3

- Soluble and dominant negative hDR3 genes with and without streptag sequences were PCR amplified from plasmid DNA and sub-cloned into eukaryotic expression vectors.
- The full length mDR3 gene was amplified via RT-PCR reaction from murine thymus tissue.
- The mDR3 splice variant missing exons 5 and 6 was also generated via RT-PCR reaction.
- Dominant negative mDR3 was PCR amplified from the full length gene and sub-cloned into a eukaryotic expression vector.
- The soluble mDR3 splice variant, which is devoid of exon 6, was commercially manufactured and PCR amplified to insert streptag sequences if required. It was sub-cloned into a eukaryotic expression vector.
- All of the generated gene constructs were transfected into eukaryotic cell lines in order to facilitate soluble protein and stable cell line production. Detection of protein expression was difficult to achieve and very few of the

transfected constructs produced detectable levels of protein despite growing in selective media.

- However, the streptag protein included in the hDR3 constructs was successfully detected via immunofluorescence.
- Furthermore, the GFP tag included in the pEGFP-N1 vector enabled the detection of dominant negative mDR3 and soluble + streptag hDR3 via Western blot and fluorescence.
- Soluble protein was never detected in the supernatant of the cells. Attempts to increase expression of soluble protein via new cloning strategies did not rectify this problem.

### 7.1.2 Chapter 3 Discussion

#### 7.1.2.1 DR3 Gene Cloning

Prior to this work, both the human and murine DR3 genes had been previously cloned. Human DR3 was originally cloned in 1996 by multiple research groups (Bodmer et al., 1997, Chinnaiyan et al., 1996, Marsters et al., 1996, Screaton et al., 1997) and the full length gene comprised 1665 bps made up of 10 exons. Murine DR3 was cloned in 2001 by Wang and co-workers and was shown to contain 1619 bps and like the human gene, was made up of 10 exons (Wang et al., 2001a). We obtained the full length human DR3 gene for use as a template for further PCR amplification from Stuart Farrow (Glaxo Wellcome, Herts, UK). Full length mDR3 was isolated by RT-PCR from thymus tissue and matched the published sequence of full length murine DR3. Additionally, one of the published murine DR3 splice variants which is devoid of exons 5 and 6 was also cloned by RT-PCR. Murine DR3

transfected constructs produced detectable levels of protein despite growing in selective media.

- However, the streptag protein included in the hDR3 constructs was successfully detected via immunofluorescence.
- Furthermore, the GFP tag included in the pEGFP-N1 vector enabled the detection of dominant negative mDR3 and soluble + streptag hDR3 via Western blot and fluorescence.
- Soluble protein was never detected in the supernatant of the cells. Attempts to increase expression of soluble protein via new cloning strategies did not rectify this problem.

### 7.1.2 Chapter 3 Discussion

#### 7.1.2.1 DR3 Gene Cloning

Prior to this work, both the human and murine DR3 genes had been previously cloned. Human DR3 was originally cloned in 1996 by multiple research groups (Bodmer et al., 1997, Chinnaiyan et al., 1996, Marsters et al., 1996, Screaton et al., 1997) and the full length gene comprised 1665 bps made up of 10 exons. Murine DR3 was cloned in 2001 by Wang and co-workers and was shown to contain 1619 bps and like the human gene, was made up of 10 exons (Wang et al., 2001a). We obtained the full length human DR3 gene for use as a template for further PCR amplification from Stuart Farrow (Glaxo Wellcome, Herts, UK). Full length mDR3 was isolated by RT-PCR from thymus tissue and matched the published sequence of full length murine DR3. Additionally, one of the published murine DR3 splice variants which is devoid of exons 5 and 6 was also cloned by RT-PCR. Murine DR3

proved difficult to amplify by conventional RT-PCR methods from thymus tissue. This may reflect the guanosine/cytosine (GC) -rich nature of the gene, as sequences which are high in GC content are notoriously difficult to amplify due to their ability to form secondary structures (Henke et al., 1997). This difficulty in amplification may also reflect the level of DR3 expression within normal tissues. Wang et al. have reported the expression of all 3 murine DR3 splice variants in thymus tissue (Wang et al., 2001a). However, the activation of T cells has been associated with an increase in the ratio of trans-membrane DR3 mRNA to total DR3 mRNA compared to the levels seen in resting T cells (Bamias et al., 2006). Thus it appears that full length DR3 may not be expressed at high levels in normal tissues making its amplification by RT-PCR difficult. The full length mDR3 gene was eventually amplified using a technique modified from a method which has been described to successfully amplify GC-rich products (Bachmann et al., 2003). In this respect, the difficulties associated with cloning the mDR3 gene may just reflect the composition of the gene.

In order to facilitate the expression of DR3 in an eukaryotic system, dominant negative forms of both human and murine DR3 genes were PCR amplified from the full length DR3 gene templates. It was essential to use dominant negative genes which did not contain a death domain because the over-expression of DR3 in eukaryotic cells results in apoptosis (Bodmer et al., 1997, Chinnaiyan et al., 1996, Marsters et al., 1996, Screaton et al., 1997, Kitson et al., 1996). A further truncated version of human DR3 was also cloned from the full length template which was devoid of both transmembrane and death domain regions in order to generate a

soluble protein. The published soluble splice variant of murine DR3 in which exon 6 is absent and an early stop codon occurs prior to the transmembrane domain was obtained commercially. Dominant negative and soluble versions of human and murine DR3 genes were cloned into appropriate eukaryotic expression vectors. Dominant negative gene sequences were cloned into the vector pDR2δEF1α. This vector contains a powerful EF1a promoter which drives high levels of protein expression (personal communication with Claire Harris, Medical Biochemistry and Immunology, Cardiff University). Soluble gene sequences were cloned into the vector Signal pigplus which contains a CD33 signal sequence and a human IgG1 Fc sequence which serve to facilitate high levels of secretion of the fusion protein (Bose et al., 2006). Not all of the soluble constructs were engineered to include the human IgG1 Fc tail. They were designed to contain the Fc tail or the streptag sequence or both. The streptag II sequence has previously been used successfully within our lab for protein detection via both fluorescence and Western blot. It was hoped that adopting a cloning strategy which generated constructs with multiple options for detecting the expressed protein might overcome the obvious difficulties associated with the absence of a commercially available DR3 antibody.

#### 7.1.2.2 DR3 Protein Expression

Protein expression from transfected cell lines was assessed by both fluorescence and Western blot methods. The streptag protein was only detectable by immunofluorescence methods whilst Western blots for either streptag or IgG1 Fc for those constructs which were tested were consistently unsuccessful. However, when attempts to overcome this protein detection difficulty were undertaken by

cloning the genes into GFP expressing vectors, positive Western blots for both GFP and the streptag protein in the cell lysate were achieved. Soluble proteins were never detected in the cell supernatant. It is possible that the GFP expressing vector is capable of achieving higher levels of protein expression than both Signal pigplus and pDR2δEF1α and that the ability to obtain positive expression by Western blot analysis was a reflection of the higher expression levels. As the production of soluble DR3 protein was of particular interest, we adopted a new cloning strategy for the soluble genes to attempt to boost protein expression. The murine and human soluble genes were amplified from the Signal pigplus vectors with primers engineered to amplify the CD33 signal sequence and the IgG1 Fc tail in addition to the gene of interest. The products of this amplification were subsequently subcloned into the pDR2δEF1α vector which we had been advised would increase soluble protein production by 10 fold. Following transfection of the soluble mDR3 construct however, protein was not detected in the cell lysate via anti-IgG1 Fc Western blot analysis.

### 7.1.3 Summary of Findings from Chapter 4

- Four peptides based on the sequence of murine DR3 were designed and purchased.
- $DR3^{-/-}$ mice were immunised with the peptides.
- Only mice immunised with peptide 2 generated specific antibodies and were selected for hybridoma production.
- Hybridoma clones were generated and screened for antibody production against the original peptide.

- Although antibody secreting hybridoma clones were produced, only 1 clone secreted a peptide specific antibody. However, this clone subsequently died.

### 7.1.4 Chapter 4 Discussion

The Kohler and Milstein protocol for antibody generation is a widely employed method which has successfully enabled the generation of antibodies against numerous different antigens. The aim of this chapter was to exploit this method in order to generate antibodies against human and murine DR3. A pre-requisite of this protocol is the availability of pure antigen with which to immunise animals. Initially it was the intention to use cells which stably expressed dominant negative DR3 or soluble DR3 proteins tagged with either streptag or human IgG1 Fc as the antigens. However, difficulty in generating stable cell lines and soluble proteins precluded this work. Thus a second method was employed to generate antibodies against mDR3 which used synthetic peptides as the immunogen. Peptides represent only a small portion of the complete protein and thus run the risk of generating antibodies which cannot recognise the native protein due to masking during protein folding. However, antibodies generated in this manner should be able to recognise linear protein during procedures such as Western blot analysis when proteins are denatured. Even anti-DR3 antibodies which are only suitable for Western blot techniques were of importance to us, thus the peptide method of antibody generation was considered appropriate. As peptides are very small molecules and unable to generate effective memory immune responses, mDR3 peptides were constructed as MAPs which contain multiple copies of the antigen on a lysine core. MAP peptides have been shown to generate an effective immune response whilst

removing the need for coupling the antigens to carrier proteins, which themselves are immunogenic (Tam, 1988). Four peptides based on the mDR3 sequence, which according to an online peptide design tool (http://peptideselect.invitrogen.com) were predicted to be capable of generating antibodies with the ability to recognise native protein, were designed and synthesised. By selecting 4 different peptides, the chances of generating a panel of antibodies which were DR3 specific, capable of recognising native protein and with the potential to recognise only specific splice variants of the gene were increased. Following immunisation of DR3 deficient mice with 3 of these peptides, immune responses were only developed against peptide number 2 which fell within cysteine-rich domain 3 of DR3. Thus it would appear that the remaining 2 peptides did not display the immunogenic properties which would be expected of a MAP peptide. Hybridoma cells were generated from the spleen cells of one of the mice immunised with peptide 2. The efficiency of hybridoma cell production proved extremely poor with only 54 out of 720 wells containing clones for analysis. Using this technique, it would not be unexpected to have at least 500 wells to test for antibody production (personal communication with Mrs Sian Llewellyn-Lacey, MRC Tissue Culture Technician, Cellular and Viral Immunology Resource, Cardiff University). Following fusion, cells were seeded into 96 well plates and were grown in the presence of a hybridoma feeding supplement in order to enhance growth. However, if the cells had initially been grown at higher densities in fewer wells, growth factors released from the surrounding cells may have further enhanced the growth of hybridoma cells enabling a greater proportion of cells to reach the densities required for analysis. This would, however, have increased the likelihood of non-antibody secreting cells over-growing those that

were secreting antibodies. Supernatant from only 6 of the clones tested reacted with the immunising peptide and of these 6, only one was specifically reactive with the peptide. Supernatant from 5 of the clones also reacted with a non-immunising peptide indicating that the lysine core which the MAPs were generated on was not entirely inert. Screening the supernatants against poly-L-lysine itself would confirm this. The one clone which appeared to be specifically reactive against the immunising peptide did not survive in culture. Thus despite attempts to generate anti-mDR3 peptide antibodies, poor immunogenicity of the peptides and poor efficiency of hybridoma generation in addition to a lack of specificity for the immunising peptide of the hybridomas produced, meant that the successful production of anti-DR3 antibodies was not achieved. The spleen from the second mouse that was immunised with peptide 2 and reacted positively with the immunising peptide in test bleeds, was frozen and remains available for hybridoma production. Following fusion of these spleen cells, they could be seeded at a higher density to encourage growth and survival and hopefully increase the number of clones available for analysis. In this manner, an anti-mDR3 antibody may still be produced from this set of experiments.

### 7.1.5 Concluding Remarks

The availability of antibodies against both human and murine DR3 was very limited prior to the commencement of this work. However, despite the limited success in generating antibodies and proteins in this study, DR3 reagents have now become more widely available. Multiple companies are now providing polyclonal human and murine anti-DR3 antibodies and a human anti-DR3 monoclonal antibody is also

available. Additionally, soluble proteins for both human and murine DR3 have been generated. There is still a distinct lack of murine monoclonal anti-DR3 antibodies available on the market although one has been generated by an independent research group (Fang et al., 2008). However, with the generation of a soluble mDR3 protein, there is potential to use this as an antigen in order to generate monoclonal antibodies. As previously mentioned, there is also still scope to generate antibodies against mDR3 using the remaining spleen from the second peptide immunised mouse that displayed a positive antibody response in chapter 4. With an improved efficiency of hybridoma production this may yield mDR3 specific antibodies. It is likely that as research in the DR3 field develops with the publication of articles, more commercially available reagents will be manufactured and DR3 research should develop at a much faster pace.

### 7.2 The Role of DR3 in the mAIA Model for RA

An important role for members of the TNFRSF in the inflammatory joint disease RA has been well documented. TNFR1 for example, via its interaction with TNFα, has been shown to significantly contribute to disease pathology in animal models of RA (Mori et al., 1996) and blockade of this receptor/ligand system has proven highly successful in clinical trials in the treatment of the disease (Bathon et al., 2000, Lipsky et al., 2000). Additionally, anti-TNF therapies are currently licensed for treatment of RA. RANK, another TNFRSF member, is also tightly linked with the destructive joint pathology associated with RA. Via interaction with its ligand RANKL, it is an essential component of the cellular differentiation pathway which results in the production of the sole bone resorbing cell type, osteoclasts (Hsu et al.,

1999). Prior to the initiation of this project, the association between the relatively newly identified member of the TNFRSF, DR3, had been specutively linked with RA in published material. Since then, DR3 has been identified as a candidate gene for association with RA and a duplication of the gene has been noted in a greater proportion of RA patients (Osawa et al., 2004). Additionally, expression of the DR3 ligand TL1A has been reported in rheumatoid synovium (Cassatella et al., 2007). DR3 also has reported roles in other inflammatory diseases including inflammatory bowel disease (Bamias et al., 2003) and atherosclerosis (Kang et al., 2005). However, no studies had been carried out *in vivo* in order to define the functional role of the DR3/TL1A pathway in inflammatory arthritis either in man or in an animal model. In order to address this issue, an important aim of this project was to evaluate the role of DR3 in a local model of RA, namely AIA. This model was induced in $DR3^{-/-}$ mice and in age-matched littermate controls. Indices of arthritis severity were compared between the groups.

### 7.2.1 Summary of Findings from Chapter 5

- $DR3^{-/-}$ mice exhibit the initial joint swelling associated with induction of AIA.
- Joint swelling in response to AIA decreased at a faster rate in DR3 deficient mice.
- Joint pathology on day 3 post-arthritis induction did not differ between $DR3^{-/-}$ and $DR3^{+/+}$ mice.
- $DR3^{-/-}$ mice are resistant to joint destruction at day 21 post-arthritis induction, with a complete absence of bone erosion.

- Articular cartilage is preserved in $DR3^{-/-}$ mice at both day 3 and day 21 post-arthritis induction.
- $DR3^{+/-}$ mice are susceptible to AIA with joint swelling following a similar pattern to that of $DR3^{+/+}$ mice.
- Joint pathology in $DR3^{+/-}$ mice was not as severe as that seen in DR3 sufficient mice at day 21 post-arthritis induction.
- Administration of the DR3 ligand TL1A to the joints of $DR3^{+/-}$ mice on the day of AIA induction did not affect joint swelling.
- However, joint destruction was significantly exacerbated according to the arthritis index.
- TL1A administration in $DR3^{+/-}$ mice also exacerbated cartilage depletion in a dose-dependent manner but had no effect in $DR3^{-/-}$ mice.
- Administration of TL1A to $DR3^{-/-}$ mice had no effect on joint swelling.
- However, although AI was not significantly affected, $DR3^{-/-}$ mice were no longer completely protected from AIA with the emergence of occasional bone erosions.

### 7.2.2 Chapter 5 Discussion

This investigation into the role of DR3 in murine AIA is the first study to be conducted investigating the pathological role that DR3 might play *in vivo* in an inflammatory model of arthritic disease. Due to the similarities seen between human RA and the AIA model, inducing DR3 deficient animals to develop AIA is a sound model for assessing the contribution that DR3 makes to the pathological processes occurring during the disease. Since $DR3^{-/-}$ mice are capable of generating

an effective antibody response, as illustrated in the assessment of serum anti-mBSA titres, they are suitable for the induction of AIA. DR3 deficient animals display a high degree of protection from AIA in terms of resolution of joint swelling and the pathological degenerative alterations occurring within the joint. This is similar to animals deficient in other TNF superfamily members, such as TNFR1 (Mori et al., 1996) and RANKL (Pettit et al., 2001), which have also been shown to display protection from such models of arthritic disease. Similar to the effects seen in TNFR1 deficient mice in the CIA model (Mori et al., 1996), DR3 knockout resulted in reduced severity of disease associated with AIA. As blockade of the TNFα/TNFR1 system is already being used as a successful treatment of the human disease in many patients, DR3 may therefore represent an alternative target for the future treatment of RA.

#### 7.2.2.1 The effect of DR3 knockout on joint swelling and cellular infiltration following AIA induction

In the absence of DR3, inflammation of the joint did arise following AIA induction. The inflammatory reaction which occurred in DR3 deficient mice displayed a comparable peak of joint swelling to wildtype littermate controls at day 1 post-arthritis induction. However, joint swelling resolved at a faster rate in the absence of DR3 implicating a pro-inflammatory role for the DR3 pathway. This is in agreement with the published role of DR3 in other inflammatory disease states such as atherosclerosis (Kang et al., 2005) and inflammatory bowel disease (Bamias et al., 2003). By day 21 post-arthritis induction, a striking reduction in cellular infiltration was evident in $DR3^{-/-}$ mice compared with controls. However, at day 3

there was no difference in cellular infiltration nor was there a significant dose-dependent effect on cellular infiltration following administration of TL1A. The lack of difference at day 3 compared to day 21 may be explained by the cell types recruited at these different stages. During the acute inflammatory phase of early AIA neutrophil infiltration predominates (McLoughlin et al., 2003) which is later taken over by monocytes/macrophages and small numbers of B cells and T cells. Neutrophils are specifically trafficked to the inflammatory joint through the action of the C-X-C chemokines such as IL-8 and growth related gene protein (GRO) (Badolato and Oppenheim, 1996). The C-C chemokines on the other hand are responsible for monocyte and T cell recruitment and these include monocyte chemotactic protein 1 (MCP-1), monocyte interacting protein 1α (MIP-1α) and regulated on activation normal T expressed and secreted (RANTES). All of these are upregulated in the synovial joint of RA patients (Badolato and Oppenheim, 1996). DR3 has been reported to induce the expression of a variety of these chemokines. For example, the activation of DR3 on THP-1 cells in concert with IFNγ stimulation has been shown to induce both the chemokines MCP-1 and IL-8 (Kang et al., 2005). However, Su et al. (2006) demonstrated that TL1A addition to primary human monocytes, only resulted in the secretion of IL-8 as they differentiated into macrophages but that MCP-1 secretion could not be detected (Su et al., 2006). Thus DR3 has the potential to affect cellular recruitment via influencing chemokine expression but the regulation of recruitment of different cell types by DR3 may be complex. In chapter 6 it was determined that the infiltration of F4/80+ cells into the joints of DR3 sufficient and deficient mice was comparable and that monocyte/macrophage cell recruitment appeared intact in the absence of DR3.

Thus the reduced cellular infiltrate evident in the joints of $DR3^{-/-}$ mice at day 21 post-arthritis induction cannot be attributed to a reduced ability to recruit monocytes/macrophages. When TL1A was added to the joints of $DR3^{+/-}$ mice on day 0 of the AIA model, no dose-dependent effect on cellular infiltration was noted. This may reflect the complex nature of the role of DR3 signalling in cellular recruitment according to time of TL1A expression during the inflammatory process. This would be in agreement with the data of Su et al. (2006) who noted differing effects of TL1A stimulated IL-8 secretion throughout the monocyte-macrophage differentiation process (Su et al., 2006). Additionally, although Kang et al. (2005) reported the induction of both MCP-1 and IL-8 from DR3 activated THP-1 cells, treatment of the same cell line with recombinant human TL1A and IFNγ resulted in IL-8 but not MCP-1 induction (Kang et al., 2005). In order to dissect the role of DR3 in cellular infiltration during models of inflammatory arthritis, it is necessary to stain for other cell types within the AIA joint such as T cells and neutrophils. The effect of DR3 on T cells in this model is a particularly interesting area of future work. Meylan et al. (2008) have demonstrated that DR3 plays an important role in two other T cell dependent animal models of autoimmune and allergic inflammation. Using the Ova-induced lung inflammation and EAE models, the authors reported reduced accumulation of T cells in the target organs of these models, namely the lungs and the spinal cord respectively (Meylan et al., 2008). Furthermore, DR3 has recently been linked with Th17 cell proliferation, as discussed in section 7.2.4, and therefore a detailed investigation into the effects of DR3 on T cell recruitment and proliferation in the AIA model might provide some interesting results. It would also be interesting to culture blood and bone marrow leukocytes from DR3 sufficient

and deficient mice and measure chemokine expression following stimulation with a panel of RA associated cytokines such as TNFα, IL-1 and TL1A. Measurement of chemokine expression within the joints of AIA mice would also provide invaluable data. Such experiments would help to generate a clearer picture of the infiltrating cells into the AIA joint which are affected by DR3/TL1A interaction and the expression of the chemokines which facilitate this recruitment.

#### 7.2.2.2 The effect of DR3 knockout on joint destruction following AIA induction

Similar to the reduction in cellular infiltration seen in DR3 deficient mice at day 21-post-arthritis induction, the increased rate of resolution of joint swelling in $DR3^{-/-}$ mice also corresponded to an improved pathological outcome within the joint, as assessed by the other disease parameters of the arthritis index including synovial hyperplasia and bone and cartilage destruction. However, again no such association was seen during the acute inflammatory phase of the disease model, with joints from $DR3^{-/-}$ mice and control mice displaying similar degrees of pathology at day 3 post-arthritis induction. Thus it appears that AIA develops in $DR3^{-/-}$ mice similar to controls during the early phase of the model, however, at a time point when maximal structural damage would be expected, DR3 deficiency confers resistance to the joint degeneration associated with AIA. When the individual features of the arthritis index were examined at day 21 post-arthritis induction, a significant reduction in all histopathological parameters was apparent. It was most intriguing that DR3 deficient mice did not develop the histopathological joint changes associated with AIA despite reaching comparable peaks in joint swelling to control mice on day 1 post-arthritis induction. This is because when TNFR1 deficient

animals were induced to develop CIA, when joint swelling did occur, albeit at a reduced incidence compared to controls, the afflicted joints went on to develop severe features of arthritic disease (Mori et al., 1996). It is possible therefore, that the role of DR3 in inflammatory joint disease might be different to that of TNFR1 with a potentially distinct role in the destruction of joint architecture, separate to any role the receptor might play in joint inflammation. In order to assess the structural damage occurring within the joint both bone erosion and cartilage depletion were analysed according to both the arthritis index and histological analysis of femoral head cartilage depletion.

One of the most interesting findings of this study was the complete absence of bone erosions in the DR3 deficient mice at day 21 following AIA induction. The destruction of bone represents one of the most debilitating consequences of inflammatory arthritis. Therefore, the apparent protection from this effect via DR3 deletion was a very exciting observation. In order to attempt to elucidate a mechanism for this effect, an investigation of osteoclast expression and potential precursors within the AIA joint was undertaken in chapter 6. As such, a discussion of the role of DR3 in bone destruction will be discussed later.

At both day 3 and day 21 post-arthritis induction, a significantly greater amount of cartilage degradation was observed in wild type animals compared to DR3 deficient mice. Thus although the AI was not different between the 2 groups at day 3 post-arthritis induction, $DR3^{-/-}$ mice were protected from the early cartilage depletion occurring within the joint and this protection was maintained at day 21.

Additionally, the administration of TL1A to $DR3^{+/-}$ mice on day 0 of the AIA model resulted in a trend towards exacerbating the depletion of cartilage when 100ng of TL1A was used. Conversely the administration of TL1A to DR3 deficient mice had no effect on cartilage degradation. Cartilage destruction can be uncoupled from bone erosion in certain models of arthritis as mice which are deficient in RANKL, a factor critical for osteoclastogenesis, do not develop bone erosions in the serum transfer model of arthritis which is generated through the transfer of serum containing anti-glucose-6-phoshate isomerase antibody from transgenic mice with a spontaneous T cell dependent arthritis. However cartilage degradation is still apparent (Pettit et al., 2001). DR3 may therefore play a specific role in cartilage destruction in AIA that could be distinct from its role in bone erosion or at least distinct from its potential effects on the activity of RANKL. The mechanisms for this however are unclear. The principle cell types thought to be responsible for cartilage destruction in the rheumatoid joint are synovial fibroblasts (Abeles and Pillinger, 2006). During RA pathogenesis, synovial fibroblasts become invasive and proliferative, contributing to the destruction of the joint. Thus synovial hyperplasia and cartilage degradation are intrinsically linked. It is therefore of particular interest that DR3 deficient mice display protection from cartilage depletion at both day 3 and day 21 post-arthritis induction in addition to displaying significantly reduced synovial hyperplasia at day 21 post-arthritis induction. Furthermore, administration of the DR3 ligand TL1A into the joints of $DR3^{+/-}$ mice resulted in a significant dose-dependent increase in synovial hyperplasia and a dose-dependent increase in cartilage degradation. This provides compelling evidence that DR3 contributes to cartilage degradation during AIA pathology. There is no published evidence regarding the expression of DR3 on

synovial fibroblasts. However, synovial fibroblasts are able to respond to a variety of stimuli such as the cytokines and growth factors produced in abundance in the rheumatoid joint (Konttinen et al., 2000). For example, TNFα stimulated synovial fibroblast cell lines derived from human knee joints display enhanced proliferation (Gitter et al., 1989) and incubation of cultured synovial fibroblasts with TNFα has been demonstrated to induce the conversion of the cartilage degrading enzyme MMP-2 from its latent to its active form (Migita et al., 1996). It is therefore possible that TL1A, via signalling through DR3, is also capable of activating synovial fibroblasts, enhancing their proliferation and migration and increasing their production of MMPs. There is published evidence to suggest that DR3 activation can result in MMP production in other cell types. Stimulation of THP-1 cells with recombinant human TL1A is reported to induce the release of MMP-9 in a dose-dependent manner (Brand et al., 2003). Activation of DR3 on the same cell line was also found to induce MMPs -1, -9 and -13 (Kim et al., 2001). All of these MMPs have been associated with the rheumatoid joint (Burrage et al., 2006) and are responsible for the degradation of cartilage. In order to fully elucidate the role of DR3/TL1A in MMP production from synovial fibroblasts, DR3 expression on this cell type requires investigation and the effect of TL1A addition to the cells on MMP expression needs to be measured. Additionally, expression of MMPs from monocytes derived from DR3 deficient mice could be examined. This has already been undertaken in IL-1 deficient mice revealing impaired production of MMPs -3 and -13 (Zwerina et al., 2007). Synovial fibroblasts are not the only cell type capable of producing MMPs involved in cartilage degradation in the rheumatoid joint. Additionally, macrophage-like synoviocytes, chondrocytes and TRAP positive cells

are also capable of proteinase secretion (Tsuboi et al., 2003). Thus should DR3 not be expressed on synovial fibroblasts, it may exert its effects on cartilage degradation via MMP induction from other cell types. Indeed, immunohistochemical analysis of the synovium from RA patients has revealed positive TL1A staining in cells with monocyte-macrophage morphology located particularly beneath the synovium. These cells also stained positively for the macrophage markers CD68 and CD14 (Cassatella et al., 2007). This positive TL1A staining was closely associated with the synoviocytes at areas of significant inflammation. Thus macrophage derived TL1A may act in an autocrine manner to induce MMP release from macrophage-like synovial fibroblasts thus contributing to cartilage degradation. Of particular note are the findings of Prehn et al. (2007) who determined that monocytes and dendritic cells could be induced by immune complex stimulation via FcγR to produce TL1A (Prehn et al., 2007). FcγR stimulation by immune complexes is also considered to play a prominent role in cartilage depletion during arthritic disease which is highlighted by reduced cartilage degradation in $Fc\gamma R^{-/-}$ mice (van Lent et al., 2006). These mice display an absence of severe cartilage depletion on day 7 post AIA induction and a complete absence of VDIPEN staining, the latter being used to illustrate the expression of MMP-induced aggrecan cleavage sites and give an indication of MMP activity within the joint (van Lent et al., 2000). Thus immune complex activation of FcγR receptors on cells in the rheumatoid joint may increase TL1A expression which can then interact with DR3 to increase MMP production, thus contributing to cartilage depletion. Another interesting observation in chapter 6, and relevant to the discussion of cartilage depletion, was the increase in TRAP+ mononuclear cells within the cellular infiltrate

of the adipose tissue and at sites of focal erosion in DR3 sufficient mice compared with DR3 deficient mice with AIA. TRAP+ cells within the human rheumatoid synovium have been reported to express MMPs -2 and -9 (Tsuboi et al., 2003) thus these TRAP+ cells may represent an additional source of MMPs within the AIA joint of DR3 sufficient animals. MMP expression within the AIA DR3 deficient mouse knee joint requires examination for example via northern blot analysis from total RNA isolated from the complete knee joint as has been previously executed in another transgenic mouse model (Salminen et al., 2002). This would provide data on the *in vivo* production of MMPs in the presence and absence of DR3 which might explain the protection from cartilage depletion noted in the DR3 deficient mice.

#### 7.2.2.3 TL1A exacerbates disease in a DR3-dependent fashion

Our results suggest that the protection from AIA seen in $DR3^{-/-}$ mice is as a result of DR3 deficiency as opposed to an effect resulting from the generation of the knockout animal. This was concluded via studying the effect of TL1A administration on the joints of animals on day 0 of the AIA protocol. This data is extremely interesting because it is widely considered that TNFα is the central cytokine sitting at the top of an inflammatory cytokine cascade, which is responsible for many of the pathological effects of RA (Feldmann and Maini, 2001). This work therefore implicates the potential importance of a novel cytokine-receptor system in the pathogenesis of RA. In the absence of an mDR3 blocking antibody, which could have been used to confirm the effect of DR3 blockade in AIA, this conclusion was reached through the use of the DR3-specific ligand TL1A. TL1A is reported to be the only

ligand for DR3 and in mouse, DR3 is the only published receptor for TL1A (Bossen et al., 2006).

The effect of TL1A administration in AIA was assessed in $DR3^{+/-}$ mice as opposed to wildtype mice in order to observe potential exacerbations of the disease within the realms of the Home Office project license. This is because $DR3^{+/-}$ mice did not develop as severe disease as DR3 sufficient mice but joint swelling and the underlying histopathology did arise and there was a significant gene dosage effect. Whilst increasing concentrations of TL1A had no significant effect on joint swelling, a dose-dependent increase in AI was seen within the joints. A significant dose-dependent increase in synovial hyperplasia and bone erosion rather than cellular infiltration and exudate accounted for this effect on the AI. The increase in the size of the bone erosions seen with increasing concentrations of TL1A was particularly striking. Thus DR3 appears to specifically effect the destructive phase of arthritic disease in terms of contributing to invasive synovial hyperplasia and the subsequent destruction of bone. When the same experiment was carried out in DR3 deficient animals, no significant effects were seen in terms of joint swelling or AI. These data suggest that DR3 via its interaction with TL1A is specifically involved in the pathological processes associated with AIA thus conferring protection from these pathological changes to the $DR3^{-/-}$ mice.

#### 7.2.2.4 DR3 deficiency does not confer complete resistance to AIA

Although when TL1A was administered to DR3 deficient animals there were no significant effects on either joint swelling or AI, as would be expected in the

absence of the only known receptor for the ligand, AI did increase from the scores seen at day 21 of $DR3^{-/-}$ mice not receiving TL1A. This was an unusual finding as there are no other known receptors for murine TL1A and an extensive investigation of the binding capabilities of the known TNF receptors and ligands revealed that only TL1A can bind mDR3 (Bossen et al., 2006). There are 2 possible reasons for this effect. Firstly, it is feasible that another receptor for TL1A exists. A decoy receptor (DcR3) which binds TL1A has been identified in humans thus the presence of another receptor for TL1A in the mouse would not be totally unexpected. Secondly, the increase in AI may just be an artifact of the TL1A preparation used which may contain impurities which are capable of exacerbating the inflammatory response.

### 7.2.3 Summary of Findings from Chapter 6

- At day 3 post-arthritis induction, osteoclast expression in the joints of $DR3^{+/+}$ and $DR3^{-/-}$ mice was comparable both in the femoral head and in the growth plate.
- At day 3 post-arthritis induction, significantly increased osteoclast expression was observed in the adipose tissue of wildtype mice.
- At day 21 post-arthritis induction, osteoclast expression in the joints of $DR3^{+/+}$ and $DR3^{-/-}$ mice was comparable both in the femoral head and in the growth plate.
- At sites of active focal bone erosion, osteoclast expression was significantly increased in $DR3^{+/+}$ mice.
- At day 3 post-arthritis induction, only low levels of F4/80+ cells were present in both the growth plate and infiltrate of $DR3^{+/+}$ and $DR3^{-/-}$ mice.

- At day 21 post-arthritis induction, there were greater numbers of F4/80+ cells in the growth plate and infiltrate of $DR3^{+/+}$ and $DR3^{-/-}$ mice and these levels were comparable.

### 7.2.4 Chapter 6 Discussion

In Chapter 5, the striking absence of bone erosions in the joints of DR3 deficient animals at day 21 post-arthritis induction and the ability of TL1A to increase bone erosion in a dose-dependent manner in $DR3^{+/-}$ mice, suggested that DR3 might play a role in the mechanisms responsible for bone destruction during arthritic disease. In order to address this point, we decided to assess the number of osteoclasts within the joints of DR3 sufficient and deficient mice at days 3 and 21 post-arthritis induction. Analysis was carried out by staining sections for TRAP, which is an osteoclast specific marker expressed both by mature osteoclasts during bone resorption (Ek-Rylander et al., 1991) and by early osteoclast precursors (Schett, 2007). TRAP staining methodology requires that joints are decalcified in EDTA for high levels of staining to be achieved. When joints are decalcified in formic acid, TRAP staining is only weak and not very reproducible. Unfortunately as formic acid was the routine method of decalcification used in this study, only those experiments that were carried out specifically to decalcify joints in EDTA were available for analysis. Thus only day 3 and day 21 experiments were assessed, and those in which TL1A was administered could not be analysed.

#### 7.2.4.1 The role of DR3 in the expression of TRAP+ cells in the AIA joint

Due to the normal physiological processes of bone turnover, TRAP expression is expected within the growth plates and cortical bone of non-diseased joints. As such, the growth plate and femoral head were analysed for TRAP expression during AIA in DR3 deficient and sufficient mice at both day 3 and day 21. No statistically significant differences in TRAP expression were evident at these locations at either timepoint. This suggests that osteoclast expression at sites distant from inflammation is unaffected by DR3 expression and that normal bone turnover is not DR3 dependent. TRAP expression in both the growth plate and femoral head in all animals is greater at day 3 to that seen at day 21. However, the TRAP staining protocol is very temperature dependent and sections from day 3 and day 21 were stained on different days when the ambient temperature would not have been the same, thus potentially affecting the degree of TRAP staining. Therefore caution must be taken in comparing the results from separate experiments and conclusions should only be drawn from sections from each individual experiment which were stained together.

TRAP expression was evident at sites of active bone erosion at day 21 post-arthritis induction in DR3 sufficient animals. As bone erosion and pannus formation were not evident in the absence of DR3, similar areas of TRAP positive expression were not seen in DR3 deficient animals. This data implicates a role for DR3 in osteoclastogenesis at sites of inflammation within the joint where cells are in direct contact with the bone surface.

A particularly interesting finding was the observation that significantly more TRAP+ cells were located within the cellular infiltrate of the adipose tissue in DR3 sufficient mice compared with $DR3^{-/-}$ mice at day 3 post-arthritis induction. These cells did not display the phenotypic multinuclearity of osteoclasts and thus may represent a precursor cell. It is unknown within the osteoclast field whether osteoclasts develop from monocytic precursors infiltrating into the joint or if they already display commitment to osteoclastogenesis upon entering the joint. Thus there are 3 possible explanations for our observation: DR3 may affect the recruitment of predisposed TRAP positive osteoclast precursor cells into the inflamed joint which are already some way down the osteoclast differentiation pathway; DR3 may affect the recruitment of monocytic osteoclast precursor cells into the joint increasing the available pool of cells capable of undergoing osteoclastogenesis; or recruitment of precursor cells may be unaffected but the process of osteoclastogenesis from precursor cells within the joint may be DR3 dependent leading to an increase in TRAP+ cells. Early osteoclastogenesis does not require direct contact with bone and thus TRAP+ cells are capable of accumulation at sites distant from the bone within the joint (Schett, 2007).

#### 7.2.4.2 Infiltration of F4/80+ cells into the joints is unaffected by DR3

To address the issue of impaired cellular infiltration into the joint, potential osteoclast precursor cells which were positive for the monocyte/macrophage marker F4/80 were analysed. Although multiple cell types have been shown to differentiate into osteoclasts *in vitro,* accumulation of macrophages within the RA joint have been shown to correlate with the severity of joint damage in the human

disease (Mulherin et al., 1996). Thus F4/80+ osteoclast precursors were selected for analysis. In order to assess whether the infiltration of these osteoclast precursor cells into the AIA joint was impaired in the absence of DR3, we stained day 3 and day 21 joint sections for F4/80. No differences were observed in F4/80+ cell staining between DR3 sufficient and deficient mice at either day 3 or day 21 post-arthritis induction, either in the growth plate, where normal physiological bone remodelling occurs or in the inflammatory infiltrate of the adipose tissue. Taken together this suggests that the infiltration of F4/80+ osteoclast precursor cells is unaffected by DR3 and that the accumulation of TRAP+ cells in the adipose tissue of DR3 sufficient mice either represent cells which are predestined to become osteoclasts prior to infiltration into the joint or that it is not the F4/80+ osteoclast precursor pool that is the important cell type involved in osteoclastogenesis in this model.

DR3 deficiency confers resistance to AIA induced bone destruction but this cannot be attributed to a reduction in basal osteoclast numbers or to the recruitment of their F4/80+ precursor cells. Data from this chapter suggests, however, that DR3 may play a role in the differentiation of osteoclasts at sites of inflammation which may or may not be derived from F4/80+ cells. The recruitment of cells which may be predestined to become osteoclasts in DR3 sufficient mice could also represent an explanation for the protection from bone erosion in DR3 deficient animals.

### 7.2.4.3 Potential mechanisms for the protection from bone erosion in the absence of DR3

As the sole bone resorbing cell, osteoclast expression within the joint was examined and an accumulation of osteoclasts at the bone/pannus interface was revealed in addition to an accumulation of TRAP+ cells in the adipose tissue in $DR3^{+/+}$ mice. We have also recently shown in an *in vitro* study that TL1A can promote osteoclastogenesis from bone marrow macrophages derived from $DR3^{+/+}$ mice but not $DR3^{-/-}$ mice in the presence of RANKL and M-CSF and also from human PBMC-derived monocytes (Bull et al., 2008). This data is particularly interesting as preservation of joint architecture is the ultimate goal of RA therapy and, as discussed in chapter 6, current anti-TNF therapies are falling short in this aim. However, this data raises a lot of questions. For example, is the reduction in bone erosion seen in $DR3^{-/-}$ mice just coupled to the overall reduction in inflammation associated with these animals during AIA? Is the increased accumulation of osteoclasts within the joints of wildtype mice compared with $DR3^{-/-}$ mice a consequence of reduced infiltration of osteoclast precursor cells or impaired osteoclastogenesis in the latter? These issues all require addressing.

In animal models for RA such as AIA and CIA, the degree of inflammation is intrinsically linked to the level of joint destruction occurring and it is not easy to distinguish between them experimentally. For example using FcγR knockout mice in the AIA model, van Lent et al. (2006) noted a direct correlation between the severity of bone destruction and the degree of cellular infiltration (van Lent et al., 2006). Thus the reduction in bone erosion in DR3 deficient mice may be regulated

by the reduction in inflammatory cells within the joints of these mice rather than due to the effect of DR3 on osteoclastogenesis. However, administration of the DR3-specific ligand into the joints of $DR3^{+/-}$ mice on day 0 of the experimental protocol resulted in a significant dose-dependent increase in bone erosion but no dose-dependent or significant effect on cellular infiltration was noted. This implies that TL1A exacerbates bone erosion in AIA via a mechanism which is uncoupled from cellular infiltration.

The accumulation of TRAP+ mononuclear cells in the adipose tissue of DR3 sufficient mice either indicates the initiation of osteoclastogenesis at this site distant from the bony surface or recruitment of osteoclast precursor cells which are already TRAP+ and predestined to differentiate into osteoclasts prior to infiltration into the joint. Osteoclast precursor cells can enter osteoclastogenesis and express TRAP independent of contact with mineralised tissue (Schett, 2007) and it is likely that it is these cells that are seen accumulating in the adipose tissue of DR3 sufficient animals which have the potential to undergo final differentiation into osteoclasts. It is entirely unknown whether or not cells are partially committed to osteoclast differentiation prior to entry into the inflamed joint, thus it is difficult to comment on whether the accumulation of these cells is due to recruitment. However, the effect of the DR3/TL1A pathway on chemokine production indicates that there is potential for this system to affect the recruitment of a "predestined" osteoclast precursor cell. However, as no difference was observed in F4/80+ cell numbers within the AIA joints of DR3 sufficient and deficient mice, the recruitment of at least this osteoclast precursor cell appears unaffected by DR3 signalling.

The process of osteoclastogenesis from osteoclast precursor cells to fully functional bone resorbing osteoclasts is well defined. The absence of TRAP positive cells within the joints of DR3 deficient mice may be explained via the effect of DR3/TL1A on this process. Other members of the TNFRSF have confirmed, although often incompletely defined roles in the process of osteoclast differentiation. RANKL for example, in concert with M-CSF, is essential for the production of mature osteoclasts (Lacey et al., 1998). TNFα, via TNFR1 engagement, is also reported to enhance osteoclastogenesis by increasing the size of the osteoclast precursor pool via the stimulation of c-fms expression (Boyce et al., 2005), through the induction of RANKL on synovial cells, osteoblasts and T cells, and also by directly binding to osteoclasts to enhance the effect of RANKL (Schett, 2007). DR3 is not known to be expressed on osteoclasts (Borysenko et al., 2006) and the effect of the DR3/TL1A pathway on osteoclastogenesis is unknown. We have demonstrated that TL1A can enhance osteoclastogenesis from murine bone marrow macrophages and human PBMC in the presence of M-CSF and RANKL. However, in the absence of RANKL and M-CSF, TL1A could not directly induce osteoclast differentiation (Bull et al., 2008). Thus, it seems that TL1A is not an essential factor for osteoclastogenesis but can promote it in the presence of RANKL and M-CSF in a DR3-dependent fashion. This is similar to the effects of TNFα on osteoclastogenesis. Although reports suggest that TNFα can directly drive osteoclastogenesis from precursor cells (Azuma et al., 2000), such studies have utilised protocols in which the precursor cells would have been exposed to RANKL in culture prior to purification. In studies where isolated myeloid cells were not previously exposed to RANKL, TNFα was unable to induce osteoclastogenesis. However, the addition of subosteoclastogenic levels of RANKL

(1ng/ml) 2-4 days prior to TNFα treatment enhanced osteoclastogenesis (Lam et al., 2000). This did not occur when RANKL and TNFα were added at the same time. In our system, RANKL (50ng/ml) and TL1A were added to the cultures at the same time and osteoclastogenesis was promoted which may imply a different effect of TL1A and TNFα in the timing of osteoclastogenesis. However, in our system, whole bone marrow cell cultures were used and thus osteoclast precursor cells may have already been exposed to RANKL resulting in a priming effect. Comparable assays would need to be performed in order to assess if TL1A and TNFα enhance osteoclastogenesis at different timepoints. The effects of osteoclastogenic factors such as TNFα are usually attributed to their ability to enhance RANKL expression on stromal cells and osteoblasts (Ross, 2000). The effect of DR3 signalling on RANKL expression in these cells has not been examined. However, DR3 is expressed on osteoblasts (Borysenko et al., 2006) raising the possibility that its signalling could induce RANKL expression on this cell type.

DR3 signalling has recently been linked with Th17 cell activity, an IL-17 secreting helper T cell subset that has published links with bone destruction. It has in fact been reported that the presence of either Th1 or Th2 cells in *in vitro* osteoclastogenesis assays has no effect on osteoclast differentiation but that Th17 cells are the only helper T cell subset capable of enhancing osteoclastogenesis (Sato et al., 2006). Using an *in vivo* model of inflammatory bone destruction, the authors have also reported a reduction in bone destruction and osteoclast formation in IL-17 deficient mice (Sato et al., 2006). It has been proposed that IL-17 is capable of promoting osteoclastogenesis through upregulating the expression of RANKL on

osteoblasts (Kotake et al., 1999). Thus IL-17 production by Th17 cells may be important in the destructive phase of inflammatory arthritis. DR3 expression on Th17 cells is reported to be greater than that seen on either Th1 or Th2 subsets and expression of the full length receptor in particular is highly upregulated (Pappu et al., 2008). In naive T cells where IL-2 signalling was blocked, TL1A was shown to enhance Th17 cell differentiation and in differentiated Th17 cell populations, TL1A enhanced cellular proliferation. This was confirmed through the use of TL1A deficient dendritic cells (DCs) which caused reduced differentiation of naive T cells into Th17 cells and reduced proliferation of Th17 cells compared with wildtype DCs (Pappu et al., 2008). Pappu et al. (2008) further explored the role of TL1A in the control of Th17 cells via the employment of the Th17 mediated myelin oligodendrocyte glycoprotein-induced experimental autoimmune encephalomyelitis model in TL1A deficient mice ($TL1A^{-/-}$). $TL1A^{-/-}$ mice displayed consistently reduced disease severity and reduced T cell infiltration throughout the course of the experiment, hypothesised to result from both reduced priming of autoreactive T cells and the reduced proliferation of Th17 cells (Pappu et al., 2008). Similarly another research group demonstrated the ability of TL1A to enhance IL-17 production with and without IL-23 stimulation from mucosal CD4 T cells and illustrated a reduction in the clinical outcome of a Th1/Th17 mediated model of colitis following anti-TL1A treatment in which CD4 T cell accumulation was again reduced (Takedatsu et al., 2008). However, more recently, Meylan et al demonstrated that DR3/TL1A interaction was not required for the differentiation of naive T cells into any of the T helper subsets and in the absence of DR3 signalling, T cell priming was normal (Meylan et al., 2008). Thus it is possible that DR3/TL1A

interactions play an important role in the differentiation of Th17 cells in inflammatory arthritis, which in turn cause the upregulation of RANKL on osteoblasts leading to increased osteoclastogenesis and bone erosion. However, the role of DR3 in the differentiation of Th17 cells continues to be debated. A first step in investigating this hypothesis would be to examine the T cell numbers within the AIA joints, examining each of the individual subsets. Additionally, IL-17 expression could be evaluated in order to indicate whether the DR3/TL1A pathway plays an important role in Th17 cell production and IL-17 mediated bone erosion.

In addition to its potential role in osteoclast formation and function, DR3 has a reported role in the control of osteoblast function. Both nontransformed and transformed (MG63 cells) human osteoblasts express the full length and soluble hDR3 receptor (Borysenko et al., 2006). Activation of DR3 on MG63 cells via cross-linking of the receptor is reported to result in apoptosis of cells when seeded at a low cell density with minimal cell contact. Addition of TL1A to these cells mediated similar effects (Borysenko et al., 2006). Thus DR3 may have a dual role in pathological bone turnover in terms of enhancing bone resorption via its effects on osteoclasts and through inhibiting bone generation via its effects on osteoblast function. By tipping the balance in favour of bone destruction, through an action on both osteoclasts and osteoblasts, DR3 may have the potential to significantly influence bone destruction during pathological inflammatory states.

### 7.2.5 DR3/TL1A expression in the rheumatoid joint

One of the most pertinent questions arising as a result of our data is where and when are DR3 and TL1A expressed in the rheumatoid joint and are they related to the expression of TNFα? Immunohistochemical staining for DR3 and TL1A in the murine AIA joints has not been possible due to both the unavailability of antibodies against these proteins and the difficulties associated with immunological staining in paraffin-embedded tissues. The construct used to generate the $DR3^{-/-}$ mice contained a LacZ cassette which enables β-galactosidase expression in those cells which normally express DR3 (Wang et al., 2001a). This could be exploited in an enzymatic reaction in order to determine DR3 expression in the AIA joint sections of DR3 deficient mice. However, enzymatic reactions can also be impaired as a result of the paraffin-embedding process and other work within this laboratory has been unable to detect β-galactosidase in these sections to date.

DR3 is expressed on many of the cells which are involved in RA pathogenesis including T cells, B cells (Screaton et al., 1997), monocytes, macrophages (Kang et al., 2005) and osteoblasts (Borysenko et al., 2006). Additionally analysis of human synovial RA tissue by Cassatella et al. (2007) revealed strong expression of TL1A on cells with monocyte-macrophage morphology but not on neutrophils, endothelial cells or lymphocytes (Cassatella et al., 2007). Thus there is a confirmed presence of TL1A within rheumatoid joints and due to the expression of DR3 on multiple immune cells, it seems reasonable to assume that DR3 will also be expressed within the rheumatoid joint. Whether or not DR3 activation occurs downstream from TNFα expression is a matter for debate. A particularly notable finding by Cassatella

et al. (2007), was that human monocytes released TL1A in response to insoluble immune complexes which are also present within rheumatoid synovial fluid but that TNFα was unable to stimulate this effect (Cassatella et al., 2007). Additionally, the production of TL1A in response to immune complexes occurred with slower kinetics than that of TNFα and was unaffected via the administration of anti-TNF antibodies (Cassatella et al., 2007). This suggests that TL1A expression may be independent of TNFα upregulation. However, Migone et al. (2002) reported the upregulation of TL1A mRNA in HUVEC cells following TNFα stimulation (Migone et al., 2002). Kang et al. (2005) also reported the upregulation of DR3 expression on monocytes when incubated with TNFα but conversely noted the induction of TNFα by THP-1 monocytic cells upon stimulation both via DR3 activation and IFNγ treatment together (Kang et al., 2005). Thus DR3/TL1A and TNFR1/TNFα may have a complex relationship in RA which requires further investigation. However, due to the presence of DR3 on multiple immune cells and the confirmed expression of TL1A within the RA joint, there is scope for involvement of DR3 signalling in multiple aspects of the disease process.

### 7.2.6 Other effects of DR3

Other published effects of DR3/TL1A interaction further complicate the role of this ligand/receptor system in models of inflammatory arthritis. Previous DR3 research has principally concentrated on its role in T cell function. Due to the original observations which suggested that DR3 might have lymphoid restricted expression this is hardly suprising. TL1A/DR3 interaction is widely reported to induce IFNγ secretion from T cells (Bamias et al., 2003, Bamias et al., 2006, Papadakis et al.,

2005) and TL1A functions as a T cell co-stimulator, increasing T cell responsiveness to IL-2 (Migone et al., 2002). In inflammatory arthritis T cells act as an additional source of RANKL and supernatant from activated CD4+ T cells can initiate osteoclastogenesis (Kong et al., 1999). This may represent a mechanism for increased osteoclastogenesis during AIA in DR3 sufficient mice compared with $DR3^{-/-}$ mice. Analysis of the ability of activated $DR3^{-/-}$ T cells to induce osteoclastogenesis would help to elucidate this issue. A published outcome of T cell costimulation by TL1A is an increased expression of IFNγ. In Crohn's disease for example, increased expression of both TL1A and DR3 has been illustrated and it has been hypothesised that their increased interaction augments IFNγ secretion thus sustaining the inflammatory response (Bamias et al., 2003). In models of inflammatory arthritis however, IFNγ is reported to have anti-inflammatory effects, with IFNγ deficient mice ($IFN\gamma^{-/-}$) displaying increased susceptibility to CIA (Manoury-Schwartz et al., 1997). Additionally, $IFN\gamma^{-/-}$ mice display more severe degenerative joint changes in response to AIA compared with wildtype controls (Williams et al., 2007). Thus the phenotype of DR3 deficient mice during AIA cannot be explained by the published role of DR3 and TL1A in the upregulation of IFNγ expression within the joint.

A further complicating factor in DR3 signalling is its ability to be expressed as multiple splice variants. There are 3 DR3 splice variants in mice (Wang et al., 2001a) and at least 13 in man (Kitson et al., 1996, Screaton et al., 1997). Bamias et al. (2006) have reported differential expression of the murine DR3 splice variants throughout lymphocyte activation. In resting T cells, full length transmembrane DR3

was expressed at a low level compared to total DR3 expression. However, upon activation, the ratio of transmembrane to total DR3 expression increased significantly (Bamias et al., 2006). Thus DR3 activity in inflammatory arthritis may be extremely complicated with expression of the full length signalling receptor being upregulated under certain conditions. However, this would be in contrast to the work of Shiozawa et al (2000) who revealed an increase in mRNA in RA patients for the transmembrane portion of DR3 compared with controls but not in mRNA for the death domain portion of DR3, suggesting a complex role for DR3 in RA (Shiozawa et al., 2000). RT-PCR analysis of murine knee joints following AIA induction may give some indication of the relative expression of the different DR3 splice variants as a result of this inflammatory disease.

### 7.2.7 DR3/TL1A as a therapeutic target for RA

The DR3/TL1A pathway is potentially a very attractive target for the treatment of RA. Should further studies support our work to suggest that blocking DR3/TL1A specifically prevents the joint degeneration associated with RA including erosion of the bone and cartilage degradation, then anti-DR3/TL1A therapy may represent a breakthrough in the treatment of the disease achieving the ultimate aim of preserving joint architecture. However, before such bold statements can be made, far more extensive studies need to be carried out in order to assess the *in vivo* effects of blocking this pathway. It has after all taken in excess of 20 years for anti-TNF treatment in RA to progress from bench to bedside. Recent work from this laboratory has provided the first evidence that inhibiting signalling through DR3 might prove an effective therapy in the treatment of RA. Using the CIA mouse

model for RA, which is currently used as the industry standard for assessing potential therapies for RA and was used in the discovery of anti-TNF treatment, Bull et al. (2008) illustrated that neutralisation of TL1A in wildtype mice through the prophylactic administration of a blocking antibody during the CIA protocol resulted in reduced disease activity. Paw scores which were clinically assessed on the basis of the degree of redness, swelling and the number of joints involved were consistently lower in the anti-TL1A treatment groups compared with both isotype and PBS treatment controls. When analysed histologically, joints from the anti-TL1A treatment group displayed a significantly reduced arthritis index (Bull et al., 2008). This data gives the first indication that blocking the DR3/TL1A pathway might be an effective treatment in RA and supports our data in the AIA model.

Considering the similarities seen between DR3 and TNFR1 function in models of RA, how likely is it that countering the DR3/TL1A pathway might provide a more effective therapy than anti-TNF treatment of RA, which is already licensed for use with a high degree of success? In the most successful clinical trials of anti-TNF therapy during RA, a maximum of 79% of patients achieved an ACR20 response. Thus despite the success of anti-TNF treatment, there is scope for improving on it. The ultimate aim is to preserve joint architecture by preventing bone and cartilage degradation. Although TNFα has reported effects on osteoclast differentiation and function, its effects on osteoblasts are unclear. Generally however, human non-tranformed and transformed osteoblasts do not respond to TNFα-induced apoptosis (Robinson et al., 2007). DR3 on the other hand, according to our data, has a potential role in osteoclastogenesis as well as being reported to cause apoptosis of osteoblasts under tightly regulated conditions (Borysenko et al., 2006). Thus DR3

may have a more important role than TNFR1 in pathological bone loss with the ability to both enhance osteoclast activity whilst causing osteoblast apoptosis. This could result in DR3 blockade being the more effective therapy choice.

Anti-TNF treatment is associated with the onset of infections, most notably tuberculosis. Use of all of the currently available anti-TNF agents has a positive association with TB incidence. Those using Infliximab for example can be up to 20 times more likely to develop TB typically from the reactivation of a latent infection (Theis and Rhodes, 2008). This reactivation of latent infection following TNFα blockade is thought to be caused by reduced recruitment of immune cells in response to TB infection, reduced macrophage activation, dysregulation of the inflammatory response and a reduction in CD4 cell activity (Ehlers, 2005). Due to the ability of DR3 to influence chemokine expression, macrophage activation and to initiate both apoptosis and cellular proliferation, it might be reasonable to assume that blockade of the DR3/TL1A pathway might confer susceptibility to certain bacterial infections. Few studies have been carried out to assess the role of DR3 in various infections. However, Meylan et al have shown that DR3 deficient mice respond normally to infection with the parasite *Toxoplasma gondii* in which host survival depends upon production of IFNγ-producing Th1 cells (Meylan et al., 2008). Thus at least in this infection, control of the pathogen is not dependent on DR3. However, further investigation regarding the effect of DR3/TL1A blockade on infection occurrence is required to determine if this potential therapy for RA might not be associated with increased occurrence of serious infections.

Before DR3/TL1A blockade can be considered an effective therapy in the treatment of human RA, far more extensive work is required to assess whether this therapy would prove more effective than those already available and what the potential side effects are of blocking this system. Generation of murine DR3 blocking antibodies would greatly enhance this research and could be tested in the CIA model for efficacy. An assessment of the responses of DR3 deficient mice to a host of infectious agents would also provide a better understanding of the potential complications of this therapy. Additionally, translation from murine models to human therapies is further complicated by the existence of decoy receptor 3 in humans but not in mice, which binds and sequesters TL1A inhibiting its signalling. Should this therapy get this far, anti-DR3/TL1A treatment would have to be fully evaluated in clinical trials, as occurred during the development of anti-TNF therapy. On the basis of current data, the DR3/TL1A axis represents a promising novel target in the treatment of RA.

### 7.6 Final conclusions

This work has shown for the first time an important role of the DR3/TL1A pathway in the AIA model of Rheumatoid Arthritis. Blockade of this pathway through gene knockout reduces the severity of all of the histopathological changes associated with the model, in particular protecting from bone and cartilage erosion. Although further investigation is required to fully elucidate the role of DR3 in this and other models of RA, our data firmly supports the DR3/TL1A pathway as a potential target in the treatment of inflammatory joint disorders.

# References

## 8. References


ABELES, A. M. & PILLINGER, M. H. (2006) The role of the synovial fibroblast in rheumatoid arthritis: cartilage destruction and the regulation of matrix metalloproteinases. *Bull NYU Hosp Jt Dis,* 64, 20-4.

ADACHI, M., SUEMATSU, S., KONDO, T., OGASAWARA, J., TANAKA, T., YOSHIDA, N. & NAGATA, S. (1995) Targeted mutation in the Fas gene causes hyperplasia in peripheral lymphoid organs and liver. *Nat Genet,* 11, 294-300.

AGGARWAL, B. B., KOHR, W. J., HASS, P. E., MOFFAT, B., SPENCER, S. A., HENZEL, W. J., BRINGMAN, T. S., NEDWIN, G. E., GOEDDEL, D. V. & HARKINS, R. N. (1985) Human tumor necrosis factor. Production, purification and characterization. *J Biol Chem,* 260, 2345-54.

AGGARWAL, S., GHILARDI, N., XIE, M. H., DE SAUVAGE, F. J. & GURNEY, A. L. (2003) Interleukin-23 promotes a distinct CD4 T cell activation state characterized by the production of interleukin-17. *J Biol Chem,* 278, 1910-4.

AKIL, M. & AMOS, R. S. (1995) ABC of rheumatology. Rheumatoid arthritis--I: Clinical features and diagnosis. *Bmj,* 310, 587-90.

AL-LAMKI, R. S., WANG, J., TOLKOVSKY, A. M., BRADLEY, J. A., GRIFFIN, J. L., THIRU, S., WANG, E. C., BOLTON, E., MIN, W., MOORE, P., POBER, J. S. & BRADLEY, J. R. (2008) TL1A both promotes and protects from renal inflammation and injury. *J Am Soc Nephrol,* 19, 953-60.

ALAMANOS, Y. & DROSOS, A. A. (2005) Epidemiology of adult rheumatoid arthritis. *Autoimmunity Reviews,* 4, 130-136.

ANDERSON, D. M., MARASKOVSKY, E., BILLINGSLEY, W. L., DOUGALL, W. C., TOMETSKO, M. E., ROUX, E. R., TEEPE, M. C., DUBOSE, R. F., COSMAN, D. & GALIBERT, L. (1997) A homologue of the TNF receptor and its ligand enhance T-cell growth and dendritic-cell function. *Nature,* 390, 175-9.

ARNETT, F. C., EDWORTHY, S. M., BLOCH, D. A., MCSHANE, D. J., FRIES, J. F., COOPER, N. S., HEALEY, L. A., KAPLAN, S. R., LIANG, M. H., LUTHRA, H. S. & ET AL. (1988) The American Rheumatism Association 1987 revised criteria for the classification of rheumatoid arthritis. *Arthritis Rheum,* 31, 315-24.

ASHKENAZI, A. & DIXIT, V. M. (1998) Death receptors: signaling and modulation. *Science,* 281, 1305-8.

AZUMA, Y., KAJI, K., KATOGI, R., TAKESHITA, S. & KUDO, A. (2000) Tumor necrosis factor-alpha induces differentiation of and bone resorption by osteoclasts. *J Biol Chem,* 275, 4858-64.

BACHMANN, H. S., SIFFERT, W. & FREY, U. H. (2003) Successful amplification of extremely GC-rich promoter regions using a novel 'slowdown PCR' technique. *Pharmacogenetics,* 13, 759-66.

BADOLATO, R. & OPPENHEIM, J. J. (1996) Role of cytokines, acute-phase proteins, and chemokines in the progression of rheumatoid arthritis. *Semin Arthritis Rheum,* 26, 526-38.

BAMIAS, G., MARTIN, C., 3RD, MARINI, M., HOANG, S., MISHINA, M., ROSS, W. G., SACHEDINA, M. A., FRIEL, C. M., MIZE, J., BICKSTON, S. J., PIZARRO, T. T., WEI, P. & COMINELLI, F. (2003) Expression,

localization, and functional activity of TL1A, a novel Th1-polarizing cytokine in inflammatory bowel disease. *J Immunol,* 171, 4868-74.
BAMIAS, G., MISHINA, M., NYCE, M., ROSS, W. G., KOLLIAS, G., RIVERA-NIEVES, J., PIZARRO, T. T. & COMINELLI, F. (2006) Role of TL1A and its receptor DR3 in two models of chronic murine ileitis. *Proc Natl Acad Sci U S A,* 103, 8441-6.
BATHON, J. M., MARTIN, R. W., FLEISCHMANN, R. M., TESSER, J. R., SCHIFF, M. H., KEYSTONE, E. C., GENOVESE, M. C., WASKO, M. C., MORELAND, L. W., WEAVER, A. L., MARKENSON, J. & FINCK, B. K. (2000) A comparison of etanercept and methotrexate in patients with early rheumatoid arthritis. *N Engl J Med,* 343, 1586-93.
BODMER, J. L., BURNS, K., SCHNEIDER, P., HOFMANN, K., STEINER, V., THOME, M., BORNAND, T., HAHNE, M., SCHROTER, M., BECKER, K., WILSON, A., FRENCH, L. E., BROWNING, J. L., MACDONALD, H. R. & TSCHOPP, J. (1997) TRAMP, a novel apoptosis-mediating receptor with sequence homology to tumor necrosis factor receptor 1 and Fas(Apo-1/CD95). *Immunity,* 6, 79-88.
BORYSENKO, C. W., FUREY, W. F. & BLAIR, H. C. (2005) Comparative modeling of TNFRSF25 (DR3) predicts receptor destabilization by a mutation linked to rheumatoid arthritis. *Biochem Biophys Res Commun,* 328, 794-9.
BORYSENKO, C. W., GARCIA-PALACIOS, V., GRISWOLD, R. D., LI, Y., IYER, A. K., YAROSLAVSKIY, B. B., SHARROW, A. C. & BLAIR, H. C. (2006) Death receptor-3 mediates apoptosis in human osteoblasts under narrowly regulated conditions. *J Cell Physiol,* 209, 1021-8.
BOSE, B., KHANNA, N., ACHARYA, S. K. & SINHA, S. (2006) Generation and characterization of a single-gene mouse-human chimeric antibody against hepatitis B surface antigen. *J Gastroenterol Hepatol,* 21, 1439-47.
BOSSEN, C., INGOLD, K., TARDIVEL, A., BODMER, J. L., GAIDE, O., HERTIG, S., AMBROSE, C., TSCHOPP, J. & SCHNEIDER, P. (2006) Interactions of tumor necrosis factor (TNF) and TNF receptor family members in the mouse and human. *J Biol Chem,* 281, 13964-71.
BOYCE, B. F., LI, P., YAO, Z., ZHANG, Q., BADELL, I. R., SCHWARZ, E. M., O'KEEFE, R. J. & XING, L. (2005) TNF-alpha and pathologic bone resorption. *Keio J Med,* 54, 127-31.
BRACKERTZ, D., MITCHELL, G. F. & MACKAY, I. R. (1977) Antigen-induced arthritis in mice. I. Induction of arthritis in various strains of mice. *Arthritis Rheum,* 20, 841-50.
BRAND, D. D., KANG, A. H. & ROSLONIEC, E. F. (2003) Immunopathogenesis of collagen arthritis. *Springer Semin Immunopathol,* 25, 3-18.
BREHME, C. S., ROMAN, S., SHAFFER, J. & WOLFERT, R. (1999) Tartrate-resistant acid phosphatase forms complexes with alpha2-macroglobulin in serum. *J Bone Miner Res,* 14, 311-8.
BRENNAN, F. M., CHANTRY, D., JACKSON, A., MAINI, R. & FELDMANN, M. (1989) Inhibitory effect of TNF alpha antibodies on synovial cell interleukin-1 production in rheumatoid arthritis. *Lancet,* 2, 244-7.
BUCAY, N., SAROSI, I., DUNSTAN, C. R., MORONY, S., TARPLEY, J., CAPPARELLI, C., SCULLY, S., TAN, H. L., XU, W., LACEY, D. L., BOYLE, W. J. & SIMONET, W. S. (1998) osteoprotegerin-deficient mice

develop early onset osteoporosis and arterial calcification. *Genes Dev,* 12, 1260-8.

BUCHAN, G., BARRETT, K., TURNER, M., CHANTRY, D., MAINI, R. N. & FELDMANN, M. (1988) Interleukin-1 and tumour necrosis factor mRNA expression in rheumatoid arthritis: prolonged production of IL-1 alpha. *Clin Exp Immunol,* 73, 449-55.

BULL, M. J., WILLIAMS, A. S., MECKLENBURGH, Z., CALDER, C. J., TWOHIG, J. P., ELFORD, C., EVANS, B. A. J., ROWLEY, T. F., SLEBIODA, T. J., TARABAN, V. Y., AL-SHAMKHANI, A. & WANG, E. C. Y. (2008) The Death Receptor 3 / TNF-like protein 1A pathway drives adverse bone pathology in inflammatory arthritis. *J Exp Med,* In Press.

BURRAGE, P. S., MIX, K. S. & BRINCKERHOFF, C. E. (2006) Matrix metalloproteinases: role in arthritis. *Front Biosci,* 11, 529-43.

CARSWELL, E. A., OLD, L. J., KASSEL, R. L., GREEN, S., FIORE, N. & WILLIAMSON, B. (1975) An endotoxin-induced serum factor that causes necrosis of tumors. *Proc Natl Acad Sci U S A,* 72, 3666-70.

CASSATELLA, M. A., PEREIRA-DA-SILVA, G., TINAZZI, I., FACCHETTI, F., SCAPINI, P., CALZETTI, F., TAMASSIA, N., WEI, P., NARDELLI, B., ROSCHKE, V., VECCHI, A., MANTOVANI, A., BAMBARA, L. M., EDWARDS, S. W. & CARLETTO, A. (2007) Soluble TNF-like cytokine (TL1A) production by immune complexes stimulated monocytes in rheumatoid arthritis. *J Immunol,* 178, 7325-33.

CHAN, F. K., CHUN, H. J., ZHENG, L., SIEGEL, R. M., BUI, K. L. & LENARDO, M. J. (2000) A domain in TNF receptors that mediates ligand-independent receptor assembly and signaling. *Science,* 288, 2351-4.

CHINNAIYAN, A. M., O'ROURKE, K., YU, G. L., LYONS, R. H., GARG, M., DUAN, D. R., XING, L., GENTZ, R., NI, J. & DIXIT, V. M. (1996) Signal transduction by DR3, a death domain-containing receptor related to TNFR-1 and CD95. *Science,* 274, 990-2.

COHEN, P. L. & EISENBERG, R. A. (1991) Lpr and gld: single gene models of systemic autoimmunity and lymphoproliferative disease. *Annu Rev Immunol,* 9, 243-69.

CONSDEN, R., DOBLE, A., GLYNN, L. E. & NIND, A. P. (1971) Production of a chronic arthritis with ovalbumin. Its retention in the rabbit knee joint. *Ann Rheum Dis,* 30, 307-15.

COOKE, T. D. & JASIN, H. E. (1972) The pathogenesis of chronic inflammation in experimental antigen-induced arthritis. I. The role of antigen on the local immune response. *Arthritis Rheum,* 15, 327-37.

CUSH, J. J. & LIPSKY, P. E. (1988) Phenotypic analysis of synovial tissue and peripheral blood lymphocytes isolated from patients with rheumatoid arthritis. *Arthritis Rheum,* 31, 1230-8.

DAGIA, N. M., GADHOUM, S. Z., KNOBLAUCH, C. A., SPENCER, J. A., ZAMIRI, P., LIN, C. P. & SACKSTEIN, R. (2006) G-CSF induces E-selectin ligand expression on human myeloid cells. *Nat Med,* 12, 1185-90.

DATTA, H. K., NG, W. F., WALKER, J. A., TUCK, S. P. & VARANASI, S. S. (2008) The cell biology of bone metabolism. *J Clin Pathol,* 61, 577-87.

DAYER, J. M., BEUTLER, B. & CERAMI, A. (1985) Cachectin/tumor necrosis factor stimulates collagenase and prostaglandin E2 production by human synovial cells and dermal fibroblasts. *J Exp Med,* 162, 2163-8.

DOUGALL, W. C., GLACCUM, M., CHARRIER, K., ROHRBACH, K., BRASEL, K., DE SMEDT, T., DARO, E., SMITH, J., TOMETSKO, M. E., MALISZEWSKI, C. R., ARMSTRONG, A., SHEN, V., BAIN, S., COSMAN, D., ANDERSON, D., MORRISSEY, P. J., PESCHON, J. J. & SCHUH, J. (2008) RANK is essential for osteoclast and lymph node development. *Genes Dev,* 13, 2412-2424.

DUMONDE, D. C. & GLYNN, L. E. (1962) The production of arthritis in rabbits by an immunological reaction to fibrin. *Br J Exp Pathol,* 43, 373-83.

EHLERS, S. (2005) Tumor necrosis factor and its blockade in granulomatous infections: differential modes of action of infliximab and etanercept? *Clin Infect Dis,* 41 Suppl 3, S199-203.

EK-RYLANDER, B., BILL, P., NORGARD, M., NILSSON, S. & ANDERSSON, G. (1991) Cloning, sequence, and developmental expression of a type 5, tartrate-resistant, acid phosphatase of rat bone. *J Biol Chem,* 266, 24684-9.

EYRE, D. (2002) Collagen of articular cartilage. *Arthritis Res,* 4, 30-5.

FANG, L., ADKINS, B., DEYEV, V. & PODACK, E. R. (2008) Essential role of TNF receptor superfamily 25 (TNFRSF25) in the development of allergic lung inflammation. *J Exp Med,* 205, 1037-48.

FELDMANN, M., BRENNAN, F. M. & MAINI, R. N. (1996) Rheumatoid arthritis. *Cell,* 85, 307-10.

FELDMANN, M. & MAINI, R. N. (2001) Anti-TNF alpha therapy of rheumatoid arthritis: what have we learned? *Annu Rev Immunol,* 19, 163-96.

FELIX, R., CECCHINI, M. G. & FLEISCH, H. (1990) Macrophage colony stimulating factor restores in vivo bone resorption in the op/op osteopetrotic mouse. *Endocrinology,* 127, 2592-4.

FERNANDEZ-TRESGUERRES-HERNANDEZ-GIL, I., ALOBERA-GRACIA, M. A., DEL-CANTO-PINGARRON, M. & BLANCO-JEREZ, L. (2006) Physiological bases of bone regeneration II. The remodeling process. *Med Oral Patol Oral Cir Bucal,* 11, E151-7.

FUJIKAWA, Y., SABOKBAR, A., NEALE, S. & ATHANASOU, N. A. (1996) Human osteoclast formation and bone resorption by monocytes and synovial macrophages in rheumatoid arthritis. *Ann Rheum Dis,* 55, 816-22.

GITTER, B. D., LABUS, J. M., LEES, S. L. & SCHEETZ, M. E. (1989) Characteristics of human synovial fibroblast activation by IL-1 beta and TNF alpha. *Immunology,* 66, 196-200.

GOLDRING, S. R. (2003) Pathogenesis of bone and cartilage destruction in rheumatoid arthritis. *Rheumatology (Oxford),* 42 Suppl 2, ii11-6.

GOUT, S., MORIN, C., HOULE, F. & HUOT, J. (2006) Death receptor-3, a new E-Selectin counter-receptor that confers migration and survival advantages to colon carcinoma cells by triggering p38 and ERK MAPK activation. *Cancer Res,* 66, 9117-24.

GRENET, J., VALENTINE, V., KITSON, J., LI, H., FARROW, S. N. & KIDD, V. J. (1998) Duplication of the DR3 gene on human chromosome 1p36 and its deletion in human neuroblastoma. *Genomics,* 49, 385-93.

HALL, A. C., HORWITZ, E. R. & WILKINS, R. J. (1996) The cellular physiology of articular cartilage. *Exp Physiol,* 81, 535-45.

HARADA, S. & RODAN, G. A. (2003) Control of osteoblast function and regulation of bone mass. *Nature,* 423, 349-55.

HENDERSON, B., REVELL, P. A. & EDWARDS, J. C. (1988) Synovial lining cell hyperplasia in rheumatoid arthritis: dogma and fact. *Ann Rheum Dis,* 47, 348-9.

HENKE, W., HERDEL, K., JUNG, K., SCHNORR, D. & LOENING, S. A. (1997) Betaine improves the PCR amplification of GC-rich DNA sequences. *Nucleic Acids Res,* 25, 3957-8.

HSU, H., LACEY, D. L., DUNSTAN, C. R., SOLOVYEV, I., COLOMBERO, A., TIMMS, E., TAN, H. L., ELLIOTT, G., KELLEY, M. J., SAROSI, I., WANG, L., XIA, X. Z., ELLIOTT, R., CHIU, L., BLACK, T., SCULLY, S., CAPPARELLI, C., MORONY, S., SHIMAMOTO, G., BASS, M. B. & BOYLE, W. J. (1999) Tumor necrosis factor receptor family member RANK mediates osteoclast differentiation and activation induced by osteoprotegerin ligand. *Proc Natl Acad Sci U S A,* 96, 3540-5.

HSU, H., SHU, H. B., PAN, M. G. & GOEDDEL, D. V. (1996) TRADD-TRAF2 and TRADD-FADD interactions define two distinct TNF receptor 1 signal transduction pathways. *Cell,* 84, 299-308.

HUSHEEM, M., NYMAN, J. K., VAARANIEMI, J., VAANANEN, H. K. & HENTUNEN, T. A. (2005) Characterization of circulating human osteoclast progenitors: development of in vitro resorption assay. *Calcif Tissue Int,* 76, 222-30.

IWANAGA, T., SHIKICHI, M., KITAMURA, H., YANASE, H. & NOZAWA-INOUE, K. (2000) Morphology and functional roles of synoviocytes in the joint. *Arch Histol Cytol,* 63, 17-31.

JOBANPUTRA, P., BARTON, P., BRYAN, S. & BURLS, A. (2002) The effectiveness of infliximab and etanercept for the treatment of rheumatoid arthritis: a systematic review and economic evaluation. *Health Technol Assess,* 6, 1-110.

KANG, Y. J., KIM, W. J., BAE, H. U., KIM, D. I., PARK, Y. B., PARK, J. E., KWON, B. S. & LEE, W. H. (2005) Involvement of TL1A and DR3 in induction of pro-inflammatory cytokines and matrix metalloproteinase-9 in atherogenesis. *Cytokine,* 29, 229-35.

KAPTEIN, A., JANSEN, M., DILAVER, G., KITSON, J., DASH, L., WANG, E., OWEN, M. J., BODMER, J. L., TSCHOPP, J. & FARROW, S. N. (2000) Studies on the interaction between TWEAK and the death receptor WSL-1/TRAMP (DR3). *FEBS Lett,* 485, 135-41.

KASSEM, M., ABDALLAH, B. M. & SAEED, H. (2008) Osteoblastic cells: differentiation and trans-differentiation. *Arch Biochem Biophys,* 473, 183-7.

KEFFER, J., PROBERT, L., CAZLARIS, H., GEORGOPOULOS, S., KASLARIS, E., KIOUSSIS, D. & KOLLIAS, G. (1991) Transgenic mice expressing human tumour necrosis factor: a predictive genetic model of arthritis. *Embo J,* 10, 4025-31.

KIM, M. Y., GASPAL, F. M., WIGGETT, H. E., MCCONNELL, F. M., GULBRANSON-JUDGE, A., RAYKUNDALIA, C., WALKER, L. S., GOODALL, M. D. & LANE, P. J. (2003) CD4(+)CD3(-) accessory cells costimulate primed CD4 T cells through OX40 and CD30 at sites where T cells collaborate with B cells. *Immunity,* 18, 643-54.

KIM, M. Y., TOELLNER, K. M., WHITE, A., MCCONNELL, F. M., GASPAL, F. M., PARNELL, S. M., JENKINSON, E., ANDERSON, G. & LANE, P. J. (2006) Neonatal and adult CD4+ CD3- cells share similar gene expression

profile, and neonatal cells up-regulate OX40 ligand in response to TL1A (TNFSF15). *J Immunol,* 177, 3074-81.
KIM, S. & ZHANG, L. (2005) Identification of naturally secreted soluble form of TL1A, a TNF-like cytokine. *J Immunol Methods,* 298, 1-8.
KIM, S. H., LEE, W. H., KWON, B. S., OH, G. T., CHOI, Y. H. & PARK, J. E. (2001) Tumor necrosis factor receptor superfamily 12 may destabilize atherosclerotic plaques by inducing matrix metalloproteinases. *Jpn Circ J,* 65, 136-8.
KIM, W. J., KANG, Y. J., SUK, K., PARK, J. E., KWON, B. S. & LEE, W. H. (2008) Comparative analysis of the expression patterns of various TNFSF/TNFRSF in atherosclerotic plaques. *Immunol Invest,* 37, 359-73.
KITSON, J., RAVEN, T., JIANG, Y. P., GOEDDEL, D. V., GILES, K. M., PUN, K. T., GRINHAM, C. J., BROWN, R. & FARROW, S. N. (1996) A death-domain-containing receptor that mediates apoptosis. *Nature,* 384, 372-5.
KNEDLA, A., NEUMANN, E. & MULLER-LADNER, U. (2007) Developments in the synovial biology field 2006. *Arthritis Res Ther,* 9, 209.
KOBAYASHI, K., TAKAHASHI, N., JIMI, E., UDAGAWA, N., TAKAMI, M., KOTAKE, S., NAKAGAWA, N., KINOSAKI, M., YAMAGUCHI, K., SHIMA, N., YASUDA, H., MORINAGA, T., HIGASHIO, K., MARTIN, T. J. & SUDA, T. (2000) Tumor necrosis factor alpha stimulates osteoclast differentiation by a mechanism independent of the ODF/RANKL-RANK interaction. *J Exp Med,* 191, 275-86.
KOHLER, G. & MILSTEIN, C. (2005) Continuous cultures of fused cells secreting antibody of predefined specificity. 1975. *J Immunol,* 174, 2453-5.
KONG, Y. Y., FEIGE, U., SAROSI, I., BOLON, B., TAFURI, A., MORONY, S., CAPPARELLI, C., LI, J., ELLIOTT, R., MCCABE, S., WONG, T., CAMPAGNUOLO, G., MORAN, E., BOGOCH, E. R., VAN, G., NGUYEN, L. T., OHASHI, P. S., LACEY, D. L., FISH, E., BOYLE, W. J. & PENNINGER, J. M. (1999) Activated T cells regulate bone loss and joint destruction in adjuvant arthritis through osteoprotegerin ligand. *Nature,* 402, 304-9.
KONTTINEN, Y. T., LI, T. F., HUKKANEN, M., MA, J., XU, J. W. & VIRTANEN, I. (2000) Fibroblast biology. Signals targeting the synovial fibroblast in arthritis. *Arthritis Res,* 2, 348-55.
KOTAKE, S., UDAGAWA, N., TAKAHASHI, N., MATSUZAKI, K., ITOH, K., ISHIYAMA, S., SAITO, S., INOUE, K., KAMATANI, N., GILLESPIE, M. T., MARTIN, T. J. & SUDA, T. (1999) IL-17 in synovial fluids from patients with rheumatoid arthritis is a potent stimulator of osteoclastogenesis. *J Clin Invest,* 103, 1345-52.
KURIHARA, N., CHENU, C., MILLER, M., CIVIN, C. & ROODMAN, G. D. (1990) Identification of committed mononuclear precursors for osteoclast-like cells formed in long term human marrow cultures. *Endocrinology,* 126, 2733-41.
LACEY, D. L., TIMMS, E., TAN, H. L., KELLEY, M. J., DUNSTAN, C. R., BURGESS, T., ELLIOTT, R., COLOMBERO, A., ELLIOTT, G., SCULLY, S., HSU, H., SULLIVAN, J., HAWKINS, N., DAVY, E., CAPPARELLI, C., ELI, A., QIAN, Y. X., KAUFMAN, S., SAROSI, I., SHALHOUB, V., SENALDI, G., GUO, J., DELANEY, J. & BOYLE, W. J. (1998) Osteoprotegerin ligand is a cytokine that regulates osteoclast differentiation and activation. *Cell,* 93, 165-76.

LAM, J., TAKESHITA, S., BARKER, J. E., KANAGAWA, O., ROSS, F. P. & TEITELBAUM, S. L. (2000) TNF-alpha induces osteoclastogenesis by direct stimulation of macrophages exposed to permissive levels of RANK ligand. *J Clin Invest,* 106, 1481-8.

LANDRE-BEAUVAIS, A. J. (2001) The first description of rheumatoid arthritis. Unabridged text of the doctoral dissertation presented in 1800. *Joint Bone Spine,* 68, 130-43.

LEAN, J. M., MATSUO, K., FOX, S. W., FULLER, K., GIBSON, F. M., DRAYCOTT, G., WANI, M. R., BAYLEY, K. E., WONG, B. R., CHOI, Y., WAGNER, E. F. & CHAMBERS, T. J. (2000) Osteoclast lineage commitment of bone marrow precursors through expression of membrane-bound TRANCE. *Bone,* 27, 29-40.

LEWTHWAITE, J., BLAKE, S., HARDINGHAM, T., FOULKES, R., STEPHENS, S., CHAPLIN, L., EMTAGE, S., CATTERALL, C., SHORT, S. & NESBITT, A. (1995) Role of TNF alpha in the induction of antigen induced arthritis in the rabbit and the anti-arthritic effect of species specific TNF alpha neutralising monoclonal antibodies.
10.1136/ard.54.5.366. *Ann Rheum Dis,* 54, 366-374.

LIPSKY, P. E., VAN DER HEIJDE, D. M., ST CLAIR, E. W., FURST, D. E., BREEDVELD, F. C., KALDEN, J. R., SMOLEN, J. S., WEISMAN, M., EMERY, P., FELDMANN, M., HARRIMAN, G. R. & MAINI, R. N. (2000) Infliximab and methotrexate in the treatment of rheumatoid arthritis. Anti-Tumor Necrosis Factor Trial in Rheumatoid Arthritis with Concomitant Therapy Study Group. *N Engl J Med,* 343, 1594-602.

MACEWAN, D. J. (2002) TNF ligands and receptors-a matter of life and death. *Br J Pharmacol,* 135, 855-75.

MAJITHIA, V. & GERACI, S. A. (2007) Rheumatoid arthritis: diagnosis and management. *Am J Med,* 120, 936-9.

MANOURY-SCHWARTZ, B., CHIOCCHIA, G., BESSIS, N., ABEHSIRA-AMAR, O., BATTEUX, F., MULLER, S., HUANG, S., BOISSIER, M. C. & FOURNIER, C. (1997) High susceptibility to collagen-induced arthritis in mice lacking IFN-gamma receptors. *J Immunol,* 158, 5501-6.

MARCH, L. & LAPSLEY, H. (2001) What are the costs to society and the potential benefits from the effective management of early rheumatoid arthritis? *Best Pract Res Clin Rheumatol,* 15, 171-85.

MARSTERS, S. A., SHERIDAN, J. P., DONAHUE, C. J., PITTI, R. M., GRAY, C. L., GODDARD, A. D., BAUER, K. D. & ASHKENAZI, A. (1996) Apo-3, a new member of the tumor necrosis factor receptor family, contains a death domain and activates apoptosis and NF-kappa B. *Curr Biol,* 6, 1669-76.

MARSTERS, S. A., SHERIDAN, J. P., PITTI, R. M., BRUSH, J., GODDARD, A. & ASHKENAZI, A. (1998) Identification of a ligand for the death-domain-containing receptor Apo3. *Curr Biol,* 8, 525-8.

MCKNIGHT, A. J., MACFARLANE, A. J., DRI, P., TURLEY, L., WILLIS, A. C. & GORDON, S. (1996) Molecular cloning of F4/80, a murine macrophage-restricted cell surface glycoprotein with homology to the G-protein-linked transmembrane 7 hormone receptor family. *J Biol Chem,* 271, 486-9.

MCLOUGHLIN, R. M., WITOWSKI, J., ROBSON, R. L., WILKINSON, T. S., HURST, S. M., WILLIAMS, A. S., WILLIAMS, J. D., ROSE-JOHN, S., JONES, S. A. & TOPLEY, N. (2003) Interplay between IFN-gamma and IL-

6 signaling governs neutrophil trafficking and apoptosis during acute inflammation. *J Clin Invest,* 112, 598-607.
MEYLAN, F., DAVIDSON, T. S., KAHLE, E., KINDER, M., ACHARYA, K., JANKOVIC, D., BUNDOC, V., HODGES, M., SHEVACH, E. M., KEANE-MYERS, A., WANG, E. C. & SIEGEL, R. M. (2008) The TNF-family receptor DR3 is essential for diverse T cell-mediated inflammatory diseases. *Immunity,* 29, 79-89.
MIGITA, K., EGUCHI, K., KAWABE, Y., ICHINOSE, Y., TSUKADA, T., AOYAGI, T., NAKAMURA, H. & NAGATAKI, S. (1996) TNF-alpha-mediated expression of membrane-type matrix metalloproteinase in rheumatoid synovial fibroblasts. *Immunology,* 89, 553-7.
MIGONE, T. S., ZHANG, J., LUO, X., ZHUANG, L., CHEN, C., HU, B., HONG, J. S., PERRY, J. W., CHEN, S. F., ZHOU, J. X., CHO, Y. H., ULLRICH, S., KANAKARAJ, P., CARRELL, J., BOYD, E., OLSEN, H. S., HU, G., PUKAC, L., LIU, D., NI, J., KIM, S., GENTZ, R., FENG, P., MOORE, P. A., RUBEN, S. M. & WEI, P. (2002) TL1A is a TNF-like ligand for DR3 and TR6/DcR3 and functions as a T cell costimulator. *Immunity,* 16, 479-92.
MORI, L., ISELIN, S., DE LIBERO, G. & LESSLAUER, W. (1996) Attenuation of collagen-induced arthritis in 55-kDa TNF receptor type 1 (TNFR1)-IgG1-treated and TNFR1-deficient mice. *J Immunol,* 157, 3178-82.
MORT, J. S. & BILLINGTON, C. J. (2001) Articular cartilage and changes in arthritis: matrix degradation. *Arthritis Res,* 3, 337-41.
MULHERIN, D., FITZGERALD, O. & BRESNIHAN, B. (1996) Synovial tissue macrophage populations and articular damage in rheumatoid arthritis. *Arthritis Rheum,* 39, 115-24.
NAKAO, A., FUKUSHIMA, H., KAJIYA, H., OZEKI, S. & OKABE, K. (2007) RANKL-stimulated TNFalpha production in osteoclast precursor cells promotes osteoclastogenesis by modulating RANK signaling pathways. *Biochem Biophys Res Commun,* 357, 945-50.
NATIONAL INSTITUTE OF HEALTH (2004) Rheumatoid Arthritis.
NEWMAN, S. J., BOND, B., CROOK, B., DARKER, J., EDGE, C. & MAYCOX, P. R. (2000) Neuron-specific localisation of the TR3 death receptor in Alzheimer's disease. *Brain Res,* 857, 131-40.
OHSHIMA, S., SAEKI, Y., MIMA, T., SASAI, M., NISHIOKA, K., NOMURA, S., KOPF, M., KATADA, Y., TANAKA, T., SUEMURA, M. & KISHIMOTO, T. (1998) Interleukin 6 plays a key role in the development of antigen-induced arthritis. *Proc Natl Acad Sci U S A,* 95, 8222-6.
ORLINICK, J. R. & CHAO, M. V. (1998) TNF-related ligands and their receptors. *Cell Signal,* 10, 543-51.
OROZCO, G., RUEDA, B. & MARTIN, J. (2006) Genetic basis of rheumatoid arthritis. *Biomed Pharmacother,* 60, 656-62.
OSAWA, K., TAKAMI, N., SHIOZAWA, K., HASHIRAMOTO, A. & SHIOZAWA, S. (2004) Death receptor 3 (DR3) gene duplication in a chromosome region 1p36.3: gene duplication is more prevalent in rheumatoid arthritis. *Genes Immun,* 5, 439-43.
PAPADAKIS, K. A., PREHN, J. L., LANDERS, C., HAN, Q., LUO, X., CHA, S. C., WEI, P. & TARGAN, S. R. (2004) TL1A synergizes with IL-12 and IL-18 to enhance IFN-gamma production in human T cells and NK cells. *J Immunol,* 172, 7002-7.

PAPADAKIS, K. A., ZHU, D., PREHN, J. L., LANDERS, C., AVANESYAN, A., LAFKAS, G. & TARGAN, S. R. (2005) Dominant role for TL1A/DR3 pathway in IL-12 plus IL-18-induced IFN-gamma production by peripheral blood and mucosal CCR9+ T lymphocytes. *J Immunol,* 174, 4985-90.

PAPPU, B. P., BORODOVSKY, A., ZHENG, T. S., YANG, X., WU, P., DONG, X., WENG, S., BROWNING, B., SCOTT, M. L., MA, L., SU, L., TIAN, Q., SCHNEIDER, P., FLAVELL, R. A., DONG, C. & BURKLY, L. C. (2008) TL1A-DR3 interaction regulates Th17 cell function and Th17-mediated autoimmune disease. *J Exp Med,* 205, 1049-62.

PESCHON, J. J., TORRANCE, D. S., STOCKING, K. L., GLACCUM, M. B., OTTEN, C., WILLIS, C. R., CHARRIER, K., MORRISSEY, P. J., WARE, C. B. & MOHLER, K. M. (1998) TNF receptor-deficient mice reveal divergent roles for p55 and p75 in several models of inflammation. *J Immunol,* 160, 943-52.

PETTIT, A. R., JI, H., VON STECHOW, D., MULLER, R., GOLDRING, S. R., CHOI, Y., BENOIST, C. & GRAVALLESE, E. M. (2001) TRANCE/RANKL knockout mice are protected from bone erosion in a serum transfer model of arthritis. *Am J Pathol,* 159, 1689-99.

PFEFFER, K., MATSUYAMA, T., KUNDIG, T. M., WAKEHAM, A., KISHIHARA, K., SHAHINIAN, A., WIEGMANN, K., OHASHI, P. S., KRONKE, M. & MAK, T. W. (1993) Mice deficient for the 55 kd tumor necrosis factor receptor are resistant to endotoxic shock, yet succumb to L. monocytogenes infection. *Cell,* 73, 457-67.

PREHN, J. L., THOMAS, L. S., LANDERS, C. J., YU, Q. T., MICHELSEN, K. S. & TARGAN, S. R. (2007) The T cell costimulator TL1A is induced by FcgammaR signaling in human monocytes and dendritic cells. *J Immunol,* 178, 4033-8.

RALPHS, J. R. & BENJAMIN, M. (1994) The joint capsule: structure, composition, ageing and disease. *J Anat,* 184 ( Pt 3), 503-9.

RINDFLEISCH, J. A. & MULLER, D. (2005) Diagnosis and management of rheumatoid arthritis. *Am Fam Physician,* 72, 1037-47.

ROBINSON, L. J., BORYSENKO, C. W. & BLAIR, H. C. (2007) Tumor necrosis factor family receptors regulating bone turnover: new observations in osteoblastic and osteoclastic cell lines. *Ann N Y Acad Sci,* 1116, 432-43.

ROMAS, E., BAKHAREVSKI, O., HARDS, D. K., KARTSOGIANNIS, V., QUINN, J. M., RYAN, P. F., MARTIN, T. J. & GILLESPIE, M. T. (2000) Expression of osteoclast differentiation factor at sites of bone erosion in collagen-induced arthritis. *Arthritis Rheum,* 43, 821-6.

ROSENBERG, L. (1971) Chemical basis for the histological use of safranin O in the study of articular cartilage. *J Bone Joint Surg Am,* 53, 69-82.

ROSS, F. P. (2000) RANKing the importance of measles virus in Paget's disease. *J Clin Invest,* 105, 555-8.

ROTHS, J. B., MURPHY, E. D. & EICHER, E. M. (1984) A new mutation, gld, that produces lymphoproliferation and autoimmunity in C3H/HeJ mice. *J Exp Med,* 159, 1-20.

ROUGHLEY, P. J. (2001) Articular cartilage and changes in arthritis: noncollagenous proteins and proteoglycans in the extracellular matrix of cartilage. *Arthritis Res,* 3, 342-7.

SALMINEN, H. J., SAAMANEN, A. M., VANKEMMELBEKE, M. N., AUHO, P. K., PERALA, M. P. & VUORIO, E. I. (2002) Differential expression

patterns of matrix metalloproteinases and their inhibitors during development of osteoarthritis in a transgenic mouse model. *Ann Rheum Dis,* 61, 591-7.
SATO, K., SUEMATSU, A., OKAMOTO, K., YAMAGUCHI, A., MORISHITA, Y., KADONO, Y., TANAKA, S., KODAMA, T., AKIRA, S., IWAKURA, Y., CUA, D. J. & TAKAYANAGI, H. (2006) Th17 functions as an osteoclastogenic helper T cell subset that links T cell activation and bone destruction. *J Exp Med,* 203, 2673-82.
SAXNE, T. & BENGT, M. (2000) Molecular markers for assessment of cartilage damage in rheumatoid arthritis. IN FIRESTEIN, G. S., PANAYI, G. S. & WOLLHEIM, F. A. (Eds.) *Rheumatoid Arthritis: New Frontiers in Pathogenesis and Treatment.* New York, Oxford University Press.
SCHETT, G. (2007) Cells of the synovium in rheumatoid arthritis. Osteoclasts. *Arthritis Res Ther,* 9, 203.
SCREATON, G. R., XU, X. N., OLSEN, A. L., COWPER, A. E., TAN, R., MCMICHAEL, A. J. & BELL, J. I. (1997) LARD: a new lymphoid-specific death domain containing receptor regulated by alternative pre-mRNA splicing. *Proc Natl Acad Sci U S A,* 94, 4615-9.
SHIOZAWA, S., KOMAI, K., KONISHI, Y., HIKASA, M., MUKAE, N., SHIOZAWA, K., KITAGAWA, M., YOSHIKAWA, N. & KAWASAKI, H. (2000) An approach to identify new genes in autoimmune diseases: lessons from rheumatoid arthritis. *Rev Immunogenet,* 2, 133-9.
SHORT, C. L. (1974) The antiquity of rheumatoid arthritis. *Arthritis Rheum,* 17, 193-205.
SIMONET, W. S., LACEY, D. L., DUNSTAN, C. R., KELLEY, M., CHANG, M. S., LUTHY, R., NGUYEN, H. Q., WOODEN, S., BENNETT, L., BOONE, T., SHIMAMOTO, G., DEROSE, M., ELLIOTT, R., COLOMBERO, A., TAN, H. L., TRAIL, G., SULLIVAN, J., DAVY, E., BUCAY, N., RENSHAW-GEGG, L., HUGHES, T. M., HILL, D., PATTISON, W., CAMPBELL, P., SANDER, S., VAN, G., TARPLEY, J., DERBY, P., LEE, R. & BOYLE, W. J. (1997) Osteoprotegerin: a novel secreted protein involved in the regulation of bone density. *Cell,* 89, 309-19.
SMITH, M. D., BARG, E., WEEDON, H., PAPENGELIS, V., SMEETS, T., TAK, P. P., KRAAN, M., COLEMAN, M. & AHERN, M. J. (2003) Microarchitecture and protective mechanisms in synovial tissue from clinically and arthroscopically normal knee joints. *Ann Rheum Dis,* 62, 303-7.
SU, W. B., CHANG, Y. H., LIN, W. W. & HSIEH, S. L. (2006) Differential regulation of interleukin-8 gene transcription by death receptor 3 (DR3) and type I TNF receptor (TNFRI). *Exp Cell Res,* 312, 266-77.
TAKAHASHI, N., AKATSU, T., UDAGAWA, N., SASAKI, T., YAMAGUCHI, A., MOSELEY, J. M., MARTIN, T. J. & SUDA, T. (1988) Osteoblastic cells are involved in osteoclast formation. *Endocrinology,* 123, 2600-2.
TAKAMI, N., OSAWA, K., MIURA, Y., KOMAI, K., TANIGUCHI, M., SHIRAISHI, M., SATO, K., IGUCHI, T., SHIOZAWA, K., HASHIRAMOTO, A. & SHIOZAWA, S. (2006) Hypermethylated promoter region of DR3, the death receptor 3 gene, in rheumatoid arthritis synovial cells. *Arthritis Rheum,* 54, 779-87.
TAKAYANAGI, H. (2007) Osteoimmunology: shared mechanisms and crosstalk between the immune and bone systems. *Nat Rev Immunol,* 7, 292-304.
TAKEDATSU, H., MICHELSEN, K. S., WEI, B., LANDERS, C. J., THOMAS, L. S., DHALL, D., BRAUN, J. & TARGAN, S. R. (2008) TL1A (TNFSF15)

regulates the development of chronic colitis by modulating both T-helper 1 and T-helper 17 activation. *Gastroenterology,* 135, 552-67.

TAM, J. P. (1988) Synthetic peptide vaccine design: synthesis and properties of a high-density multiple antigenic peptide system. *Proc Natl Acad Sci U S A,* 85, 5409-13.

THEIS, V. S. & RHODES, J. M. (2008) Review article: minimizing tuberculosis during anti-tumour necrosis factor-alpha treatment of inflammatory bowel disease. *Aliment Pharmacol Ther,* 27, 19-30.

TSUBOI, H., MATSUI, Y., HAYASHIDA, K., YAMANE, S., MAEDA-TANIMURA, M., NAMPEI, A., HASHIMOTO, J., SUZUKI, R., YOSHIKAWA, H. & OCHI, T. (2003) Tartrate resistant acid phosphatase (TRAP) positive cells in rheumatoid synovium may induce the destruction of articular cartilage. *Ann Rheum Dis,* 62, 196-203.

VAANANEN, H. K. & LAITALA-LEINONEN, T. (2008) Osteoclast lineage and function. *Arch Biochem Biophys,* 473, 132-8.

VAN LENT, P. L., GREVERS, L., LUBBERTS, E., DE VRIES, T. J., NABBE, K. C., VERBEEK, S., OPPERS, B., SLOETJES, A., BLOM, A. B. & VAN DEN BERG, W. B. (2006) Fcgamma receptors directly mediate cartilage, but not bone, destruction in murine antigen-induced arthritis: uncoupling of cartilage damage from bone erosion and joint inflammation. *Arthritis Rheum,* 54, 3868-77.

VAN LENT, P. L., VAN VUUREN, A. J., BLOM, A. B., HOLTHUYSEN, A. E., VAN DE PUTTE, L. B., VAN DE WINKEL, J. G. & VAN DEN BERG, W. B. (2000) Role of Fc receptor gamma chain in inflammation and cartilage damage during experimental antigen-induced arthritis. *Arthritis Rheum,* 43, 740-52.

WANG, E. C., KITSON, J., THERN, A., WILLIAMSON, J., FARROW, S. N. & OWEN, M. J. (2001a) Genomic structure, expression, and chromosome mapping of the mouse homologue for the WSL-1 (DR3, Apo3, TRAMP, LARD, TR3, TNFRSF12) gene. *Immunogenetics,* 53, 59-63.

WANG, E. C., THERN, A., DENZEL, A., KITSON, J., FARROW, S. N. & OWEN, M. J. (2001b) DR3 regulates negative selection during thymocyte development. *Mol Cell Biol,* 21, 3451-61.

WARZOCHA, K., RIBEIRO, P., CHARLOT, C., RENARD, N., COIFFIER, B. & SALLES, G. (1998) A new death receptor 3 isoform: expression in human lymphoid cell lines and non-Hodgkin's lymphomas. *Biochem Biophys Res Commun,* 242, 376-9.

WEINBERG, J. B., PIPPEN, A. M. & GREENBERG, C. S. (1991) Extravascular fibrin formation and dissolution in synovial tissue of patients with osteoarthritis and rheumatoid arthritis. *Arthritis Rheum,* 34, 996-1005.

WEN, L., ZHUANG, L., LUO, X. & WEI, P. (2003) TL1A-induced NF-kappaB activation and c-IAP2 production prevent DR3-mediated apoptosis in TF-1 cells. *J Biol Chem,* 278, 39251-8.

WILLIAMS, A. S., RICHARDS, P. J., THOMAS, E., CARTY, S., NOWELL, M. A., GOODFELLOW, R. M., DENT, C. M., WILLIAMS, B. D., JONES, S. A. & TOPLEY, N. (2007) Interferon-gamma protects against the development of structural damage in experimental arthritis by regulating polymorphonuclear neutrophil influx into diseased joints. *Arthritis Rheum,* 56, 2244-54.

WILLIAMS, R. O., FELDMANN, M. & MAINI, R. N. (1992) Anti-tumor necrosis factor ameliorates joint disease in murine collagen-induced arthritis. *Proc Natl Acad Sci U S A*, 89, 9784-8.

WILLIAMS, R. O., MASON, L. J., FELDMANN, M. & MAINI, R. N. (1994) Synergy between anti-CD4 and anti-tumor necrosis factor in the amelioration of established collagen-induced arthritis. *Proc Natl Acad Sci U S A*, 91, 2762-6.

WILLIAMS, T. W. & GRANGER, G. A. (1968) Lymphocyte in vitro cytotoxicity: lymphotoxins of several mammalian species. *Nature*, 219, 1076-7.

WONG, B. R., JOSIEN, R. & CHOI, Y. (1999) TRANCE is a TNF family member that regulates dendritic cell and osteoclast function. *J Leukoc Biol*, 65, 715-24.

WOOLEY, P., GRIMM, M. & RADIN, E. (2005) The Structure and Function of Joints. IN WJ., K. & LW., M. (Eds.) *Arthritis and Allied Conditions A Textbook of Rheumatology*. Philadelphia, Lippincott Williams and Wilkins.

WORDSWORTH, B. P., LANCHBURY, J. S., SAKKAS, L. I., WELSH, K. I., PANAYI, G. S. & BELL, J. I. (1989) HLA-DR4 subtype frequencies in rheumatoid arthritis indicate that DRB1 is the major susceptibility locus within the HLA class II region. *Proc Natl Acad Sci U S A*, 86, 10049-53.

YASUDA, H., SHIMA, N., NAKAGAWA, N., YAMAGUCHI, K., KINOSAKI, M., MOCHIZUKI, S., TOMOYASU, A., YANO, K., GOTO, M., MURAKAMI, A., TSUDA, E., MORINAGA, T., HIGASHIO, K., UDAGAWA, N., TAKAHASHI, N. & SUDA, T. (1998) Osteoclast differentiation factor is a ligand for osteoprotegerin/osteoclastogenesis-inhibitory factor and is identical to TRANCE/RANKL. *Proc Natl Acad Sci U S A*, 95, 3597-602.

ZWERINA, J., REDLICH, K., POLZER, K., JOOSTEN, L., KRONKE, G., DISTLER, J., HESS, A., PUNDT, N., PAP, T., HOFFMANN, O., GASSER, J., SCHEINECKER, C., SMOLEN, J. S., VAN DEN BERG, W. & SCHETT, G. (2007) TNF-induced structural joint damage is mediated by IL-1. *Proc Natl Acad Sci U S A*, 104, 11742-7.

# Appendix

Appendix I

1. Bull, M.J., Williams, A.S., & Wang, E.C.Y. (2005) Poster presentation. The role of death receptor 3 in a murine model for Rheumatoid Arthritis. **20th Annual Post-Graduate Research Day**, Cardiff University.
2. Bull, M.J., Williams, A.S., Mecklenburgh, Z., Calder, C.J., Twohig, J.P., Elford, C., Evans, B.A.J., Rowley, T.F., Slebioda, T.J., Taraban, V.J., Al-Shamkhani, A. & Wang, E.C.Y. (2006) Oral presentation. The role of death receptor 3 in a murine model for Rheumatoid Arthritis. **I3-IRG Annual Conference**, Millennium Stadium, Cardiff.
3. Bull, M.J., Williams, A.S., Mecklenburgh, Z., Calder, C.J., Twohig, J.P., Elford, C., Evans, B.A.J., Rowley, T.F., Slebioda, T.J., Taraban, V.J., Al-Shamkhani, A. & Wang, E.C.Y. (2005) Oral presentation. The role of death receptor 3 in a murine model for Rheumatoid Arthritis. **21st Annual Post-Graduate Research Day**, Cardiff University.
4. Bull, M.J., Williams, A.S., Mecklenburgh, Z., Calder, C.J., Twohig, J.P., Elford, C., Evans, B.A.J., Rowley, T.F., Slebioda, T.J., Taraban, V.J., Al-Shamkhani, A. & Wang, E.C.Y. (2008) Oral presentation. The role of death receptor 3 in a murine model for Rheumatoid Arthritis. **DR3 Symposium**, Cardiff University.
5. Williams, A.S., Bull, M.J., Mecklenburgh, Z., Calder, C.J., Twohig, J.P., Elford, C., Evans, B.A.J., Rowley, T.F., Slebioda, T.J., Taraban, V.J., Al-Shamkhani, A. & Wang, E.C.Y. (2008) Oral presentation. The role of death receptor 3 in inflammatory arthritis. ***British Society for Immunology***, Glasgow, Scotland.
6. Wang, E.C.Y., Bull, M.J., Mecklenburgh, Z., Calder, C.J., Twohig, J.P., Elford, C., Evans, B.A.J., Rowley, T.F., Slebioda, T.J., Taraban, V.J., Al-Shamkhani, A. & Williams, A.S. (2008) Poster presentation (won the Industry Poster Award runner-up prize). Proof of principle for targeting of the DR3/TL1A pathway as therapy for inflammatory arthritis. ***MRC IIB Vaccines and Immunotherapies Showcase***, Sanger Institute, Cambridge.
7. Wang, E.C.Y., Bull, M.J. & Williams, A.S (2007) Oral presentation. The role of death receptor 3 in antigen-induced arthritis. ***13th International Congress of Immunology***, Rio de Janeiro, Brazil.

ished September 29, 2008

# IN THIS ISSUE

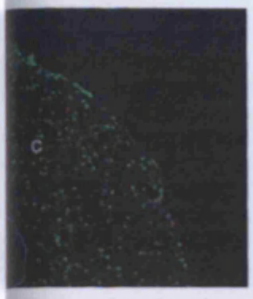

ctive thymocytes (green) ted in the cortex (C) before g the medulla (M).

## Autoimmunity fought in the cortex

In the best-case scenario, self-attacking T cells are ousted before they have a chance to leave the thymus. That essential process, which eliminates autoreactive thymocytes from the get-go, is known to occur in the thymic medulla. Now, on page 2575, McCaughtry et al. provide solid evidence that this elimination also occurs in the thymic cortex.

Although immunologists have reported T cell deletion in the cortex before, their results were made ambiguous by the transgenic mice models they used. These mice expressed T cell receptors specific for a self-peptide earlier in development than they are normally expressed. One fear was that those T cells were being deleted before they had a chance to migrate into the medulla. To quell that concern, McCaughtry's team generated a transgenic mouse in which the receptors are turned on at the appropriate time. Turns out, the earlier models were correct.

T cells reacting to ubiquitous self-antigens were deleted in the cortex alone, before entering the medulla. Furthermore, the medulla-based transcription factor AIRE, which mediates T cell deletion, did not seem to be required in the cortical deletions. Local dendritic cells, however, were needed. Without them, a large fraction of autoreactive T cell clones survived.

The locale of T cell deletion may depend on the antigen involved. Tissue-specific self-antigens are produced only in the medulla, whereas ubiquitous self-antigens, such as house-keeping peptides and the antigen recognized in the authors' mouse model, are widespread and can be handled in the cortex, at the site of first encounter. Now that the question of location has been settled, future studies can focus on learning how cortical dendritic cells control T cells gone awry.

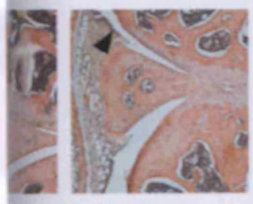

cking DR3 (right) had ed arthritic inflammation rrowheads) and bone (blue arrowheads).

## Death receptor chews up bone

Arthritis sufferers might find some relief in a new compound found to ease bone damage in mice. Bull et al. (page 2457) prevented joint erosion when they crippled a member of the TNF receptor superfamily, Death Receptor 3 (DR3), by blocking its ligand, TL1A.

Patients with rheumatoid arthritis are more likely to have extra copies of the gene that codes for DR3. A causative role for DR3 in disease pathology, however, had not been shown. Bull et al. now find that mice lacking DR3 are freed from the bone damage usually caused by antigen-induced arthritis. And blocking TL1A curtailed the bone erosion typical of collagen-induced arthritis in mice.

Back in the dish, the team investigated how this receptor–ligand pair might induce bone destruction in humans. They found that the addition of TL1A to ordinary monocytes from human blood enhanced the generation of bone-resorbing osteoclasts. Although how TL1A leads to osteoclast differentiation is not yet clear, its DR3 receptor is known to activate NFκB, which is required for osteoclast formation.

A few stones remain unturned in the hunt for vandals, as obstructing TL1A didn't eliminate bone destruction altogether. Still, the researchers point out that the anti-TL1A antibody did ameliorate much of the damage.

in-4 (red) and EAAT2 colocalize in normal spine.

## Pain in the brain

A severe and unusual disorder often confused with multiple sclerosis (MS) has now become a little less mysterious. On page 2473, Hinson and colleagues demonstrate how the disease's distinguishing autoantibody disrupts glutamate regulation.

Neuromyelitis optica (NMO), also known as Devic's disease, results in MS-like lesions in the optic nerves and along the spine. Yet unlike MS, NMO is associated with production of a specific autoantibody known as NMO-IgG. Clinicians use NMO-IgG to diagnose the disease, but they don't know how the antibody contributes to its symptoms—sight impairment, paraplegia, and loss of limb, bladder, and bowel sensation.

In 2005, the same group identified NMO-IgG's target as aquaporin-4, a water channel protein concentrated in astrocyte membranes along the blood-brain barrier. However, the finding was somewhat perplexing because myelin damage occurs on nerve cells, not on astrocytes. Now the team confirms that astrocytes are indeed the relevant target, and show how autoantibody binding can lead to demyelination. Clue: when astrocytes hurt, their duties lapse, too.

When NMO-IgG binds to aquaporin-4, they show, the levels of the astrocyte glutamate transporter EAAT2 drop. And no transporter, no glutamate regulation. Astrocytes themselves aren't sensitive to changes in glutamate levels, but neurons and oligodendrocytes are. These cells rely on

Published September 29, 2008

Text by Amy Maxmen
amaxmen@rockefeller.edu

EAAT2 to mop up excess glutamate from extracellular space. Accumulation of the neurotransmitter can be toxic to myelin-making oligodendrocytes.

After spelling out the pathway in astrocyte in vitro assays, the team examined human tissue. Sure enough, NMO lesions along cadaver spines lacked both aquaporin-4 and EAAT2. Lesions from MS patients show no such deficiencies, highlighting another way in which the demyelinating disorders differ.

If the groups' results are confirmed in vivo, drug development could be straightforward. Therapeutic trials for glutamate antagonists, created to treat other neurodegenerative diseases like Lou Gehrig's disease (or ALS), are already underway.

## Friend to the brain, foe to the spine

Shouting during a World Cup match and shouting during a funeral will be met with different reactions. Context is equally important in a cytokine outburst, find Lees et al. on page 2633. Regional responses to interferon-γ (IFNγ) dictated whether the spinal cord or cerebellum came under fire in mice with EAE, a mouse model of human multiple sclerosis (MS). In other words, both outburst and audience matter.

IFNγ, the signature T helper (Th)-1 cytokine, contributes to CNS inflammation during EAE. But not all forms of EAE are alike. In classical EAE, the T cell attack is focused on the spinal cord. But in atypical disease, the cerebellum and brain stem are the primary victims. A prior study suggested that the ratio of interleukin (IL)-17 to IFNγ determines whether disease pathology occurs in the spine or brain, with increasing levels of IL-17 associated with disease in the brain. But the data from Lees et al. instead show that lesion location is mainly controlled by the brain's response to IFNγ.

When transferred into wild-type mice, the authors show, myelin-specific Th1 cells attacked the spinal cord. But when transferred into mice lacking the IFNγ receptor, the cells instead attacked the cerebellum and brain stem, sparing the spinal cord. The production of IL-17 by the transferred T cells was comparable in both settings. However, the production of IL-17 by non-T cells predominated in the cerebellum, suggesting that IL-17–producing cells contribute to atypical disease but do not determine its location.

In agreement with past reports, however, transferring mixed populations of IFNγ- and IL-17–producing cells resulted in a mixed disease phenotype, with increasing numbers of IFNγ producers causing progressively more spinal cord disease.

Why IFNγ induces inflammation in one tissue and not another remains unknown—particularly because no obvious regional differences in the expression of the receptor were detected. The authors suspect that IFNγ triggers a localized production of T cell–attracting chemokines in the spine.


Inflammation (arrows) is focused on the cerebellum, not the spine, in mice lacking the IFNγ receptor.

## Giving imatinib a hand

Researchers have discovered a new a way to make the anticancer drug imatinib more effective. By suppressing the oncogene *AHI-1*, Zhou and colleagues were able to hold chronic myeloid leukemia (CML) in check (page 2657).

Imatinib is currently the most popular targeted therapy for CML. The leukemia is associated with the abnormal fusion of *BCR* with a kinase gene, *ABL*, which results in a perpetually active kinase known as BCR-ABL. Imatinib, a tyrosine kinase inhibitor, slows down the spread of cancer by blocking BCR-ABL activity. But the drug doesn't work in everyone and patients often relapse, most likely because the drug only targets mature cells, leaving CML stem cells behind. Scientists have therefore been hunting for complementary therapies that act on pathways left undeterred by kinase inhibitors.

Mutated versions of the recently identified protein AHI-1, whose function is unknown, have been shown to be highly expressed in leukemic stem cells—the same cells that express BCR-ABL in patients with CML. Here, Zhou et al. show that expressing AHI-1 in stem cells turns the cells cancerous in vitro, and these cells caused lethal leukemia when transferred into mice. When expressed in BCR-ABL–positive cells, AH1-1 exacerbated the growth-promoting effects of the fusion protein.

AHI-1's growth-promoting activity was attributed to the ability of AHI-1 to bind to BCR-ABL, along with an activated version of the downstream signaling protein JAK2. Cells expressing this complex were resistant to the kinase-blocking action of imatinib. Indeed, blocking AHI-1 in cells from imatinib-resistant CML patients restored the cells' sensitivity to the drug.

With this finding, the race is on to find a drug to block AH1-1. As other studies have recently suggested, the cure for CML and other leukemias may not lie in a miracle drug, but rather in a carefully concocted cocktail of targeted therapies.

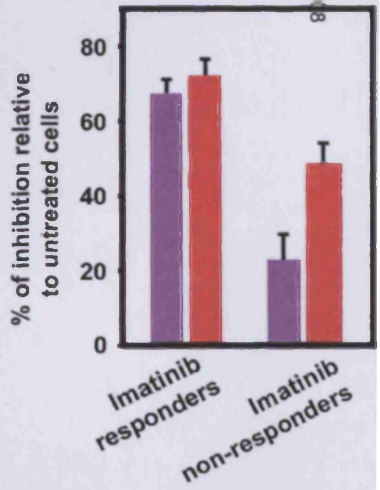


A combination of imatinib and an AHI-1 blocker (red) killed more cells from imatinib-resistant CML patients than did imatinib alone (purple).

Published September 29, 2008

BRIEF DEFINITIVE REPORT

# The Death Receptor 3–TNF-like protein 1A pathway drives adverse bone pathology in inflammatory arthritis

Melanie Jane Bull,[1] Anwen Siân Williams,[2] Zarabeth Mecklenburgh,[1] Claudia Jane Calder,[1] Jason Peter Twohig,[1] Carole Elford,[3] Bronwen Alice James Evans,[3] Tania F. Rowley,[4] Tomasz J. Slebioda,[4] Vadim Y. Taraban,[4] Aymen Al-Shamkhani,[4] and Eddie Chung Yern Wang[1]

[1]Department of Medical Biochemistry and Immunology, [2]Department of Rheumatology, and [3]Department of Child Health, School of Medicine, Heath Park, Cardiff CF14 4XN, Wales, UK
[4]Cancer Sciences Division, University of Southampton School of Medicine, Southampton SO16 6YD, England, UK

**Rheumatoid arthritis (RA) is a chronic inflammatory disease of synovial joints that is associated with cartilage and bone destruction. Death Receptor 3 (DR3), a tumor necrosis factor (TNF) receptor superfamily member, has recently been associated with the pathogenesis of RA. We demonstrate that absence of DR3 confers resistance to the development of adverse bone pathology in experimental antigen-induced arthritis (AIA). DR3$^{ko}$ mice exhibited a reduction in all histopathological hallmarks of AIA but, in particular, failed to develop subchondral bone erosions and were completely protected from this characteristic of AIA. In contrast, TNF-like protein 1A (TL1A), the ligand for DR3, exacerbated disease in a dose- and DR3-dependent fashion. Analysis of osteoclast number within AIA joint revealed a reduction in areas susceptible to bone erosion in DR3$^{ko}$ mice, whereas in vitro osteoclastogenesis assays showed that TL1A could directly promote osteoclastogenesis in mouse and man. Treatment with antagonistic anti-TL1A mAb protected animals in a systemic model of RA disease collagen-induced arthritis. We therefore conclude that the DR3–TL1A pathway regulates joint destruction in two murine models of arthritis and represents a potential novel target for therapeutic intervention in inflammatory joint disease.**

CORRESPONDENCE
Eddie Chung Yern Wang
WangEC@cf.ac.uk

Rheumatoid arthritis (RA) is a chronic inflammatory disease affecting ~1% of the global population (1). RA is characterized by infiltration of synovial joints by immune cells, principally macrophages, T cells, plasma cells, and hyperplasia of the synovial lining. This eventually results in the destructive phase of disease causing damage to cartilage and bone. It is widely accepted that cytokines and their receptors play a central role in the pathogenesis of RA, thus TNFα, IL-1, and IL-6 have been identified as key mediators of the disease (2–4). The role played by members of the TNF receptor superfamily (TNFRSF) in pathological bone resorption has also become widely accepted, with RANK and RANKL acting as crucial factors in differentiation of osteoclasts (5), the primary cell type involved in bone degradation.

DR3 (TRAMP, LARD, Apo3, Wsl1, and TNFRSF25) is a member of the TNFRSF and shows closest homology to TNFR1 (6). Like TNFR1, DR3 contains four extracellular cysteine-rich repeats and is capable of signaling both apoptosis via caspase 8 activation and cell survival via the activation of NFκB (7–9). The biological function of DR3 is an area of growing interest. In the immune system, DR3 has been shown to affect negative selection during thymocyte development (10) and can modulate T cell (11–13) and NKT cell function (14). It has also been associated with inflammatory diseases such as irritable bowel disease (15, 16) and atherosclerosis (17). Interestingly, DR3,

M.J. Bull and A.S. Williams contributed equally to this paper.



The Rockefeller University Press $30.00
J. Exp. Med. Vol. 205 No. 11 2457-2464
www.jem.org/cgi/doi/10.1084/jem.20072378

Published September 29, 2008



along with its only known ligand, TNF-like protein 1A (TL1A) (18), has been linked with RA. Duplication of the DR3 gene is more prevalent in RA patients compared with controls (19), whereas TL1A$^+$ mononuclear phagocytes have been identified in rheumatoid synovium and soluble TL1A has been detected in synovial fluid of patients (20). However, functional analysis of the in vivo role of the DR3–TL1A pathway in RA has not yet been reported.

To address this, we have generated mice lacking the DR3 gene (DR3$^{ko}$) on a C57BL/6 background (10) and used a salient model of experimental arthritis to elucidate functional aspects of DR3 activity. Antigen-induced arthritis (AIA) is a local model of disease which displays many pathological features of RA including cellular infiltration, synovial hyperplasia, pannus formation, cartilage depletion, and bone destruction (21). We show that DR3 is essential for the development of adverse joint pathology in AIA and that anti-TL1A treatment can protect from the systemic model of disease, collagen-induced arthritis (CIA). These results imply an important in vivo function for DR3 in the pathogenesis of inflammatory arthritis and provide proof of principle that countering this pathway may represent a novel therapy for RA.

## RESULTS AND DISCUSSION

### DR3$^{ko}$ mice show reduced inflammatory response to AIA compared with DR3$^{wt}$ controls

To investigate the in vivo role of DR3 in inflammatory arthritis, we induced AIA in DR3$^{ko}$ mice and DR3$^{wt}$ controls. All mice developed an inflammatory reaction in response to intraarticular injection of methylated BSA, with both DR3$^{ko}$ and DR3$^{wt}$ mice exhibiting a similar pattern of joint swelling over a 21-d time course. Comparable knee joint swelling measurements were noted in DR3$^{ko}$ and DR3$^{wt}$ mice at the peak of response, 1 d after mBSA injection. Thereafter, swelling resolved in both but faster in the absence of DR3 (Fig. 1 A).

We next assessed whether more rapid resolution of joint swelling was translated to improved pathological outcome in DR3$^{ko}$ mice. Examination of histopathological severity was performed on joint sections taken during the acute inflammatory phase when TNFα, IL-1β, and IL-6 reach a peak and destructive pathology first becomes detectable (3 d after induction) and when there is maximal evidence of structural damage within the joint (21 d after induction) (21). The severity of arthritis (arthritis index [AI]) was quantified in hematoxylin and eosin (H&E)–stained sections by grading parameters as described in Materials and methods. On day 3 after arthritis induction, DR3$^{wt}$ (Fig. 1 B) and DR3$^{ko}$ mice (Fig. 1 C) did not differ histopathologically. By day 21, DR3$^{wt}$ mice had developed arthritis characterized by extensive cellular infiltration, synovial hyperplasia, formation of a thick pannus, and bone erosions (Fig. 1 D). In contrast, DR3$^{ko}$ mice displayed mild pathological features of arthritis, showing general absence of synovial hyperplasia, lack of pannus formation, and no evidence of bone erosion (Fig. 1 E). Indeed, all scoring parameters were either absent or significantly milder in DR3$^{ko}$ compared with DR3$^{wt}$ mice (Fig. 1 F). This translated into a significant reduction in the AI (Fig. 1 G).

As a second outcome measure of structural damage to the joint, we assessed proteoglycan depletion from articular cartilage on the femoral head using Safranin O/Fast Green staining 21 d after arthritis induction. In DR3$^{wt}$ mice, cartilage was severely depleted, as illustrated by lack of red Safranin O staining resulting in an obvious tidemark (Fig. 1 H). DR3$^{ko}$ mice did not display much cartilage depletion (Fig.1 I), retaining similar levels of Safranin O staining as nonarthritic control left knees (not depicted). Collectively, this data indicate that there is considerable protection against degenerative AIA disease pathology in DR3$^{ko}$ mice.

### TL1A exacerbates disease in a DR3-dependent fashion

To confirm that resistance to AIA was DR3 specific, TL1A was injected with mBSA on day 0 of the AIA model at escalating

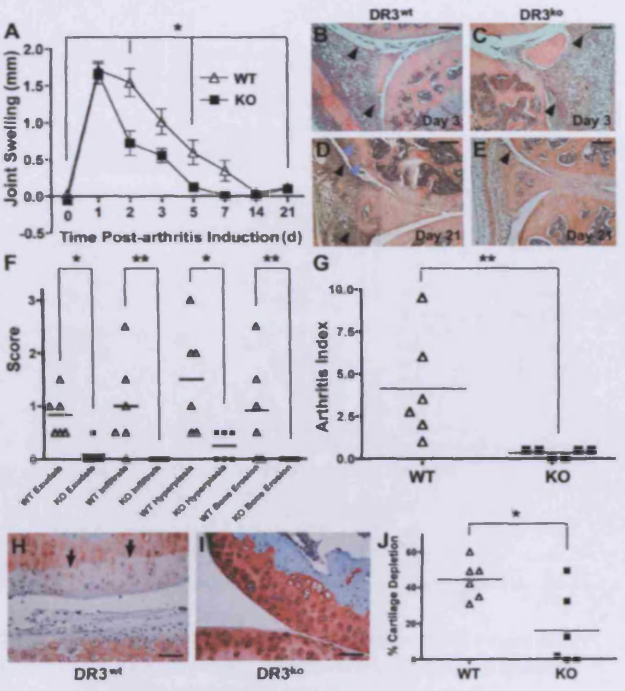


**Figure 1. Protection against AIA in DR3$^{ko}$ mice.** (A) Joint swelling after intraarticular injection of mBSA. Data are mean ± SEM from $n = 6$ DR3$^{wt}$ (△) or DR3$^{ko}$ (■) mice. Two-way analysis of variance (ANOVA) shows significance at $P < 0.02$ (*). One representative experiment of three is shown. (B–E) Representative images from DR3$^{wt}$ (B) and DR3$^{ko}$ (C) mice, 3 d after arthritis induction, and DR3$^{wt}$ (D) and DR3$^{ko}$ (E) mice, 21 d after arthritis induction. Bars, 200 µm. Inflammatory tissue (black arrowheads) and erosions (blue arrowheads) are shown. (F) Breakdown of each component of the AI. *, $P < 0.05$; **, $P < 0.01$. (G) AI scores from DR3$^{wt}$ and DR3$^{ko}$ mice. **, $P < 0.01$. Lines mark means of graphed points. (H and I) Representative images of collagen around knee joints from DR3$^{wt}$ (H) and DR3$^{ko}$ (I) mice. Sections were stained with Safranin O/Fast Green to visualize collagen in red. Tidemark of cartilage depletion (arrows) is shown. Bars, 50 µm. (J) Estimated cartilage depletion from DR3$^{wt}$ and DR3$^{ko}$ mice. *, $P < 0.05$. Each point in the summary graphs represents a single 6 DR3$^{wt}$ (△) or DR3$^{ko}$ (■) animal.

ublished September 29, 2008



quantities up to 100 ng. DR3$^{het}$ mice were chosen as they showed intermediate AI scores compared with DR3$^{wt}$ mice (Figs. 1 G and 2 A). Consequently, exacerbation or amelioration of disease after TL1A injection could be quantified, irrespective of the inherent variability in the model. Coadministration of TL1A resulted in significant dose-dependent exacerbation of disease in DR3$^{het}$ mice (Fig. 2 A). This was strikingly illustrated by the effect on size of bone erosions and severity of bone destruction, which increased in a dose-dependent fashion after TL1A injection (Fig. 2, B and C). In contrast, TL1A had no significant effect on arthritis progression in DR3$^{ko}$ mice over the concentration range studied (Fig. 2 D). Representative images of DR3$^{ko}$ mice receiving 1 and 100 ng TL1A show the continued absence of bone erosions (Fig. 2, E and F). TL1A therefore exacerbates AIA and, in particular, adverse bone pathology in a DR3-dependent manner.

### DR3 expression promotes osteoclastogenesis in AIA

Because DR3$^{ko}$ mice were protected from the development of subchondral bone erosions in AIA, we elected to quantify the number of bone-resorbing osteoclasts within the joint at two distinct sites of epiphyseal bone. Osteoclasts are clearly visualized as large red multinucleated cells with tartrate-resistant acid phosphatase (TRAP). TRAP expression in DR3$^{wt}$ and DR3$^{ko}$ mice was comparable in the femoral head (Fig. 3, A–C) and growth plate (not depicted). However, in the periosteum at areas adjacent to pannus formation, where focal bone erosions could be visualized at high magnification, TRAP staining was significantly greater in DR3$^{wt}$ mice than at equivalent areas in DR3$^{ko}$ mice (Fig. 3, D–F). These data implicate a role for DR3 in generation of osteoclasts at sites of bone pathology but not in influencing osteoclastogenesis in areas away from the pannus.

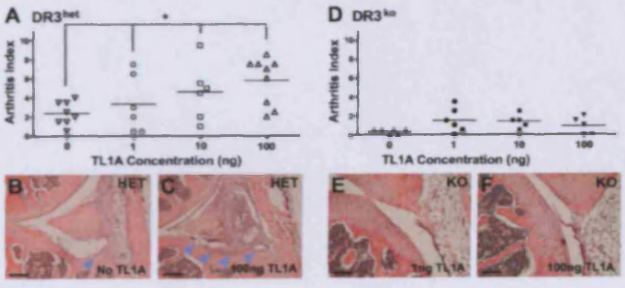


**Figure 2. TL1A promotes adverse bone pathology of AIA in a DR3-dependent manner.** (A) AI with increasing administration of TL1A in DR3$^{het}$ mice. Horizontal lines mark means of graphed points. Open symbols represent DR3$^{het}$ mice; filled symbols represent DR3$^{ko}$ mice. (B and C) Representative images from DR3$^{het}$ mice with no (B) or 100 ng (C) TL1A added. Bone erosions (arrowheads) are shown. (D) AI with increasing administration of TL1A to DR3$^{ko}$ mice. (E and F) Representative images from DR3$^{ko}$ mice with 1 (E) or 100 (F) ng TL1A added. Bars, 200 µm. One-way ANOVA showed significance of TL1A addition to DR3$^{het}$ but not DR3$^{ko}$ mice. *, $P < 0.05$. Each point in the summary graphs represents a single animal. One representative experiment of two is shown.

### DR3$^{ko}$ mice show normal myeloid infiltration within joints in AIA

Recruitment of mononuclear cells to the subintimal synovial lining layer and to periarticular adipose tissue adjacent to the meniscus is a process characteristic of the AIA model and RA patient joints. Indeed, the degree of macrophage (osteoclast precursor) infiltration within rheumatoid joint has been correlated with severity of structural damage in human disease. To assess whether reduction in osteoclast number was caused by impaired recruitment of these cells to the joint, we performed immunohistochemical analysis of F4/80 expression in sections from DR3$^{ko}$ and DR3$^{wt}$ mice on days 3 and 21 after arthritis induction. On day 3, some F4/80 expression was detected in the periarticular adipose tissue, which did not differ significantly between DR3$^{wt}$ and DR3$^{ko}$ mice (Fig. 3, G–I). By day 21, F4/80 staining was markedly increased with strong F4/80 expression visualized microscopically in both

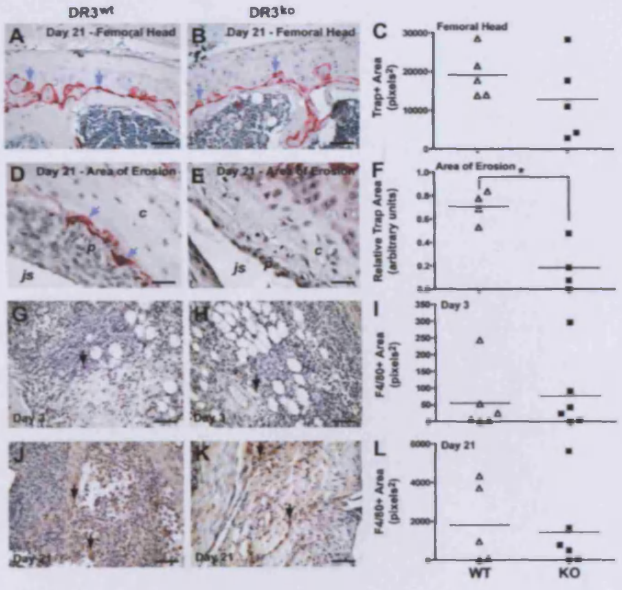


**Figure 3. TRAP and F4/80 expression in joints of DR3$^{wt}$ and DR3$^{ko}$ mice.** Sections were stained for TRAP or F4/80 as described in Materials and methods. Horizontal lines mark means of graphed points. (A and B) Representative images of TRAP staining at day 21 after arthritic induction from DR3$^{wt}$ (A) and DR3$^{ko}$ (B) mice. Red TRAP$^+$ staining (arrows) is shown. (C) Summary of TRAP staining in femoral head at day 21. (D and E) Representative images of TRAP staining around areas of bone erosion at day 21 after arthritic induction from DR3$^{wt}$ mice (D) and equivalent areas from DR3$^{ko}$ mice (E). Red TRAP$^+$ staining (arrows) is shown; *js*, joint space; *p*, pannus; *c*, cartilage. (F) DR3$^{ko}$ mice show significantly reduced TRAP$^+$ staining compared with DR3$^{wt}$ mice. *, $P < 0.05$. (G and H) Representative images of F4/80 staining from DR3$^{wt}$ (G) and DR3$^{ko}$ (H) mice, 3 d after arthritis induction. (I) Summary of day-3 data. (J and K) Representative images of F4/80 staining from DR3$^{wt}$ (J) and DR3$^{ko}$ (K) mice, 21 d after induction of arthritis. F4/80-positive cells (arrows) are shown. (L) Summary of day-21 data. Each point in the summary graphs represents a single DR3$^{wt}$ (△) or DR3$^{ko}$ (■) animal. Bars, 50 µm. One representative experiment of two is shown.

Published September 29, 2008



$DR3^{ko}$ and $DR3^{wt}$ mice. Quantification of $F4/80^+$ cells again revealed no significant difference in expression between $DR3^{wt}$ and $DR3^{ko}$ mice (Fig. 3, J–L). Overall, these data suggest that absence of DR3 does not impair recruitment of myeloid cells to the joint, nor does it affect overall numbers of basal mature osteoclasts in the femoral head. Neither hypothesis can explain the reduction in osteoclast numbers in areas of bone pathology in $DR3^{ko}$ mice.

### TL1A promotes osteoclastogenesis in vitro in a DR3-dependent fashion

We therefore tested the possibility that TL1A could directly promote differentiation of osteoclasts. To achieve this, we used an in vitro system of osteoclastogenesis from adherent BM-derived cells (BMC). BM macrophages (BMM) from $DR3^{wt}$ mice were confirmed to express DR3 (Fig. 4 A). BMC from $DR3^{wt}$ and $DR3^{ko}$ mice did not differ in their ability to generate osteoclasts in the presence of soluble RANK-L and M-CSF as measured by the formation of multinucleated $TRAP^+$ cells (Fig. 4 B). However, TL1A addition significantly enhanced development of osteoclasts from $DR3^{wt}$ but not $DR3^{ko}$ BMC (Fig. 4, B–D). TL1A in the absence of RANK-L and M-CSF could not generate osteoclasts (Fig. 4 E). The functional capacity of in vitro–generated osteoclasts to destroy bone was visualized by toluidine blue staining of pits in the ivory discs (Fig. 4 F). This data indicates that TL1A is not necessary for osteoclastogenesis per se, but promotes it in the presence of RANK-L and M-CSF and in a DR3-dependent fashion. In support of our murine data and highlighting the significance of these results for humans, TL1A significantly promoted osteoclastogenesis from monocytes derived from human peripheral blood (Fig. 4 G).

### Anti-TL1A neutralizing antibody ameliorates AIA and CIA

To test the therapeutic potential of countering the DR3–TL1A pathway, we generated an antagonistic rat mAb to murine TL1A (Fig. 5, A and B) and applied it in AIA and the systemic model of disease. CIA is the industry standard for testing potential therapeutic agents against RA. A single treatment of anti-TL1A at the point of arthritic induction in AIA resulted in more rapid resolution of swelling that mirrored our observations in $DR3^{ko}$ mice (Fig. 5 C). In CIA, clinical signs of arthritis became apparent in control mice on day 25 (Fig. 5 D). Disease activity was assessed by assigning scores to each paw according to degree of redness, swelling, and joint involvement. Paw scores in anti-TL1A–treated mice were consistently lower than in control IgG2a-treated mice, reaching significance on days 27 and 28 (Fig. 5 E). Disease activity in control IgG2a-treated mice was characterized by leukocyte infiltration of synovial tissues and variable degrees of bone erosion (Fig. 5 F). Specimens from anti-TL1A–treated mice demonstrated mild changes by comparison (Fig. 5 G). The AI in anti-TL1A–treated mice was significantly less than in IgG2a-treated controls (Fig. 5 H). These data are consistent with the protection against AIA observed in $DR3^{ko}$ mice and suggest that countering the DR3–TL1A pathway may be therapeutic against RA in man.

### The role of the DR3–TL1A axis in driving adverse bone pathology in inflammatory arthritis

Our findings show that $DR3^{ko}$ mice are resistant to the adverse joint pathology that is typical in AIA and are consistent with an essential role for the DR3–TL1A pathway in development of inflammatory arthritis. $DR3^{ko}$ mice elicited an initial inflammatory reaction in response to AIA induction, such that at day 3 after arthritis induction, there was no difference in histopathological scoring or level of inflammatory cell infiltrate between control and $DR3^{ko}$ mice. Resolution of inflammation, however, occurred at a faster rate in $DR3^{ko}$ mice, as indicated by reduction in joint swelling over the course of the study and reduction in all histopathological parameters measured at day 21 after arthritic induction. Of particular note was the absence of bone erosion and marked reduction in cell infiltrate in $DR3^{ko}$ mice in later stages of disease. Comparable numbers of infiltrating $F4/80^+$ macrophages were present in joints of $DR3^{wt}$ and $DR3^{ko}$ mice, despite the observed differences in joint pathology. Therefore, the mechanisms involved in initiating the inflammatory reaction and in recruitment of myeloid cells into the joint appear

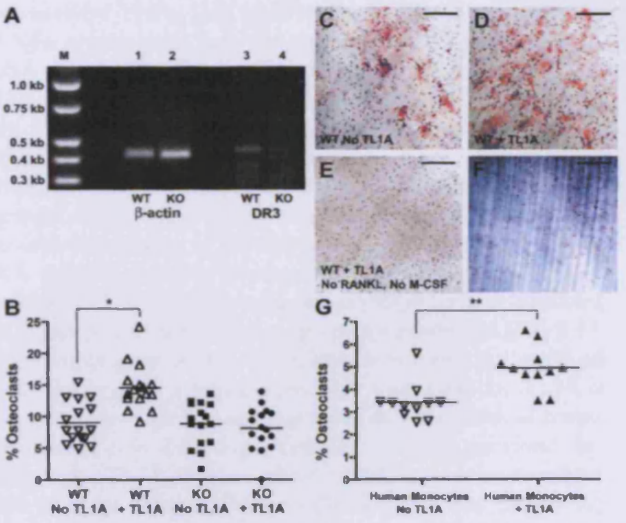


**Figure 4. TL1A promotes DR3-dependent in vitro osteoclastogenesis.** (A) RT-PCR of DR3 in BMM. In vitro osteoclastogenesis assays were performed as described in Materials and methods. Osteoclast numbers were estimated by counting multinucleated $TRAP^+$ cells. (B) Effect of TL1A on proportion of osteoclasts generated in presence of RANKL and M-CSF. *, $P = 0.0003$. Each point represents a single ivory disc from experiments on $DR3^{wt}$ (open symbols) or $DR3^{ko}$ (filled symbols) mice. Four discs from four mice were counted for each treatment. Lines mark means of graphed points. One representative experiment of two is shown. (C–E) TRAP staining of BM cells from $DR3^{wt}$ mice on discs with RANK-L + M-CSF and no TL1A (C) or 10 ng/ml TL1A (D) and TL1A (E), but no RANKL and M-CSF. Bars, 50 µm. (F) Toluidine blue staining of ivory discs showing pit-forming ability of osteoclasts generated in vitro. Bar, 150 µm. (G) Effect of TL1A on osteoclastogenesis from adherent human peripheral blood mononuclear cells and proportion of osteoclasts in cultures shown with (▽) or without (▲) exogenous TL1A added. **, $P = 0.0013$. One representative experiment of two is shown.

Published September 29, 2008



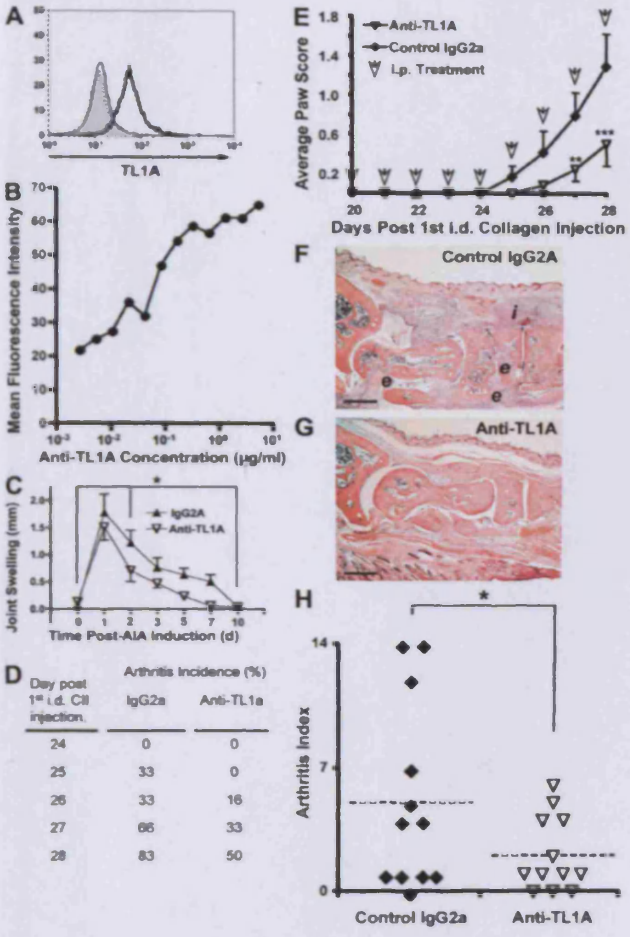


**Figure 5. Early therapeutic intervention with anti-TL1A antibody arrests development of arthritis.** (A) Binding of rat anti-TL1A mAb (TAN 2-2) to J558L cells transfected with plasmid encoding membrane-bound TL1A. Shaded histogram and dotted line represent binding of isotype control and TAN 2-2 to plasmid only transfected cells, respectively. Binding of isotype control and TAN 2-2 to TL1A-expressing cells is represented by a thin and thick line, respectively. (B) Titration of TAN 2-2 binding to J558L cells expressing membrane-bound TL1A. (C) Time course of swelling in AIA after anti-TL1A mAb treatment. Data are mean ± SEM from mice treated with control IgG2A (▲) or anti-TL1A (▽) mAb. One representative experiment of two is shown. *, $P < 0.02$ by two-way ANOVA. CIA was induced as described in Materials and methods. All data were derived from six mice for each treatment. (D) Arthritis incidence tabulated over 28-d time course. (E) Arthritis severity as a mean paw score from day 20 when dosing schedule for anti-TL1A and control IgG2a was started. Data are mean ± SEM. Timing of injections are shown (arrows). (F and G) Representative images of H&E-stained sections from control IgG2a (F) and anti-TL1A (G). *i*, intense synovial infiltration; e, aggressive bone erosion. Bars, 200 µm. (H) Analysis of AI of CIA in control IgG2a and anti-TL1A–treated mice. Dotted horizontal line depicts mean for each group. *, $P < 0.05$; **, $P = 0.01$; ***, $P = 0.006$.

intact in the absence of DR3. Because of this, we chose to investigate differentiation of osteoclasts, discovering that osteoclast differentiation in vitro and bone erosion in vivo was exacerbated by exogenous TL1A in control but not DR3$^{ko}$ mice. These DR3-dependent effects confirm that TL1A is a specific functional ligand for DR3 and identifies the control of osteoclasts as a novel function for DR3. The potential of countering the DR3–TL1A pathway as a therapy was proven by amelioration of CIA and AIA using a neutralizing anti-TL1A mAb. Interestingly, anti-TL1A therapy was not totally protective. The possibility remains that there may be secondary ligands for DR3 and TL1A as implicated for TL1A by recent data in renal inflammation (22), but detailed studies have shown no other TNFSF/TNFRSF family members that bind murine DR3 or murine TL1A (18), whereas human TL1A binds Decoy Receptor 3 (11), a mouse homologue of which has not been found.

This is the first paper reporting that signaling through DR3 on myeloid cells promotes osteoclastogenesis, although it is clear from our data that it is not a prerequisite for, nor can it induce, this differentiation in the absence of RANK-L and M-CSF. In this respect, it mirrors functions that have been reported for TNFα (23). However, a function independent of TNFα is suggested by a recent paper showing that macrophages produce TL1A independent of TNF activity (20). TL1A expression, including release of active soluble forms of the protein, can be induced on human monocytes by FcγR stimulation through soluble (24) and insoluble immune complexes purified from RA synovial fluid (20). The majority of stromal macrophages in RA synovial tissue express TL1A, and in vitro stimulation of monocytes with PEG precipitates from RA samples results in production of nanogram quantities of soluble TL1A (20). This suggests very high levels in localized RA joint akin to the levels we used to exacerbate AIA (Fig. 2 A). The implication is that in inflammatory arthritis, myeloid cells may exhibit a positive feedback loop whereby TL1A is triggered through ICs and can drive differentiation of bone-destroying cells if the right cytokine milieu is provided. Intriguingly, TL1A also has varied effects on human osteoblast cell lines in vitro, inhibiting differentiation and promoting quiescence at low densities but inducing death at high densities (25). We therefore propose that the DR3–TL1A pathway may act as a switch that is capable of directly activating osteoclast but also inhibiting osteoblast differentiation and, in so doing, disregulate the homeostatic balance of degradation and formation in normal bone into the detrimental situation observed in destructive bone pathologies such as RA. Although our in vitro data supports this proposal, some caution is necessary in interpreting the contribution of direct TL1A-driven osteoclastogenesis to arthritic bone damage in vivo, as inflammation and bone erosion cannot be dissociated in AIA or CIA. The possibility remains that the resistance of DR3$^{ko}$ mice to bone erosion is secondary to DR3–TL1A-dependent control of other parts of the inflammatory process.

In this respect, our data also show that cartilage depletion is significantly reduced in DR3$^{ko}$ mice (Fig. 1). Cartilage depletion

Published September 29, 2008

is attributed to the effects of matrix metalloproteinases (MMPs), levels of which are raised in RA joint. In vitro experiments on human cell lines have shown that DR3 activation can induce the production of MMP-1, -9, and -13 in THP-1s (17). These MMPs have all been associated with RA joint pathology (26). In addition, it is also established that TL1A plays an important role in T cell function. TL1A has been shown to costimulate IL-2 responsiveness (11) and synergize with the TCR and IL-12/IL-18 pathways to induce IFNγ release (15, 27, 28). TL1A also amplifies cytokine release by NKT cells (14) and T cells (13) and regulates the development of proinflammatory Th17 cells (12, 16), which are reported to aid osteoclastogenesis in autoimmune arthritis (29). The action of TL1A on T cells may also be regulated by differential expression of splice variants of DR3 (27). The exact role of TL1A and DR3 on lymphocytes in inflammatory arthritis remains to be elucidated, but it is interesting to note that we find normal anti-mBSA Ab levels in serum, unchanged T cell proliferation to mBSA in draining lymph nodes of $DR3^{ko}$ mice after AIA induction, and normal in vitro generation of Th17 cells from $DR3^{ko}$ splenocytes (unpublished data).

In summary, we have induced inflammatory arthritis in $DR3^{ko}$ mice and found that they exhibit strong resistance to the adverse pathology observed in AIA. We show DR3-dependent TL1A-driven exacerbation of bone damage in vivo and promotion of osteoclastogenesis in vitro. We also show that anti-TL1A therapy ameliorates disease. Our data suggest that the DR3–TL1A pathway is an important component of inflammatory responses in joint disease and, as such, identifies a potential therapeutic target for treatment of diseases like RA but with potential impact in other diseases involving disrupted bone physiology.

## MATERIALS AND METHODS

**Animals.** The DR3 mouse colony was founded from animals supplied by Cancer Research UK, London. All experiments were undertaken in male WT ($DR3^{+/+}$), heterozygous ($DR3^{+/-}$), and KO ($DR3^{-/-}$) mice, which have been described previously (10). DBA 1J mice were acquired from Harlan, UK. Animals were used at 6–8 wk of age. All procedures were approved by the Local Research Ethics Committee and performed in strict accordance with Home Office–approved licenses PPL 30/1999 and 30/2361.

**Induction of murine AIA.** AIA was induced as previously described (30). In brief, mice were s.c. immunized on two occasions, 1 wk apart, with 1 mg/ml mBSA with an equal volume of CFA. An additional i.p. injection of 100 μl of heat-inactivated *Bordetella pertussis* toxin was administered with the first immunization. AIA was induced in the hind right knee joint via an intraarticular injection of 10 mg/ml mBSA (6 μl), administered 21 d after the initial immunization. To assess the effect of TL1A or anti-TL1A administration, AIA was induced via mBSA injection in conjunction with 1, 10, or 100 ng of soluble TL1A (R&D Systems) or 100 ng of anti-TL1A mAb.

**Generation of a rat anti-mouse TL1A monoclonal antibody.** Rats were immunized with a soluble recombinant TL1A protein consisting of a human IgG1 Fc domain, with an additional hinge-like region at the C terminus, linked to the extracellular domain of mouse TL1A (177–252). The protein was produced in Chinese hamster ovary cells and was purified by immunoaffinity chromatography using an anti-human Fc mAb. Anti-TL1A mAb was generated by standard hybridoma technology and hybridoma supernatants were screened for binding to recombinant soluble and membrane-expressed TL1A. To generate cells expressing membrane-anchored TL1A, PCR fragments encoding the entire coding sequence of mouse TL1A were cloned into the mammalian expression vectors pEF1/V5-His A and pcDNA3.1 (Invitrogen), and plasmids were then transfected into J558L or 293T cells. Stable J558L cell lines expressing membrane-anchored TL1A were selected in Geneticin (400 μg/ml)-containing media. Splenic cDNA or IMAGE clone 30740802 was used as a template for PCR reactions to generate TL1A-encoding DNA fragments. Further selection of neutralizing anti-TL1A mAbs was based on the ability to block binding of soluble recombinant TL1A-Fc to anti-CD3/CD28–stimulated T cells.

**Anti-TL1A therapy in CIA.** CIA was induced as previously described (31). In brief, 2 mg/ml of chicken type II collagen (CII; Sigma-Aldrich) was emulsified with an equal volume of complete Freund's adjuvant and 100 μl of collagen/adjuvant mixture injected intradermally into several sites near the base of the tail of 7-wk-old male DBA/1J mice. A second identical booster was administered to each mouse 21 d after the first injection. The day of the first immunization was designated as day 0. Mice were randomly assigned to one of three treatment groups on day 20. Animals received nine daily 100-μl injections containing either 2.5 mg/kg of anti-TL1A or LEAF purified control rat IgG2a (Cambridge Biosciences) dissolved in sterile PBS or PBS alone administered by the i.p. route from day 20. Thereafter, arthritis incidence and severity was assessed daily until termination on day 28 when the disease severity limits were attained in IgG2a and PBS controls. The incidence of CIA was assessed as the percentage of mice developing arthritis among all mice. The severity of arthritis in each paw (paw score) was evaluated by using an established in-house scoring system: 0, normal; 1, mild but definite swelling in the ankle or wrist joint or redness and swelling limited to individual digits regardless of the number of digits affected; 2, moderate swelling of ankle or wrist; 3, severe redness and swelling of the ankle or wrist and proximal phalangeal joints; and 4, maximally inflamed limb with involvement of multiple joints, no ankylosis.

**Assessment of arthritis.** Joint swelling was assessed on days 1, 2, 3, 5, 7, 14, and 21 after arthritis induction by measuring the difference between hind right (AIA) and hind left (control) knee joint diameters using an analogue micrometer. Animals were killed on day 3 or 21 for assessment of inflammatory and pathological changes within the joint. Histological assessment was performed as previously described (30). All joints were fixed in neutral buffered formal saline and decalcified with 10% formic acid for 2 wk at 4°C before embedding in paraffin wax. Serial sections of 7-μm thickness were taken and stained routinely with H&E for analysis. Two blinded independent observers scored the sections for cellular infiltration (0–5), cellular exudate (0–3), synovial hyperplasia (0–3), and bone erosion (0–3), with 0 representing a normal joint. The sum of all parameters gave the AI. Sections were additionally stained with Safranin O and Fast Green to assess cartilage depletion.

**RT-PCR.** BMM were generated as previously described (32). RNA was extracted from BMM cultures using RNeasy (QIAGEN) after manufacturer's instructions, whereas cDNA was generated and RT-PCR performed according to standard Invitrogen protocols. PCR primers were as follows: β-actin, forward 5′-CGGCCAGGTCATCACTATTG-3′ and reverse 5′-CTCAGTAACCCGCCTAG-3′ giving a 410-bp product; and DR3, forward 5′-CTAAGGCTTGCACTGCTGTCT-3′ and reverse 5′-GAGCATCTCATACTGCTGGTC-3′ giving a 457-bp product. The PCR consisted of 33 cycles with a 59°C annealing temperature.

**TRAP staining for osteoclasts.** For TRAP staining, joints were decalcified in EDTA (7%), rehydrated, and incubated with TRAP staining solution containing 0.1 M acetate buffer, 0.5 M sodium tartrate, 10 mg/ml naphthol AS-MX phosphate, 100 μl Triton X-100, and 0.3 mg/ml Fast Red Violet LB salt for 3 h at 37°C. Sections were then counterstained with hematoxylin before mounting in DPX. Images were captured using a digital camera (N457; Olympus), and TRAP positive cells were analyzed using Photoshop CS3. 5 (Adobe). Randomly chosen selected areas were used for analysis.

Published September 29, 2008

**Immunohistochemistry for F4/80 expression.** F4/80 expression was detected using an anti-rat HRP-DAB staining kit (R&D Systems) according to the manufacturer's instructions. In brief, sections were rehydrated and endogenous peroxidase activity was blocked. Antigen unmasking was achieved by incubating the sections in 0.1% prewarmed Trypsin EDTA in PBS for 30 min at 37°C. After blocking steps, sections were incubated overnight with 4 µg/ml of rat anti-F4/80 antibody (Invitrogen) or isotype control diluted in PBS followed by secondary antibody as per the manufacturer's instructions. Positively labeled cells were visualized using a streptavidin-HRP conjugate and DAB chromogen. Sections were counterstained with hematoxylin, dehydrated, and mounted in DPX. Images were captured using a digital camera (N457), and F4/80 positive cells were analyzed using Photoshop. Randomly selected areas were used for analysis.

**In vitro osteoclastogenesis assays.** BMC were removed from femurs of DR3$^{tg}$ and DR3$^{tg}$ mice by centrifugation after removal of the proximal end. BMC were resuspended in α-MEM supplemented with 10% FCS, 2 mM L-glutamine, and antibiotics (MEM-10) and $5 \times 10^5$ cells added to ivory discs. After 2 h at 37°C, nonadherent cells were removed by transfer of ivory discs to new wells with fresh media supplemented with 50 ng/ml RANKL and 25 ng/ml M-CSF with or without 10 ng/ml TL1A. All media were replenished after 3 d. TRAP staining was performed according to the manufacturer's instructions (Sigma-Aldrich) after 7 d. Six fields of view on each disc were counted for TRAP-positive multinucleated cells. For human osteoclastogenesis assays, peripheral blood mononuclear cells were used as a source for adherent cells and cultures were maintained for 21 d before TRAP staining.

**Statistical analysis.** Readouts could not be assumed to be normally distributed as they were histological scores or percentages. Therefore, nonparametric Mann-Whitney *U* tests were used for statistical analysis. One-way unpaired and two-way ANOVAs were used when testing the influence of third parameters such as time or dose. Analyses were performed on GraphPad Prism v4. *P* values of $<0.05$ were considered significant and values of $<0.01$ were considered highly significant.

This work was funded by the Medical Research Council, through a Medical Research Council Career Establishment Grant awarded to E.C.Y. Wang (G0300180), a Medical Research Council Collaboration Grant (G0500617), the Wellcome Trust and two PhD studentships, one part-funded by the I3 Interdisciplinary Research Group, Cardiff University.

The authors have no conflicting financial interests.

**Submitted: 6 November 2007**
**Accepted: 2 September 2008**

## REFERENCES

1. Feldmann, M., F.M. Brennan, and R.N. Maini. 1996. Rheumatoid arthritis. *Cell*. 85:307–310.
2. Williams, R.O., M. Feldmann, and R.N. Maini. 1992. Anti-tumor necrosis factor ameliorates joint disease in murine collagen-induced arthritis. *Proc. Natl. Acad. Sci. USA*. 89:9784–9788.
3. Abramson, S.B., and A. Amin. 2002. Blocking the effects of IL-1 in rheumatoid arthritis protects bone and cartilage. *Rheumatology (Oxford)*. 41:972–980.
4. Boe, A., M. Baiocchi, M. Carbonatto, R. Papotan, and O. Serlupi-Crescenzi. 1999. Interleukin 6 knock-out mice are resistant to antigen-induced experimental arthritis. *Cytokine*. 11:1057–1064.
5. Asagiri, M., and H. Takayanagi. 2007. The molecular understanding of osteoclast differentiation. *Bone*. 40:251–264.
6. Kitson, J., T. Raven, Y.P. Jiang, D.V. Goeddel, K.M. Giles, K.T. Pun, C.J. Grinham, R. Brown, and S.N. Farrow. 1996. A death domain-containing receptor that mediates apoptosis. *Nature*. 384:372–375.
7. Bodmer, J.L., K. Burns, P. Schneider, K. Hofmann, V. Steiner, M. Thome, T. Bornand, M. Hahne, M. Schroter, K. Becker, et al. 1997. TRAMP, a novel apoptosis mediating receptor with sequence homology to tumor necrosis factor receptor 1 and Fas(Apo-1/CD95). *Immunity*. 6:79–88.
8. Screaton, G.R., X.N. Xu, A.L. Olsen, A.E. Cowper, R. Tan, A.J. McMichael, and J.I. Bell. 1997. LARD: a new lymphoid-specific death domain containing receptor regulated by alternative pre-mRNA splicing. *Proc. Natl. Acad. Sci. USA*. 94:4615–4619.
9. Marsters, S.A., J.P. Sheridan, C.J. Donahue, R.M. Pitti, C.L. Gray, A.D. Goddard, K.D. Bauer, and A. Ashkenazi. 1996. Apo-3, a new member of the tumor necrosis factor receptor family, contains a death domain and activates apoptosis and NF-kappa B. *Curr. Biol.* 6:1669–1676.
10. Wang, E.C., A. Thern, A. Denzel, J. Kitson, S.N. Farrow, and M.J. Owen. 2001. DR3 regulates negative selection during thymocyte development. *Mol. Cell. Biol.* 21:3451–3461.
11. Migone, T.S., J. Zhang, X. Luo, L. Zhuang, C. Chen, B. Hu, J.S. Hong, J.W. Perry, S.F. Chen, J.X. Zhou, et al. 2002. TL1A is a TNF-like ligand for DR3 and TR6/DcR3 and functions as a T cell costimulator. *Immunity*. 16:479–492.
12. Pappu, B.P., A. Borodovsky, T.S. Zheng, X. Yang, P. Wu, X. Dong, S. Weng, B. Browning, M.L. Scott, L. Ma, et al. 2008. TL1A-DR3 interaction regulates Th17 cell function and Th17-mediated autoimmune disease. *J. Exp. Med.* 205:1049–1062.
13. Meylan, F., T.S. Davidson, E. Kahle, M. Kinder, K. Acharya, D. Jankovic, V. Bundoc, M. Hodges, E.M. Shevach, A. Keane-Myers, et al. 2008. The TNF-family receptor DR3 is essential for diverse T cell-mediated inflammatory diseases. *Immunity*. 29:79–89.
14. Fang, L., B. Adkins, V. Deyev, and E.R. Podack. 2008. Essential role of TNF receptor superfamily 25 (TNFRSF25) in the development of allergic lung inflammation. *J. Exp. Med.* 205:1037–1048.
15. Bamias, G., C. Martin III, M. Marini, S. Hoang, M. Mishina, W.G. Ross, M.A. Sachedina, C.M. Friel, J. Mize, S.J. Bickston, et al. 2003. Expression, localization, and functional activity of TL1A, a novel Th1-polarizing cytokine in inflammatory bowel disease. *J. Immunol.* 171:4868–4874.
16. Takedatsu, H., K.S. Michelsen, B. Wei, C.J. Landers, L.S. Thomas, D. Dhall, J. Braun, and S.R. Targan. 2008. TL1A (TNFSF15) regulates the development of chronic colitis by modulating both T-Helper 1 and T-Helper 17 activation. *Gastroenterology*. 135:552–567.
17. Kang, Y.J., W.J. Kim, H.U. Bae, D.I. Kim, Y.B. Park, J.E. Park, B.S. Kwon, and W.H. Lee. 2005. Involvement of TL1A and DR3 in induction of pro-inflammatory cytokines and matrix metalloproteinase-9 in atherogenesis. *Cytokine*. 29:229–235.
18. Bossen, C., K. Ingold, A. Tardivel, J.L. Bodmer, O. Gaide, S. Hertig, C. Ambrose, J. Tschopp, and P. Schneider. 2006. Interactions of tumor necrosis factor (TNF) and TNF receptor family members in the mouse and human. *J. Biol. Chem.* 281:13964–13971.
19. Osawa, K., N. Takami, K. Shiozawa, A. Hashiramoto, and S. Shiozawa. 2004. Death receptor 3 (DR3) gene duplication in a chromosome region 1p36.3: gene duplication is more prevalent in rheumatoid arthritis. *Genes Immun.* 5:439–443.
20. Cassatella, M.A., G.P. da Silva, I. Tinazzi, F. Facchetti, P. Scapini, F. Calzetti, N. Tamassia, P. Wei, B. Nardelli, V. Roschke, et al. 2007. Soluble TNF-like cytokine (TL1A) production by immune complexes stimulated monocytes in rheumatoid arthritis. *J. Immunol.* 178:7325–7333.
21. Simon, J., R. Surber, G. Kleinstauber, P.K. Petrow, S. Henzgen, R.W. Kinne, and R. Brauer. 2001. Systemic macrophage activation in locally-induced experimental arthritis. *J. Autoimmun.* 17:127–136.
22. Al-Lamki, R.S., J. Wang, A.M. Tolkovsky, J.A. Bradley, J.L. Griffin, S. Thiru, E.C. Wang, E. Bolton, W. Min, P. Moore, et al. 2008. TL1A both promotes and protects from renal inflammation and injury. *J. Am. Soc. Nephrol.* 19:953–960.
23. Lam, J., S. Takeshita, J.E. Barker, O. Kanagawa, F.P. Ross, and S.L. Teitelbaum. 2000. TNF-alpha induces osteoclastogenesis by direct stimulation of macrophages exposed to permissive levels of RANK ligand. *J. Clin. Invest.* 106:1481–1488.
24. Prehn, J.L., L.S. Thomas, C.J. Landers, Q.T. Yu, K.S. Michelsen, and S.R. Targan. 2007. The T cell costimulator TL1A is induced by FcgammaR signaling in human monocytes and dendritic cells. *J. Immunol.* 178:4033–4038.
25. Borysenko, C.W., V. Garcia Palacios, R.D. Griswold, Y. Li, A.K. Iyer, B.B. Yaroslavskiy, A.C. Sharrow, and H.C. Blair. 2006. Death receptor-3 mediates apoptosis in human osteoblasts under narrowly regulated conditions. *J. Cell. Physiol.* 209:1021–1028.

26. Burrage, P.S., K.S. Mix, and C.E. Brinckerhoff. 2006. Matrix metalloproteinases: role in arthritis. *Front. Biosci.* 11:529–543.
27. Bamias, G., M. Mishina, M. Nyce, W.G. Ross, G. Kollias, J. Rivera-Nieves, T.T. Pizarro, and F. Cominelli. 2006. Role of TL1A and its receptor DR3 in two models of chronic murine ileitis. *Proc. Natl. Acad. Sci. USA.* 103:8441–8446.
28. Papadakis, K.A., D. Zhu, J.L. Prehn, C. Landers, A. Avanesyan, G. Lafkas, and S.R. Targan. 2005. Dominant role for TL1A/DR3 pathway in IL-12 plus IL-18-induced IFN-gamma production by peripheral blood and mucosal CCR9+ T lymphocytes. *J. Immunol.* 174:4985–4990.
29. Sato, K., A. Suematsu, K. Okamoto, A. Yamaguchi, Y. Morishita, Y. Kadono, S. Tanaka, T. Kodama, S. Akira, Y. Iwakura, et al. 2006. Th17 functions as an osteoclastogenic helper T cell subset that links T cell activation and bone destruction. *J. Exp. Med.* 203:2673–2682.
30. Williams, A.S., M. Mizuno, P.J. Richards, D.S. Holt, and B.P. Morgan. 2004. Deletion of the gene encoding CD59a in mice increases disease severity in a murine model of rheumatoid arthritis. *Arthritis Rheum.* 50:3035–3044.
31. Campbell, I.K., J.A. Hamilton, and I.P. Wicks. 2000. Collagen-induced arthritis in C57BL/6 (H-2b) mice: new insights into an important disease model of rheumatoid arthritis. *Eur. J. Immunol.* 30:1568–1575.
32. Calder, C.J., L.B. Nicholson, and A.D. Dick. 2005. A selective role for the TNF p55 receptor in autocrine signaling following IFN-gamma stimulation in experimental autoimmune uveoretinitis. *J. Immunol.* 175:6286–6293.